

**Product distributions and efficiencies for ethanol oxidation in
proton exchange membrane electrolysis cells**

By

Rakan Mohammad Altarawneh

A thesis submitted to the School of Graduate Studies in partial fulfillment of
the requirements for the degree of
Doctor of Philosophy

Department of Chemistry
Memorial University
St. John's, Newfoundland
Canada

August 2018

Abstract

Ethanol is an attractive fuel for direct alcohol fuel cells (DAFCs). In comparison with other organic fuels, ethanol has a high energy density. Therefore, direct ethanol fuel cells (DEFCs) are considered to be highly attractive power sources for electronic devices and vehicles. In addition, ethanol can be oxidized in an ethanol electrolysis cell (EEC) to produce hydrogen for use in fuel cells. Although ethanol has a high energy density and DEFCs have a high theoretical efficiency (98%), these are based on complete oxidation of ethanol to CO₂, while the main products from DEFCs and EECs are acetic acid and acetaldehyde. A good understanding of what happens during ethanol oxidation in fuel cell hardware is therefore a crucial step in the evolution of these technologies. It is particularly important in the development of new catalysts to improve cell efficiencies and performances by facilitating the complete oxidation of ethanol.

The methods reported here provide information on the efficiency and product distribution for ethanol oxidation in a DEFC or EEC. They are based on polymer electrolyte membrane (PEM) fuel cell technology. In comparison with those reported in the literature, our methodologies are shown to have advantages over them by detecting the fuel itself and reaction products from both the anode and cathode exhausts. The amounts of ethanol consumed and acetic acid and acetaldehyde produced were determined by proton NMR spectroscopy while CO₂ was measured with a non-dispersive infrared CO₂ monitor. The efficiencies of these cells are dependent on the cell potential, crossover of ethanol, and stoichiometry of the ethanol oxidation reaction (i.e. the average number of electrons transferred per ethanol molecule). The stoichiometry of the EOR (ethanol oxidation reaction) was determined by using different methods in this work: an electrochemical method, analysis of the amount of ethanol consumed (ΔC) and from the product

distribution (faradaic and chemical). It was found that the results from these methods were in a good agreement.

In addition, the effects of fuel and product crossover were closely examined. It was shown that analysis of only the anode exhaust solution leads to an underestimation of ethanol and products due to crossover through the membrane to the cathode. To obtain accurate product distributions, the anode and cathode exhausts were combined. In addition, the chemical reaction between ethanol and oxygen that occurs in a DEFC was avoided by making measurement in an EEC with N₂ gas at the cathode.

The stoichiometry, efficiency, and product distribution for ethanol electrolysis in fuel cell hardware has been determined at 80 °C for various anodes prepared with commercial Pt/C, PtRu/C, and PtSn/C catalysts. Also, synergetic effects between these catalysts were studied by using mixed and bilayer electrodes. It was found that bilayer electrodes increased the overall efficiency of the cell by increasing the faradaic efficiency while maintaining high potential efficiency.

An octahedral PtNi catalyst was prepared by using a literature method and tested in our system. In comparison to a Pt, this catalyst was shown to increase selectivity towards complete oxidation (to carbon dioxide) at low potentials and thereby increase efficiency. These results are contrary to those reported in the literature for this catalyst in a conventional electrochemical cell, and demonstrate the importance of the new methodologies in the evaluation and study of new catalysts for ethanol oxidation.

Dedicated to my Dad and Mom for their love and support.

Acknowledgements

I would like to express my deep and sincere gratitude to my supervisor Prof. Peter Pickup for giving me the opportunity to work in his group and also for his kindness, guidance, motivation, support and patience while doing the research. I could not have asked for a better advisor for my program.

I would also like to thank my supervisory committee, Prof. Francesca Kerton and Prof. David Thompson for the advice, support and time they have dedicated throughout my program.

I want to acknowledge all the faculty members of the chemistry department who sat on my comprehensive exam committee, examined my seminars and taught me courses throughout the years. I wish to extend my warmest thanks to the staff at Memorial University for their help. I thank my lab-mates for their assistance, discussion and for sharing their experience. I also wish them good luck for their PhD. I also thank Dr. Pasha Majidi for his kind help during the initial stage of this work.

Financial support from the School of Graduate Studies, Mu'tah University, and Prof. Pickup's NSERC grants are gratefully acknowledged.

Last but not least, I would have not been able to achieve any of my successes if it was not for the support of my parents, my family and friends. Their constant support and encouragement keeps me motivated. My deepest appreciation to everyone who helped and encouraged me during my PhD.

Table of Contents

Abstract.....	ii
Acknowledgements.....	v
List of Tables	x
List of Figures.....	xi
List of Abbreviations	xvii
List of Symbols.....	xix
1. Introduction.....	2
1.1 Introduction to Fuel Cells.....	2
1.2 Proton Exchange Membrane Fuel Cells (PEMFCs)	4
1.2.1 Introduction	4
1.2.2 Proton Exchange Membranes (PEM).....	8
1.2.3 Electrodes	9
1.2.4 Oxygen Reduction Reaction (ORR).....	10
1.3 Direct Alcohol Fuel Cells (DAFCs).....	11
1.3.1 Introduction	11
1.3.2 Direct Ethanol Fuel Cells (DEFCs).....	13
1.3.3 Performance and Efficiency	15
1.3.4 Effects of Crossover	19
1.3.5 Mechanisms for the Electrochemical Oxidation of Ethanol.....	19
1.3.6 Product Analysis from DEFCs	28
1.3.7 Bi and Trimetallic Catalysts	30
1.3.8 Proton Exchange Membrane Electrolysis Cells (PEM-ECs)	31
1.4 Thesis Objectives	33
References	34
2. Experimental.....	51
2.1 Chemicals and Materials.....	51
2.2 Preparation of Electrodes and MEAs	53
2.3 Electrochemical Measurements.....	54
2.4 Product Analysis Instrumentation.....	55

2.4.1 Non-Dispersive Infrared (NDIR) Carbon Dioxide Detector	56
2.4.2 Nuclear Magnetic Resonance (NMR)	56
2.5 Catalyst Characterization Techniques	56
2.5.1 X-Ray Diffraction (XRD).....	56
2.5.2 Inductively Coupled Plasma Optical Emission Spectroscopy (ICP-OES).....	57
2.5.3 Thermogravimetric Analysis (TGA)	57
2.5.4 Transmission Electron Microscopy (TEM).....	58
References	58
3. Determination of the Efficiency of Ethanol Oxidation in a Proton Exchange Membrane Electrolysis Cell	62
3.1 Introduction	62
3.2 Experimental	65
3.2.1 The Cell	65
3.2.2 Ethanol and Product Analysis.....	67
3.3 Results and Discussion.....	70
3.3.1 Operation of the Cell in Crossover Mode.....	70
3.3.2 Operation of the Cell in Anode Polarization Mode.....	73
3.3.3 Discussion.....	84
3.4 Conclusions	87
References	88
4. Product Distributions and Efficiencies for Ethanol Oxidation in a Proton Exchange Membrane Electrolysis Cell.....	98
4.1 Introduction	98
4.2 Experimental	101
4.2.1 The Cell	101
4.2.2 Ethanol and Product Analysis.....	102
4.3. Results and Discussion.....	103
4.3.1 Polarization Curves.....	103
4.3.2. Stoichiometry (n_{av}) from the Consumption of Ethanol and Product Yields.....	105
4.3.3 Product Distributions	107
4.3.4 Efficiencies	110

4.4 Conclusions	114
References	114
5. Pt and PtRu Catalyst Bilayers Increase Efficiencies for Ethanol Oxidation in Proton Exchange Membrane Electrolysis and Fuel Cells	122
5.1 Introduction	122
5.2 Experimental	124
5.3 Results and Discussion.....	125
5.3.1 Polarization Curves.....	125
5.3.2 Product Distributions.....	129
5.3.3 Stoichiometry and Efficiency	131
5.3.4 Reaction Rates	133
5.3.5 Mechanisms	137
5.4 Conclusions	139
References	140
6. Determination of the Stoichiometry of Ethanol Oxidation from the Flow Rate Dependence of the Current in a Proton Exchange Membrane Electrolysis Cell.....	146
6.1 Introduction	146
6.2 Experimental	148
6.3 Results and Discussion.....	150
6.3.1 Polarization Curves.....	150
6.3.2 Stoichiometry (n_{av}) from the Flow Rate Dependence of the Current.	151
6.3.3 Discrepancies Between n_{av} Values from Eq. 6.5 and Chemical Analysis.....	155
6.4 Conclusions	160
References	161
7. Product Distributions and Efficiencies for Ethanol Electrolysis at PtNi Octahedra.....	166
7.1 Introduction	166
7.2 Experimental	168
7.2.1 Chemicals and Materials	168
7.2.2 Synthesis of the PtNi/C Catalyst	169
7.2.3 Physical Characterization	169
7.2.4 Electrochemical Characterization.....	170

7.3 Results and Discussion.....	171
7.3.1 Physical Characterization of the PtNi/C Catalyst.....	171
7.3.2 Electrochemical Measurements.....	174
7.3.3 Stoichiometry and Product distribution.....	185
7.3.4 Efficiency.....	190
7.4 Conclusions.....	193
References.....	193
8. Summary and Future Work.....	200
8.1 Summary.....	200
8.2 Future Work.....	202
References.....	203
A. CO ₂ and NMR Measurements.....	206
A1. CO ₂ Measurements.....	206
A1.1 Faradaic Yield.....	206
A1.2 Chemical Yield.....	207
A2. NMR Measurements.....	207
A3. Faradaic Yields of Acetic Acid and Acetaldehyde.....	207
B. Current and CO ₂ Traces for Pt black.....	210
C. Current and CO ₂ Traces for Pt/C, PtRu/C and PtSn/C.....	217
D. Current and CO ₂ Traces for Pt/C and PtRu/C catalyst bilayers.....	224
E. Determination of the stoichiometry of ethanol oxidation from the flow rate dependence of the current in a proton exchange membrane electrolysis cell.....	224
F. Product distributions and efficiencies for ethanol oxidation at PtNi octahedra.....	224

List of Tables

Table 1.1. Faradaic yields of CO ₂ and acetic acid from a cell operating with O ₂ or N ₂ /H ₂ at the cathode. Reprinted from Reference, ⁸² Copyright (2010), with permission from Elsevier.	32
Table 3.1. Experimental (NMR) and calculated (eq. 3.7) concentrations of ethanol exiting a cell operating in anode polarization with 0.100 M ethanol supplied to the anode at 0.2 mL min ⁻¹ . Averages and standard deviations for three consecutive experiments are presented.	77
Table 3.2. Summary chemical analysis results for the anode and cathode exhausts of a cell operating in anode polarization mode with 0.100 M ethanol at a flow rate of 0.2 mL min ⁻¹ . Chemical yields are given, based the measured quantities of products and the amount of ethanol consumed. Averages and standard deviations for three consecutive experiments are presented.	78
Table 3.3. Faradaic yields for CO ₂ , acetic acid and acetaldehyde from a cell operating in anode polarization mode with 0.100 M ethanol at a flow rate of 0.2 mL min ⁻¹ . CO ₂ and acetic acid yields are based on the combined analyses from the anode and cathode. Averages and standard deviations for three consecutive experiments are presented.	79
Table 3.4. Summary of n_{av} values obtained in this work.	80
Table 3.5. Summary of product yields and calculated n_{av} values from literature reports of ethanol oxidation at 50 °C and 80 °C. AL is acetaldehyde, AA is acetic acid.	87
Table 7.1. Surface areas and utilizations of the PtNi/C and Pt/C catalysts.	176
Table 7.2. n_{av} vs. potential for the oxidation of 0.100 M ethanol (0.2 mL min ⁻¹) at PtNi/C anode at 80 °C.	186

List of Figures

Figure 1.1. Schematic diagram of a proton exchange membrane fuel cell.....	5
Figure 1.2. Schematic diagram of a membrane electrode assembly (MEA).	6
Figure 1.3. The general structure of Nafion.....	8
Figure 1.4. Schematic illustration of a DEFC.....	14
Figure 1.5. Polarization curve for a DEFC obtained from this work.....	16
Figure 1.6. Calculated reaction network and reaction barriers (units, eV) for (a) ethanol oxidation on Pt(111) and (b) acetyl oxidation on Pt(100). The insets show mechanisms in more detail. Reprinted from Reference, ⁷⁵ Copyright (2006), with permission from Elsevier. Reprinted (Adapted) with permission from Reference. ⁸⁶ Copyright (2008) American Chemical Society.....	22
Figure 1.7. Ethanol electro-oxidation on a nanostructured mesoporous platinum (MPPt) electrode in 0.01 M ethanol + 0.5 M H ₂ SO ₄ . CVs (A) and MSCVs for m/z = 22 (B), m/z = 29 (C) and m/z = 15 (D). $v = 2 \text{ mV s}^{-1}$; $T = 25 \text{ }^\circ\text{C}$. Reprinted from Reference, ⁹² Copyright (2016), with permission from Elsevier.....	24
Figure 1.8. Selected IR spectra for the EOR (0.5 M CH ₃ CH ₂ OH) recorded at 1 mVs^{-1} in a) 0.1 M HClO ₄ /H ₂ O and b) 0.1 M HClO ₄ /D ₂ O. Inset: A magnification of the 1800–1600 cm^{-1} region of the spectrum recorded at 1.0 V, which shows the presence of two bands at 1713 and 1685 cm^{-1} . Reprinted from Reference, ⁹¹ Copyright (2016), with permission from Elsevier.....	27
Figure 1.9. ¹³ C NMR spectrum for the anode exhaust from a DEFC at 80 °C and 0.2 V with 2 M ethanol and a PtRu/C anode. Reprinted from Reference, ⁹⁶ Copyright (2009), with permission from Elsevier.....	29

Figure 2.1. Photograph of the 5 cm ² single-anode cell.	52
Figure 2.2. Schematic diagram of the nine-anode fuel cell. Reprinted from reference ¹	53
Figure 3.1. Schematic diagrams of the two cell configurations employed in this work.	67
Figure 3.2. Schematic diagram of the product collection system employed in anode polarization experiments.	68
Figure 3.3. NMR spectrum of the anode exhaust solution from oxidation of 0.100 M ethanol at 0.7 V and 50 °C in anode polarization mode.....	69
Figure 3.4. Current at 0.7 V vs. flow rate for oxidation of 0.102 M ethanol in crossover mode at 50 °C (points) and best fit curve calculated by using eq. 3.6 with $I_{lim} = 22.4$ mA and $n_{av} = 4.43$	71
Figure 3.5. Experimental vs. calculated (eq. 3.7 with $I_{lim} = 22.4$ mA and $n_{av} = 4.43$) concentrations of ethanol exiting a cell under the conditions for Figure 3.4.	72
Figure 3.6. Polarization curves for oxidation of 0.100 M ethanol at 0.5 mL min ⁻¹ in anode polarization mode at 50 °C (o) and 80 °C (●).	74
Figure 3.7. Current vs. flow rate for oxidation of 0.100 M ethanol at 50 °C in anode polarization mode at 0.45 V (◇), 0.55 V (●), and 0.70V (□) with best fit curves calculated by using eq. 3.6 with $I_{lim} = 17.5$ mA and $n_{av} = 4.84$, $I_{lim} = 38.2$ mA and n_{av} $= 5.13$, and $I_{lim} = 83.7$ mA, $n_{av} = 3.31$, respectively.	75
Figure 3.8. Current vs. flow rate for oxidation of 0.100 M ethanol at 80 °C in anode polarization mode at 0.4 V (◇), 0.50 V (●), and 0.70 V (□) with best fit curves calculated by using eq. 3.6 with $I_{lim} = 25.3$ mA and $n_{av} = 7.68$, $I_{lim} = 63.9$ mA and n_{av} $= 7.00$, and $I_{lim} = 86.8$ mA, $n_{av} = 5.55$, respectively.	84
Figure 4.1. Schematic diagram of the product collection system.	102

Figure 4.2. Polarization curves for the oxidation of 0.100 M ethanol (0.5 mL min ⁻¹) at Pt/C, PtRu/C, and PtSn/C anodes at 80 °C.	105
Figure 4. 3. n_{av} vs. potential for the oxidation of 0.100 M ethanol (0.2 mL min ⁻¹) at Pt/C, PtRu/C, and PtSn/C anodes at 80 °C. Solid points were calculated from the CO ₂ , acetic acid, and acetaldehyde yields by using eq. 4.4. Open points were calculated from the ethanol consumed by using eq. 4.6. Lines are drawn through the averages of the values from eqs. 4.4 and 4.6.	106
Figure 4. 4. Faradaic yields of CO ₂ vs. potential for oxidation of 0.100 M ethanol at Pt/C (□), PtRu/C (●), and PtSn/C (◇) anodes at 80 °C.	108
Figure 4.5. Chemical yields of CO ₂ , acetic acid, and acetaldehyde as a function of potential for oxidation of 0.100 M ethanol at Pt/C, PtRu/C, and PtSn/C anodes at 80 °C.	109
Figure 4. 6. Predicted efficiency vs. current density for DEFCs operating at 80 °C with 0.1 M ethanol at 0.5 mL min ⁻¹ with Pt/C (□), PtRu/C (●) and PtSn/C (◇) anodes.	113
Figure 5.1. Polarization curves for the oxidation of 0.100 M ethanol (0.5 mL min ⁻¹) at Pt (····), PtRu (- - -), Pt+ PtRu (●), Pt on PtRu (▲) and PtRu on Pt (■) anodes at 80°C.	126
Figure 5.2. Schematic diagrams of some of the reactions and transport processes within bilayer anodes.	128
Figure 5.3. Faradaic yields of CO ₂ (A), acetic acid (B), and acetaldehyde (C) vs. potential for oxidation of 0.100 M ethanol (0.2 mL min ⁻¹) at Pt (····), PtRu (- - -), Pt + PtRu (●), Pt on PtRu (▲) and PtRu on Pt (■) anodes at 80 °C.	130
Figure 5.4. n_{av} from eq. 5.5 vs. potential for the oxidation of 0.100 M ethanol (0.2 mL min ⁻¹) at Pt (····; data for 2 different anodes), PtRu (- - -), Pt + PtRu (●), Pt on PtRu (▲) and PtRu on Pt (■) anodes at 80 °C.	131

Figure 5.5. Predicted efficiency vs. power density (A) and current density (B) for DEFCs operating with 0.100 M ethanol at 80 °C at Pt (⋯), PtRu (- - -), Pt + PtRu (●), Pt on PtRu (▲) and PtRu on Pt (■) anodes. 133

Figure 5.6. Ethanol consumption rate vs. potential for the oxidation of 0.100 M ethanol (0.2 mL min⁻¹ and 80 °C) at Pt (⋯), PtRu (- - -), Pt+ PtRu (●), Pt on PtRu (▲) and PtRu on Pt (■) anodes..... 134

Figure 5.7. Product production rates vs. potential for the oxidation of 0.100 M ethanol (0.2 mL min⁻¹ and 80 °C) at Pt (⋯), PtRu (- - -), Pt + PtRu (●), Pt on PtRu (▲) and PtRu on Pt (■) anodes..... 136

Figure 6.1. Polarization curves for the oxidation of 0.100 M ethanol at 0.02 (○), 0.05 (■), 0.09 (□) , 0.2 (▲) and 0.5 (●) mL min⁻¹ at a PtRu/C anode and 80 °C.151

Figure 6.2. Plots of current vs. flow rate for selected data from Figure 6.1 (points) together with the best fits to eq. 6.5 (lines). 152

Figure 6.3. n_{av} vs. potential for the oxidation of 0.100 M ethanol at a PtRu/C anode at 80 °C. Black (●) points were obtained by using eq. 6.5, red (○) points are from the amount of ethanol consumed, blue (□) and green (■) points are from the faradaic and chemical yields of products, respectively. For clarity, error bars are only shown for the data from eq. 6.5. 153

Figure 6.4. n_{av} vs. potential for the oxidation of 0.100 M ethanol at PtSn/C (green triangles), Pt/C + PtRu/C (red squares) and Pt/C on PtRu/C bilayer (black circles) anodes at 80 °C. Solid points are from eq. 6.5, while open points are from chemical analysis (averages from the amount of ethanol consumed and yields of products). For clarity, error bars are only shown for the values from eq. 6.5. 154

Figure 6.5. n_{av} vs. potential for the oxidation of 0.100 M ethanol at a Pt/C anode at 80 °C, from eq. 6.5 using the currents at all flow rates (●), the amount of ethanol consumed (○), and the faradaic (□) and chemical (■) yields of products. Triangular (purple) data points were obtained by fitting eq. 6.5 to the currents at 0.09, 0.2, and 0.5 mL min⁻¹..... 156

Figure 6.6. Plots of current (●) and n_{av} (○) vs. flow rate for the oxidation of 0.100 M ethanol at a Pt/C anode, at 0.4 V and 80 °C. The dashed line is the best fit obtained from a simulation based on a linear dependence of n_{av} on ethanol concentration (see text), while the dotted line was obtained by using in eq. 6.5 with $n_{av} = 5.33$ from chemical analysis. 157

Figure 6.7. Plots of current (solid points) and n_{av} (open point) vs. flow rate for the oxidation of 0.100 M ethanol at a Pt/C anode at 80 °C, at 0.2 V (▲), 0.3 V (■), and 0.35 (●) V. Lines show simulations of the current based on $n_{av}(0.1 M) = 4.1$ and $dn_{av}/dC = -79 M^{-1}$ at 0.2 V, $n_{av}(0.1 M) = 4.5$ and $dn_{av}/dC = -75 M^{-1}$ at 0.3 V, and $n_{av}(0.1 M) = 6.2$ and $dn_{av}/dC = -58 M^{-1}$ at 0.35 V..... 159

Figure 6.8. n_{av} vs. potential for the oxidation of 0.100 M ethanol at a PtRu/C on Pt/C bilayer anode at 80 °C. Solid points are from eq. 6.5 (● for 0.02 to 0.5 mL min⁻¹; ■ for 0.09 to 0.5 mL min⁻¹), while open points are from chemical analysis (average and standard deviation from the amount of ethanol consumed and yields of products). 160

Figure 7.1. X-ray diffraction pattern of the PtNi/C catalyst before treatment with acetic acid.172

Figure 7.2. TEM images of the PtNi/C catalyst before treatment with acetic acid. 174

Figure 7.3. CVs obtained for the PtNi/C and Pt/C catalysts in 1.0 M sulfuric acid solution at ambient temperature and a scan rate of 100 mV s⁻¹. The dotted line is for the as-

prepared PtNi/C catalyst, the dashed and solid lines are for the PtNi/C catalyst after treatment with acetic acid for 2 h and 4 h, respectively, while the long-dashed line is for Pt/C.	177
Figure 7.4. CVs of PtNi/C and Pt/C in solution of 0.1M ethanol + 1.0 M sulfuric acid at scan rate of 10 mVs ⁻¹ . The dotted line is for the as prepared PtNi/C catalyst, the dashed and solid lines are for the PtNi/C catalyst after treatment with acetic acid for 2 h and 4 h, respectively, while the long-dashed line for Pt/C.....	180
Figure 7.5. Polarization curves for the oxidation of 0.100 M ethanol in a nine-anode PEM cell in crossover mode at Pt/C and different samples of PtNi/C at 0.5 mL min ⁻¹ and 80 °C.	182
Figure 7.6. Faradaic yields of CO ₂ for the oxidation of 0.100 M ethanol in a nine-anode PEM cell in crossover mode at Pt/C and different samples of PtNi/C at 0.2 mL min ⁻¹ , 0.5 V and 80 °C.....	183
Figure 7.7. Polarization curves for the oxidation of 0.100 M ethanol in anode polarization mode at Pt/C, PtRu/C and PtNi/C at 0.5 mL min ⁻¹ and 80 °C.	185
Figure 7.8. <i>n_{av}</i> vs. potential for the oxidation of 0.100 M ethanol (0.2 mL min ⁻¹) at Pt/C and PtNi/C anodes at 80 °C.	186
Figure 7.9. Faradaic and chemical yields of CO ₂ , acetic acid, and acetaldehyde as a function of potential for oxidation of 0.100 M ethanol at a PtNi/C anode at 80 °C.	188
Figure 7.10. Chemical yields of CO ₂ vs. potential for oxidation of 0.100 M ethanol at Pt/C and PtNi/C anodes at 80 °C.	189
Figure 7.11. Efficiency vs. current density (A) and power density (B) for DEFCs operating with 0.100 M ethanol at 80 °C at PtNi/C and Pt/C anodes.	192

List of Abbreviations

AA	Acetic acid
AAEMFC	Alkaline anion exchange membrane fuel cell
AAL	Acetaldehyde
AFC	Alkaline fuel cell
CFP	Carbon fiber paper
CO	Carbon monoxide
CO ₂	Carbon dioxide
CV	Cyclic voltammetry
DAFC	Direct alcohol fuel cell
DEFC	Direct ethanol fuel cell
DEMS	Differential electrochemical mass spectrometry
DFT	Density functional theory
DHE	Dynamic hydrogen electrode
DMFC	Direct methanol fuel cell
D ₂ O	Deuterium oxide
EEC	Ethanol electrolysis cell
EOR	Ethanol oxidation reaction
FTIR	Fourier transform infrared spectroscopy
GC	Gas chromatography
HFC	Hydrogen fuel cell
HPLC	High performance liquid chromatography

ICP-OES	inductively coupled plasma optical emission spectroscopy
MEA	Membrane electrode assembly
MOR	Methanol oxidation reaction
NDIR	Non-dispersive infrared
NMR	Nuclear magnetic resonance
OCP	Open circuit potential
ORR	Oxygen reduction reaction
PEFC	Polymer electrolyte fuel cell
PEM	Proton exchange membrane
PEM-EC	Proton exchange membrane electrolysis cell
PEMFC	Proton exchange membrane fuel cell
RHE	Reversible hydrogen electrode
RT	Room temperature
SCE	Saturated calomel electrode
SHE	Standard hydrogen electrode
SPEFC	Solid polymer electrolyte fuel cell
TEM	Transmission electron microscopy
TGA	Thermogravimetric analysis
XRD	X-ray diffraction

List of Symbols

A	Ampere
Å	Ångstrom
C	Coulomb
ca.	Approximately
ε	Efficiency
ε_{rev}	Theoretical efficiency
ε_{E}	Potential efficiency
ε_{F}	Faradaic efficiency
e^-	Electron
E°	Standard potential
E	Potential
E_{n}	Energy
E_{rev}	Reversible cell potential
eV	Electron volt
F	Faraday constant
G	Gibbs energy
λ	Wavelength
H	Enthalpy
h	Hour
i	Current
I_{lim}	Limiting current
j	Current density

min	Minute
η	Overpotential
n	Electrons transferred in a reaction
n_{av}	Average number of electrons
N	Moles of product
Θ	Diffraction angle
Ω	Ohm
u	Flow rate
ppm	Parts per million
Q	Charge
R	Gas constant
s	Second
t	Time
D_e	Energy density
D_p	Power density
v	Volume
V	Voltage (volts)
W	Watts
X_{ad}	Species adsorbed on electrode surface

Chapter 1

Introduction

1. Introduction

1.1 Introduction to Fuel Cells

Fossil fuels are currently the primary source for the world energy supply, the combustion of which produces a huge amount of greenhouse gases (mainly CO₂). These greenhouse gases cause environmental problems, particularly global warming and resulting climate change. Meanwhile, the dwindling sources as well as the significant increase in the rate of annual consumption of fossil fuels lead to an increasing depletion rate. Thus, some of the most important future challenges have been identified to be global warming, depletion of fossil fuels, and volatile prices of crude oil.¹⁻⁵ Therefore, it is necessary to develop alternative types of affordable, renewable and cleaner power sources with low CO₂ emissions. Electro-oxidation of some low molecular weight molecules such as hydrogen, formic acid, methanol and ethanol in fuel cells can be considered as good alternative sources of power.⁶⁻¹³

A fuel cell is an electrochemical device that converts the chemical energy of a fuel into electricity. They are considered attractive power sources with much potential for electronic devices and vehicles. The hydrogen fuel cell has been studied for a long time but the major obstacles that limit the commercialization of the hydrogen fuel cells are the production, storage and transportation of hydrogen. Alternative fuels have been investigated and proposed. The most common and studied fuels are liquids such as methanol and ethanol, which can be used as a fuel in fuel cells instead of hydrogen.

In general, the principle of the fuel cell was discovered accidentally by Sir William Grove in 1839. In an electrolyte solution, two platinum electrodes were connected directly instead of using a battery to connect them during electrolysis of water. Thus, the polarity was reversed and a small

amount of current was produced by combining hydrogen and oxygen at the surface of electrode, which later became known as a hydrogen fuel cell.¹⁴

A proper understanding of the fuel cell principles developed at the beginning of second half of the 20th century. Before that there were only a few studies and the development of fuel cells was slow. However, in the 1959, Francis Thomas Bacon, developed a new hydrogen fuel cell by using nickel as electrodes and alkaline electrolytes.¹⁴ In the early 1960s, the first application of fuel cells was achieved successfully with space technology and was more convenient than using batteries. The NASA space program successfully used hydrogen as a fuel in polymer electrolyte membrane fuel cells (PEMFCs) and alkaline fuel cells (AFCs) to provide electricity, heat and pure water for space shuttle applications and vehicles.¹⁵⁻¹⁸ In the past, the development of fuel cells was restricted because of the limited knowledge of materials and the high cost of fuel cells.¹⁹

In recent years, fuel cells have been of great interest because they are considered as a renewable source of power with potentially electrical efficiencies, are much more safe and have longer lifetimes compared with other power sources (like batteries).^{11,20,21} Interest in them has increased drastically, especially when many institutions, companies and groups around the world have started to focus on overcoming the challenges of commercializing fuel cells. Many companies throughout the world like Toyota, Honda, Mercedes and Hyundai have developed proton exchange membrane fuel cells as a power source by using hydrogen and methanol as fuels instead of using the internal combustion engine in their cars.²² High efficiency commercial fuel cells have not yet been manufactured, but fuel cells are increasingly being used in the public and private sectors. They are attractive power sources for transportation, electronic devices such as mobile phones and laptop computers as well as to generate power for lighting and heating.^{20,21}

Important parameters should be taken into consideration when studying fuel cells such as energy and power density. Fuels such as hydrogen, methanol and ethanol can be assessed and compared based on these parameters. The energy density can be defined as the amount of energy stored in the fuel cell system per unit volume or mass. The power density is the amount of power produced from the fuel cell per unit volume, mass or area, where power is in units of watts (W) and is defined as the amount of energy produced per unit time (Joule/s). The theoretical energy mass density (D_e) and the power density (D_p) can be calculated by eqs. 1.1 and 1.2, respectively.

$$D_e = - \frac{\Delta G^\circ}{3600 M} \quad (1.1)$$

$$D_p = \text{current density} \times E_{cell} \quad (1.2)$$

Where M = is the molar mass of the fuel (46.07 g/mol for ethanol).

1.2 Proton Exchange Membrane Fuel Cells (PEMFCs)

1.2.1 Introduction

Many types of fuel cells are available throughout the world, typically categorized by the type of electrolyte material. The catalysts, operating temperature and even the electrochemical reaction in the fuel cell is determined by the type of electrolyte. Furthermore, these different types of fuel cell have different performances (power outputs), operating temperatures, efficiencies and applications.^{20,21,23–25} Recently, solid polymer electrolyte membrane fuel cells have become a dominate type due to the convenience, high conductivity, and thermal, mechanical and chemical stability of the electrolyte. In particular, proton exchange membrane fuel cells (PEMFCs; Figure 1.1) are the most developed type of polymer electrolyte membrane fuel cell.^{11,21,22,26,27}

PEMFCs are being widely used for transport applications because of their high power density, high efficiency, durability, low weight, quick start-up and low operating temperature.^{21,22,26,27} The central part of a PEMFC is composed of a membrane and electrode assembly (MEA), which consists of two electrodes and a solid electrolyte (proton exchange membrane), as shown in Figure 1.2. The solid electrolyte serves as separator between the electrodes and between the fuel and oxidant, and as bridge for proton transport from the anode to the cathode. The fuel is oxidized electrochemically at the anode to produce electrons and protons. The electrons travel through the external circuit to the cathode to generate power while the protons (H^+) migrate through the membrane to the cathode to complete the electrochemical reaction via reduction of oxygen.

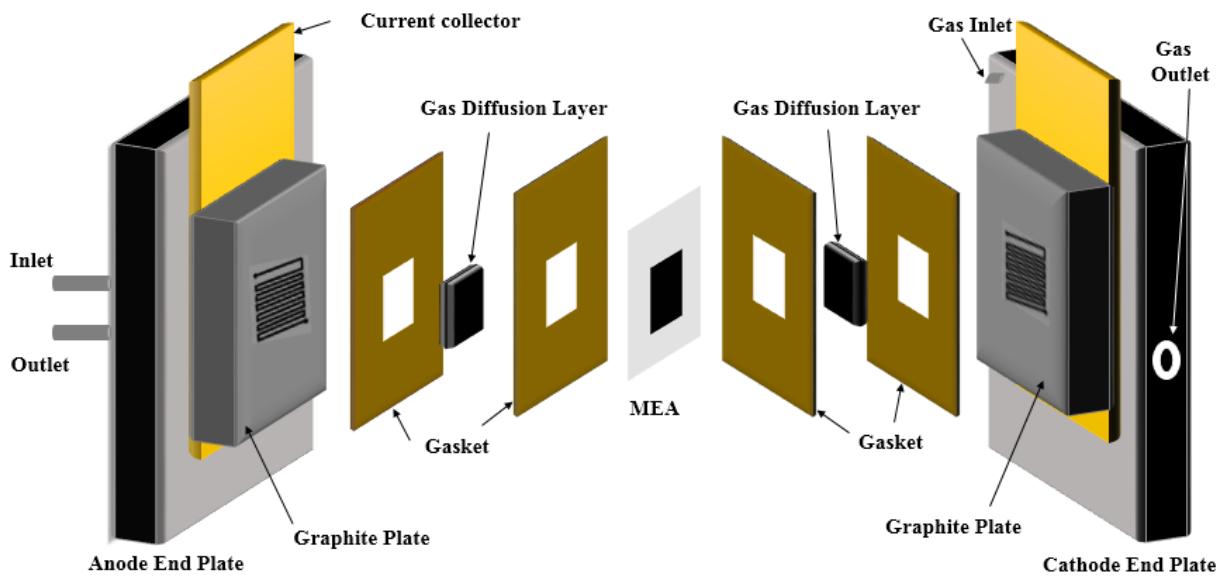


Figure 1.1. Schematic diagram of a proton exchange membrane fuel cell.

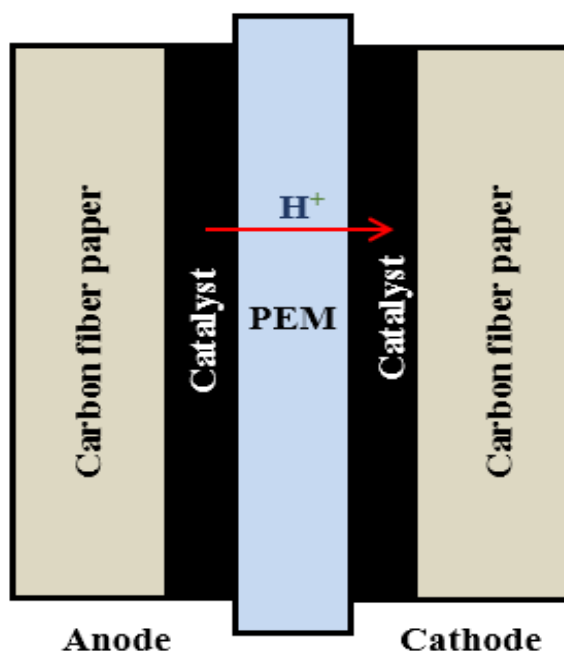


Figure 1.2. Schematic diagram of a membrane electrode assembly (MEA).

The first-generation of fuel cells used hydrogen as a fuel and oxygen (air) as an oxidant, which provides a simple reaction with a high thermodynamic standard potential (1.229 V) and a higher theoretical energy density (33.3 kWh kg⁻¹). Over the past years, PEM-type hydrogen fuel cells (HFCs) have been used in many applications including for stationary power and transportation.^{28–33} Many companies have manufactured vehicles operating with HFCs include buses, boats, motorcycles and bicycles. Countries including the USA, Canada, Germany, Brazil, China, United Kingdom and Japan have significantly used HFCs.^{34–38}

In HFCs, hydrogen gas is oxidized at the anode (eq. 1.3) to generate electrons and hydrogen ions.



Whereas, oxygen is reduced at the cathode to produce water according to eq. 1.4.



Hence, the overall reaction in HFCs is given by eq. 1.5.



where E° is the standard electrode potentials versus the standard hydrogen (reference) electrode (SHE). The standard cell potential (E°_{cell}) is $E^\circ_{\text{cell}} = E^\circ_{\text{cathode}} - E^\circ_{\text{anode}}$.

The final product from HFCs is water which means no CO₂ emission. Since HFCs are commercially available, high-pure hydrogen is required in order to preserve a proper electrochemical performance and efficiency.³⁹ The production of pure hydrogen is one of the main obstacles to widespread use HFCs because there is no natural resource of hydrogen and production costs are high. Hydrogen is mainly produced by electrolysis or by steam reforming of alcohols, gasoline and hydrocarbons such as natural gas and coal. The gasoline, natural gas and coal resources would increase the greenhouse effect by producing high CO₂ emissions.

The kinetics of the hydrogen oxidation reaction (HOR) are very fast which means that the reaction is controlled only by mass transfer limitations.¹⁹ However, the production of hydrogen by electrolysis of water has low efficiency.⁴⁰ Whereas, the hydrogen produced from the electrolysis and steam reforming methods of alcohols, gasoline and hydrocarbons will contain carbon monoxide (CO) and this decreases the performance and efficiency of HFCs. This can be attributed to the poisoning effect of CO; even small amount of CO block the active sites of catalysts (normally Pt or Pt-based catalysts) and thus prevent the adsorption of hydrogen on the catalyst surface.¹⁹

Other obstacles that limit the applications of HFCs are high hydrogen flammability and hydrogen storage, which are serious challenge for transportation.^{41,42} Considerable effort has been made to develop new fuel cells that have a similar design as HFCs but operate with other kinds of fuel, as described in Section 1.3.

1.2.2 Proton Exchange Membranes (PEM)

The proton exchange membrane (PEM) is an important part of PEMFCs, as mentioned above. The most common acidic PEM used in PEMFCs is Nafion[®], which is a type of perfluorosulfonic acid membrane, developed at the end of 1960s by DuPont.^{43,44} The Nafion polymer consists of a hydrophobic backbone (polytetrafluoroethylene, PTFE) which maintains the stability of the membrane and short perfluorinated side chains that terminate in a hydrophilic sulfonic acid groups (-SO₃H). Figure 1.3 shows the general structure of Nafion. The high electronegativity of the acid groups in the presence of water provides a good medium for high proton conductivity. The operating temperature of Nafion membrane fuel cells should not normally exceed 100 °C. The limited operating temperature of these types of cells can be explained as follows: for high proton conductivity, the Nafion membrane requires a high content of water. The migration of protons through the PEM is due to the dissociation of the terminal sulfonic acid groups in the presence of water.^{45,46} Increasing the temperature to more than 100 °C can lead to dehydration, causing the proton conductivity to decrease significantly.

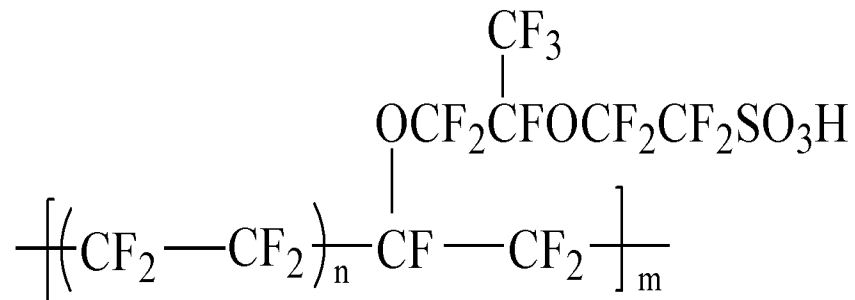


Figure 1.3. The general structure of Nafion.

Improving the performance and increasing the power density and efficiency of fuel cells can be achieved by enhancing the proton conductivity, stability and electrical insulation of the Nafion membranes as well as preventing crossover of fuel and oxidant through the membrane.⁴⁷⁻

⁵⁰ However, the major drawbacks of PEMFCs are low operating efficiency and high cost. Consequently, further development and research are required to overcome these drawbacks and then increase the efficiency. Recently, Nafion membranes have been modified with phosphotungstic acid (PWA) to form PWA-Nafion composite membranes, which generally decrease crossover and increase the proton conductivity compared with unmodified Nafion, resulting in a high performance of DEFCs.⁵¹

1.2.3 Electrodes

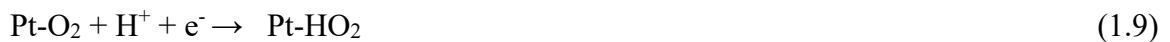
A PEMFC electrode is mainly composed of two layers, a diffusion layer and a catalyst layer. The catalyst layers are normally made up of a Pt or Pt based catalyst while the diffusion layers are comprised of two layers, a support layer (also called backing layer) (usually carbon fiber paper, glassy carbon or carbon cloth) and a micro-porous layer.^{48,50} The latter consists of a mixture of a hydrophobic polymer and carbon powder. The hydrophobic polymer (usually PTFE) allows reactive species access to the catalyst and inhibits water condensation. Generally, the electrodes (anode and cathode) are made from a high surface area carbon-based material that is covered with a layer of catalyst nanoparticles which is active to oxidize the fuel or reduce the oxidant. The catalyst (metals) should be mixed with Nafion solution and carbon powder in the presence of solvent (normally isopropanol and water) before being applied to the diffusion layer. The Nafion and carbon are used to enhance the ionic and electronic conductivities of the catalyst layer, respectively. Platinum is the most common catalyst that has been used for both the anode and the cathode in PEMFCs because of its high activity compared with other metals.

1.2.4 Oxygen Reduction Reaction (ORR)

Oxygen (in air) is usually used as the oxidant at the cathode in fuel cells. It combines with electrons and protons from the anode to form water with a high thermodynamic potential (1.229 V). However, the oxygen reduction reaction (ORR) is complex and has very slow (sluggish) kinetics relative to the hydrogen oxidation reaction, resulting a significant potential loss which limits the performance of PEMFCs.⁵² The ORR can occur through two pathways according to equations 1.6 and 1.7:



The first equation represents the full reduction and is referred to as the direct four electron pathway. Since the cathode potential affects the standard cell potential ($E^\circ_{\text{cell}} = E^\circ_{\text{cathode}} - E^\circ_{\text{anode}}$), the first pathway is more favored and efficient because of its high thermodynamic standard potential (1.229 V). Whereas the second reaction (Eq. 1.7), referred to as partial reduction (indirect two-electron pathway), which is unfavored and less efficient with a lower thermodynamic standard potential (0.67 V). Furthermore, the second pathway involves hydrogen peroxide which has detrimental effect on the electrode and membrane.⁵² The most widely used electrocatalyst is platinum and the crystalline facets and particles shape of Pt have a significant effect on the ORR.^{53,54} A possible reaction mechanism for the full oxygen reduction is as follows:⁵⁵





Thus, water is the only the product at the cathode. However, due to the sluggish kinetics of the ORR on Pt, a high loading of Pt is required at the cathode to avoid a loss in performance. But the high cost of Pt has forced many studies to focus on using Pt-based catalysts and controlling the morphology of the catalyst surface in order to achieve higher ORR efficiency.⁵⁶⁻⁵⁸ Furthermore, other factors can have a significant effect on the ORR efficiency such as crossover of fuel through the membrane to the cathode, which is described in section 1.3.4.

1.3 Direct Alcohol Fuel Cells (DAFCs)

1.3.1 Introduction

Direct alcohol fuel cells are a relatively new type of power source and are regarded as one of the most promising alternative renewable energy technologies. A DAFC is a type of PEMFC which is fueled directly with an alcohol. It avoids the need for reforming and overcomes the problems with hydrogen. In DAFCs, liquid fuels such as methanol and ethanol can be used and have advantages over hydrogen because they can be easily handled, transported, and stored and have higher volumetric energy densities.^{21,31-33,39,59}

In DAFCs, a liquid fuel is fed directly to the anode generating electrons from the oxidation reaction, while air (or pure oxygen) is passed through the cathode for the reduction reaction. Proton exchange membranes (normally Nafion) and platinum-based catalysts are often used in DAFCs.⁶⁰ However, another type of DAFC using high a pH environment that can be operated at low temperature has been developed, which is called an alkaline fuel cell or anion-exchange membrane fuel cell (AEMFC).⁶⁰ AEMFCs are technically similar to PEMFCs with some differences such as operating in an alkaline electrolyte, anion (OH^-) migration through the membrane to the anode and

water consumption at the cathode, which are opposite to the PEMFC. The reversed direction of the anions (OH⁻) decreases the crossover of fuel to the cathode and the abundance of OH⁻ ions increases the rate of the fuel oxidation reaction and thus provides better kinetic.^{61–64} However, the main obstacle with AEMFCs is the low conductivity and low stability of the solid anion-exchange membrane which is lower than the conductivity of PEMs. This is exacerbated by the formation of carbonate when the carbon dioxide produced reacts with hydroxyl ions, resulting damage the MEA and a significant loss in performance and efficiency. Consequently, the PEMFC is still the most promising type of fuel cells.

Direct methanol fuel cells (DMFCs) can be operated at low temperature which makes them an attractive power source for portable devices. Methanol is obtained from natural gas or biomass. Additionally, various studies have shown that the complete oxidation of methanol to CO₂ is achieved by using platinum-based catalysts under most conditions. However, the complete oxidation of methanol only provides six electrons (equation 1.12) and the power density of methanol is only 6.1 kWh kg⁻¹.^{65–69}

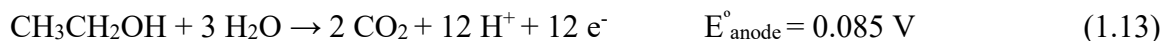


The methanol oxidation reaction (MOR) has very slow kinetics relative to the hydrogen oxidation reaction, which results in much lower power densities and lower system efficiency. This is due to the poisoning effect of adsorbed CO (CO_{ad}), formed as an intermediate on the surface of the catalyst (see Section 1.3.5). Furthermore, methanol is relatively volatile, toxic and has low power density. However, ethanol is a good fuel choice for overcoming some of the problems with methanol. In fact, ethanol is less toxic and has a higher energy density. It also can be produced from agricultural bioprocesses and is considered a renewable energy source. Additionally, ethanol has been proven by researchers to have a lower crossover rate because of its higher molar mass.⁷⁰

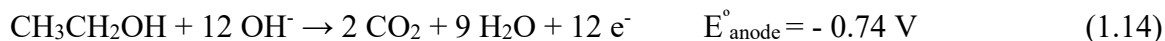
1.3.2 Direct Ethanol Fuel Cells (DEFCs)

Ethanol has some advantages over hydrogen and methanol such as its theoretical energy density of around 8.0 kWh kg⁻¹, which is higher than for methanol (6.1 kWh kg⁻¹) and reasonably close to gasoline (10 kWh kg⁻¹). Moreover, ethanol has low toxicity, simple handling and storage, and is produced in large quantities from biomass. Hence, direct ethanol fuel cells (DEFCs) have been a topic of interest in the last decades.⁷¹⁻⁷³ However, the high energy density of ethanol is based on complete oxidation to CO₂, which generates 12 electrons but is difficult to achieve with high selectivity.

In DEFCs, the anode is directly fed with ethanol and the cathode is fed with air. The ethanol and oxygen transfer through the diffusion layers to the anode and cathode catalyst layers, respectively, where the ethanol is oxidized and the oxygen is reduced. The ethanol should be oxidized to CO₂ at the anode (eq. 1.13) while oxygen is reduced to water at the cathode (eq. 1.4).



Whereas, the reactions at the anode and at the cathode in an alkaline fuel cell are described by equations 1.14 and 1.15, respectively for complete ethanol oxidation.



Thus, the overall reaction of ethanol in DEFCs is described according to eq. 1.16.



The oxidation of ethanol in a PEM-FC generates electrons and protons. The electrons travel through the external circuit while the protons migrate through the membrane to the cathode as shown in Figure 1.4.

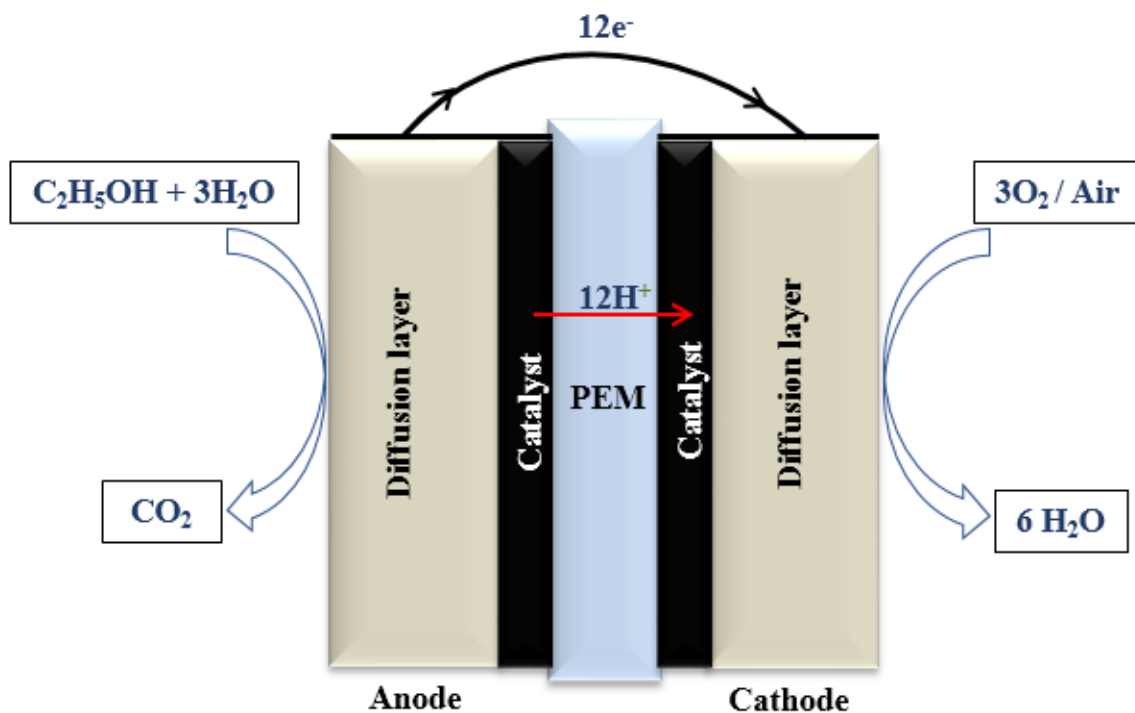


Figure 1.4. Schematic illustration of a DEFC.

The ethanol oxidation reaction (EOR) is complex and involves many intermediates and products due to the presence of a C-C bond. In addition, many parameters influence the rate and selectivity of ethanol oxidation, including the catalyst composition, operating temperature, ethanol concentration and cell potential. Since the EOR has very slow kinetics, high temperature and high overpotentials are required to enhance the performance and efficiency.

1.3.3 Performance and Efficiency

General insight regarding the evaluation of the performance of a fuel cell can be obtained from the potential-current output (polarization curve). The potential difference of the cell, between the anode and cathode, is a key parameter to describe the behavior of the cell, which uses to determine potential efficiency (see below) and power density. At the beginning, it is important to distinguish between different concepts of potential when describing the behavior of the cell. The standard cell potential (E_{cell}°) is the theoretical Nernst potential of the cell when it is operating reversibly under standard thermodynamic conditions (activities are one). The reversible cell potential (E_{rev}) (also called equilibrium potential (E_{eq})) is the theoretical potential difference between the electrodes for a cell under thermodynamically reversible conditions with no current flowing. It is based on the bulk activities of reactants and products according to the Nernst equation. The actual cell potential (E_{cell}) is the potential of the cell when it is running at non-standard condition and it is measured experimentally.

Figure 1.5 shows a polarization curve of a DEFC obtained in this work. The straight line at the top represents the reversible cell potential. E_{rev} is the highest potential that can be obtained for a fuel cell. In contrast, the open circuit potential (OCP) is the potential difference between the electrodes when there is no current flow. Whereas E_{cell}° and E_{rev} are calculated theoretically from thermodynamic data, OCP is measured experimentally. Polarization measurements show a loss of fuel cell performance (the actual cell potential, E_{cell} is less than the theoretical reversible cell potential, E_{rev}), which is attributed to factors that lead to increased overpotentials, particularly the kinetic polarization, ohmic resistance polarization, and concentration polarization as shown in Figure 1.5.

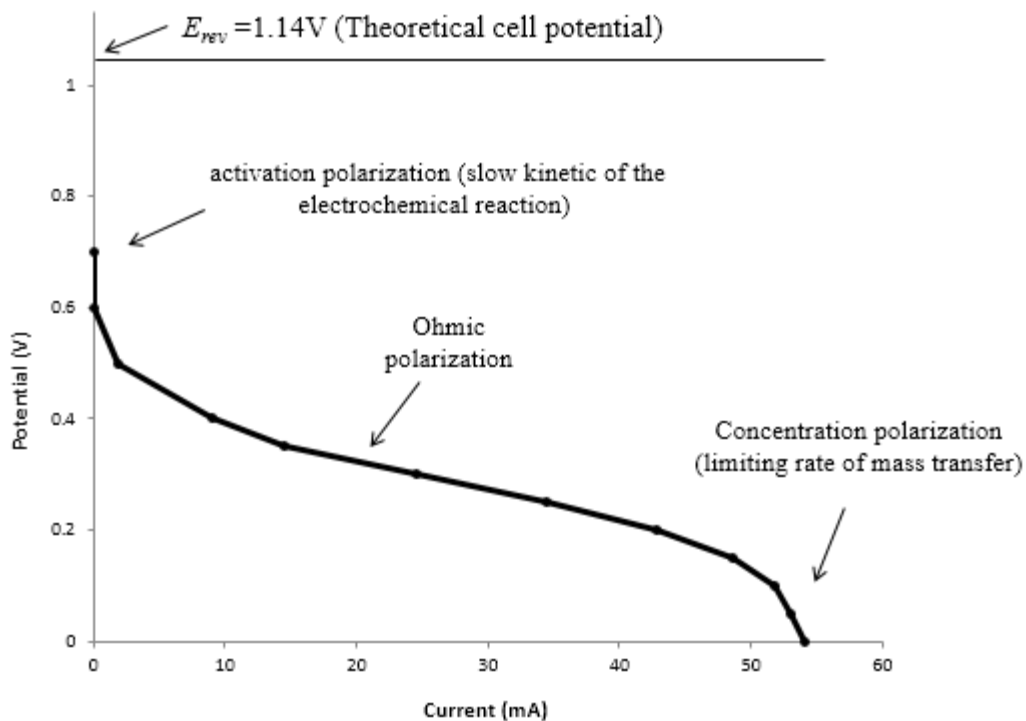


Figure 1.5. Polarization curve for a DEFC obtained from this work.

The difference between the actual potential (E_{cell}) and reversible potential (equilibrium potential) is called overpotential. It can be seen from this figure that the OCP is lower than the E_{rev} which can be attributed to a mixed potential due to crossover of ethanol (described in section 1.3.4). As the current increases the overpotential increases and thus the cell potential decreases until it reaches zero. The polarization curve can be divided into three regions: the low and intermediate current regions are controlled (main factor that causes increase in overpotential) by the slow kinetics of reactions (EOR and ORR) and ohmic resistance, respectively. The low and intermediate current regions can be modelled and analyzed with the Tafel equation and Ohm's law, respectively. The ohmic resistance (ohmic polarization) increases with increasing resistance of the membrane to proton conduction and the electrodes to electron flow. In the high current region, the cell potential drops significantly due to concentration polarization (mass transfer

limitation) and can reach a limiting current under certain conditions. This is due to the mass transport resistance of the fuel and oxidant to the catalyst surface through the diffusion layer.

In a DEFC, a high overpotential is required to force the reactions to occur due to their slow kinetics. The overpotential would be positive for the EOR (anodic reaction) and negative for the ORR (cathodic reaction). A fuel cell with the highest potential (lowest overpotential) and high limiting current would have the best performance.

Moreover, the basics of thermodynamics and electrochemistry are required to understand the performance and efficiency of fuel cells. The reversible cell potential (E_{rev}) of DEFCs at equilibrium under standard conditions can be derived from the thermodynamic data of the overall combustion reaction of ethanol (eq. 1.17): $\Delta G^\circ = -1325 \text{ kJ mol}^{-1}$; $\Delta H^\circ = -1366 \text{ kJ mol}^{-1}$,^{74,75}

$$E_{rev} = -\frac{\Delta G^\circ}{nF} = \frac{1325 \times 10^3}{12 \times 96485} = E^\circ_{cathode} - E^\circ_{anode} = 1.144 \text{ V} \quad (1.17)$$

Where ΔG° is the Gibbs free energy and ΔH° is the enthalpy change of the overall reaction under standard conditions (1.0 atm, 298.15 K and liquid phase for water and alcohols), while F is the Faraday constant (96485 C mol⁻¹) and n = 12 is the number of electrons transferred per molecule of ethanol for the complete oxidation. The standard cell potential of a DEFC is lower than that of a HFC (1.229 V).

The theoretical energy conversion efficiency (thermodynamic efficiency) is given by eq. 1.18.

$$\varepsilon_{rev} = \frac{\Delta G^\circ}{\Delta H^\circ} = \frac{1325}{1366} = 0.97 \quad (1.18)$$

Hence, the theoretical energy conversion efficiency of DEFCs is 97% at ambient temperature, which is much better than that of a HFC (83%) and internal combustion engine (43%) under the same conditions.⁷⁶

The potential efficiency (\mathcal{E}_E) is the ratio between the operating (actual) potential (E_{cell}) and reversible cell potential (E_{rev}) and is described by eq. 1.19:

$$\mathcal{E}_E = \frac{E_{cell}}{E_{rev}} \quad (1.19)$$

The faradic efficiency (\mathcal{E}_F) is defined as the ratio of the actual average number of electrons obtained per molecule of ethanol (n_{av}) to the theoretical value of 12 (for complete oxidation to CO₂) (eq. 1.20):⁷⁷

$$\mathcal{E}_F = \frac{n_{av}}{12} \quad (1.20)$$

It is a very important parameter for the evaluation of catalyst efficiency since one of the major problems in DEFCs is the incomplete oxidation of ethanol. n_{av} can be determined by electrochemical methods (e.g. flow rate dependence of the current⁷⁸) and from the product distribution.

The overall efficiency of a DEFC (\mathcal{E}_{cell}) can be calculated from the theoretical energy conversion efficiency (\mathcal{E}_{rev}), the potential efficiency (\mathcal{E}_E), the faradaic efficiency (\mathcal{E}_F), and losses of ethanol due to crossover through the membrane and reaction with oxygen (\mathcal{E}_C) according to eq. 1.21.^{71,74,75}

$$\mathcal{E}_{cell} = \mathcal{E}_{rev} \times \mathcal{E}_E \times \mathcal{E}_F \times \mathcal{E}_C \quad (1.21)$$

1.3.4 Effects of Crossover

Crossover is the diffusion of species through the membrane from the anode to the cathode or vice versa, resulting in a decrease in performance and efficiency. This is one of the main obstacles that limit the commercialization of DAFCs. Various factors influence the crossover rate, including operating temperature, fuel concentration and membrane thickness. A decrease in crossover rate is found with decreasing operating temperature and fuel concentration, and increasing membrane thickness.^{79–83} Nevertheless, decreasing the temperature decreases the selectivity, performance and efficiency, while using a thicker membrane increases the cell resistance.

In DEFCs, ethanol diffuses through the membrane to the cathode where it reacts chemically with oxygen without producing a current. In addition, oxygen can crossover to the anode resulting in chemical reaction with ethanol. These processes lead to a decrease in the concentration of fuel at the anode and losses in both the potential efficiency and fuel efficiency ($\mathcal{E}_F \times \mathcal{E}_C$). Furthermore, there is competitive adsorption at the cathode between the ethanol and oxygen resulting in a significant decrease in cathode potential and a further decrease in performance and efficiency. This decrease in the cathode potential is known as a mixed potential since both the EOR and ORR occur at the same electrode, leading to a decrease in cell potential (E_{cell}) and thus a further decrease in the potential efficiency.^{75,84}

1.3.5 Mechanisms for the Electrochemical Oxidation of Ethanol

According to the preferred oxidation-reduction reaction in a DEFC, ethanol should be oxidized electrochemically to carbon dioxide at the anode, while oxygen is reduced at the cathode. The complete electro-oxidation of ethanol generates 12 e⁻. However, the high theoretical efficiency

(97%) and energy density of the DEFC is based on complete oxidation of ethanol to CO₂, while the main products from DEFCs are acetaldehyde (eq. 1.22) and acetic acid (eq. 1.23), which only involve 2 and 4 electrons, respectively [eg.^{11,12,63,72,74,78,81}].



Indeed, the formation of acetaldehyde and acetic acid decrease the efficiency of DEFCs and may cause environmental concerns. Therefore, to fully utilize the high energy density of ethanol, complete oxidation to CO₂ should be achieved via C-C bond cleavage. Therefore, understanding the reaction mechanism is necessary in order to allow high activity catalysts to be designed and to improve the efficiency and performance of DEFCs. Consequently, the reaction mechanism has been widely studied theoretically (computationally) and experimentally to provide the understanding required to develop efficient catalysts. The purpose of this section is to briefly describe some of the theoretical studies^{86,87} and experiments by using differential electrochemistry mass spectroscopy (DEMS),^{85,88-90} voltammetry,⁹¹⁻⁹³ gas chromatography,^{94,95} nuclear magnetic resonance (NMR)⁹⁶⁻⁹⁹ and in situ infrared spectroscopy (IR)^{75,91} that have been performed to study the mechanism of EOR.

Among all the catalysts that have been examined up to now, platinum (Pt) is widely used and has relatively high activity for cleavage of the C-C bond of ethanol.^{86,90} However, due to the slow kinetics of the EOR, high overpotentials are required to force the reaction to occur. At low applied potentials, where many active sites are available for C-C bond breaking due to the low oxygen coverage (OH_{ad}), poisoning species produced by the dissociative adsorption of ethanol, such as CO, will form readily and adsorb (accumulate) at the Pt surface. The production of poisoning

species causes a decrease of the catalytic activity by inhibiting the adsorption and further oxidation of ethanol.^{86,87,100} In this situation, the coverage of adsorbed hydroxyl species (OH_{ad}) limits the rate of production of CO_2 , which is described later in this section.

Higher applied potentials favor the formation of OH_{ad} species, and thus the Pt surface has higher activity to remove poisoning species (CO_{ad}). However, the cleavage of the C-C bond is the rate limiting step and it decreases significantly in the presence of a high coverage of OH_{ad} species at the Pt surface.^{86,87,92} Under these circumstances, CO_2 formation reflects the rate of C-C bond cleavage and oxidation of adsorbed CH_x species.¹⁰¹ This simple mechanistic model provides a working explanation of why pure Pt has been found to be an inefficient catalyst for the complete oxidation of ethanol. Consequently, increasing the efficiency of Pt and other catalysts requires control of adsorbed oxygenated species to achieve complete oxidation of ethanol to CO_2 .^{86,87,92}

Figure 1.6 shows a theoretical description (based on computational results) of some of the possible products and intermediates of ethanol electro-oxidation on a Pt electrode at room temperature.^{75,86} The insets in Figure 1.6 show mechanisms in more detail for some important pathways.⁷⁵ In general, ethanol adsorbs initially in a series of dehydrogenation steps at low potentials on the Pt surface, forming acetaldehyde, which is the favorable path with lower energy barriers than other paths such as C-C bond breaking, β -hydroxyl- and α -dehydrogenation (Figure 1.6a). The acetaldehyde can desorb from the electrode surface as the final product or it can be easily oxidized or readsorbed via α -dehydrogenation to form adsorbed acetyl ($\text{CH}_3\text{CO}_{\text{ad}}$).⁸⁶ These processes are illustrated in Figure 1.6:

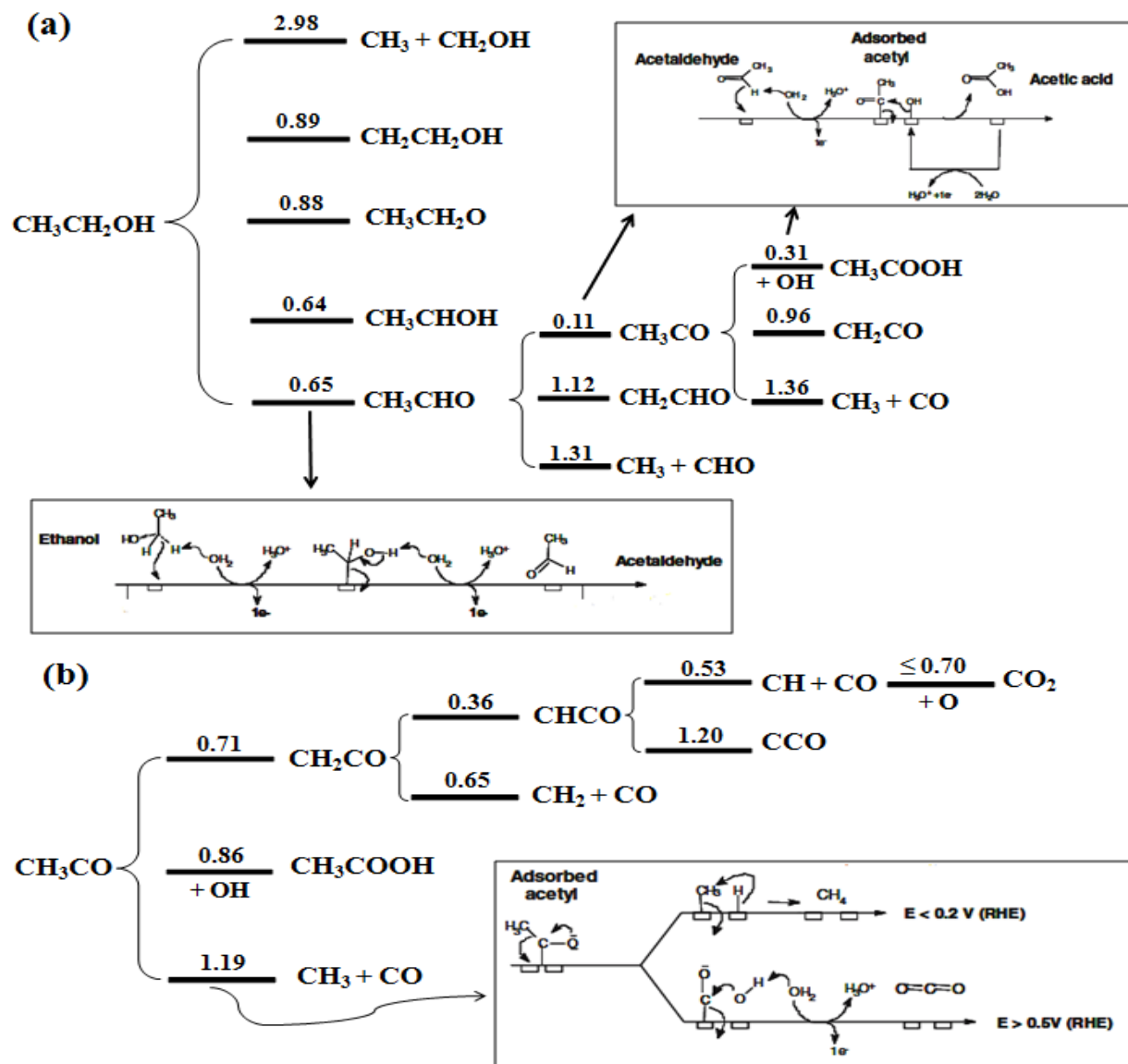


Figure 1.6. Calculated reaction network and reaction barriers (units, eV) for (a) ethanol oxidation on Pt(111) and (b) acetyl oxidation on Pt(100). The insets show mechanisms in more detail. Reprinted from Reference,⁷⁵ Copyright (2006), with permission from Elsevier. Reprinted (Adapted) with permission from Reference.⁸⁶ Copyright (2008) American Chemical Society.

In fact, adsorbed acetyl is the key intermediate for the electro-oxidation of ethanol to both acetic acid and CO_2 .^{86,102} Thus, $\text{CH}_3\text{CO}_{\text{ad}}$ can be further oxidized in the presence of OH_{ad} species to acetic acid, which is effectively a final product, or it can be further oxidized by breaking the C-

C or C-H bond (maximum rate at 0.3 – 0.4 V vs. RHE), which leads to formation of adsorbed intermediates such as CO_{ad} and CH_{x,ad} through the lowest energy channel or path as shown in Figure 1.6b. The CH₃ species can interact with adsorbed H at a very low potential (around < 0.2 V) to form methane (eq. 1.24), or, in the presence of OH_{ad} (> 0.5 V), can form CO₂ (eq. 1.25):^{91,101}



The CH₃ species produced at low potentials (0.2 – 0.4 V) where no adsorbed H species are available will accumulate and may interact with OH species at high potentials to lead to higher CO₂ yields (based on eq. 1.25).

It is clear from Figure 1.6 that the dissociative adsorption of water (≥ 0.5 V vs. RHE) to form OH_{ad} at the electrode surface (eq. 1.26) is necessary for further oxidation of adsorbed CO to CO₂ (eq. 1.27), which releases free sites on the electrode surface for further ethanol and intermediate species to adsorb and oxidize.^{86,102}



Therefore, bi or tri-metallic Pt based catalysts (section 1.3.7) have been used (Pt is often modified with other metals like Ru and Sn) to enhance the dissociative adsorption of water at low applied potentials which thus promote the oxidative removal of adsorbed intermediates (CO_{ad}, CH_{x,ad} and CH₃CO_{ad}) on adjacent Pt sites.^{86,102} Consequently, the activity of ethanol electro-oxidation is enhanced and the performance of the DEFC improves.

Recently, differential electrochemistry mass spectroscopy (DEMS) has provided much information about the electro-oxidation mechanism of ethanol by detecting gaseous and volatile

species such as CO_2 , CO and acetaldehyde. Acetic acid cannot be detected by DEMS, since it is not volatile enough. Furthermore, voltammetry (particularly CV and CO stripping) can be used to study the behavior of CO and OH . Figure 1.7 shows cyclic voltammograms (CVs) and the corresponding mass spectroscopic voltammograms (MSCVs) for ethanol oxidation on a Pt electrode.⁹²

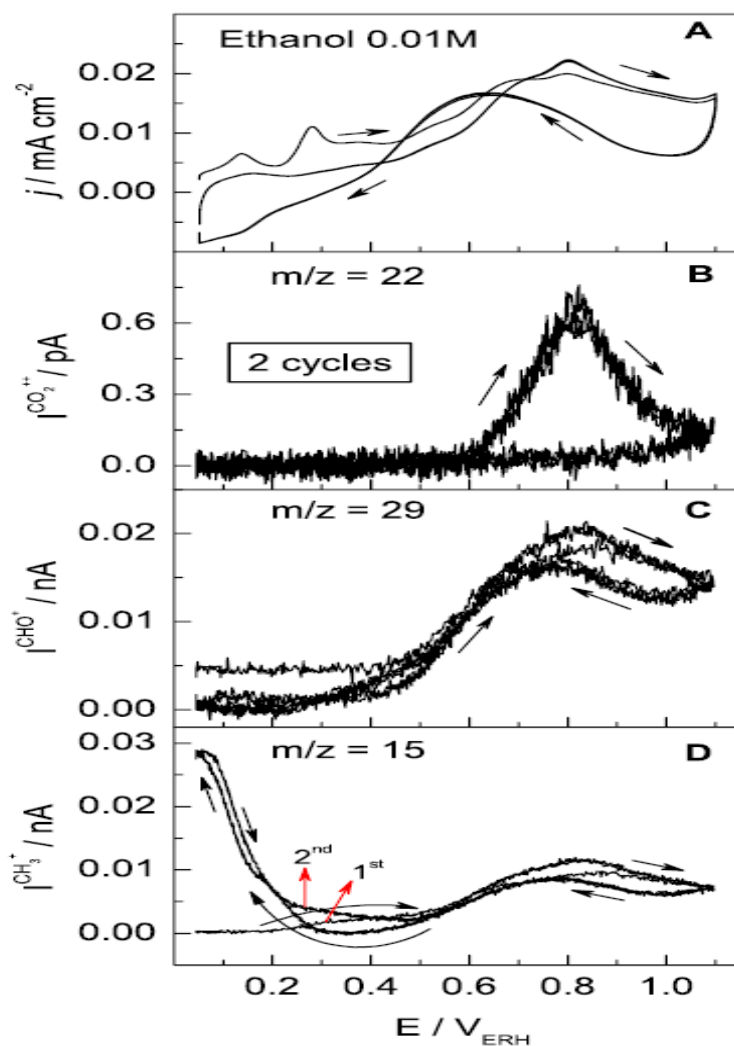


Figure 1.7. Ethanol electro-oxidation on a nanostructured mesoporous platinum (MPPt) electrode in 0.01 M ethanol + 0.5 M H_2SO_4 . CVs (A) and MSCVs for $m/z = 22$ (B), $m/z = 29$ (C) and $m/z = 15$ (D). $v = 2 \text{ mV s}^{-1}$; $T = 25 \text{ }^\circ\text{C}$. Reprinted from Reference,⁹² Copyright (2016), with permission from Elsevier.

The signals at $m/z = 22, 29$ and 15 correspond to CO_2^+ , CHO^+ and CH_3^+ respectively. The latter fragment is produced from both acetaldehyde and methane. It is clear from Figure 1.7A that the faradaic current at low potentials (< 0.38 V) is related to the adsorption/desorption of hydrogen and/or ethanol, dehydrogenation of ethanol and/or formation of methane, whereas the electro-oxidation of ethanol starts at potentials of around 0.38 V and increases up to 0.8 V and then decreases.⁹² The onset of electro-oxidation of ethanol at 0.38 V and decrease at high potentials may be explained by the effect of poisoning species; CO_{ad} at low potentials and OH_{ad} at high potentials, as mentioned previously in this section. Figures 1.7B and 1.7C show CO_2 and acetaldehyde formation, respectively, over a wide range of potentials. The CO_2 formation starts at around 0.5 V which is attributed to an increasing dissociative adsorption of water (based on eqs. 1.26 and 1.27), while the CO_2 formation at low and high potentials drops to zero due to the poisoning effects described above. The signal at $m/z = 15$ is due to methane at low potentials as shown in the inset of Figure 1.7b (and eq. 1.24), while at high potentials is due to acetaldehyde and is similar to m/z signal 29.

Electrochemical in-situ Fourier transform infrared spectroscopy (EC-FTIRS) has also been used to elucidate the reaction mechanism by identifying the reaction products and adsorbed intermediate species involved in the electrochemical reactions. Figure 1.8 shows IR spectra recorded during ethanol oxidation at a Pt electrode with 0.5 M ethanol in $\text{HClO}_4/\text{H}_2\text{O}$ and $\text{HClO}_4/\text{D}_2\text{O}$ electrolytes.⁹¹ Enhancing the signal-to-noise ratio and subtracting the background was accomplished by using the potential difference technique. Consequently, negative and positive peaks correspond to reaction products (appearing species) and reactants (disappearing species), respectively. Here, the reference spectrum was recorded at 0.05 V and then the potential was increased by 0.1 V up to 1.2 V vs. RHE. From the IR spectra, in both H_2O and D_2O , a negative

band at 2007 cm^{-1} was formed at around 0.25 V and corresponds to linearly adsorbed CO. The intensity of this band increased as the potential was increased up to around 0.6 V vs. RHE, and then its intensity decreased, which indicates that CO_{ad} was the main species blocking (poison) the active sites of Pt at low applied potentials. In the H_2O electrolyte, the negative band at 2343 cm^{-1} corresponds to CO_2 . This band appears at 0.5 V and increased as the potential was increased up to 0.8 V , which indicates that CO_2 formation was due to oxidative removal of CO_{ad} by OH_{ad} species, and then decreases at high potentials due to high coverage of OH_{ad} species. These observations are in good agreement with the data in Figure 1.7. This band was not observed in the D_2O electrolyte due to the IR region being dominated by a strong band from D_2O .⁹¹

The negative band at 1713 cm^{-1} in both electrolytes corresponds to the C=O stretching in acetaldehyde and acetic acid. In H_2O electrolyte, this band is not accurately observed due to the strong band from water at around 1615 cm^{-1} . When both acetic acid and acetaldehyde are formed, the band at 1713 cm^{-1} (which corresponds to both acetic acid and acetaldehyde) will be higher than the band at 1685 or 1280 cm^{-1} (correspond only to acetic acid).⁹¹ However, as seen from the IR spectra, the intensity of the 1713 cm^{-1} band increases significantly at higher potentials, which indicates that both acetaldehyde and acetic acid formation is promoted at higher potentials. Acetyl species are not formed under the conditions used here. The positive bands in the D_2O electrolyte at around 1392 and 2901 cm^{-1} correspond to adsorbed acetaldehyde species.⁹¹ The intensity of these bands increases with increasing potential, which indicates that ethanol adsorbs initially in a series of dehydrogenation steps at low potentials, leading to the formation adsorbed acetaldehyde. This means that ethanol and acetaldehyde adsorb on the electrode surface at very low potentials and then they start to desorb with increasing potentials producing in this case free active sites for C-C bond breaking.

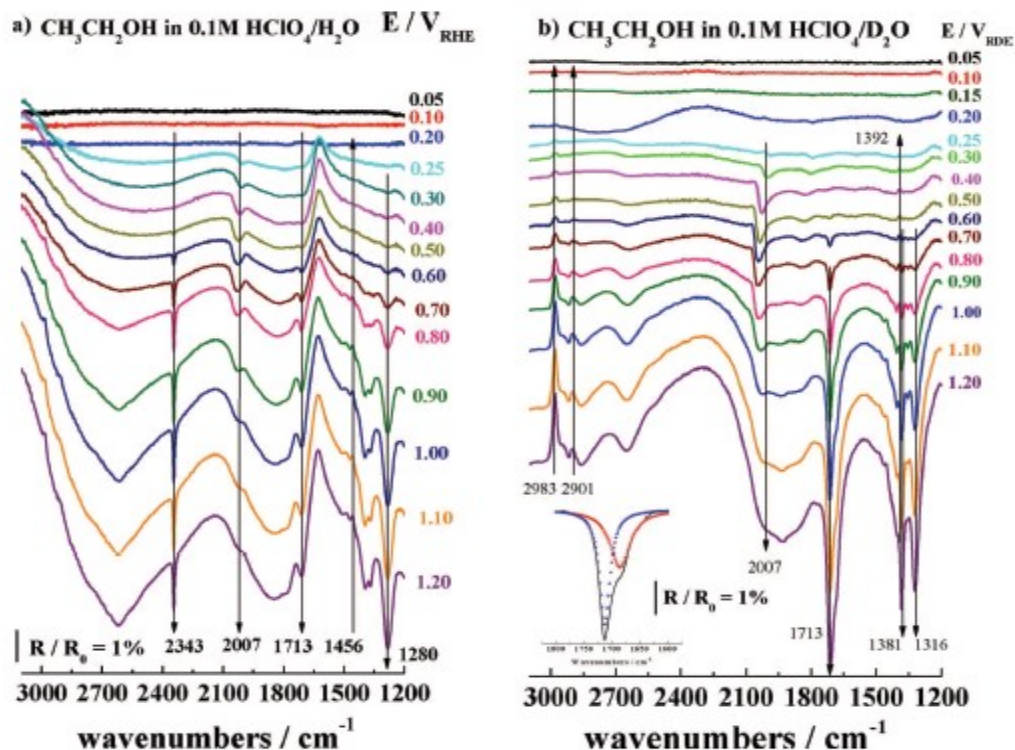


Figure 1.8. Selected IR spectra for the EOR (0.5 M $\text{CH}_3\text{CH}_2\text{OH}$) recorded at 1 mVs^{-1} in a) 0.1 M $\text{HClO}_4/\text{H}_2\text{O}$ and b) 0.1 M $\text{HClO}_4/\text{D}_2\text{O}$. Inset: A magnification of the $1800\text{--}1600 \text{ cm}^{-1}$ region of the spectrum recorded at 1.0 V, which shows the presence of two bands at 1713 and 1685 cm^{-1} . Reprinted from Reference,⁹¹ Copyright (2016), with permission from Elsevier.

From the results discussed in this section, the formation of acetaldehyde and acetic acid can be explained as follows. The onset for acetaldehyde formation is observed at intermediate potentials. At low potentials, the formation of CO_{ad} and $\text{CH}_{\text{x,ad}}$ dominate due to the higher activity of the catalyst for cleavage of the C-C bonds of ethanol and acetaldehyde. Increasing the potentials (up to potentials where no dissociative adsorption of water takes place) leads to an increase in the coverage of CO_{ad} species and a decrease in the activity of the catalyst for cleavage of the C-C bond, which then hinders the further re-adsorption of acetaldehyde, resulting in incomplete oxidation to acetaldehyde. At high potentials where dissociative adsorption of water takes place

significantly, OH species will form and interact with CO_{ad} resulting in free active sites at the electrode surface that enhance the further adsorption and oxidation of ethanol leading to higher CO₂, acetic acid and acetaldehyde formation. Afterwards, the catalyst activity decreases at higher potentials ($E > 0.8V$) due to the high coverage of OH species leading to the hindrance the C-C bond cleavage. Therefore, acetic acid is formed significantly while the formation of CO₂ declines with increasing potential.

At low potentials, CO_{ad} formation is favored from the dissociative adsorption of acetaldehyde more than ethanol, which indicates that acetaldehyde may be the more favorable path to CO₂ than direct C-C bond cleavage of ethanol. In conclusion, poisoning species and C-C bond cleavage play a central role in determining the efficiency of DEFCs.

1.3.6 Product Analysis from DEFCs

Although not common, a number of research groups have determined product yields from DEFCs or under fuel cell operating conditions. Rousseau et al.⁷⁴ used HPLC to determine the product distribution at various catalysts in a DEFC at 80 °C. It was found that acetic acid was the main product at a Pt catalyst. Also, modification of Pt with Sn increased the acetic acid formation, while the addition of Ru did not affect the product distribution of the PtSn. Sun et al.⁸⁵ have studied the effect of temperature and ethanol concentration on the CO₂ yield from a DEFC using DEMS. The CO₂ yield was increased significantly with higher temperatures and lower ethanol concentrations. Similar studies were reported for ethanol oxidation in DEFCs using gas chromatography (GC) by Nakagawa et al.⁹⁰ and by Seweryn et al.¹⁰³. Nakagawa et al. reported that acetaldehyde was the main product at Pt, PtRu and PtRuRh at 80 °C, while the Pt catalyst gave the highest selectivity for CO₂. In addition, James and Pickup⁹⁵ used gas chromatography, a

conductivity cell (and/or titration with base) and a NDIR CO₂ detector successfully to measure the concentrations of acetaldehyde, acetic acid and CO₂, respectively produced during ethanol oxidation in a DEFC. James and Pickup⁸² studied the effect of oxygen on the product yields in DEFCs. They reported that using oxygen at the cathode leads to overestimation of product yields due to crossover.

NMR has been used successfully to measure the concentration of residual ethanol as well as acetic acid and acetaldehyde produced during ethanol oxidation in a DEFC. Figure 1.9 shows the ¹³C NMR spectrum for the anode exhaust from a DEFC with a PtRu/C catalyst, with methanol used as an internal standard. The observed products were acetic acid, acetaldehyde and derivatives of acetaldehyde (gem-dihydroxyethane at 88 ppm, methoxyhydroxyethane at 96 and 54 ppm, and ethoxyhydroxyethane at 94 and 63 ppm).⁹⁶

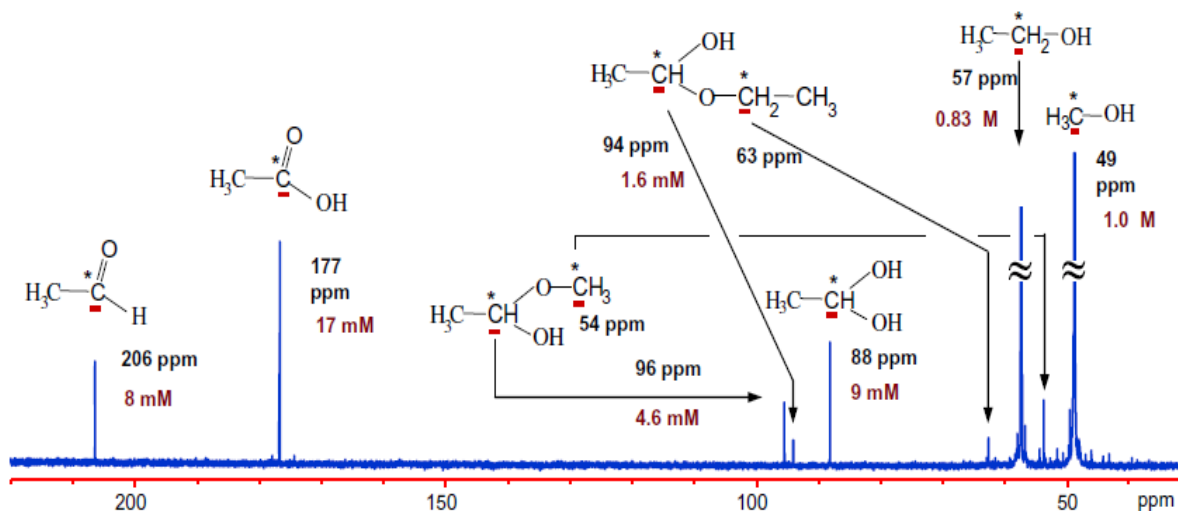


Figure 1.9. ¹³C NMR spectrum for the anode exhaust from a DEFC at 80 °C and 0.2 V with 2 M ethanol and a PtRu/C anode. Reprinted from Reference,⁹⁶ Copyright (2009), with permission from Elsevier.

1.3.7 Bi and Trimetallic Catalysts

Although platinum (Pt) has relatively high activity for cleavage of the C–C bond of ethanol, it exhibits very slow kinetics for both the EOR and ORR leading to significant losses in performance and efficiency. The primary reason for the slow kinetics on Pt is the CO_{ad} poisoning effect described in section 1.3.5. However, there are many strategies that can be used to overcome or reduce the poisoning effect and thus increase the overall cell performance. For EOR, many groups have developed new catalysts by modifying the Pt with other metals and controlling the morphology (crystalline facets) of the catalyst surface.^{104–112} Metals such as Ru,^{90,110,113,114} Sn,^{93,94,105,115} Ni,^{116–121} Rh,^{104,107,110,112} Pd,^{57,110} Cu,^{58,122} Ir,^{105,106,110} and others like Co, Au, Os, Eu and Fe^{57,58,110,123,124} can be used to enhance the bifunctional mechanism and/or ligand (electronic) effect of the catalyst.

The bifunctional mechanism can be described as follows: Pt is modified with oxyphilic metals to form bi or trimetallic alloyed catalysts that enhance the dissociative adsorption of water at low overpotential to form OH_{ad}. The OH can adsorb on the oxyphilic metals even more strongly than CO. Since the dissociative adsorption of water to form OH_{ad} is necessary for the complete oxidation of CO_{ad} and CH_{x,ad} to CO₂, the CO and CH_x can react with OH_{ad} to form CO₂, leading to a decrease in the poisoning effect of CO. Furthermore, these metals can promote the ligand effect, which is defined as a change in the electronic structure of Pt (decrease the electron density in the d-orbitals and thereby decrease the backdonation of electrons from Pt to CO), which can lead to weakening of the CO_{ad} bond resulting in high CO tolerance and a significant decrease in the poisoning effect on Pt. Thus, the bifunctional mechanism and ligand effect can release sufficient free Pt active sites for further adsorption and oxidation, leading to enhanced activity for ethanol electro-oxidation and improved performance in DEFCs.

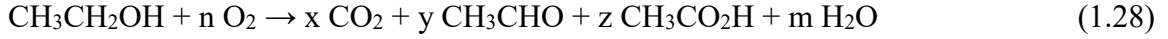
However, an ensemble of three to four Pt atoms are needed to provide an active site for cleavage the C-C bond of ethanol.⁷⁵ Using too much of a secondary and/or tertiary metal dilutes the Pt sites and can also result in a OH_{ad} coverage that is too high, leading to significant OH poisoning and a decrease in selectivity, performance and efficiency. Therefore, controlling the ratio between the metals on the catalyst surface is very important to obtain the optimum selectivity and performance. In DEFCs, PtRu and PtSn have been shown to give the best performance at low overpotentials compared to Pt.^{75,108,125} However, the selectivity for the complete oxidation to CO_2 is significantly lower than at Pt and acetic acid becomes the main product. From all the work up to now, it is clear that there is often an inverse relationship between the selectivity and performance of catalysts in DEFCs. Further work is required on the development of new anode catalysts in order to increase the selectivity and performance of the catalysts simultaneously. The newest approach is to employ catalyst nanoparticles with different shapes and structure, such as the PtNi octahedral used in Chapter 7, core-shell particles with a Pt shell over an electropositive core to provide a ligand effect,¹²⁶ or and oxide shell on a Pt core¹⁰⁹.

1.3.8 Proton Exchange Membrane Electrolysis Cells (PEM-ECs)

All experimental results in this work were performed in a PEM-EC. The PEM-EC employed commercial DEFC hardware operated with nitrogen instead of oxygen or air. Nitrogen was used to avoid the chemical reaction (eq. 1.28) between ethanol and oxygen described in section 1.3.4. Determination of the overall efficiency of a DEFC and the evaluation of anode catalysts requires accurate methods for the measurement of n_{av} , and this is very difficult (and has not been achieved) in a DEFC. Using oxygen at the cathode, as in a DEFC, leads to overestimation of the products

and electrochemical consumption of ethanol due to crossover, and so yields inaccurate n_{av} values.

In the absence of oxygen, the cathodic reaction is represented by eq. 1.29.



The overall reaction of the ethanol oxidation in a PEM-EC is represented in eq. 1.30.



Recently, the anode exhaust was analyzed to investigate the effect of oxygen on the product distribution at ambient and elevated temperature.^{82,95} It was found that the yields of CO_2 and acetic acid increased significantly with oxygen at the cathode compared to the yields when a mixture of nitrogen and hydrogen was used as shown in Table 1.1.

Table 1.1. Faradaic yields of CO_2 and acetic acid from a cell operating with O_2 or N_2/H_2 at the cathode. Reprinted from Reference,⁸² Copyright (2010), with permission from Elsevier.

Current (mA)	T (°C)	Acetic acid		CO ₂	
		N ₂ /H ₂	O ₂	N ₂ /H ₂	O ₂
20	Ambient	26.5%	42.1%	5.7%	6.6%
40	Ambient	34.8%	48.4%	2.7%	4.0%
60	Ambient	45.2%	57.1%	1.7%	2.5%
80	Ambient	55.5%	61.8%	1.4%	2.0%
50	80	28.0%	49.4%	14.1%	20.0%
100	80	34.6%	54.2%	13.5%	25.4%
150	80	40.9%	46.7%	15.6%	25.0%
200	80	40.7%	46.1%	18.6%	24.0%

Accurate measurement of the product distribution is very important in the evaluation of catalysts, and for understanding the mechanisms and how the rates of pathways to the desired products can be enhanced. This can lead to development of more efficient catalyst for commercialization of DEFCs and ethanol electrolysis cells (EECs). In addition to providing

accurate product distributions, EECs can be used to produce hydrogen in a process referred to as electrochemical reforming.^{127,128}

1.4 Thesis Objectives

The first objective of this thesis was to develop simple and fast methodologies that can be routinely used to comprehensively evaluate and compare commercial and new catalysts for the oxidation of ethanol. These methodologies should be able to quantify ethanol consumption and product distributions during electro-oxidation of ethanol in both EECs and DEFCs. This would allow n_{av} and faradaic efficiencies to be routinely determined. A secondary objective was to evaluate an electrochemical method for determining n_{av} by comparing the results with those from chemical analysis of the cell exhaust (chapter 6). In addition, investigating the crossover of ethanol and products through the membrane was undertaken by analysis of the anode and cathode exhausts separately (chapter 3).

The third objective of this thesis was to study and compare various commercial catalysts in order to understand how their performance and selectivity influence EEC and DEFC efficiency. This was achieved after combining the anode and cathode exhaust to measure the product distributions, average number of electrons and efficiencies as a function of potentials at elevated temperature in fuel cell hardware (chapter 4).

Another objective of this thesis was to examine the effects catalyst mixtures and bilayers on the product distribution and efficiency. It has been clearly shown that catalysts bilayers increase the faradaic efficiency while maintaining the high potential efficiency (chapter 5).

The final objective of this thesis was to study the effect of octahedral PtNi alloy catalyst nanoparticles on the selectivity, performance and efficiency of the EOR in fuel cell hardware at elevated temperature and compare it with the commercial catalysts (chapter 7).

References

1. M. Hoel, S. Kvemdokk, Depletion of fossil fuels and the impacts of global warming, *Resour. Energy Econ.* 18 (1996) 115–136.
2. M. Höök, X. Tang, Depletion of fossil fuels and anthropogenic climate change-A review, *Energy Policy.* 52 (2013) 797–809.
3. S. Shafiee, E. Topal, When will fossil fuel reserves be diminished?, *Energy Policy.* 37 (2009) 181–189.
4. N. Abas, A. Kalair, N. Khan, Review of fossil fuels and future energy technologies, *Futures.* 69 (2015) 31–49.
5. S.H. Mohr, J. Wang, G. Ellem, J. Ward, D. Giurco, Projection of world fossil fuels by country, *Fuel.* 141 (2015) 120–135.
6. J.W. Gosselink, Pathways to a more sustainable production of energy: Sustainable hydrogen - A research objective for Shell, *Int. J. Hydrogen Energy.* 27 (2002) 1125–1129.
7. X. Yu, P.G. Pickup, Recent advances in direct formic acid fuel cells (DFAFC), *J. Power Sources.* 182 (2008) 124–132.
8. C. Lamy, E.M. Belgsir, J.M. Léger, Electrocatalytic oxidation of aliphatic alcohols:

- Application to the direct alcohol fuel cell (DAFC), *J. Appl. Electrochem.* 31 (2001) 799–809.
9. C. Lamy, A. Lima, V. LeRhun, F. Delime, C. Coutanceau, J.M. Léger, Recent advances in the development of direct alcohol fuel cells (DAFC), *J. Power Sources.* 105 (2002) 283–296.
 10. U.B. Demirci, Direct liquid-feed fuel cells: Thermodynamic and environmental concerns, *J. Power Sources.* 169 (2007) 239–246.
 11. M.Z.F. Kamarudin, S.K. Kamarudin, M.S. Masdar, W.R.W. Daud, Review: Direct ethanol fuel cells, *Int. J. Hydrogen Energy.* 38 (2013) 9438–9453.
 12. M.A.F. Akhairi, S.K. Kamarudin, Catalysts in direct ethanol fuel cell (DEFC): An overview, *Int. J. Hydrogen Energy.* 41 (2016) 4214–4228.
 13. S.P.S. Badwal, S. Giddey, A. Kulkarni, J. Goel, S. Basu, Direct ethanol fuel cells for transport and stationary applications - A comprehensive review, *Appl. Energy.* 145 (2015) 80–103.
 14. W.G.C. Ryan O’hayre, S. Cha, *Fuel Cell Fundamentals*, Wiley. (2016) 603.
 15. P. Costamagna, S. Srinivasan, Quantum jumps in the PEMFC science and technology from the 1960s to the year 2000: Part I. Fundamental scientific aspects, *J. Power Sources.* 102 (2001) 242–252.
 16. A.D.S. Tantram, Fuel cells: past, present and future, *Energy Policy.* 2 (1974) 55–66.
 17. T.R. Ralph, “Principles of Fuel Cells,” *Platin. Met. Rev.* 50 (2006) 200–201.

18. K. Prater, The renaissance of the solid polymer fuel cell, *J. Power Sources*. 29 (1990) 239–250.
19. L. Carrette, K.A. Friedrich, U. Stimming, Fuel Cells: Principles, Types, Fuels, and Applications, *ChemPhysChem*. 1 (2000) 162–193.
20. U. Lucia, Overview on fuel cells, *Renew. Sustain. Energy Rev.* 30 (2014) 164–169.
21. O.Z. Sharaf, M.F. Orhan, An overview of fuel cell technology: Fundamentals and applications, *Renew. Sustain. Energy Rev.* 32 (2014) 810–853.
22. R.E. Rosli, A.B. Sulong, W.R.W. Daud, M.A. Zulkifley, T. Husaini, M.I. Rosli, E.H. Majlan, M.A. Haque, A review of high-temperature proton exchange membrane fuel cell (HT-PEMFC) system, *Int. J. Hydrogen Energy*. 42 (2017) 9293–9314.
23. S. Mekhilef, R. Saidur, A. Safari, Comparative study of different fuel cell technologies, *Renew. Sustain. Energy Rev.* 16 (2012) 981–989.
24. M. Nacef, A.M. Affoune, Comparison between direct small molecular weight alcohols fuel cells' and hydrogen fuel cell's parameters at low and high temperature. Thermodynamic study, *Int. J. Hydrogen Energy*. 36 (2011) 4208–4219.
25. S. Abdullah, S.K. Kamarudin, U.A. Hasran, M.S. Masdar, W.R.W. Daud, Development of a conceptual design model of a direct ethanol fuel cell (DEFC), *Int. J. Hydrogen Energy*. 40 (2015) 11943–11948.
26. W.R.W. Daud, R.E. Rosli, E.H. Majlan, S.A.A. Hamid, R. Mohamed, T. Husaini, PEM fuel cell system control: A review, *Renew. Energy*. 113 (2017) 620–638.

27. A. Chandan, M. Hattenberger, A. El-Kharouf, S. Du, A. Dhir, V. Self, B.G. Pollet, A. Ingram, W. Bujalski, High temperature (HT) polymer electrolyte membrane fuel cells (PEMFC)-A review, *J. Power Sources*. 231 (2013) 264–278.
28. P.J. Vergragt, Transition management for sustainable personal mobility, *IEEE Eng. Manag. Rev.* 34 (2006) 27.
29. E. Díaz, M. Epstein, M. Romero, J. González-Aguilar, Performance assessment of concentrated solar power plants based on carbon and hydrogen fuel cells, *Int. J. Hydrogen Energy*. 3 (2018) 0–10.
30. V. Das, S. Padmanaban, K. Venkitesamy, R. Selvamuthukumar, F. Blaabjerg, P. Siano, Recent advances and challenges of fuel cell based power system architectures and control – A review, *Renew. Sustain. Energy Rev.* 73 (2017) 10–18.
31. M. Farooque, H.C. Maru, Fuel Cells — The Clean and Efficient Power Generators, *IEEE Xplore*. 89 (2001) 1819–1829.
32. X. Huang, Z. Zhang, J. Jiang, Fuel Cell Technology for Distributed Generation: An Overview, 2006 *IEEE Int. Symp. Ind. Electron.* (2006) 1613–1618.
33. M.W. Ellis, M.R. Von Spakovsky, D.J. Nelson, Fuel cell systems: efficient, flexible energy conversion for the 21st century, *Proc. IEEE*. 89 (2001) 1808–1818.
34. B. Johnston, M.C. Mayo, A. Khare, Hydrogen: The energy source for the 21st century, *Technovation*. 25 (2005) 569–585.
35. T. Hua, R. Ahluwalia, L. Eudy, G. Singer, B. Jermer, N. Asselin-Miller, S. Wessel, T. Patterson, J. Marcinkoski, Status of hydrogen fuel cell electric buses worldwide, *J. Power*

- Sources. 269 (2014) 975–993.
36. P.E.V. de Miranda, E.S. Carreira, U.A. Icardi, G.S. Nunes, Brazilian hybrid electric-hydrogen fuel cell bus: Improved on-board energy management system, *Int. J. Hydrogen Energy*. 42 (2017) 13949–13959.
 37. D. Gao, Z. Jin, J. Zhang, J. Li, M. Ouyang, Development and performance analysis of a hybrid fuel cell/battery bus with an axle integrated electric motor drive system, *Int. J. Hydrogen Energy*. 41 (2016) 1161–1169.
 38. J.P. Stempien, S.H. Chan, Comparative study of fuel cell, battery and hybrid buses for renewable energy constrained areas, *J. Power Sources*. 340 (2017) 347–355.
 39. A. Kirubakaran, S. Jain, R.K. Nema, A review on fuel cell technologies and power electronic interface, *Renew. Sustain. Energy Rev.* 13 (2009) 2430–2440.
 40. W . C . Röntgen, On a New Kind of Rays Author, *American Association for the Advancement of Science Stable*, 3 (2018) 227–231.
 41. K. Mazloomi, C. Gomes, Hydrogen as an energy carrier: Prospects and challenges, *Renew. Sustain. Energy Rev.* 16 (2012) 3024–3033.
 42. M. Pudukudy, Z. Yaakob, M. Mohammad, B. Narayanan, K. Sopian, Renewable hydrogen economy in Asia - Opportunities and challenges: An overview, *Renew. Sustain. Energy Rev.* 30 (2014) 743–757.
 43. K.A. Mauritz, R.B. Moore, State of understanding of Nafion, *Chem. Rev.* 104 (2004) 4535–4585.

44. R. Tiwari, E. Garcia, The state of understanding of ionic polymer metal composite architecture: A review, *Smart Mater. Struct.* 20 (2011).
45. T.J. Peckham, J. Schmeisser, M. Rodgers, S. Holdcroft, Main-chain, statistically sulfonated proton exchange membranes: the relationships of acid concentration and proton mobility to water content and their effect upon proton conductivity, *J. Mater. Chem.* 17 (2007) 3255.
46. Y.S. Kim, L. Dong, M.A. Hickner, T.E. Glass, V. Webb, J.E. McGrath, State of water in disulfonated poly(arylene ether sulfone) copolymers and a perfluorosulfonic acid copolymer (nafion) and its effect on physical and electrochemical properties, *Macromolecules.* 36 (2003) 6281–6285.
47. D.E. Curtin, R.D. Lousenberg, T.J. Henry, P.C. Tangeman, M.E. Tisack, Advanced materials for improved PEMFC performance and life, *J. Power Sources.* 131 (2004) 41–48.
48. S. Gamburgzev, A.J. Appleby, Recent progress in performance improvement of the proton exchange membrane fuel cell (PEMFC), *J. Power Sources.* 107 (2002) 5–12.
49. S.J. Lee, S. Mukerjee, J. McBreen, Y.W. Rho, Y.T. Kho, T.H. Lee, Effects of Nafion impregnation on performances of PEMFC electrodes, *Electrochim. Acta.* 43 (1998) 3693–3701.
50. S. Litster, G. McLean, PEM fuel cell electrodes, *J. Power Sources.* 130 (2004) 61–76.
51. H. Kim, S. Lee, S. Kim, C. Oh, J. Ryu, J. Kim, E. Park, S. Hong, K. No, Membrane crystallinity and fuel crossover in direct ethanol fuel cells with Nafion composite membranes containing phosphotungstic acid, *J. Mater. Sci.* 52 (2017) 2400–2412.
52. Y.J. Deng, G.K.H. Wiberg, A. Zana, M. Arenz, On the oxygen reduction reaction in

- phosphoric acid electrolyte: Evidence of significantly increased inhibition at steady state conditions, *Electrochim. Acta.* 204 (2016) 78–83.
53. S. Sui, X. Wang, X. Zhou, Y. Su, S. Riffat, C. Liu, A comprehensive review of Pt electrocatalysts for the oxygen reduction reaction: Nanostructure, activity, mechanism and carbon support in PEM fuel cells, *J. Mater. Chem. A.* 5 (2017) 1808–1825.
 54. H.A. Gasteiger, B.N. Grgur, P.N. Ross, Oxygen reduction reaction on Pt (111): effects of bromide, *Electrochim. Acta.* 467 (1999) 157–163.
 55. A.S. Aricò, S. Srinivasan, V. Antonucci, DMFCs: From Fundamental Aspects to Technology Development, *Fuel Cells.* 1 (2001) 133–161.
 56. J. Stacy, Y.N. Regmi, B. Leonard, M. Fan, The recent progress and future of oxygen reduction reaction catalysis: A review, *Renew. Sustain. Energy Rev.* 69 (2017) 401–414.
 57. S. Lankiang, M. Chiwata, S. Baranton, H. Uchida, C. Coutanceau, Oxygen reduction reaction at binary and ternary nanocatalysts based on Pt, Pd and Au, *Electrochim. Acta.* 182 (2015) 131–142.
 58. S.D. Lankiang, S. Baranton, C. Coutanceau, Electrocatalytic behaviour towards oxygen reduction reaction of carbon-supported $Pt_xM_yAu_z$ (M = Ni, Cu, Co) binary and ternary catalysts, *Electrochim. Acta.* 242 (2017) 287–299.
 59. B. Braunschweig, D. Hibbitts, M. Neurock, A. Wieckowski, Electrocatalysis: A direct alcohol fuel cell and surface science perspective, *Catal. Today.* 202 (2013) 197–209.
 60. B.C. Ong, S.K. Kamarudin, S. Basri, Direct liquid fuel cells: A review, *Int. J. Hydrogen Energy.* 42 (2017) 10142–10157.

61. D.R. Dekel, Review of cell performance in anion exchange membrane fuel cells, *J. Power Sources*. 375 (2018) 158–169.
62. Y.S. Li, T.S. Zhao, R. Chen, Cathode flooding behaviour in alkaline direct ethanol fuel cells, *J. Power Sources*. 196 (2011) 133–139.
63. L. An, R. Chen, Recent progress in alkaline direct ethylene glycol fuel cells for sustainable energy production, *J. Power Sources*. 329 (2016) 484–501.
64. S.Y. Shen, T.S. Zhao, Q.X. Wu, Product analysis of the ethanol oxidation reaction on palladium-based catalysts in an anion-exchange membrane fuel cell environment, *Int. J. Hydrogen Energy*. 37 (2012) 575–582.
65. L.J. Burcham, I.E. Wachs, The origin of the support effect in supported metal oxide catalysts: In situ infrared and kinetic studies during methanol oxidation, *Catal. Today*. 49 (1999) 467–484.
66. S. Wasmus, A. Küver, Methanol oxidation and direct methanol fuel cells: a selective review, *J. Electroanal. Chem.* 461 (1999) 14–31.
67. J.N. Tiwari, R.N. Tiwari, G. Singh, K.S. Kim, Recent progress in the development of anode and cathode catalysts for direct methanol fuel cells, *Nano Energy*. 2 (2013) 553–578.
68. X. Li, A. Faghri, Review and advances of direct methanol fuel cells (DMFCs) part I: Design, fabrication, and testing with high concentration methanol solutions, *J. Power Sources*. 226 (2013) 223–240.
69. S.S. Munjewar, S.B. Thombre, R.K. Mallick, Approaches to overcome the barrier issues of passive direct methanol fuel cell – Review, *Renew. Sustain. Energy Rev.* 67 (2017) 1087–

1104.

70. S. Song, W. Zhou, Z. Liang, R. Cai, G. Sun, Q. Xin, V. Stergiopoulos, P. Tsiakaras, The effect of methanol and ethanol cross-over on the performance of PtRu/C-based anode DAFCs, *Appl. Catal. B Environ.* 55 (2005) 65–72.
71. L. An, T.S. Zhao, Y.S. Li, Carbon-neutral sustainable energy technology: Direct ethanol fuel cells, *Renew. Sustain. Energy Rev.* 50 (2015) 1462–1468.
72. J. Friedl, U. Stimming, Model catalyst studies on hydrogen and ethanol oxidation for fuel cells, *Electrochim. Acta.* 101 (2013) 41–58.
73. A. Lan, A. S. Mukasyan, Perovskite-based Catalysts for Direct Ethanol Fuel Cells, 2 (2007) 1–10.
74. S. Rousseau, C. Coutanceau, C. Lamy, J.M. Léger, Direct ethanol fuel cell (DEFC): Electrical performances and reaction products distribution under operating conditions with different platinum-based anodes, *J. Power Sources.* 158 (2006) 18–24.
75. F. Vigier, S. Rousseau, C. Coutanceau, J.M. Leger, C. Lamy, Electrocatalysis for the direct alcohol fuel cell, *Top. Catal.* 40 (2006) 111–121.
76. C. Lamy, C. Coutanceau, J. Leger, *The Direct Ethanol Fuel Cell: a Challenge to Convert Bioethanol*, Wiley, 2009.
77. H. Wang, Z. Jusys, R.J. Behm, Ethanol electrooxidation on a carbon-supported Pt catalyst: Reaction kinetics and product yields, *J. Phys. Chem. B.* 108 (2004) 19413–19424.
78. P. Majidi, P.G. Pickup, Determination of the average number of electrons released during

- the oxidation of ethanol in a direct ethanol fuel cell, *Electrochim. Acta.* 182 (2015) 856–860.
79. X. Ren, T.E. Springer, S. Gottesfeld, Water and Methanol Uptakes in Nafion Membranes and Membrane Effects on Direct Methanol Cell Performance, *J. Electrochem. Soc.* 147 (2000) 92.
 80. Q. Wang, G. Wang, X. Lu, C. Chen, Z. Li, G. Sun, Investigation of Methanol Crossover and Water Flux in an Air- Breathing Direct Methanol Fuel Cell, *Int. J. Electrochem. Sci.* 10 (2015) 2939–2949.
 81. R. Lawson, C. Wang, J. Hong, J. Ma, B. Fang, D. Chu, Nafion-Bimevox Composite Membrane for Fuel Cell Applications, *J. Electrochem. Soc.* 154 (2007) B48.
 82. D.D. James, P.G. Pickup, Effects of crossover on product yields measured for direct ethanol fuel cells, *Electrochim. Acta.* 55 (2010) 3824–3829.
 83. Z. Zuo, Y. Fu, A. Manthiram, Novel blend membranes based on acid-base interactions for fuel cells, *Polymers (Basel).* 4 (2012) 1627–1644.
 84. S. Song, W. Zhou, J. Tian, R. Cai, G. Sun, Q. Xin, S. Kontou, P. Tsiakaras, Ethanol crossover phenomena and its influence on the performance of DEFC, *J. Power Sources.* 145 (2005) 266–271.
 85. S. Sun, M.C. Halseid, M. Heinen, Z. Jusys, R.J. Behm, Ethanol electrooxidation on a carbon-supported Pt catalyst at elevated temperature and pressure: A high-temperature/high-pressure DEMS study, *J. Power Sources* 190 (2009) 2-13.
 86. H.F. Wang, Z.P. Liu, Comprehensive mechanism and structure-sensitivity of ethanol

- oxidation on platinum: New transition-state searching method for resolving the complex reaction network, *J. Am. Chem. Soc.* 130 (2008) 10996–11004. doi:10.1021/ja801648h.
87. R. Kavanagh, X.M. Cao, W.F. Lin, C. Hardacre, P. Hu, Origin of low CO₂ selectivity on platinum in the direct ethanol fuel cell, *Angew. Chemie - Int. Ed.* 51 (2012) 1572–1575.
88. H. Wang, Z. Jusys, R.J. Behm, Ethanol Electrooxidation on a Carbon-Supported Pt Catalyst: Reaction Kinetics and Product Yields Ethanol Electrooxidation on a Carbon-Supported Pt Catalyst: Reaction Kinetics and Product Yields, (2004) 19413–19424.
89. O. Guillén-Villafuerte, G. García, M.C. Arévalo, J.L. Rodríguez, E. Pastor, New insights on the electrochemical oxidation of ethanol on carbon-supported Pt electrode by a novel electrochemical mass spectrometry configuration, *Electrochem. Commun.* 63 (2016) 48–51.
90. N. Nakagawa, Y. Kaneda, M. Wagatsuma, T. Tsujiguchi, Product distribution and the reaction kinetics at the anode of direct ethanol fuel cell with Pt/C, PtRu/C and PtRuRh/C, *J. Power Sources.* 199 (2012) 103–109.
91. J. Torrero, F.J. Pérez-Alonso, M.A. Peña, C. Domínguez, A.O. Al-Youbi, S.A. Al-Thabaiti, S.N. Basahel, A.A. Alshehri, S. Rojas, In Situ Infrared Study of the Electrooxidation of Ethanol and Acetaldehyde in Acid Electrolyte, *ChemElectroChem.* 3 (2016) 1072–1083.
92. J. Flórez-Montaño, G. García, O. Guillén-Villafuerte, J.L. Rodríguez, G.A. Planes, E. Pastor, Mechanism of ethanol electrooxidation on mesoporous Pt electrode in acidic medium studied by a novel electrochemical mass spectrometry set-up, *Electrochim. Acta.* 209 (2016) 121–131.

93. H. Ishitobi, Y. Ino, N. Nakagawa, Anode catalyst with enhanced ethanol electrooxidation activity by effective interaction between Pt-Sn-SiO₂ for a direct ethanol fuel cell, *Int. J. Hydrogen Energy*. 42 (2017) 26897–26904.
94. R.M. Antoniassi, A. Oliveira Neto, M. Linardi, E. V. Spinacé, The effect of acetaldehyde and acetic acid on the direct ethanol fuel cell performance using PtSnO₂/C electrocatalysts, *Int. J. Hydrogen Energy*. 38 (2013) 12069–12077.
95. D.D. James, D. V. Bennett, G. Li, A. Ghumman, R.J. Helleur, P.G. Pickup, Online analysis of products from a direct ethanol fuel cell, *Electrochem. Commun.* 11 (2009) 1877–1880.
96. Y. Paik, S.S. Kim, O.H. Han, Spatial distribution of reaction products in direct ethanol fuel cell, *Electrochem. Commun.* 11 (2009) 302–304.
97. O.H. Han, Nuclear magnetic resonance investigations on electrochemical reactions of low temperature fuel cells operating in acidic conditions, *Prog. Nucl. Magn. Reson. Spectrosc.* 72 (2013) 1–41.
98. O.H. Han, Direct Alcohol Fuel Cells Investigated by NMR Spectroscopy at the Korea Basic Science Institute, *J. Anal. Sci. Technol.* 2 (2011) A168–A172.
99. I. Kim, O.H. Han, S.A. Chae, Y. Paik, S.H. Kwon, K.S. Lee, Y.E. Sung, H. Kim, Catalytic reactions in direct ethanol fuel cells, *Angew. Chemie - Int. Ed.* 50 (2011) 2270–2274.
100. J. Rossmeisl, J.K. Nørskov, C.D. Taylor, M.J. Janik, M. Neurock, Calculated phase diagrams for the electrochemical oxidation and reduction of water over Pt(111), *J. Phys. Chem. B.* 110 (2006) 21833–21839.
101. H. Wang, Z. Jusys, R.J. Behm, Electrooxidation of acetaldehyde on carbon-supported Pt,

- PtRu and Pt₃Sn and unsupported PtRu_{0.2} catalysts: A quantitative DEMS study, *J. Appl. Electrochem.* 36 (2006) 1187–1198.
102. W. Du, G. Yang, E. Wong, N.A. Deskins, A.I. Frenkel, D. Su, X. Teng, Platinum-tin oxide core-shell catalysts for efficient electro-oxidation of ethanol, *J. Am. Chem. Soc.* 136 (2014) 10862–10865.
103. J. Seweryn, A. Lewera, High selectivity of ethanol electrooxidation to carbon dioxide on platinum nanoparticles in low temperature polymer electrolyte membrane direct ethanol fuel cell, *Appl. Catal. B Environ.* 144 (2014) 129–134.
104. A. Kowal, S.L. Gojković, K.S. Lee, P. Olszewski, Y.E. Sung, Synthesis, characterization and electrocatalytic activity for ethanol oxidation of carbon supported Pt, Pt-Rh, Pt-SnO₂ and Pt-Rh-SnO₂ nanoclusters, *Electrochem. Commun.* 11 (2009) 724–727.
105. J. Tayal, B. Rawat, S. Basu, Bi-metallic and tri-metallic Pt-Sn/C, Pt-Ir/C, Pt-Ir-Sn/C catalysts for electro-oxidation of ethanol in direct ethanol fuel cell, *Int. J. Hydrogen Energy.* 36 (2011) 14884–14897.
106. W. Du, Q. Wang, D. Saxner, N.A. Deskins, D. Su, J.E. Krzanowski, A.I. Frenkel, X. Teng, Highly Active Iridium / Iridium-Tin / Tin Oxide Heterogeneous Nanoparticles as Alternative Electrocatalysts for the Ethanol Oxidation Reaction, *J. Am. Chem. Soc.* (2011) 15172–15183.
107. D.A. Cantane, W.F. Ambrosio, M. Chatenet, F.H.B. Lima, Electro-oxidation of ethanol on Pt/C, Rh/C, and Pt/Rh/C-based electrocatalysts investigated by on-line DEMS, *J. Electroanal. Chem.* 681 (2012) 56–65.

108. J.-M. Jin, T. Sheng, X. Lin, R. Kavanagh, P. Hamer, P. Hu, C. Hardacre, A. Martinez-Bonastre, J. Sharman, D. Thompsett, W.-F. Lin, The origin of high activity but low CO₂ selectivity on binary PtSn in the direct ethanol fuel cell, *Phys. Chem. Chem. Phys.* 16 (2014) 9432–9440.
109. W. Du, G. Yang, E. Wong, N.A. Deskins, A.I. Frenkel, D. Su, X. Teng, Platinum-Tin Oxide Core – Shell Catalysts for Efficient Electro- Oxidation of Ethanol, *J. Am. Chem. Soc.* 136 (2014) 10862–10865.
110. T. Sheng, W.-F. Lin, C. Hardacre, P. Hu, Significance of β -dehydrogenation in ethanol electro-oxidation on platinum doped with Ru, Rh, Pd, Os and Ir, *Phys. Chem. Chem. Phys.* 16 (2014) 13248–13254.
111. D. Li, H. Lv, Y. Kang, N.M. Markovic, V.R. Stamenkovic, Progress in the Development of Oxygen Reduction Reaction Catalysts for Low-Temperature Fuel Cells, *Annu. Rev. Chem. Biomol. Eng.* 7 (2016) 509–532.
112. A. Bach Delpeuch, F. Maillard, M. Chatenet, P. Soudant, C. Cremers, Ethanol oxidation reaction (EOR) investigation on Pt/C, Rh/C, and Pt-based bi- and tri-metallic electrocatalysts: A DEMS and in situ FTIR study, *Appl. Catal. B Environ.* 181 (2016) 672–680.
113. O. Sahin, H. Kivrak, A comparative study of electrochemical methods on Pt-Ru DMFC anode catalysts: The effect of Ru addition, *Int. J. Hydrogen Energy.* 38 (2013) 901–909.
114. P. Liu, A. Logadottir, J.K. Nørskov, Modeling the electro-oxidation of CO and H₂/CO on Pt, Ru, PtRu and Pt₃Sn, *Electrochim. Acta.* 48 (2003) 3731–3742.

115. E. Antolini, F. Colmati, E.R. Gonzalez, Ethanol oxidation on carbon supported (PtSn)alloy/SnO₂ and (PtSnPd)alloy/SnO₂ catalysts with a fixed Pt/SnO₂ atomic ratio: Effect of the alloy phase characteristics, *J. Power Sources*. 193 (2009) 555–561.
116. B. Li, H. Fan, M. Cheng, Y. Song, F. Li, X. Wang, R. Wang, Porous Pt–NiO_x nanostructures with ultrasmall building blocks and enhanced electrocatalytic activity for the ethanol oxidation reaction, *RSC Adv*. 8 (2018) 698–705.
117. N. Erini, V. Beermann, M. Gocyla, M. Gliech, M. Heggen, R.E. Dunin-Borkowski, P. Strasser, The Effect of Surface Site Ensembles on the Activity and Selectivity of Ethanol Electrooxidation by Octahedral PtNiRh Nanoparticles, *Angew. Chemie - Int. Ed*. 56 (2017) 6533–6538.
118. S. Il Choi, S. Xie, M. Shao, J.H. Odell, N. Lu, H.C. Peng, L. Protsailo, S. Guerrero, J. Park, X. Xia, J. Wang, M.J. Kim, Y. Xia, Synthesis and characterization of 9 nm Pt-Ni octahedra with a record high activity of 3.3 A/mgPt for the oxygen reduction reaction, *Nano Lett*. 13 (2013) 3420–3425.
119. L.S. Parreira, J.C.M. Da Silva, M. D’Villa -Silva, F.C. Simões, S. Garcia, I. Gaubeur, M.A.L. Cordeiro, E.R. Leite, M.C. Dos Santos, PtSnNi/C nanoparticle electrocatalysts for the ethanol oxidation reaction: Ni stability study, *Electrochim. Acta*. 96 (2013) 243–252.
120. Z. Zhang, L. Xin, K. Sun, W. Li, Pd-Ni electrocatalysts for efficient ethanol oxidation reaction in alkaline electrolyte, *Int. J. Hydrogen Energy*. 36 (2011) 12686–12697.
121. K.W. Park, J.H. Choi, B.K. Kwon, S.A. Lee, Y.E. Sung, H.Y. Ha, S.A. Hong, H. Kim, A. Wieckowski, Chemical and electronic effects of Ni in Pt/Ni and Pt/Ru/Ni alloy

- nanoparticles in methanol electrooxidation, *J. Phys. Chem. B.* 106 (2002) 1869–1877.
122. W. Hong, J. Wang, E. Wang, Facile synthesis of PtCu nanowires with enhanced electrocatalytic activity, *Nano Res.* 8 (2015) 2308–2316.
 123. C. Te Hsieh, J.Y. Lin, Fabrication of bimetallic Pt-M (M = Fe, Co, and Ni) nanoparticle/carbon nanotube electrocatalysts for direct methanol fuel cells, *J. Power Sources.* 188 (2009) 347–352.
 124. Y.W. Lee, M. Kim, Z.H. Kim, S.W. Han, One-Step Synthesis of Au@Pd Core-Shell Nanooctahedron, *J. Am. Chem. Soc.* 131 (2009) 17036–17037.
 125. E. Antolini, F. Colmati, E.R. Gonzalez, Effect of Ru addition on the structural characteristics and the electrochemical activity for ethanol oxidation of carbon supported Pt-Sn alloy catalysts, *Electrochem. Commun.* 9 (2007) 398–404.
 126. B.W. Zhang, T. Sheng, Y.X. Wang, X.M. Qu, J.M. Zhang, Z.C. Zhang, H.G. Liao, F.C. Zhu, S.X. Dou, Y.X. Jiang, S.G. Sun, Platinum-Cobalt Bimetallic Nanoparticles with Pt Skin for Electro-Oxidation of Ethanol, *ACS Catal.* 7 (2017) 892–895.
 127. H.K. Ju, S. Giddey, S.P.S. Badwal, R.J. Mulder, Electro-catalytic conversion of ethanol in solid electrolyte cells for distributed hydrogen generation, *Electrochim. Acta.* 212 (2016) 744–757.
 128. C. Lamy, T. Jaubert, S. Baranton, C. Coutanceau, Clean hydrogen generation through the electrocatalytic oxidation of ethanol in a Proton Exchange Membrane Electrolysis Cell (PEMEC): Effect of the nature and structure of the catalytic anode, *J. Power Sources.* 245 (2014) 927–936.

Chapter 2

Experimental

2. Experimental

2.1 Chemicals and Materials

All chemicals and materials were used as received in this work, except for Nafion membranes. Chemicals used include: anhydrous ethanol (Commercial Alcohols Inc.), acetic acid (99.7%, Caledon Lab. Chemicals), acetaldehyde (Sigma-Aldrich), sulphuric acid (Fisher Scientific), hydrochloric acid (Sigma-Aldrich), propanol (J. T. Baker), hydrogen peroxide (30%, ACP Chemicals Inc.), oleylamine (70%, Aldrich Chem. Co.), oleic acid (90%, Aldrich Chem. Co.), benzyl ether (98%, Alfa Aesar), tungsten hexacarbonyl ($W(CO)_6$, 97%, Alfa Aesar) and Nafion solution (5%, DuPont). Industrial grade nitrogen from Air Liquide was used in fuel cell experiments. CO_2 (Air Liquide) was used in detector calibration. The as-received Nafion™ 115 and 117 membranes were pre-treated before using as follows: they were cut into square pieces and heated in 3% H_2O_2 for 1 h at 80°C with stirring, then rinsed and immersed in distilled water for 15 min at ambient temperature, followed by immersion in 1 M sulfuric acid for two hours at 80 °C with stirring. Finally, the membranes were heated at 80°C for 3 h in distilled water with stirring, rinsed and then stored in deionized water. ¹

The cells used in this work were a 5 cm² single-anode commercial fuel cell (Figure 2.1) from Fuel Cell Technology Inc., a nine-anode cell (Figure 2.2) constructed by using a custom built 9-anode plate in 5 cm² fuel cell from Electro Chem Inc.,² and a conventional glass cell for voltammetry (see Section 2.3). The cells were operated as electrolysis cells in all experiments. Nafion® 115 and 117 membranes were the only PEMs used in this work. All homemade electrodes used Toray™ (TGP-H-090; 0.26 mm) carbon fiber paper (CFP) that had been wet-proofed with 10wt.% PTFE. Commercial Pt anodes and cathodes (4 mg cm⁻² loading of Pt black on wet-proofed

Toray™ CFP; TGP-H-090) that were used in many of the experiments were donated by Ballard Power Systems. Carbon supported Pt (Pt/C; HiSPEC™ 13100, 70% Pt on a high surface area advanced carbon support; Alfa Aesar; Lot# M22A026), carbon supported PtRu alloy (PtRu/C; HiSPEC™ 12100, 50% Pt and 25% Ru on a high surface area advanced carbon support; Alfa Aesar; Lot# P17B047, carbon supported PtSn (PtSn/C; 40% HP PtSn alloy (3:1 atom%) on Vulcan XC-72; BASF Fuel Cell Inc.; Lot# F0060910), platinum acetylacetonate (Pt(acac)₂, 97%, Aldrich Chem. Co.), nickel acetylacetonate (Ni(acac)₂, 95%, Aldrich Chem. Co.) and carbon black (Vulcan XC-72, Cabot) were also used in this work.



Figure 2.1. Photograph of the 5 cm² single-anode cell.

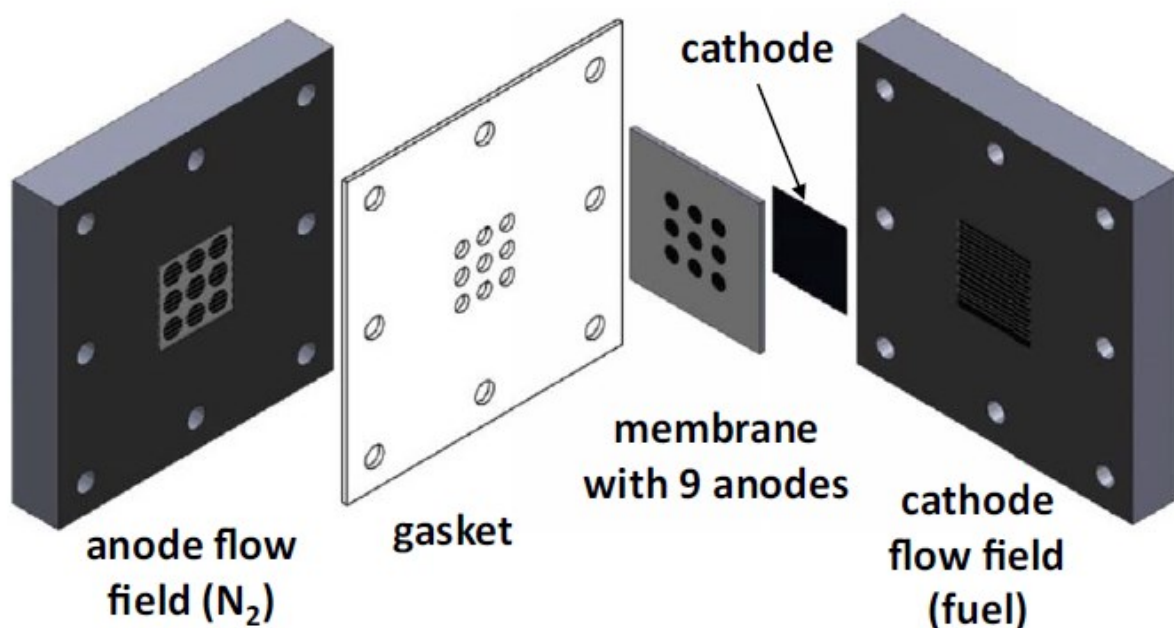


Figure 2.2. Schematic diagram of the nine-anode fuel cell. Reprinted from reference¹.

2.2 Preparation of Electrodes and MEAs

Electrodes were prepared by applying a catalyst ink over a 5 cm² piece of carbon fiber paper (Toray, 0.26 mm), then drying in a fume hood overnight at ambient temperature. Homemade electrodes described in this work were prepared using literature methods.³ The ink was prepared by thoroughly dispersing the catalyst in an appropriate mixture of 5% Nafion® solution (Aldrich) and iso-propanol and the resulting mixture was sonicated for ca. 30 min. A number of Pt based catalysts were prepared and the details are described in the relevant chapters.

MEAs were prepared by pressing the electrodes onto each side of a Nafion membrane at ambient temperature at a pressure of ca. 1.5 MPa.

2.3 Electrochemical Measurements

Electrochemical measurements were conducted with a Hokuto Denko HA-301 potentiostat or with an Arbin® Instruments multi-channel potentiostat. Logger Pro3 software was used for recording CO₂ detector signals.

Cyclic voltammetry measurements were carried out in a conventional three electrode glass cell using a BioLogic SP-50 potentiostat/galvanostat. This instrument used EC-Lab electrochemical software for recording results.

The fuel cell hardware can be operated as a fuel cell (section 1.3.2), in an anode polarization mode (section 1.3.8), or in a crossover mode.⁴ In the crossover mode, ethanol was fed through the cathode while N₂ was passed through the anode. Then the ethanol would cross through the membrane to the anode where it is electrochemically oxidized. The nine-anode cell consists of small anodes and thereby was operated in this mode in all experiments to avoid the loss of ethanol due to crossover and because the steady flux of ethanol through the membrane provided information on the reaction stoichiometry. The 5 cm² cell was also operated in this mode in the work at the beginning of chapter 3, in order to test and develop the analytical methodology under controlled mass transport conditions (the rate of ethanol oxidation is limited by its diffusion rate through the membrane) and without any loss of ethanol due to crossover.

Although the cathode was supplied with N₂ in all experiments in this work, it acts as a dynamic hydrogen reference electrode (DHE). Since the cathode reaction is $H^+ + e^- \rightarrow 0.5 H_2$, it is unnecessary to supply hydrogen to the cathode or to use a reference electrode.⁵ This has been demonstrated by comparing anode polarization curves for a direct methanol fuel cell measured relative the cathode, and relative to a separate, edge-type DHE.⁶ The hydrogen evolving cathode (DHE) can be considered as a better reference electrode than edge-type DHE. The latter reference

electrode can be incorporated into DEFC by attaching two Pt wires to a region of the membrane, but the main problem is the dehydration of membrane outside the active region which can result in an unstable and inaccurate potential.

Temperature control of the cells was achieved using a Cole-Parmer temperature controller (type K thermocouple, model 89810-02) from which two cartridge heaters were inserted inside two holes in the body of the anode and cathode end plates (each plate has a cartridge heater and a thermocouple is connected to the anode plate). The temperature controller reading was stable ($\pm 0.1^\circ\text{C}$) throughout the experiments. Regarding to the reproducibility and error, we have conducted many preliminary experiments to establish the reproducibility and the consistency of the cell assembly. Polarization curves and flow rate experiments (chapter 6) were repeated at least twice for each electrode. Since the use of t-test indicates that the results are not significantly different, averages of the results were used and reported in this work. Chapter 3 provides some data on precision and accuracy, and additional information about the reproducibility is shown in chapter 5 with a 2nd Pt/C electrode.

The use of 0.1 M ethanol in this work represents a compromise between electrochemical performance (power density) and faradaic efficiency (determined primarily by the CO₂ yield, which decreases with increasing ethanol concentration ⁷). Data in the literature for CO₂ yields obtained with Pt/C catalysts covers ethanol concentrations from 0.01 M ⁷ to 2 M ⁸, and so we have selected an intermediate value for this work.

2.4 Product Analysis Instrumentation

To determine the product distributions in the EOR, two main instruments were used. For CO₂ analysis, a commercial CO₂ detector was used. Whereas the analysis of the residual ethanol, acetic

acid as well as acetaldehyde and its derivatives were carried out using nuclear magnetic resonance (NMR). The calculation of yields from these measurements is described in Appendix A.

2.4.1 Non-Dispersive Infrared (NDIR) Carbon Dioxide Detector

All of the CO₂ measurements reported in this work were carried out using a commercial Telaire 7001 CO₂ detector. The detector provides stable and accurate readings due to its dual beam Non-Dispersive Infrared technology with a gas flow-through inlet.

2.4.2 Nuclear Magnetic Resonance (NMR)

Nuclear magnetic resonance was used in the determination of residual ethanol and acetic acid and acetaldehyde produced in the EOR. A Bruker AVANCE III 300 MHz was used at ambient temperature with a BACS auto-sampler and the software was Topspin 3.0 with ICON. Fumaric acid was used as an internal standard, so that the concentrations of the ethanol and reaction products were measured against the peak area of the fumaric acid.

Due to the high volatility of acetaldehyde it was important that all samples from the anode and cathode exhausts were cooled quickly in a mixture of ice and dry ice after exiting the fuel cell. The NMR analysis is discussed in the proceeding chapter.

2.5 Catalyst Characterization Techniques

2.5.1 X-Ray Diffraction (XRD)

X-ray diffraction (XRD) patterns for catalysts were obtained on an X-ray diffractometer (Rigaku Ultima IV) using a copper x-ray source (Cu K α radiation, $\lambda = 1.5406 \text{ \AA}$) and a scintillation counter detector by Dr. Wanda Aylward of Core Research Equipment and Instrument Training

(CREAIT). The x-ray powder diffraction was used to identify crystalline components of the catalysts synthesized in this work and to determine particle sizes at a scan rate of 1.5 degrees per minute. The scan range was from 10 degrees to 90 degrees and the sample was ground in a mortar before measurements.

2.5.2 Inductively Coupled Plasma Optical Emission Spectroscopy (ICP-OES)

ICP-OES measurements were carried out on a Perkin Elmer 5300 DV by Adam Beaton of CREAIT. The sample for ICP-OES was prepared by mixing ca. 6 mg of catalyst with 6 mL of HCl and 2 mL of HNO₃ and heated at 65 °C for 22 h. The final solution was filtered and diluted to 15 mL of water and then analyzed using the ICP-OES. Calibration curves were prepared using various concentrations of Pt, and Ni in 2% HNO₃.

2.5.3 Thermogravimetric Analysis (TGA)

TGA experiments were conducted using a TA instrument Q500 thermogravimetric analyzer with thermal advantage software. Experiments were conducted under an air atmosphere. TGA is a method of thermal analysis uses to measure the mass of a sample over time as a function of temperature. In this work, increasing the temperature (up to 800 °C) of a sample leads to changes in the composition of the sample including evaporation of water (ca. 100 °C) and burning of carbon (ca. 600 °C), the content of each was determined by the difference in mass. Eventually, the mass of metals was determined due to the very high vaporization temperatures of the transition metals involved.

2.5.4 Transmission Electron Microscopy (TEM)

Transmission electron microscopy (TEM) was used to study the morphology of the PtNi/C octahedral catalyst including the particle size and distribution. TEM experiments were carried out at the University of New Brunswick (The Microscopy and Microanalysis Facility) by Steven Cogswell using a JEOL 2011 200 keV scanning transmission electron microscope.

The sample was prepared by carefully grinding PtNi/C powder and was dispersed in 100% ethanol and sonicated. Then pipetting a drop of the sample solution onto the TEM grid which has a carbon suspension film and allowed to dry overnight. The chemical analysis was carried out using an Energy Dispersive X-ray Analysis (EDAX) system.

References

1. L. Napoli, M. J. Lavorante, J. Franco, A. Sanguinetti, H. Fasoli, Effects on Nafion® 117 Membrane using Different Strong Acids in Various Concentrations, *Journal of New Materials for Electrochemical Systems*, 16 (2013) 151-156.
2. T.M. Brueckner, P.G. Pickup, Kinetics and Stoichiometry of Methanol and Ethanol Oxidation in Multi-Anode Proton Exchange Membrane Cells, *J. Electrochem. Soc.* 164 (2017) F1172–F1178.
3. G. Li, P.G. Pickup, Decoration of carbon-supported Pt catalysts with Sn to promote electro-oxidation of ethanol, *J. Power Sources*. 173 (2007) 121–129.
4. P. Majidi, R.M. Altarawneh, N.D.W. Ryan, P.G. Pickup, Determination of the efficiency of methanol oxidation in a direct methanol fuel cell, *Electrochim. Acta.* 199 (2016) 210–217.

5. D.D. James, P.G. Pickup, Measurement of carbon dioxide yields for ethanol oxidation by operation of a direct ethanol fuel cell in crossover mode, *Electrochim. Acta.* 78 (2012) 274–278.
6. G. Li, P.G. Pickup, Measurement of single electrode potentials and impedances in hydrogen and direct methanol PEM fuel cells, *Electrochim. Acta.* 49 (2004) 4119–4126.
7. S. Sun, M.C. Halseid, M. Heinen, Z. Jusys, R.J. Behm, Ethanol electrooxidation on a carbon-supported Pt catalyst at elevated temperature and pressure: A high-temperature/high-pressure DEMS study, *J. Power Sources*, 190 (2009) 2-13.
8. S. Rousseau, C. Coutanceau, C. Lamy, J.M. Leger, Direct ethanol fuel cell (DEFC): Electrical performances and reaction products distribution under operating conditions with different platinum-based anodes, *J. Power Sources*, 158 (2006) 18-24.

Chapter 3

Determination of the Efficiency of Ethanol Oxidation in a Proton Exchange Membrane Electrolysis Cell

The principal author (Rakan M. Altarawneh) contributed to all aspects of the project as the main researcher including: literature review, performing all of the experiments, collecting and analyzing the data, designing some of the experiments, presenting and discussing the data and writing the first draft of the manuscript. The co-author (Pasha Majidi) conducted preliminary work and assisted with the initial experiments.

The corresponding author (Prof. Peter G. Pickup) was the principal investigator and developed the initial ideas for this research. He oversaw all aspects of the project, including supervision of the principal author (Rakan M. Altarawneh), the design of experiments, data analysis; he finalized and submitted the manuscript.

This chapter has been published as: -

(R.M. Altarawneh, P. Majidi, P.G. Pickup, Determination of the efficiency of ethanol oxidation in a proton exchange membrane electrolysis cell, *J. Power Sources*, 351 (2017) 106-114).

The raw data is provided in Appendix B.

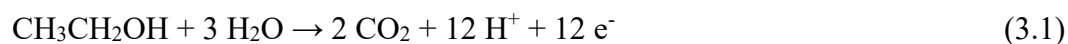
3. Determination of the Efficiency of Ethanol Oxidation in a Proton Exchange Membrane Electrolysis Cell

3.1 Introduction

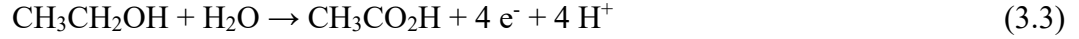
The electrochemical oxidation of ethanol is of fundamental importance to the development of our understanding of organic electrocatalysis^{1,2} and has growing applications in energy technology²⁻⁵ and sensors.^{6,7} Direct ethanol fuel cells^{8,9} (DEFC) offer the potential for efficient and clean energy production from biomass, while ethanol electrolysis¹⁰⁻¹² provides a renewable source of hydrogen for fuel cells. Electrochemical oxidation is widely used as an ethanol sensing mechanism in breath alcohol analyzers (breathalyzer).

In addition to measurement of electrochemical kinetics under a wide range of conditions, a full understanding of electrochemical ethanol oxidation requires knowledge of the stoichiometry (n_{av} = average number of electrons transferred per ethanol molecule),^{13,14} product distribution,^{13,15,16} and the nature and coverage of adsorbed intermediates.¹⁷⁻²¹ Since the efficiency of a fuel cell or electrolysis cell is proportional to n_{av} ,¹⁴ the reaction stoichiometry plays a critical role in the development of energy technologies based on electrochemical ethanol oxidation. It also influences the sensitivity of ethanol sensors, and variations in n_{av} with time and operating conditions will cause errors in breathalyzer measurements.

The complete oxidation of ethanol to carbon dioxide, which provides the highest theoretical energy efficiency for a fuel cell or electrolyzer, involves the transfer of 12 electrons as shown in eq. 3.1.



However, the main products formed during electrochemical oxidation are generally acetaldehyde (eq. 3.2) and acetic acid (eq. 3.3), which generate only 2 and 4 electrons, respectively.



Ethyl acetate²²⁻²⁵ from condensation of ethanol with the acetic acid, ethane,²⁶ methane,²⁶⁻²⁸ ethane-1,1-diol,^{23,25} ethoxyhydroxyethane,^{23,25} and formic acid²⁹ have also been observed as minor products. In addition to greatly decreasing the energy efficiency of DEFCs and ethanol electrolyzers, the formation of acetaldehyde, acetic acid and other byproducts can decrease the effectiveness of both the anode and cathode catalysts, and has the potential to create significant environmental problems.

The efficiency of a DEFC (\mathcal{E}_{cell}) is determined by the theoretical energy conversion efficiency (\mathcal{E}_{rev} ; thermodynamic efficiency), the potential efficiency ($\mathcal{E}_E = E_{cell}/E_{rev}$, where E_{cell} is the operating potential and E_{rev} is the reversible cell potential), and the faradaic efficiency (\mathcal{E}_F), according to eq. 3.4.^{9, 15}

$$\mathcal{E}_{cell} = \mathcal{E}_{rev} \cdot \mathcal{E}_E \cdot \mathcal{E}_F \quad (3.4)$$

The faradic efficiency is the ratio of the average number of electrons obtained per molecule of ethanol to the maximum of 12 for the complete oxidation to CO_2 ($\mathcal{E}_F = n_{av}/12$), and is determined by the product distribution according to eq. 3.5,¹⁶

$$12 \cdot \mathcal{E}_F = n_{av} = \sum n_i f_i \quad (3.5)$$

where n_i is the number of electrons transferred to form product i and f_i is the fraction of ethanol converted to product i . Accurate use of eq. 3.5 required all products to be identified and accurately quantified.

A recent analysis of low carbon power sources for vehicles has concluded that polymer electrolyte membrane (PEM) DEFCs, together with batteries, offer the best alternative to internal combustion engines.³⁰ However, this is based on the assumption that DEFCs that can operate at

50% efficiency will be developed, which will require n_{av} to be close to 12. Currently, the best efficiencies are ca. 11% for acid PEM DEFCs and ca. 23% for alkaline cells.⁹ It has generally been found that increasing the electrochemical performance (potential efficiency) of the anode catalyst by combining Pt with other metals, such as Ru and Sn, in bi- and tri-metallic catalysts decreases the faradaic efficiency.^{4,15,31,32} However, in most cases, the faradaic efficiencies (or product distributions) of new catalysts have not been reported.

The development of better catalysts for ethanol fuel cells and electrolyzers²⁻⁵ requires accurate methodologies for routine determination of n_{av} . Although it can be estimated from product distributions by use of eq. 3.5,¹⁶ it has been shown that product analysis at the anode of a DEFC does not provide an accurate measure of the product distribution because of crossover of products through the membrane to the cathode, and chemical formation of products due to the crossover of ethanol and oxygen through the membrane.^{24,31,33} Furthermore, accurate measurement of products exiting the cathode is difficult due to the high volatility of acetaldehyde²⁹ and condensation of acetic acid.³³ Although the effects of reaction with oxygen are not present in an electrolysis cell, analysis of products that crossover to the cathode remains a problem.³³

Previously, it has been shown that n_{av} for ethanol oxidation can be determined in DEFC hardware from the variation of the current (I) as a function of the flow rate (u) of the ethanol solution by use of eq. 3.6.³⁴

$$I = n_{av}FC_{in}u \left(1 - \exp \left(- \frac{I_{lim}}{n_{av}FC_{in}u} \right) \right) \quad (3.6)$$

where C_{in} is the concentration of ethanol entering the cell and I_{lim} is the limiting current at high flow rates. Although this equation was developed for a cell operating in crossover mode (Figure 3.1A), the simplest configuration for development of the theory,³⁵ it has subsequently been shown

to also be valid for methanol oxidation in a normal electrolysis cell (anode polarization mode; Figure 3.1B), and a model has been developed to account for losses due to crossover.³⁵

The purpose of the work described in this chapter was to extend the use of eq. 3.6 to an ethanol electrolysis cell operating normally (i.e. in anode polarization mode), to verify its accuracy by measuring ethanol consumption and product distributions, and to assess the effects of ethanol crossover. Proton nuclear magnetic resonance (¹H NMR) spectroscopy was used to measure the concentrations of acetaldehyde, acetic acid and residual ethanol exiting the cell, while CO₂ was analyzed with a commercial non-dispersive infrared (NDIR) detector.³⁶ Analyses of the anode and cathode exhausts were performed separately in order to quantify the crossover of ethanol and products through the membrane. Previously, ¹H NMR has been used to quantify products from ethanol oxidation with molecular catalysts,³⁷ while solution and solid-state ¹³C NMR have been used to identify and quantify ethanol and product distributions within and exiting a DEFC,^{23,25} and in a cell with a liquid electrolyte.³⁸

This work was performed in an electrolysis cell rather than a DEFC in order to avoid the consumption of ethanol by chemical reaction with oxygen that would be supplied to the cathode in a DEFC. Accurate separation the effects of electrochemical and chemical oxidation of ethanol in a DEFC has not yet been achieved.

3.2 Experimental

3.2.1 The Cell

Commercial fuel cell hardware (5 cm² active area; Fuel Cell Technology Inc.) was used for all electrochemical measurements. The anode inlet and both outlets of the cell were modified with stainless steel tubing that connected directly to the graphite flow field plates. The flow field

channels were sealed with ethyl-2-cyanoacrylate³⁹ in order to minimize absorption of ethanol and reaction products into the graphite plates.³³ Membrane and electrode assemblies (MEA) were prepared by pressing (room temperature; ca.1.5 MPa) two electrodes consisting of 4 mg cm⁻² Pt black on Toray™ (TGP-H-090) carbon fiber paper onto a Nafion™ 115 membrane in the cell.⁴⁰

The two modes of operation employed are shown schematically in Figure 3.1. In both cases, the cell was operated as an electrolysis cell, not a fuel cell. Measurements were made under steady state conditions at constant cell potentials using a Hokuto Denko HA-301 potentiostat. The flow rate of the 0.1 M ethanol (Commercial Alcohols Inc.) solution was controlled with a syringe pump. N₂ was passed through the anode (crossover mode) or cathode (anode polarization mode) at 9-32 mL min⁻¹. In both cases, the cathode reaction is $H^+ + e^- \rightarrow \frac{1}{2} H_2$ and so the cathode acts a dynamic hydrogen electrode (DHE) and provides a relatively stable reference potential. The cell was operated at 50 °C in initial experiments in order to achieve a suitable balance of products, limit ethanol crossover, and optimize the product collection procedure. It was then operated at 80 °C to provide higher CO₂ yields and more stringent testing.

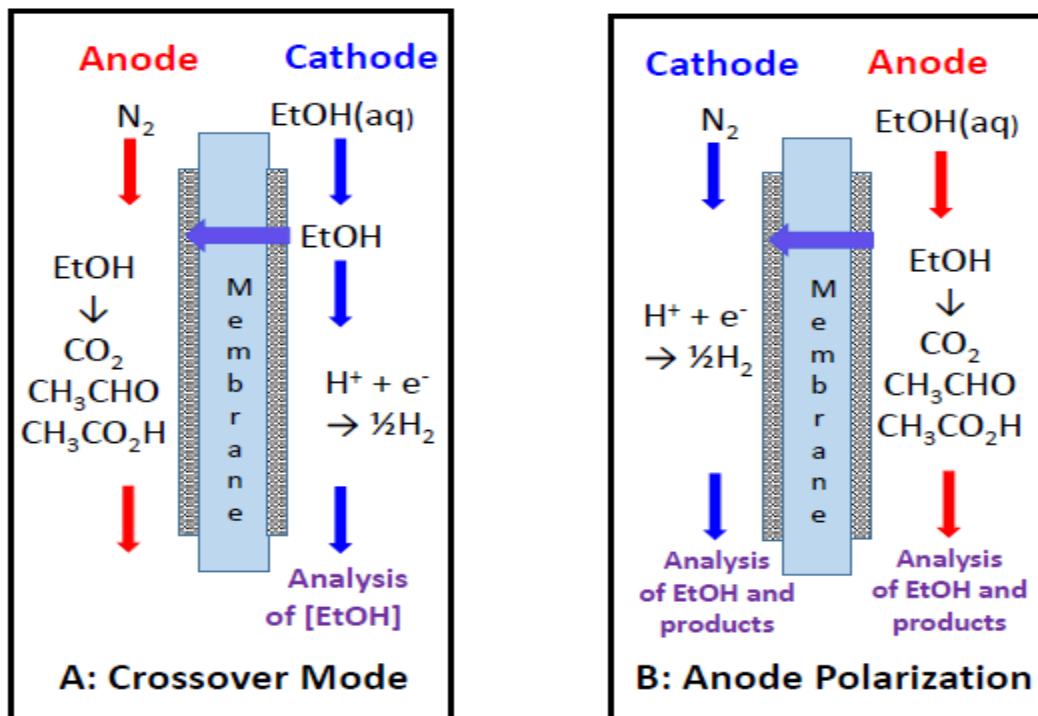


Figure 3.1. Schematic diagrams of the two cell configurations employed in this work.

3.2.2 Ethanol and Product Analysis

For the experiment in crossover mode, the cathode solution was collected in a sealed vial cooled with ice. The residual ethanol concentration was determined by ^1H NMR. The cell was operated at the selected fuel flow rate for at least 10 min before collecting a sample for analysis. Analysis of products and residual ethanol when the cell was operated in anode polarization mode was complicated by crossover of all species through the membrane. In addition, the mixtures of gases (N_2 and CO_2) with volatile liquid components (acetaldehyde and ethanol) that are obtained make it difficult to obtain accurate analyses of all components.³³ Here, ^1H NMR spectroscopy was used to measure ethanol, acetic acid, and acetaldehyde separately in the anode and cathode exhausts, while CO_2 was determined in each exhaust by using a NDIR detector.³⁶ The experimental design shown schematically in Figure 3.2 allowed residual ethanol and all products to be

determined in both exhausts from a single experiment. CO₂ from the cathode (N₂ stream) was measured in real time with a Telaire 7001 CO₂ monitor following condensation of ethanol, water and products that had crossed the membrane in a 200 mL cold trap. The current and CO₂ readings were allowed to stabilize, and then averaged over a period of at least 100 s. The trap was cooled with ice, dry ice or liquid N₂ in the various experiments, but quantitative collection of acetaldehyde (boiling point 20 °C) was not achieved in most experiments. Use of liquid N₂ is complicated by condensation of the CO₂.

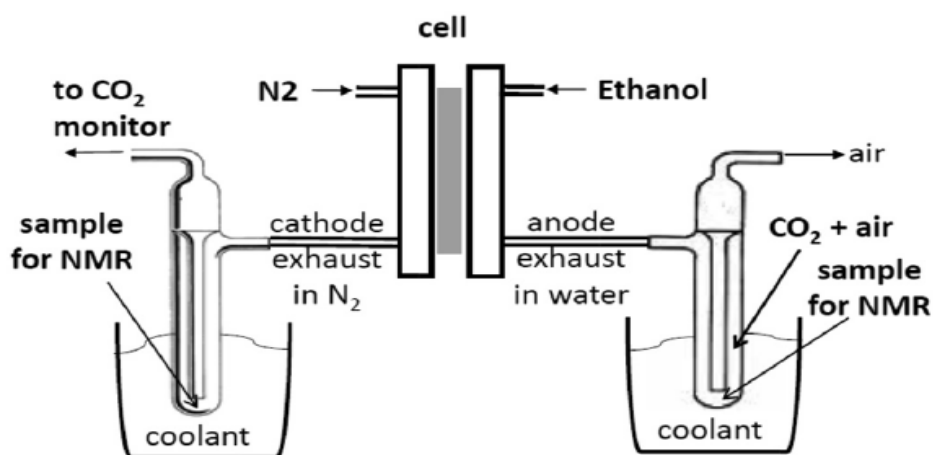


Figure 3.2. Schematic diagram of the product collection system employed in anode polarization experiments.

The anode exhaust solution was collected in a ca. 200 mL trap cooled with ice in the experiments at 50 °C and dry ice in the experiments at 80 °C. At the end of each experiment, a sample of the solution was collected for analysis by ¹H NMR, and then the CO₂ in the trap was flushed through the CO₂ monitor with N₂ at 9-35 mL min⁻¹. The CO₂ concentration was integrated until it reached the reading for the air initially in the trap.

For analysis by ¹H NMR, 400 mL samples collected from the anode and cathode exhausts were mixed with 100 mL of D₂O containing 32 mM fumaric acid as an internal standard, which

gives a singlet peak in the spectra at 6.72 ppm. Spectra were recorded on a Bruker AVANCE III 300 spectrometer. The D₂O in the sampled provided the field frequency lock and spectra were referenced to sodium 3-(trimethylsilyl)-2,2,3,3-tetradeuteriopropionic propionate at 0 ppm. Figure 3.3 shows an example of an NMR spectrum of a sample from the anode exhaust. The residual ethanol concentration was determined from the triplet at 1.10 ppm.

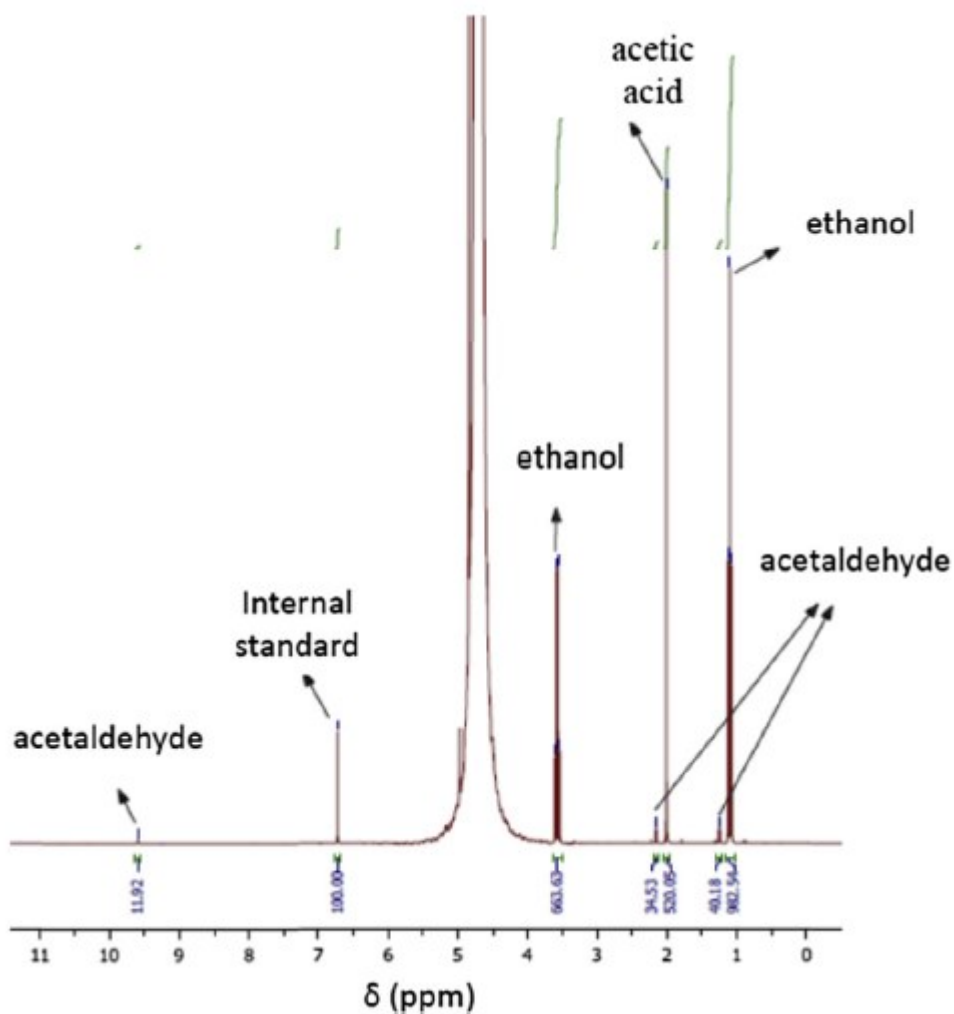


Figure 3.3. NMR spectrum of the anode exhaust solution from oxidation of 0.100 M ethanol at 0.7 V and 50 °C in anode polarization mode.

The only products detected in the exhaust solution were acetic acid (singlet at 2.01 ppm) and acetaldehyde (doublet at 2.15 ppm). Acetaldehyde forms a dimer under the conditions of these

experiments,⁴¹ as indicated by the doublet at 1.24 ppm, and so the integral of this peak was included to give a single acetaldehyde concentration. Ethyl acetate was not detected.

Analysis of the cell exhausts was performed in triplicate at 0.2 mL min⁻¹ only, since uncertainties became too large at higher and lower flow rates. This flow rate gave sufficient consumption of ethanol, while sample collection times were reasonable (to evaluate precision/reproducibility) and reasonably stable cell performances could be maintained.

3.3 Results and Discussion

3.3.1 Operation of the Cell in Crossover Mode

Initially, the cell was operated in crossover mode in order to develop the analytical methodology under well controlled mass transport conditions and without complications due to loss of ethanol due to crossover.³⁵ This allowed us to test the cell, and the assumptions made in the derivation of eq. 3.6. These include the assumption of linear concentration gradients of ethanol across the membrane, that ethanol is quantitatively oxidized at the anode, and that the pressure drop across the membrane, concentration gradient in solution perpendicular to the flow direction, and lateral diffusion along the flow field are all negligible.³⁴

The cell was operated in the limiting current region at 0.7 V and 50 °C (as demonstrated previously³⁴) with ethanol solution supplied through the cathode flow field (negative electrode) so that it had to cross through the membrane to reach the anode, where it was electrochemically oxidized. N₂ was passed through the anode flow field to prevent interference from oxygen. Figure 3.4 shows experimental data and theoretical (eq. 3.6) plots of current vs. fuel flow rate for 0.102 M ethanol supplied to the cathode. The best fit of the theoretical curve to the experimental data points was obtained with $n_{av} = 4.43$ and $I_{lim} = 22.4$ mA. These are within the ranges previously

reported for these conditions.³⁴ In order to check the assumption that all of the ethanol reaching the anode was being oxidized, the ethanol concentration in the solution exiting the cathode flow field was measured by NMR spectroscopy. Since ethanol should only cross the membrane or exit the cathode flow field, a discrepancy in the residual ethanol concentration would indicate that some ethanol reaching the anode was not oxidized, that one or more assumption were invalid, or that there were other losses (leakage) due to the hardware.

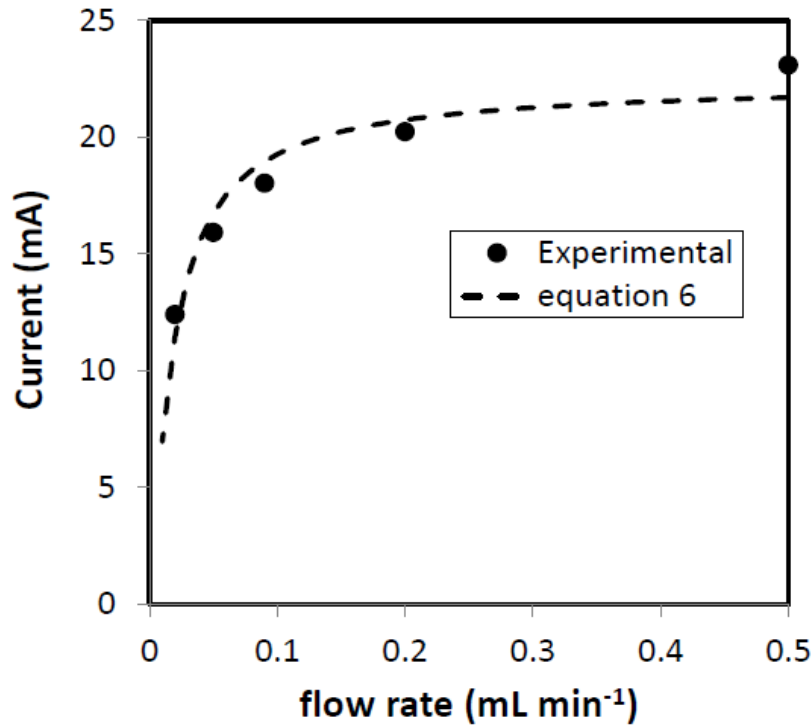


Figure 3.4. Current at 0.7 V vs. flow rate for oxidation of 0.102 M ethanol in crossover mode at 50 °C (points) and best fit curve calculated by using eq. 3.6 with $I_{lim} = 22.4$ mA and $n_{av} = 4.43$.

Figure 3.5 shows the measured concentrations of the residual ethanol content in the cathode exhaust (C_{out}) at different flow rates as a function of the expected ethanol exhaust concentrations calculated from eq. 3.7³⁵ for $I_{lim} = 22.4$ mA and $n_{av} = 4.43$.

$$C_{out} = C_{in} \exp\left(-\frac{I_{lim}}{n_{av}FC_{in}u}\right) \quad (3.7)$$

The good linearity of this plot ($R^2 = 0.984$) and slope (0.953) close to one indicates that the oxidation of ethanol at the anode was quantitative without significant loss of ethanol into the N_2 stream, and that the assumptions implicit in eq. 3.6 are reasonable. The uncertainties observed in Figure 3.5 arise from a number of factors, including variations in n_{av} with flow rate, changes in the cell performance with time, and failure to reach a steady state concentration at the lowest flow rate because of the long time-scale required.³⁴

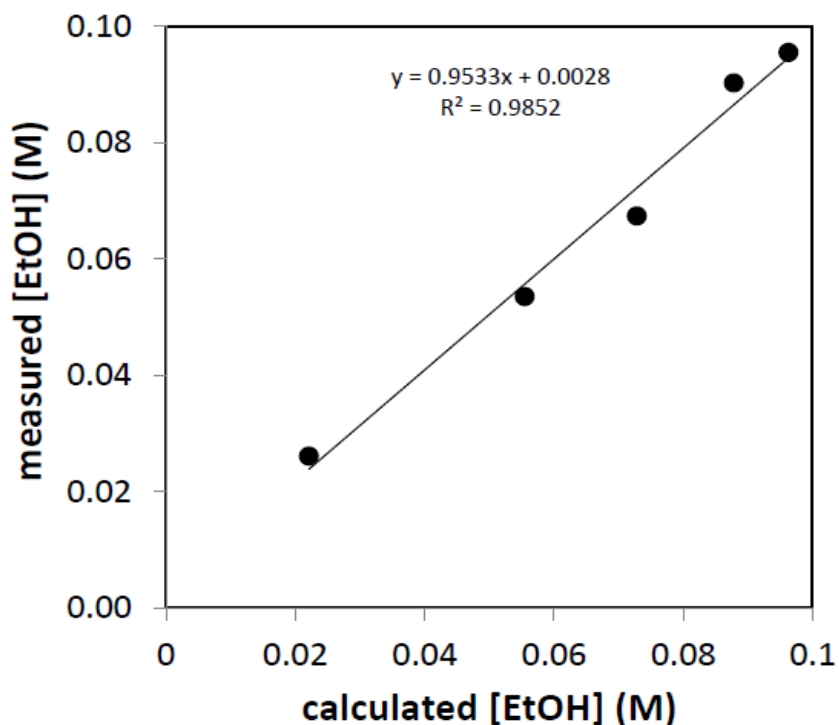


Figure 3.5. Experimental vs. calculated (eq. 3.7 with $I_{lim} = 22.4$ mA and $n_{av} = 4.43$) concentrations of ethanol exiting a cell under the conditions for Figure 3.4.

If it is assumed that ethanol was oxidized quantitatively in this experiment, and that there were no losses of ethanol, values of n_{av} can be obtained directly from the concentrations of ethanol in the cathode exhaust by using eq. 3.8.

$$n_{av} = I/uF(C_{in} - C_{out}) \quad (3.8)$$

Application of this equation to the experimental data in Figures 3.4 and 3.5 gave an average n_{av} of 4.4 ± 0.7 . The agreement of this value with that obtained from eq. 3.6 again indicates that losses of ethanol were not significant.

3.3.2 Operation of the Cell in Anode Polarization Mode

When operating the cell in anode polarization mode, an aqueous solution of 0.100 M ethanol was fed to the anode flow field, where ethanol is oxidized to generate electrons, protons, carbon dioxide, acetaldehyde, and acetic acid. This is the normal mode of operation of an ethanol electrolysis cell, and is also used to evaluate performances of anode catalysts and catalyst layers for DEFCs. Nitrogen was fed to the cathode flow field to avoid interference from oxygen and to provide a stable reference potential from the reduction of protons to hydrogen (DHE). The aim was to fully analyze the ethanol oxidation efficiency by determining n_{av} , accounting for any crossover losses, and complete accounting of the fate of ethanol consumption by analysis of the ethanol oxidation products.

3.3.2.1 Mass Transport Limited Region: High Current and Low Crossover

Figure 3.6 shows polarization curves obtained in anode polarization mode at 50 °C and 80 °C with 0.100 M ethanol supplied to the anode. At 80 °C the current reached a limiting value at 0.6 V. The slight decrease at 0.7 V can be attributed to a decrease in n_{av} (see below). At 50 °C the current was at, or close to, the limiting value at 0.7 V. The increase in current when the temperature was increased is due to effects of temperature on the mass transport rate, electrochemical kinetics, and n_{av} .

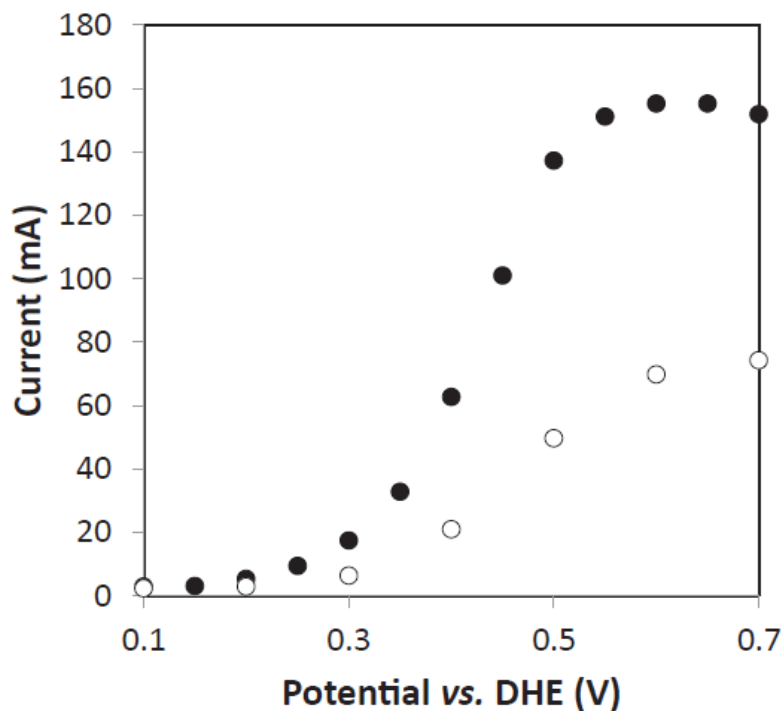


Figure 3.6. Polarization curves for oxidation of 0.100 M ethanol at 0.5 mL min⁻¹ in anode polarization mode at 50 °C (o) and 80 °C (●).

Figure 3.7 (□) shows the dependence of the experimental current at 0.7 V on the flowrate at 50 °C. The best fit theoretical curve (dashed line) from eq. 3.6 is also shown. It has previously been shown for methanol oxidation that eqs. 3.6 and 3.7 are both valid under these conditions.³⁵ The best fit parameters of $n_{av} = 3.31$ and $I_{lim} = 83.7$ mA are reasonable and so support the use of eq. 3.6 here. However, the central importance of n_{av} in determining the efficiencies of ethanol fuel cells and electrolysis cells makes it essential to know the accuracy of this methodology. To determine this, it is necessary to determine the product distribution, and ensure that all of the ethanol entering the cell is accounted for.

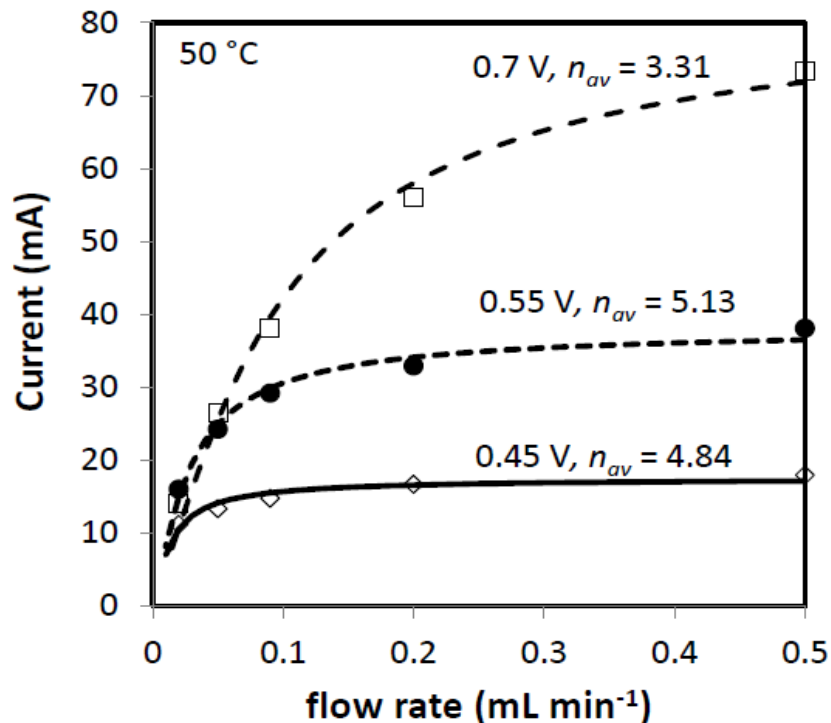


Figure 3.7. Current vs. flow rate for oxidation of 0.100 M ethanol at 50 °C in anode polarization mode at 0.45 V (◇), 0.55 V (●), and 0.70V (□) with best fit curves calculated by using eq. 3.6 with $I_{lim} = 17.5$ mA and $n_{av} = 4.84$, $I_{lim} = 38.2$ mA and $n_{av} = 5.13$, and $I_{lim} = 83.7$ mA, $n_{av} = 3.31$, respectively.

Results of the chemical analysis of products and residual ethanol exiting the cell, obtained under the conditions used to determine n_{av} at 0.7 V in Figure 3.7, are presented in the first row of Tables 3.1 - 3.3. Table 3.1 shows a comparison between the experimental and calculated ethanol exhaust concentrations (C_{out}) obtained by ¹H NMR and based on the measured currents (eq. 3.7), respectively. It can be seen that only 1.3% of the ethanol entering the cell was detected in the cathode exhaust at 0.7 V, indicating that there was little crossover of ethanol at this potential. Under mass transport limited conditions, all of the ethanol entering the anode catalyst layer should have been oxidized before reaching the membrane.³⁵ The small amount of ethanol that was detected in the cathode exhaust may indicate that the cell was not quite at the mass transport limit

(see Figure 3.6), or may have been due to crossover through inactive regions of the MEA at the edges. The total ethanol measured in the cell exhaust at 0.7 V was somewhat higher than the calculated value for $n_{av} = 3.3 \pm 0.3$, suggesting that n_{av} had been underestimated by use of eq. 3.6. Indeed, use of eq. 3.8 to calculate n_{av} from the amount of ethanol consumed yielded a value of 3.9 ± 0.2 .

The measured product distribution for these experiments at 0.7 V (Table 3.2) clearly demonstrates the effects of crossover,³³ and also shows a poor mass balance. Similar amounts of CO₂ were measured in the anode and cathode exhausts, showing that there was facile crossover of CO₂ to the cathode. The chemical yield of CO₂ was 7.6% from the combined analyses. In contrast, there was much less crossover of acetic acid, with only 4.4% of the total chemical yield of 62% appearing at the cathode. This can be attributed to the low volatility of acetic acid.³³ Acetaldehyde was also predominantly observed at the anode, although in this case the anode to cathode ratio does not accurately reflect the amount of crossover, since the low mass balance (“sum” column in Table 3.2) can be attributed primarily to inefficient collection of acetaldehyde from the cathode gas stream.³³ This was confirmed by later experiments (below) in which the acetaldehyde collection efficiency was improved.

Table 3.1. Experimental (NMR) and calculated (eq. 3.7) concentrations of ethanol exiting a cell operating in anode polarization with 0.100 M ethanol supplied to the anode at 0.2 mL min⁻¹. Averages and standard deviations for three consecutive experiments are presented.

T (°C)	Potential (V)	C_{out} (mM)			
		anode	cathode	total	eq. 3.7
50	0.70	52 ± 3	1.3 ± 0.4	53 ± 3	45.6
50	0.55	75 ± 5	4.0 ± 1.1	79 ± 4	79.3
50	0.45	79 ± 2	7.7 ± 1.0	87 ± 1	89.4
80	0.70	59.2 ± 0.9	5.0 ± 0.7	64.2 ± 1.2	61.5
80	0.50	66 ± 1	7.5 ± 0.9	73.4 ± 0.4	75.3
80	0.40	71 ± 1	15.7 ± 0.8	86.9 ± 0.4	90.3

The chemical yields of CO₂ and acetic acid given in Table 3.2 were used to estimate n_{av} by using eq. 3.5. Since the measured acetaldehyde yield was known to be inaccurate, a value estimated by mass balance ($f_{carbon\ dioxide} + f_{acetic\ acid} + f_{acetaldehyde} = 1$) was used. This gave $n_{av} = 4.0 \pm 0.2$, while use of the measured acetaldehyde yield (i.e. assuming that C_{out} was inaccurate) gave $n_{av} = 3.6 \pm 0.4$, which was not statistically different.

Table 2.2. Summary chemical analysis results for the anode and cathode exhausts of a cell operating in anode polarization mode with 0.100 M ethanol at a flow rate of 0.2 mL min⁻¹. Chemical yields are given, based the measured quantities of products and the amount of ethanol consumed. Averages and standard deviations for three consecutive experiments are presented.

T (°C)	potential (V)	%CO ₂		%Acetic acid		%acetaldehyde		sum*	<i>n_{av}</i>
		anode	cathode	anode	cathode	anode	cathode		
50	0.70	4.2 ± 0.3	3.4 ± 0.1	59 ± 6	2.7 ± 0.2	8.9 ± 0.6	0.3 ± 0.2	78 ± 7%	4.0 ± 0.2
50	0.55	6.2 ± 1.4	4.5 ± 0.4	53 ± 2	13 ± 3	13 ± 6	1.9 ± 0.8	92 ± 8%	4.4 ± 0.2
50	0.45	8.0 ± 0.7	5.1 ± 0.5	27.2 ± 0.4	7.1 ± 0.6	27 ± 6	6.9 ± 1.5	81 ± 8%	4.0 ± 0.1
80	0.70	13.3 ± 0.4	10.6 ± 0.9	36 ± 2	11.9 ± 0.4	6.0 ± 1.2	2.6 ± 0.3	80 ± 3%	5.3 ± 0.1
80	0.50	18.6 ± 0.6	11.9 ± 0.1	39 ± 2	14.1 ± 0.6	8.5 ± 0.9	3.7 ± 0.3	96 ± 1%	6.1 ± 0.1
80	0.40	26.8 ± 1.4	8.8 ± 0.3	33 ± 4	16.6 ± 0.8	9.9 ± 1.4	4.8 ± 0.8	100 ± 5%	6.6 ± 0.2

* Mass balance varies due to variations in the acetaldehyde collection efficiency.

Because of the difficulty in obtaining accurate acetaldehyde analyses, and the expectation that faradaic yield of CO₂ and acetic acid obtained by NDIR and ¹H-NMR were accurate, *n_{av}* values were also determined from the CO₂ and acetic acid analyses and the charge balance. Faradaic yields (*F_i*) are presented in Table 3.3 together with *n_{av}* calculated by using eq. 3.9.

$$n_{av} = 12 / (F_{carbon\ dioxide} + 3 F_{acetic\ acid} + 6 F_{acetaldehyde}) \quad (3.9)$$

The *n_{av}* of 4.1 ± 0.2 calculated in this way is not statistically different from the value in Table 3.2 based on the mass balance. Consequently, it can be concluded that failure to obtain a quantitative analysis of the acetaldehyde produced by the cell does not significantly compromise the accuracy of *n_{av}*. A summary of the *n_{av}* values obtained by the various procedures is given in

Table 3.4, where it can be seen that there is very good agreement between the values from eqs. 3.5, 3.8 and 3.9 (t tests show that the differences were not significant). However, eq. 3.6 significantly underestimated n_{av} in this case, which can be attributed to a systematic error due to a slow decrease in the cell performance over the course of the experiment.

Table 3.3. Faradaic yields for CO₂, acetic acid and acetaldehyde from a cell operating in anode polarization mode with 0.100 M ethanol at a flow rate of 0.2 mL min⁻¹. CO₂ and acetic acid yields are based on the combined analyses from the anode and cathode. Averages and standard deviations for three consecutive experiments are presented.

T (°C)	Potential (V)	CO₂ yield	acetic acid yield	acetaldehyde yield from charge balance	n_{av}
50	0.70	24 ± 1%	63 ± 4%	13 ± 5%	4.1 ± 0.2
50	0.55	27 ± 2%	57 ± 6%	15 ± 5%	4.1 ± 0.2
50	0.45	41 ± 1%	36 ± 2%	24 ± 1%	4.15 ± 0.01
80	0.70	53 ± 2%	35 ± 1%	12 ± 2%	5.2 ± 0.2
80	0.50	61 ± 2%	35 ± 1%	4 ± 3%	6.3 ± 0.1
80	0.40	66 ± 1%	31 ± 1%	3.0 ± 0.8%	6.8 ± 0.1

When the temperature of the cell was raised to 80 °C, the current at 0.7 V increased significantly (Figure 3.6), while the amount of ethanol consumed decreased (Table 3.1). The increased current and efficiency are consistent with the higher n_{av} (5.55 at 80 °C vs. 3.31 at 50 °C) obtained by fitting the currents to eq. 3.6. A similar difference in the ethanol consumed is obtained from eq. 3.7 (Table 3.1). The product analyses at 80 °C also show an increase in the efficiency for ethanol oxidation to CO₂ (Tables 3.2 and 3.3), with n_{av} increasing to 5.2 - 5.3, which is consistent with the values of 5.6 ± 0.3 and 5.4 ± 0.2 from eqs. 3.6 and 3.8, respectively (Table 3.4). The increased CO₂ yield at 80 °C vs. 50 °C is consistent with literature reports (see Table 3.5). It can

also be seen from the data in Table 3.1 that there was considerably more crossover of ethanol to the cathode at 80 °C relative to 50 °C.

Table 3.4. Summary of n_{av} values obtained in this work.

Mode	Temp (C)	Potential (V)	n_{av}			
			i vs. u (eq. 3.6)	Ethanol consumed (eq. 3.8)	Faradaic yields (eq. 3.9)	Chemical yields (eq. 3.5)
Crossover	50	0.70	4.4 ± 0.2	4.4 ± 0.7	*	*
Anode pol.	50	0.70	3.3 ± 0.3	3.9 ± 0.2	4.1 ± 0.2	4.0 ± 0.2
Anode pol.	50	0.55	5.1 ± 0.2	4.7 ± 0.4	4.1 ± 0.2	4.4 ± 0.2
Anode pol.	50	0.45	4.8 ± 0.2	3.8 ± 0.2	4.15 ± 0.01	4.0 ± 0.1
Anode pol.	80	0.70	5.6 ± 0.3	5.4 ± 0.2	5.2 ± 0.2	5.3 ± 0.1
Anode pol.	80	0.50	7.0 ± 0.1	6.0 ± 0.1	6.3 ± 0.1	6.1 ± 0.1
Anode pol.	80	0.40	7.7 ± 0.2	6.5 ± 0.3	6.8 ± 0.1	6.6 ± 0.2

* Not determined

3.3.2.2 Low Current Region with Crossover

Experiments were also performed at potentials below the mass transport limited region in order to explore the use of eq. 3.6 to determine n_{av} under the mixed kinetic and mass transport conditions employed in fuel cells and electrolysis cells. Under these conditions, the concentration of ethanol does not drop to zero at the anode-membrane interface, and this results in crossover of

ethanol to the cathode.³⁵ Since, the derivation of eqs. 3.6 and 3.7 assumes that all of the ethanol reaching the anode is oxidized,³⁴ loss of ethanol by crossover would be expected to result in errors. Indeed, this was observed for methanol oxidation at potentials below the limiting current region, and the model was adapted in order to account for and quantify crossover.³⁵ Here, the loss of ethanol into the cathode exhaust was quantified by NMR and current *vs.* flow rate data were analyzed by using both models (eq. 3.6 and a finite difference simulation with crossover) to assess the influence of ethanol crossover. n_{av} values from product analyses were used to assess the accuracy of the n_{av} values obtained from analysis of *I vs. u* curves.

Figure 3.7 (●) shows current as a function of flow rate at 50 °C for an experiment at 0.55 V, which provided only 46% of the current at 0.7 V. Fitting of these data to eq. 3.6 gave $n_{av} = 5.13$ and $I_{lim} = 38.2$ mA. The measured ethanol exhaust concentrations are given in row 2 of Table 3.1, where it can be seen that there was significant crossover of ethanol to the cathode. Approximately 4% of the ethanol entering the cell was detected in the cathode exhaust, which corresponds to 19% of $(C_{in} - C_{out-T})$, where C_{out-T} is the sum of the ethanol concentrations in the anode (C_{out-A}) and cathode (C_{out-C}) exhausts. C_{out} calculated with eq. 3.7 was 79.3 mM for $n_{av} = 5.13$, which agrees well with the experimental total (C_{out-T}) of 79 mM.

In order to investigate whether the crossover of ethanol caused an error in the n_{av} obtained from eq. 3.6, the experimental *I vs. u* and C_{out-A} data were fitted to the simulation³⁵ that includes a crossover parameter. The best fit gave $n_{av} = 5.19$ and $I_{lim} = 39.2$ mA, and 4.8% loss of ethanol due to crossover. The crossover loss from the simulation agrees well with the experimental value of $4.0 \pm 1.1\%$, while the insignificant change in n_{av} shows that this small amount of crossover does not compromise the accuracy of eq. 3.6. I_{lim} was increased slightly in the simulation because it is the limiting current that would be observed in the absence of crossover.

Full product analysis for the anode and cathode exhausts was used to test the accuracy of the n_{av} of 5.1 ± 0.2 obtained from I vs. u , and the results are shown in row 2 of Tables 3.2 and 3.3. The analysis provided a good mass balance, with $n_{av} = 4.4 \pm 0.2$ (Table 3.2), which agreed within the experimental uncertainty with the n_{av} of 4.1 ± 0.2 from the faradaic yields of CO₂ and acetic acid (Table 3.3). Equation 3.7, based on the amount of ethanol consumed, gave a similar value of 4.7 ± 0.4 . The reasonable agreement of all of these n_{av} values indicates that eq. 3.6 provides a useful measure of n_{av} under these conditions.

Figure 3.7 (\diamond) shows current as a function of flow rate for an experiment at 0.45 V, which provided only 21% of the current at 0.7 V. Fitting of these data to eq. 3.6 gave $n_{av} = 4.84$ and $I_{lim} = 17.5$ mA, and use of these parameters in eq. 3.7 gave $C_{out} = 89.4$ mM at 0.2 mL min⁻¹. The exhaust concentrations are given in row 3 of Table 3.1, where it can be seen that there was increased crossover of ethanol to the cathode relative to the experiments at 0.55 V and 0.7 V. The measured C_{out-T} was slightly higher than the value from eq. 3.7, suggesting that the n_{av} of 4.84 may have been slightly overestimated by use of eq. 3.6. Indeed, calculation of n_{av} from the amount of ethanol consumed (eq. 3.8) gave a lower value of 3.8 ± 0.2 . This conjecture was supported by analysis of the products, which provided $n_{av} = 4.0 \pm 0.1$ based on the mass balance (Table 3.2) and $n_{av} = 4.15 \pm 0.01$ based on the charge balance (Table 3.3).

It should be noted that n_{av} values obtained from the flow rate dependence of the current (eq. 3.6) represent averages over the range of flow rates employed, and should not necessarily match those measured from ethanol and product analysis at a specific flow rate. Since the CO₂ yield increases with decreasing ethanol concentration, and the average concentration of ethanol in the flow field decreases with decreasing flow rate, n_{av} increases with decreasing flow rate.³⁴ In the experiments at 0.45 V, the average ethanol concentration in the anode flow field was ca. 89 mM

at 0.2 mL min^{-1} , but only 80 mM over the range of $0.02 - 0.5 \text{ mL min}^{-1}$. This can adequately explain the higher n_{av} from eq. 3.6.

In order to assess the effect of crossover on the n_{av} from eq. 3.6, the experimental I vs. u and C_{out-A} data at 0.45 V were fitted to the simulation with crossover. The best fit gave $n_{av} = 4.98$, $I_{lim} = 18.6 \text{ mA}$, and 10.4% loss of ethanol due to crossover. The measured loss due to crossover was $7.7 \pm 1.0\%$, and so again the value from the simulation is reasonable. The slightly higher n_{av} from the simulation relative to eq. 3.6 should be more accurate, although the difference is not statistically significant.

Current vs flow rate data at $80 \text{ }^\circ\text{C}$ for two potentials (0.4 and 0.5 V) below the mass transport controlled region are shown in Figure 3.8. Fitting of eq. 3.6 to these data sets gave $n_{av} = 7.68$ at 0.4 V and $n_{av} = 7.00$ at 0.5 V, which are both significantly higher than the value of 5.55 obtained at 0.7 V. This decreasing n_{av} with increasing potential is consistent with literature reports,^{42,43} as are the higher values relative to those obtained at $50 \text{ }^\circ\text{C}$ (Table 3.4). Analysis of the ethanol (Table 3.1) and products (Tables 3.2 and 3.3) exiting the cell gave somewhat lower n_{av} values than eq. 3.6, as can be seen from the summaries in Table 3.4. This can be attributed to the effect of flow rate on n_{av} . The ethanol exhaust concentrations in Table 3.1 indicate that ca. 15.7% and 7.5% of the ethanol entering the cell crossed over to the cathode at 0.4 V and 0.5 V, respectively. Simulations show that these levels of crossover would make n_{av} values from eq. 3.6 ca. 2-5% too low.

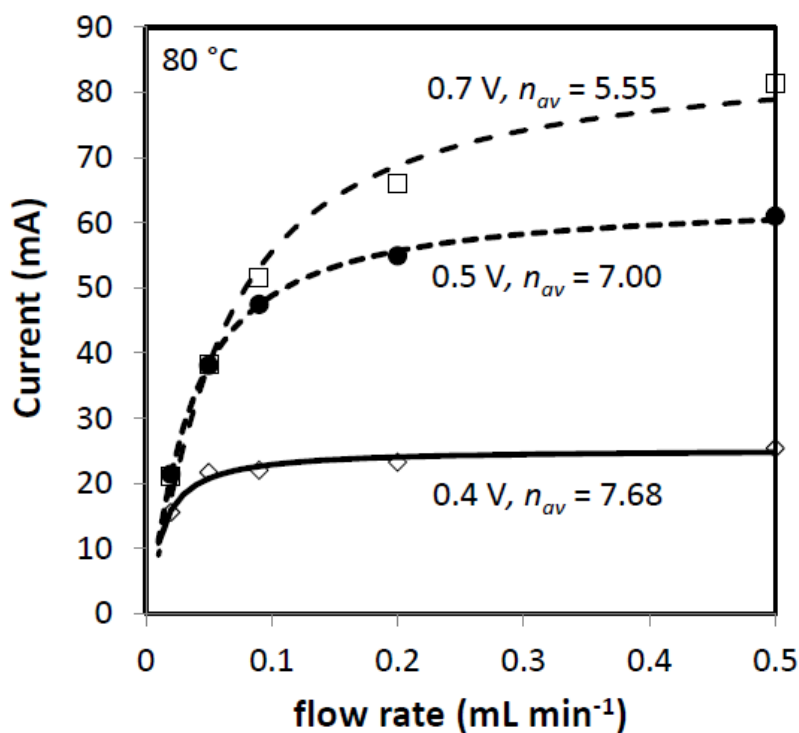


Figure 3.8. Current vs. flow rate for oxidation of 0.100 M ethanol at 80 °C in anode polarization mode at 0.4 V (\diamond), 0.50 V (\bullet), and 0.70 V (\square) with best fit curves calculated by using eq. 3.6 with $I_{lim} = 25.3$ mA and $n_{av} = 7.68$, $I_{lim} = 63.9$ mA and $n_{av} = 7.00$, and $I_{lim} = 86.8$ mA, $n_{av} = 5.55$, respectively.

3.3.3 Discussion

It is clear from the results in Table 4 that all four methods for determining n_{av} give similar results under a variety of conditions. There are significant uncertainties in all cases, and there may be some systematic errors. Crossover of ethanol would be expected to cause an error when eq. 3.6 is used, although modelling of this indicates that it was not a significant source of error (< 5%) here. Loss of acetaldehyde during sample collection would also lead to a systematic error, but this has been accounted for by using the mass and charge balances. n_{av} values obtained from the mass and changes balances did not differ significantly, indicating good accuracy.

From inspection of the results in Table 3.4, it can be seen that the flow rate dependence of the current (eq. 3.6) provides a valuable method for routine determination of n_{av} . It can be applied as a simple extension of a polarization experiment, and can track changes in the stoichiometry as the operating conditions (e.g. T, C_{in} , pressure) of the cell are changed. In combination with a simple, inexpensive, commercial CO₂ detector, it can provide the product distribution from eq. 3.9 with charge balance, if it is assumed that the only products are CO₂, acetic acid and acetaldehyde. A conductivity sensor can also be employed to monitor acetic acid production.⁴⁴ Where necessary, the results can be verified and refined by analysis of the combined exhaust solutions by NMR or chromatography. The product distribution and n_{av} can be obtained from just the ethanol and acetic acid concentrations by applying eq. 3.8 to obtain n_{av} and solving eq. 3.5 with mass balance. This simplifies the analytical procedure considerably, and potential errors due to the loss of ethanol into the gas stream can be avoided if the CO₂ does not need to be measured.

We have applied eq. 3.6 and the comprehensive analysis methodology reported here to a DEFC (i.e. with air at the cathode), but have not achieved a satisfactory accounting of the crossover effects and production of CO₂, acetic acid and acetaldehyde by the chemical reaction of ethanol with oxygen. Although comprehensive analysis of the products and residual ethanol should provide this information, changes in the current and product distributions with time produced unacceptable uncertainties. Consequently, the anode polarization data presented here provide the best estimates available for the stoichiometry and product distribution of ethanol oxidation in a DEFC.

The n_{av} values reported in Table 3.4 and product distributions reported in Tables 3.2 and 3.3 are consistent with literature reports, and follow similar trends. Representative product distributions from the literature are presented in Table 3.5, together with n_{av} for each distribution

calculated with eq. 3.5 for chemical yields or eq. 3.9 for faradaic yields. Where only the CO₂ yield was reported, the range of n_{av} given is for 0% acetic acid to 0% acetaldehyde. At 50 °C, the literature n_{av} values range from 2.1 to 4.2, while those in Table 3.4 range from 3.3 to 5.1. The higher values in this work, which are due to the higher CO₂ yields (Table 3.3), can be attributed to the use of a high loading of Pt black (4 mg cm⁻²) compared with low loadings of 20% Pt on carbon (0.028 - 0.04 mg cm⁻²) in the literature reports.^{16,42} At 80 °C, the literature n_{av} values range from 2.6 to 7.3 while those in Table 3.4 range from 5.2 to 7.7, again showing good compatibility in light of the high Pt loading and low ethanol concentration employed here. The n_{av} values in Table 3.5 are generally much higher at 80 °C than 50 °C, as found in this work (Table 3.4).

Generally, it can be seen from the data in Table 3.5 that the CO₂ yield decreases as the anode potential is increased, and the results in Table 3.4 also follow this trend. This can be attributed to the effect of oxide formation on the Pt surface, which is necessary to oxidize the adsorbed CO intermediate, but restricts the number of contiguous site available for ethanol adsorption.^{42,45} Consequently, for efficient oxidation of ethanol, it is important to avoid oxide formation on Pt. This requires a second, oxophilic component, such as Ru or Sn, to provide the oxide required to form CO₂ at lower potentials.^{32,46,47} However, since the dissociation of the C-C bond of ethanol requires 3 adjacent Pt sites,^{48,49} the presence of a second metal on the Pt surface can inhibit dissociation and causes a decrease in CO₂ formation. Consequently, the surface coverage of the second metal must be low, or it should be present as a separate phase. Oxide supports can provide the required oxide sites and have been shown to increase activities while maintaining high efficiency for the complete oxidation.⁵⁰⁻⁵⁶ It is an approach that offers great potential for the development of efficient DEFCs. However, further work is required in order to establish that oxide supported catalysts produce high stoichiometries under fuel cell conditions.

Table 3.5. Summary of product yields and calculated n_{av} values from literature reports of ethanol oxidation at 50 °C and 80 °C. AAL is acetaldehyde, AA is acetic acid.

T (°C)	catalyst	Pt loading (mg cm ⁻²)	[EtOH] (mol cm ⁻³)	potential (V) <i>reference</i> ^a	Yield ^b			n_{av}	Ref.
					%AAL	%AA	%CO ₂		
50	20% Pt/C	0.028	0.1	scan	37	60	2.7	3.0	16
50	20% Pt/C	0.04	0.1	0.48 <i>RHE</i>	-	-	7.8	2.1-4.2	42
80	20% Pt/C	0.04	0.1	0.48 <i>RHE</i>	-	-	25.7	2.55-4.83	42
80	60% Pt/C	3.0	2.0	-0.4 to -0.6 <i>cathode</i>	47.5	32.5	20	4.7	15
80	Pt black	4.0	0.5	-	41.9	39.5	18.6	3.09	44
80	Pt black	4.0	0.1	0.4 <i>DHE</i>	-	-	56	3.8-6.8	57
80	63% Pt/C	1.0	0.5	-0.1 <i>cathode</i>	14	65	21	5.4	31
80	63% Pt/C	1.0	0.5	-0.2 <i>cathode</i>	29	57	14	4.6	31
80	18% Pt/C	1.0	0.2	-0.1 <i>cathode</i>	15	47	37	6.7	58
80	18% Pt/C	1.0	0.2	-0.2 <i>cathode</i>	21	31	47	7.3	58

- Not reported.

^a Cathode is the oxygen electrode of a fuel cell.

^b Faradaic or chemical (italics) yields.

3.4 Conclusions

The flow rate dependence of the current for a fuel cell operated in anode polarization mode can provide a good estimate of the stoichiometry (n_{av}) of ethanol oxidation at a DEFC anode, or in a PEM electrolysis cell. Errors due to crossover are typically <5%. The stoichiometry can also be conveniently obtained from analysis of the ethanol in the anode and cathode exhausts by NMR, which also provides the rate of crossover of ethanol through the membrane. NMR analysis also

provides the yield of acetic acid, which allows the yields of acetaldehyde and CO₂ to be estimate from n_{av} . This is important because of the experimental difficulty of quantitative collection of the acetaldehyde. Furthermore, it will be important in the determination of product distributions from DEFCs where the chemical reaction of ethanol with oxygen also produces acetaldehyde, acetic acid, and CO₂.

References

1. M.T.M. Koper, S.C.S. Lai, E. Herrero, Mechanisms of the oxidation of carbon monoxide and small organic molecules at metal electrodes, in: Fuel Cell Catalysis, John Wiley, 2009, pp. 159-207.
2. Y. Wang, S.Z. Zou, W.B. Cai, Recent Advances on Electro-Oxidation of Ethanol on Pt- and Pd-Based Catalysts: From Reaction Mechanisms to Catalytic Materials, Catalysts. 5 (2015) 1507-1534.
3. E. Antolini, Catalysts for direct ethanol fuel cells, J. Power Sources. 170 (2007) 1-12.
4. J. Friedl, U. Stimming, Model catalyst studies on hydrogen and ethanol oxidation for fuel cells, Electrochim. Acta. 101 (2013) 41-58.
5. M.A.F. Akhairi, S.K. Kamarudin, Catalysts in direct ethanol fuel cell (DEFC): An overview, Int. J. Hydrogen Energy. 41 (2016) 4214-4228.
6. J.G. Wigmore, R.M. Langille, Six Generations of Breath Alcohol Testing Instruments: Changes in the Detection of Breath Alcohol Since 1930. An Historical Overview, Can. Soc. Forensic Sci. J. (2009) 276-283.
7. M.R. Rahman, J.T.S. Allan, M.Z. Ghavidel, L.E. Prest, F.S. Saleh, E.B. Easton, The application of power-generating fuel cell electrode materials and monitoring methods to breath alcohol sensors Sens Actuators, B Chem. 228 (2016) 448-457.

8. S.P.S. Badwal, S. Giddey, A. Kulkarni, J. Goel, S. Basu, Direct ethanol fuel cells for transport and stationary applications – A comprehensive review, *Appl. Energy* 145 (2015) 80-103.
9. L. An, T.S. Zhao, Y.S. Li, Carbon-neutral sustainable energy technology: Direct ethanol fuel cells, *Renew. Sustain. Energy Rev.* 50 (2015) 1462-1468.
10. V. Bambagioni, M. Bevilacqua, C. Bianchini, J. Filippi, A. Lavacchi, A. Marchionni, F. Vizza, P.K. Shen, Self-Sustainable Production of Hydrogen, Chemicals, and Energy from Renewable Alcohols by Electrocatalysis, *ChemSusChem* 3 (2010) 851-855.
11. C. Lamy, T. Jaubert, S. Baranton, C. Coutanceau, Clean hydrogen generation through the electrocatalytic oxidation of ethanol in a Proton Exchange Membrane Electrolysis Cell (PEMEC): Effect of the nature and structure of the catalytic anode, *J. Power Sources* 245 (2014) 927-936.
12. A.R. de la Osa, A.B. Calcerrada, J.L. Valverde, E.A. Baranova, A. de Lucas-Consuegra, Electrochemical reforming of alcohols on nanostructured platinum-tin catalyst-electrodes, *Appl. Catal. B Env.* 179 (2015) 276-284.
13. H. Hitmi, E.M. Belgsir, J.M. Leger, C. Lamy, R.O. Lezna, A kinetic analysis of the electro-oxidation of ethanol at a platinum electrode in acid medium, *Electrochim. Acta* 39 (1994) 407- 415.
14. F. Vigier, C. Coutanceau, A. Perrard, E.M. Belgsir, C. Lamy, Development of anode catalysts for a direct ethanol fuel cell, *J. Appl. Electrochem.* 34 (2004) 439-446.
15. S. Rousseau, C. Coutanceau, C. Lamy, J.M. Leger, Direct ethanol fuel cell (DEFC): Electrical performances and reaction products distribution under operating conditions with different platinum-based anodes, *J. Power Sources* 158 (2006) 18-24.

16. H. Wang, Z. Jusys, R.J. Behm, Ethanol Electrooxidation on a Carbon-Supported Pt Catalyst: Reaction Kinetics and Product Yields, *J. Phys. Chem. B* 108 (2004) 19413-19424.
17. B. Beden, M.C. Morin, F. Hahn, C. Lamy, "In situ" analysis by infrared reflectance spectroscopy of the adsorbed species resulting from the electrosorption of ethanol on platinum in acid medium, *J. Electroanal. Chem.* 229 (1987) 353-366.
18. T. Iwasita, W. Vielstich, The electrochemical oxidation of ethanol on platinum: A SNIFTIRS study, *J. Electroanal. Chem.* 257 (1988) 319-324.
19. F. Vigier, C. Coutanceau, F. Hahn, E.M. Belgsir, C. Lamy, On the mechanism of ethanol electro-oxidation on Pt and PtSn catalysts: electrochemical and in situ IR reflectance spectroscopy studies, *J. Electroanal. Chem.* 563 (2004) 81-89.
20. D.M. dos Anjos, F. Hahn, J.M. Leger, K.B. Kokoh, G. Tremiliosi, J.M. Feliu, E. Herrero, P. Waszczuk, A. Crown, S. Mitrovski, A. Wieckowski, In situ FTIRS studies of the electrocatalytic oxidation of ethanol on Pt alloy electrodes, *J. Solid State Electrochem.* 11 (2007) 1567-1573.
21. A.B. Delpuch, F. Maillard, M. Chatenet, P. Soudant, C. Cremers, *Appl. Catal. B Env.* 181 (2016) 672-680.
22. Q. Wang, G.Q. Sun, L. Cao, L.H. Jiang, G.X. Wang, S.L. Wang, S.H. Yang, Q. Xin, High performance direct ethanol fuel cell with double-layered anode catalyst layer, *J. Power Sources* 177 (2008) 142-147.
23. Y. Paik, S.S. Kim, O.H. Han, Spatial distribution of reaction products in direct ethanol fuel cell, *Electrochem. Commun.* 11 (2009) 302-304.

24. A. Jablonski, P.J. Kulesza, A. Lewera, Oxygen permeation through Nafion 117 membrane and its impact on efficiency of polymer membrane ethanol fuel cell, *J. Power Sources* 196 (2011) 4714-4718.
25. I. Kim, O.H. Han, S.A. Chae, Y. Paik, S.H. Kwon, K.S. Lee, Y.E. Sung, H. Kim, *Angew. Chem. Int. Ed. Engl.* 50 (2011) 2270-2274.
26. H. Wang, Z. Jusys, R.J. Behm, Ethanol electro-oxidation on carbon-supported Pt, PtRu and Pt₃Sn catalysts: A quantitative DEMS study, *J. Power Sources* 154 (2006) 351-359.
27. K. Taneda, Y. Yamazaki, Study of direct type ethanol fuel cells: Analysis of anode products and effect of acetaldehyde, *Electrochim. Acta* 52 (2006) 1627-1631.
28. Y. Katayanagi, Y. Yamazaki, Effect of Fuel Flow Rate, Fuel Concentration, and O₂ Concentration of the Cathode Gas on the CO₂ Evolution of a Direct Ethanol Fuel Cell, *Electrochemistry* 78 (2010) 976-981.
29. F.C. Simoes, D.M. dos Anjos, F. Vigier, J.M. Leger, F. Hahn, C. Coutanceau, E.R. Gonzalez, G. Tremiliosi, A.R. de Andrade, P. Olivi, K.B. Kokoh, Electroactivity of tin modified platinum electrodes for ethanol electrooxidation, *J. Power Sources* 167 (2007) 1-10.
30. S. Ramachandran, U. Stimming, Well to wheel analysis of low carbon alternatives for road traffic, *Energy Environ. Sci.* 8 (2015) 3313-3324.
31. N. Nakagawa, Y. Kaneda, M. Wagatsuma, T. Tsujiguchi, Product distribution and the reaction kinetics at the anode of direct ethanol fuel cell with Pt/C, PtRu/C and PtRuRh/C, *J. Power Sources* 199 (2012) 103-109.
32. J.M. Jin, T. Sheng, X. Lin, R. Kavanagh, P. Hamer, P.J. Hu, C. Hardacre, A. Martinez-Bonastre, J. Sharman, D. Thompsett, W.F. Lin, The origin of high activity but low CO₂

- selectivity on binary PtSn in the direct ethanol fuel cell, *Phys. Chem. Chem. Phys.* 16 (2014) 9432-9440.
33. D.D. James, P.G. Pickup, Effects of crossover on product yields measured for direct ethanol fuel cells, *Electrochim. Acta* 55 (2010) 3824-3829.
 34. P. Majidi, P.G. Pickup, Determination of the average number of electrons released during the oxidation of ethanol in a direct ethanol fuel cell, *Electrochim. Acta* 182 (2015) 856-860.
 35. P. Majidi, R.M. Altarawneh, N.D.W. Ryan, P.G. Pickup, Determination of the efficiency of methanol oxidation in a direct methanol fuel cell, *Electrochim. Acta* 199 (2016) 210-217.
 36. A. Ghumman, G. Li, D.V. Bennett, P. Pickup, Online analysis of carbon dioxide from a direct ethanol fuel cell, *J. Power Sources* 194 (2009) 286-290.
 37. Y. Liu, S.-F. Zhao, S.-X. Guo, A.M. Bond, J. Zhang, Electrooxidation of Ethanol and Methanol Using the Molecular Catalyst [$\{\text{Ru}_4\text{O}_4(\text{OH})_2(\text{H}_2\text{O})_4\}(\gamma\text{-SiW}_{10}\text{O}_{36})_2$], *J. Am. Chem. Soc.* 138 (2016) 2617- 2628.
 38. L. Huang, E.G. Sorte, S.G. Sun, Y.Y.J. Tong, A straightforward implementation of in situ solution electrochemical ^{13}C NMR spectroscopy for studying reactions on commercial electrocatalysts: ethanol oxidation, *Chem. Commun.* 51 (2015) 8086-8088.
 39. K. Alayavalli, D.L. Bourell, *Rapid Prototyp. J.* 16 (2010) 268-274.
 40. C. Song, P.G. Pickup, Effect of Hot Pressing on the Performance of Direct Methanol Fuel Cells, *J. Appl. Electrochem* 34 (2004) 1065-1070.

41. A. Scheithauer, E. von Harbou, H. Hasse, T. Gruetzner, C. Rijksen, D. Zollinger, W.R. Thiel, ^1H - and ^{13}C -NMR spectroscopic study of chemical equilibria in the system acetaldehyde + water, *AIChE J.* 61 (2015) 177-187.
42. S. Sun, M.C. Halseid, M. Heinen, Z. Jusys, R.J. Behm, Ethanol electrooxidation on a carbon-supported Pt catalyst at elevated temperature and pressure: A high-temperature/high-pressure DEMS study, *J. Power Sources* 190 (2009) 2-13.
43. V. Rao, C. Cremers, U. Stimming, L. Cao, S.G. Sun, S.Y. Yan, G.Q. Sun, Q. Xin, Electro-oxidation of Ethanol at Gas Diffusion Electrodes A DEMS Study, *J. Electrochem. Soc.* 154 (2007) B1138-B1147.
44. D.D. James, D.V. Bennett, G.C. Li, A. Ghumman, R.J. Helleur, P.G. Pickup, Online analysis of products from a direct ethanol fuel cell, *Electrochem. Commun.* 11 (2009) 1877-1880.
45. R. Kavanagh, X.M. Cao, W.F. Lin, C. Hardacre, P. Hu, Origin of Low CO_2 Selectivity on Platinum in the Direct Ethanol Fuel Cell, *Angew. Chem. Int. Ed. Engl.* 51 (2012) 1572-1575.
46. Y.X. Wang, Y.J. Mi, N. Redmon, J. Holiday, Understanding Electrocatalytic Activity Enhancement of Bimetallic Particles to Ethanol Electro-oxidation. 1. Water Adsorption and Decomposition on Pt_nM ($n = 2, 3, \text{ and } 9$; $\text{M} = \text{Pt}, \text{Ru}, \text{ and } \text{Sn}$), *J. Phys. Chem. C* 114 (2010) 317.
47. Z.F. Xu, Y. Wang, Effects of Alloyed Metal on the Catalysis Activity of Pt for Ethanol Partial Oxidation: Adsorption and Dehydrogenation on Pt_3M ($\text{M} = \text{Pt}, \text{Ru}, \text{Sn}, \text{Re}, \text{Rh}, \text{ and } \text{Pd}$), *J. Phys. Chem. C* 115 (2011) 20565-20571.

48. S.E. Evarts, I. Kendrick, B.L. Wallstrom, T. Mion, M. Abedi, N. Dimakis, E.S. Smotkin, Ensemble Site Requirements for Oxidative Adsorption of Methanol and Ethanol on Pt Membrane Electrode Assemblies, *ACS Catal.* 2 (2012) 701-707.
49. H.F. Wang, Z.P. Liu, Comprehensive Mechanism and Structure-Sensitivity of Ethanol Oxidation on Platinum: New Transition-State Searching Method for Resolving the Complex Reaction Network, *J. Am. Chem. Soc.* 130 (2008) 10996-11004.
50. J. Mann, N. Yao, A.B. Bocarsly, Characterization and Analysis of New Catalysts for a Direct Ethanol Fuel Cell, *Langmuir* 22 (2006) 10432.
51. A. Kowal, M. Li, M. Shao, K. Sasaki, M.B. Vukmirovic, J. Zhang, N.S. Marinkovic, P. Liu, A.I. Frenkel, R.R. Adzic, Ternary Pt/Rh/SnO₂ electrocatalysts for oxidizing ethanol to CO₂, *Nat. Mater.* 8 (2009) 325.
52. E.A. Baranova, A. Tavasoli, T. Amir, *Electrocatalysis* 2 (2011) 89.
53. W.X. Du, Q. Wang, D. Saxner, N.A. Deskins, D. Su, J.E. Krzanowski, A.I. Frenkel, X.W. Teng, Highly Active Iridium/Iridium–Tin/Tin Oxide Heterogeneous Nanoparticles as Alternative Electrocatalysts for the Ethanol Oxidation Reaction, *J. Amer. Chem. Soc.* 133 (2011) 15172. 54.
54. J.C. Castro, M.H.M.T. Assumpcao, R.F.B. de Souza, E.V. Spinace, A.O. Neto, *Electrocatalysis* 4 (2013) 159.
55. M. Li, D.A. Cullen, K. Sasaki, N.S. Marinkovic, K. More, R.R. Adzic, Ternary Electrocatalysts for Oxidizing Ethanol to Carbon Dioxide: Making Ir Capable of Splitting C–C Bond, *J. Amer. Chem. Soc.* 135 (2013) 132.

56. L.A. Soares, C. Morais, T.W. Napporn, K.B. Kokoh, P. Olivi, Beneficial effects of rhodium and tin oxide on carbon supported platinum catalysts for ethanol electrooxidation, *J. Power Sources* 315 (2016) 47-55.
57. D.D. James, P.G. Pickup, Measurement of carbon dioxide yields for ethanol oxidation by operation of a direct ethanol fuel cell in crossover mode, *Electrochim. Acta* 78 (2012) 274-278.
58. J. Seweryn, A. Lewera, High selectivity of ethanol electrooxidation to carbon dioxide on platinum nanoparticles in low temperature polymer electrolyte membrane direct ethanol fuel cell, *Appl. Catal. B Environ.* 144 (2014) 129.

Chapter 4

Product Distributions and Efficiencies for Ethanol

Oxidation in a Proton Exchange Membrane

Electrolysis Cell

The principal author (Rakan M. Altarawneh) contributed to all aspects of the project as the main researcher including: literature review, performing all of the experiments, collecting and analyzing the data, designing some of the experiments, presenting and discussing the data and writing the first draft of the manuscript.

The corresponding author (Prof. Peter G. Pickup) was the principal investigator and developed the initial ideas for this research. He oversaw all aspects of the project, including supervision of the principal author (Rakan M. Altarawneh), the design of experiments, data analysis; he finalized and submitted the manuscript.

This chapter has been published as: -

(R.M. Altarawneh, P.G. Pickup, Product Distributions and Efficiencies for Ethanol Oxidation in a Proton Exchange Membrane Electrolysis Cell, *J. Electrochem. Soc.*, 164 (2017) F861-F865).

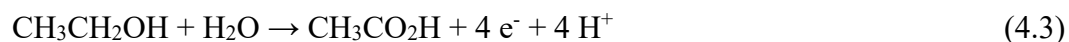
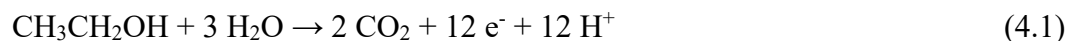
The raw data is provided in Appendix C.

4. Product Distributions and Efficiencies for Ethanol Oxidation in a Proton Exchange Membrane Electrolysis Cell

4.1 Introduction

The electrochemical oxidation of ethanol in cells with proton exchange membrane (PEM) electrolytes is of central importance to the development of energy technologies based on bio-ethanol. PEM-based direct ethanol fuel cell (DEFC)^{1,2} power systems are potentially one of the best alternatives to internal combustion engines,³ although their efficiencies will need to be increased significantly. Alternatively, ethanol electrolysis cells (EEC) can be used to produce hydrogen.⁴⁻⁶ In an EEC, ethanol is oxidized at the anode and protons are reduced to hydrogen at the cathode. In a DEFC, ethanol is oxidized at the anode and oxygen is reduced to water at the cathode. The attraction of these technologies arises from their high theoretical efficiencies and the perception that emissions will be low. However, the incomplete oxidation of ethanol at all known catalysts currently results in low efficiency cells and large amounts of byproducts.²

To achieve high energy efficiencies in EECs and DEFCs the faradaic efficiency (ϵ_F) for the electrochemical oxidation of ethanol to carbon dioxide (eq. 4.1) must be high.^{2,7} However, in practice low yields of CO₂ have generally been reported, with the major products being acetaldehyde (eq. 4.2) and acetic acid (eq. 4.3).



The faradaic efficiency is the ratio of the average number of electrons transferred per molecule of ethanol (n_{av}) to the maximum of 12 for the complete oxidation to CO₂ ($\epsilon_F = n_{av}/12$). It is determined by the product distribution according to eq. 4.4,⁸

$$n_{av} = \sum n_i f_i \quad (4.4)$$

where n_i is the number of electrons transferred to form product i and f_i is the fraction of ethanol converted to product i . The importance of n_{av} in determining the efficiency of ethanol oxidation technologies makes product analysis of central importance in the development of better anode catalysts.⁹

Although there have been many advances in the electrochemical performances (potential efficiency) of ethanol oxidation catalysts,⁹⁻¹² high faradaic efficiencies remain elusive. Pt alloys with metals such as Ru and Sn can increase the potential efficiency greatly, but there is generally a decrease in faradaic efficiency.^{7,9,13,14} In contrast, alloying Pt with Rh increases the faradaic efficiency, but decreases the potential efficiency.^{15,16} Currently, one of the best approaches appears to be to combine PtRh alloy nanoparticle catalysts with Sn oxide based support materials.^{17,18}

There have been many mechanistic studies of the oxidation of ethanol in liquid electrolyte cells at ambient temperature,^{9,11,19} with intermediates and products identified in many cases by infrared spectroscopy and/or differential electrochemical mass spectrometry (DEMS).^{9,11} In combination with computational studies,^{20,21} these have provided a good understanding of factors that influence the product distribution at ambient temperature. However, there have been relatively few studies of product distributions for ethanol oxidation at elevated temperatures, in either liquid electrolytes or PEM cells. Sun et al.²² conducted a comprehensive DEMS study of CO₂ production at a carbon supported Pt (Pt/C) electrode in aqueous sulfuric acid over a temperature range of 23–100 °C. CO₂ formation was found to increase with increasing temperature, decreasing ethanol

concentration, and decreasing potential between 0.48 and 0.68 V vs. RHE. Measurements of products from PEM-DEFCs have mainly been made by analyzing the anode exhaust solution only,^{7,13, 23-30} which provides inaccurate results due to crossover of products to the cathode, and chemical oxidation of ethanol by the oxygen supplied to the cathode.^{26,31} The latter problem can be avoided by using nitrogen and/or hydrogen at the cathode,³¹ while the loss of products by crossover can be addressed by analysis of the cathode exhaust.^{30, 31} However, these methods have only been applied simultaneously in one study.³² In that work, the effects of crossover were quantified and various methods for determining n_{av} at a Pt black anode were assessed.

The purpose of the work described in this chapter was to investigate and compare the potential dependences of product distributions and n_{av} for ethanol oxidation at commercial carbon supported Pt, PtRu and PtSn catalysts at 80 °C in a PEM electrolysis cell. Proton nuclear magnetic resonance (¹H-NMR) spectroscopy was used to measure the concentrations of acetaldehyde, acetic acid and residual ethanol exiting the cell, while CO₂ was analyzed with a commercial non-dispersive infra-red (NDIR) detector.³² The accuracy of the n_{av} values obtained by product analysis has been verified by comparison with the amount of ethanol consumed.

This is only the second study in which errors due to crossover and the chemical oxidation of ethanol by oxygen have been avoided.³² It provides the first accurate determination of products yields and stoichiometry for ethanol oxidation at carbon supported and alloy catalysts, and the first comparison of efficiencies between different catalysts.

4.2 Experimental

4.2.1 The Cell

A commercial fuel cell (5 cm² active area; Fuel Cell Technology Inc.) was operated as an electrolysis cell by supplying 0.1 M ethanol (Commercial Alcohols Inc.) solution to the anode at 0.2 or 0.5 mL min⁻¹ with a syringe pump and N₂ to the cathode at 35 mL min⁻¹. The cathode acts as a dynamic hydrogen electrode (DHE) and provides a relatively stable reference potential. The anode inlet and both outlets of the cell were modified with stainless steel tubing that connected directly to the graphite flow field plates. The flow field channels were sealed with ethyl-2-cyanoacrylate³³ in order to minimize absorption of ethanol and reaction products into the graphite plates.³¹ The cell was operated at 80 °C in all experiments.

Anodes were prepared using the following commercial catalysts. The carbon supported Pt catalyst (Pt/C) was HiSPECTM 13100, 70% Pt on a high surface area advanced carbon support (Alfa Aesar; Lot# M22A026). The carbon supported PtRu alloy catalyst (PtRu/C) was HiSPECTM 12100, 50% Pt and 25% Ru on a high surface area advanced carbon support (Alfa Aesar; Lot# P17B047). The carbon supported PtSn alloy catalyst (PtSn/C) was 40% HP PtSn alloy (3:1 atom%) on Vulcan XC-72 (BASF Fuel Cell Inc.; Lot# F0060910). Catalyst suspensions were prepared by sonication of the catalyst (21-39 mg) in ca. 0.2-0.4 mL of a 1:1 mixture of 1-propanol and Nafion solution (Dupont; 5% Nafion) for 3 h at ambient temperature. An appropriate amount of the suspension was spread onto Toray carbon fiber paper (CFP; TGP-H-090) with a spatula to give a metal loading of 3.2 mg cm⁻². Cathodes consisted of 4 mg cm⁻² Pt black on TGP-H-090.

Membrane and electrode assemblies (MEA) were prepared by pressing (room temperature; ca. 1.5 MPa) an anode and cathode onto a NafionTM 115 membrane in the cell.³⁴ Electrochemical

measurements were made under steady state conditions at constant cell potentials using a Hokuto Denko HA-301 potentiostat.

4.2.2 Ethanol and Product Analysis

The product collection apparatus is shown schematically in Figure 4.1. Ethanol and reaction products from the anode and cathode were combined before analysis. Liquids were collected in a trap cooled with a mixture of ice and dry ice, while CO₂ remaining in the N₂ stream was measured in real time with a commercial non-dispersive infrared CO₂ monitor (Telaire 7001).³⁵ The current and CO₂ readings were allowed to stabilize, and then averaged over a period of at least 100 s.

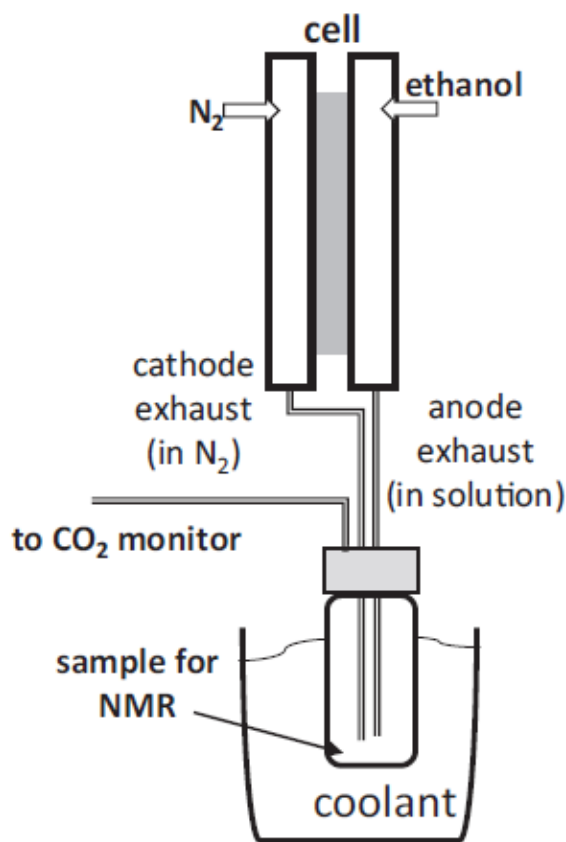


Figure 4.1. Schematic diagram of the product collection system.

For analysis by $^1\text{H-NMR}$, 400 μL samples collected from the trap were mixed with 100 μL of D_2O containing 32 mM fumaric acid as an internal standard, which gives a singlet peak in the spectra at 6.72 ppm.³² Spectra were recorded on a Bruker AVANCE III 300 spectrometer. The D_2O in the sampled provided the field frequency lock and spectra were referenced to sodium 3-(trimethylsilyl)-2,2,3,3-tetradeuteropropionic propionate at 0 ppm. The residual ethanol concentration was determined from the triplet at 1.10 ppm. The residual ethanol concentration was determined from the triplet at 1.10 ppm. The only products detected in the exhaust solution were acetic acid (singlet at 2.01 ppm) and acetaldehyde (doublet at 2.15 ppm). Acetaldehyde forms a dimer under the conditions of these experiments,³⁶ as indicated by a doublet at 1.24 ppm, and so the integral of the 1.24 ppm peak was added to give a single acetaldehyde concentration.

4.3. Results and Discussion

4.3.1 Polarization Curves

Figure 4.2 compares polarization curves for the oxidation of 0.1 M ethanol at the Pt/C, PtRu/C, and PtSn/C anodes. As expected from many previous studies,^{10,12} the current for ethanol oxidation at low potentials was much higher at the PtRu/C anode than the Pt/C anode. However, the current at the PtRu/C anode levelled off at potentials above 0.5 V, while the current at the Pt/C anode increased sharply to a peak at ca. 0.6 V that was approximately double the current at the PtRu/C anode. The plateau in the current at the PtRu/C anode suggests that it became limited by ethanol diffusion through the CFP backing layer, in which case this mass transport limited current (i_{lim}) can be described by eq. 4.5.³⁷

$$i_{lim} = n_{av}FADC/l \quad (4.5)$$

Where A is the area of the electrode, D is the diffusion coefficient, C is the concentration of ethanol, and l is the thickness of the CFP. Since changing the catalyst can only change n_{av} in eq. 4.5, the higher currents at the Pt/C anode at potentials ≥ 0.45 V in Figure 4.2 suggest that n_{av} was much higher than at the PtRu/C anode over this potential range.

The currents at the PtSn/C anode in Figure 4.2 were similar to those at the Pt/C anode at potentials below 0.35 V, but lower than those for both the Pt/C and PtRu/C anodes at higher potentials. The relatively poor performance of this electrode may be due to the lower loading of metal on the carbon support (40% vs. 70% and 75% for Pt/C and PtRu/C, respectively). The lower limiting current relative to the PtRu/C anode may indicate a lower n_{av} or may be due to an additional diffusion limitation in the catalyst layer, which was thicker because of the larger amount of carbon support. The PtSn/C catalyst employed here is same type as the PtSn₃/C catalysts from E-TEK employed and characterized by several other groups.³⁸ The 20% PtSn₃/C catalyst has been shown to be superior to 20% Pt/C from E-TEK for ethanol oxidation in a DEFC.³⁹ However, it is clearly inferior to the more advanced Johnson Matthey Pt/C and Pt/Ru/C catalysts from Alfa Aesar. The lower masses of Pt in the PtSn/C and PtRu/C anodes relative to the Pt/C anode was not a significant factor here, since the loading of the Pt/C catalyst could be decreased to match their Pt masses without a significant decrease in performance.

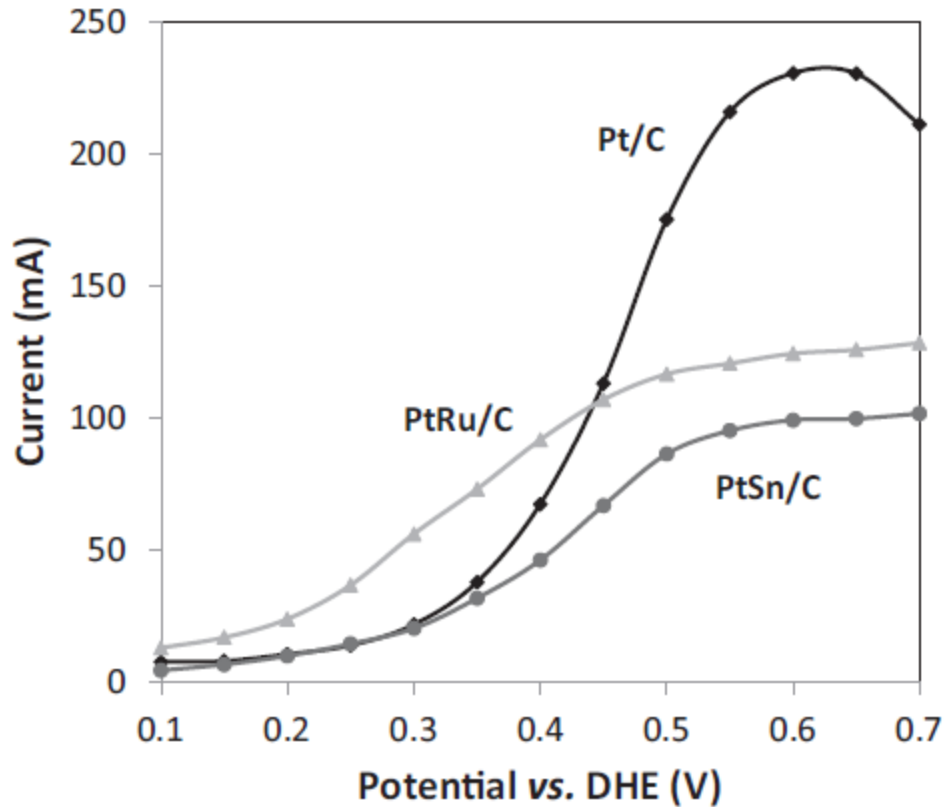


Figure 4.2. Polarization curves for the oxidation of 0.100 M ethanol (0.5 mL min^{-1}) at Pt/C, PtRu/C, and PtSn/C anodes at $80 \text{ }^\circ\text{C}$.

4.3.2. Stoichiometry (n_{av}) from the Consumption of Ethanol and Product Yields

If it is assumed that there were no losses of ethanol from the cell or during collection of the liquids from the combined anode (liquid + CO_2) and cathode ($\text{N}_2 + \text{CO}_2 + \text{condensed liquids}$) exhausts, n_{av} can be obtained directly from the concentration of ethanol in the exhaust liquid (C_{out}) by using eq. 4.6:

$$n_{av} = i/uF(C_{in} - C_{out}) \quad (4.6)$$

where i is the average current, and u and C_{in} are the flow rate and concentration, respectively, of the ethanol solution entering the cell. In these experiments 3.2% to 65.8% of the ethanol entering the cell was consumed electrochemically. Results for ethanol oxidation at the Pt/C, PtRu/C, and

PtSn/C anodes are plotted as a function of potential in Figure 4.3, together with values calculated from the product yields by using eq. 4.4. The two methods gave similar values, with small differences that can be attributed to experimental uncertainty.

It can be seen from the data in Figure 4.3 that n_{av} was much higher at the Pt/C anode than at the PtRu/C and PtSn/C anodes. The maximum n_{av} was 7.9 at 0.5 V, while values of 5.8 and 4.5 were obtained for PtSn/C and PtRu/C at this potential. These differences are consistent with the higher yields of CO₂ that have generally been reported for ethanol oxidation at Pt relative to PtRu and PtSn.^{7,13,35}

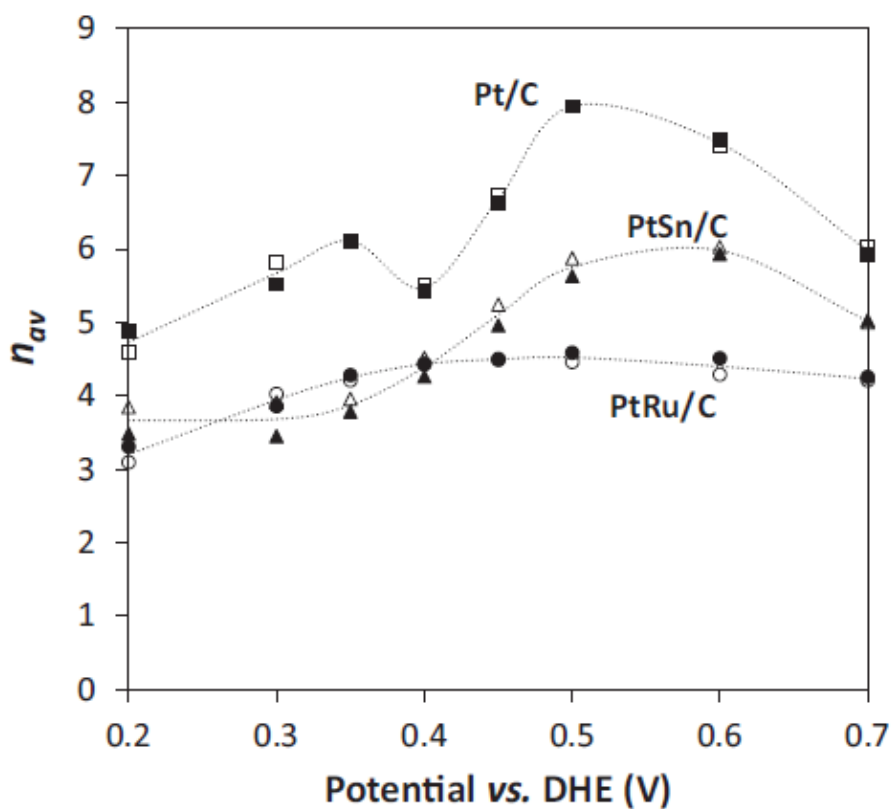


Figure 4.3. n_{av} vs. potential for the oxidation of 0.100 M ethanol (0.2 mL min⁻¹) at Pt/C, PtRu/C, and PtSn/C anodes at 80 °C. Solid points were calculated from the CO₂, acetic acid, and acetaldehyde yields by using eq. 4.4. Open points were calculated from the ethanol consumed by using eq. 4.6. Lines are drawn through the averages of the values from eqs. 4.4 and 4.6.

Interestingly, the potential dependences were significantly different for the three catalysts. Whereas n_{av} varied over only a narrow range at PtRu/C, from 3.2 to 4.5, PtSn/C gave a significant peak at ca. 0.55 V, while there were two peaks for Pt/C. The peak at 0.5 V for Pt/C can be attributed to CO₂ production via the oxidation of adsorbed CO (CO_{ads}),^{40–42} while the peak of $n_{av} = 6.1$ at 0.35 V suggests that there may be a pathway to CO₂ that does not involve CO_{ads} as an intermediate.

4.3.3 Product Distributions

Although n_{av} is the key parameter that determines the fuel efficiency of a DEFC or EEC, accurate determination of the product distribution is also very important. In addition to verifying the accuracy of n_{av} values obtained from eq. 4.6, it provides crucial information for analysis of the reaction kinetics, and the quantities of byproducts produced by the cell. Since acetaldehyde is an intermediate that can be recycled through the cell, whereas acetic acid is a terminal product, knowledge of their ratio is necessary to determine the overall system efficiency, and the final amount of acetic acid produced.

Figure 4.4 shows faradaic yields of CO₂ vs. potential for the three different anodes. These results parallel the n_{av} data in Figure 4.3 because changes in n_{av} are dominated by changes in the production of CO₂, due to the higher number of electrons transferred. However, the faradaic yields exaggerate the amount of CO₂ produced for the same reason. They are shown here to allow comparisons with literature reports, where faradaic yields have normally been presented.

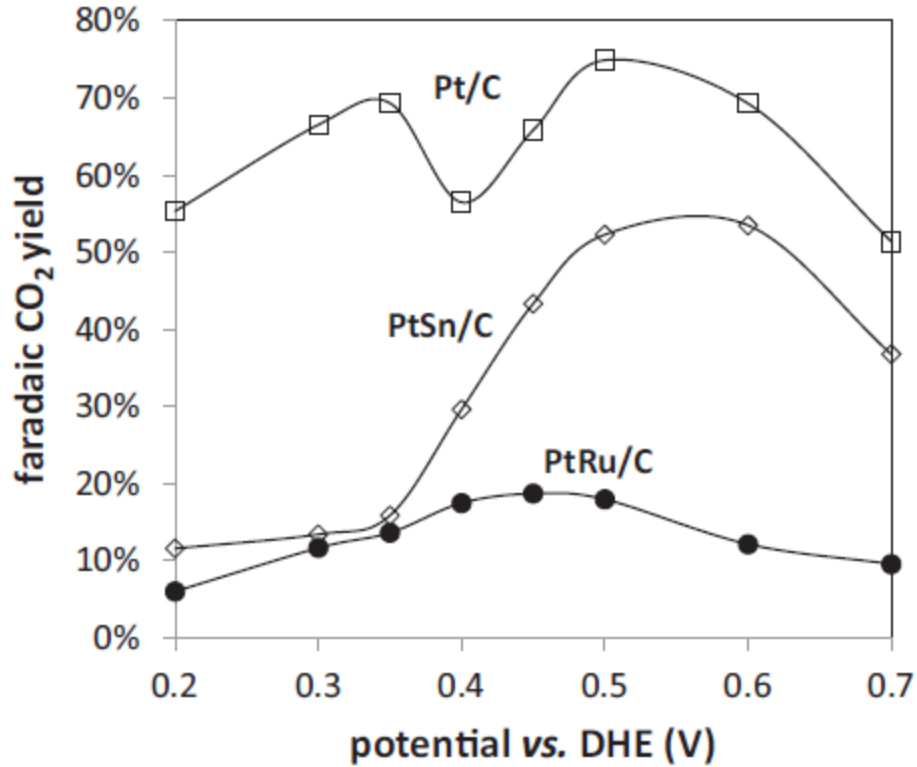


Figure 4.4. Faradiac yields of CO₂ vs. potential for oxidation of 0.100 M ethanol at Pt/C (□), PtRu/C (●), and PtSn/C (◇) anodes at 80 °C.

Figure 4.5 shows chemical yields of CO₂, acetic acid, and acetaldehyde as a function of potential. These are based only on the measured quantities of these three products, and have been calculated by using eq. 4.7:

$$\text{Chemical yield of } i = N_i / (N_{\text{carbon dioxide}} + N_{\text{acetic acid}} + N_{\text{acetaldehyde}}) \quad (4.7)$$

where N_i is the number of moles of ethanol required to produce the amount of product i measured in the exhaust from the cell. The measured amount of ethanol consumed by the cell was not used here in order to minimize the uncertainty, and to obtain yields that would produce independent values of n_{av} when used in eq. 4.4. However, it should be noted that the amount of ethanol required to form the measured products agreed very well with the measured decrease in ethanol

concentration. The sum of ethanol plus products exiting the cell was $99.3 \pm 1.1\%$ of the ethanol entering the cell averaged over the three data sets. This indicates that there was not a significant loss of ethanol or products, and that no other products were formed in significant ($>1\%$) quantities. This is an important result because it means that NMR analysis alone can provide the product distribution, with the yield of CO_2 calculated from the mass balance. Other minor products that have been reported include ethyl acetate,^{23,28} ethane,⁴⁰ methane,⁴⁰ ethane-1,1-diol,²⁸ and ethoxyhydroxyethane²⁸. None of these products were detected in this work.

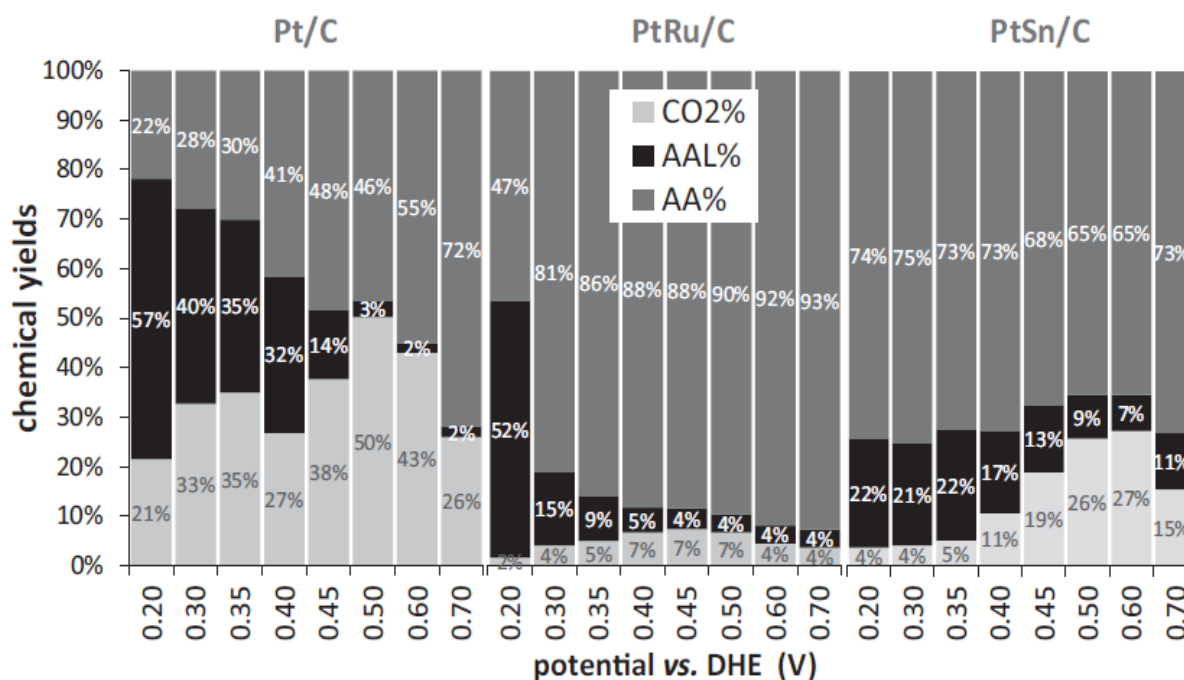


Figure 4.5. Chemical yields of CO_2 , acetic acid, and acetaldehyde as a function of potential for oxidation of 0.100 M ethanol at Pt/C, PtRu/C, and PtSn/C anodes at 80 °C.

It can be seen from the data in Figure 4.5 that the highest chemical yields of CO_2 were 50% for Pt/C at 0.5 V, 7% for PtRu/C at 0.45 V, and 27% for PtSn/C at 0.6 V. At lower potentials, which are necessary for the potential efficiency to be reasonable, the CO_2 yield remained substantial for Pt/C but dropped to very low values ($\leq 5\%$ for potentials of ≤ 0.35 V) for PtRu/C

and PtSn/C. At low potentials, Pt/C also gave high yields of acetaldehyde, which can be further oxidized to CO₂ and acetic acid if recycled and thereby increase the overall faradaic efficiency.

PtRu/C provided high selectivity for the oxidation of ethanol to acetic acid, which can be attractive for production of H₂ from ethanol electrolysis because acetic acid is an important commodity.² At low potentials, large amounts of acetaldehyde were also produced. PtSn/C also produced predominantly acetic acid, but the sample used here did not produce high enough currents at low potentials to be useful. The Pt/C catalyst was superior for faradaic efficiency, while the PtRu/C provided better potential efficiency and better efficiency for acetic acid production.

Comparative product distributions from the literature have previously been tabulated and reviewed.^{9,32} Many new catalysts that show improved activities and/or selectivity for the complete oxidation of ethanol at ambient temperature in liquid electrolytes have been developed.^{9,11} However, we are not aware of any reports of product distributions for ethanol oxidation at elevated temperature or in polymer electrolyte cells for these advanced catalysts.

4.3.4 Efficiencies

4.3.4.1 Ethanol Electrolysis Cell

The energy efficiency for production of hydrogen from the electrolysis of ethanol involves a number of factors, including the electrical energy required for the electrolysis and the various losses from incomplete oxidation of the ethanol and crossover to the cathode.⁵ However, in theory all of the residual ethanol and products can be collected without a significant loss of energy. Consequently, only the electrical energy input and the energy density of the ethanol (8.0 kWh kg⁻¹) will be considered here.

The electrical energy consumed (W_e) is given by eq. 4.8,⁵

$$W_e = (33 \text{ kWh kg}^{-1}) E_{cell} / 1.229 \quad (4.8)$$

where E_{cell} is the applied cell potential, the energy density of the hydrogen produced is 33 kWh kg^{-1} and the thermodynamic potential for electrolysis of water is 1.229 V . Consequently the energy consumed is proportional to the cell potentials vs. DHE in Figure 4.2. The PtRu/C anode therefore produced the highest electrical efficiency at currents up to ca. 100 mA while the Pt/C anode was more efficient at higher currents and could produce hydrogen at higher rates. Pt/C provides the added advantages of lower ethanol consumption and lower amounts of byproducts that would need to be utilized to maintain the overall efficiency of the system. At 0.5 V and 35 mA cm^{-2} the cell with the Pt/C anode consumed ca. 13 kWh kg^{-1} of electrical energy to provide hydrogen with an energy density of 33 kWh kg^{-1} . Based on the measured n_{av} of 7.94 , this would require ca. 5.8 kg of ethanol per kg of hydrogen, corresponding to 46 kWh kg^{-1} of chemical energy. The total energy input was therefore ca. 59 kWh kg^{-1} with concurrent production of ca. 3.5 kg of acetic acid. Electrolysis of water typically requires 50 kWh kg^{-1} , making this a potentially attractive technology for co-production of hydrogen and acetic acid, if the current density can be increased to be competitive with the ca. 1 A cm^{-2} level currently used for water electrolysis.⁵

4.3.4.2 Direct Ethanol Fuel Cell

Since n_{av} cannot be accurately determined in a DEFC because of the chemical reaction of ethanol with oxygen, values from ethanol electrolysis (Figure 4.3) are used here to estimate the efficiencies of DEFCs. This, for the first time, allows catalysts to be compared based on the overall efficiency that they will provide. If the loss of ethanol due to crossover is neglected for simplicity, the overall efficiency of a DEFC (\mathcal{E}_{DEFC}) can be calculated by using eq. 4.9:

$$\mathcal{E}_{DEFC} = \mathcal{E}_{rev} \times \mathcal{E}_E \times \mathcal{E}_F \quad (4.9)$$

where ε_{rev} is the theoretical efficiency of 96% at 80°C, ε_E is the potential efficiency ($\varepsilon_E = E_{cell}/E_{rev}$, where E_{rev} is the reversible cell potential of ca. 1.15 V), and $\varepsilon_F = n_{av}/12$. The potential efficiency includes losses due to the anode (η_{anode}) and cathode ($\eta_{cathode}$) overpotentials as well as the ohmic resistance of the cell (R) (eq. 4.10).

$$\varepsilon_E = (E_{rev} - \eta_{cathode} - \eta_{anode} - iR)/E_{rev} \quad (4.10)$$

If it is assumed that the overpotential of the DHE cathode was negligible, ($\eta_{anode} + iR$) is given approximately by the difference between the cell potential in Figure 4.2 and the standard potential of +0.084 V for reaction 4.1. In order to assess the effects that the different anodes would have on the efficiency of a DEFC through equations 4.9 and 4.10, values of $\eta_{cathode}$ were modelled by fitting a representative⁴³ iR corrected cathode polarization curve to a Tafel relationship (eq. 4.11), with $b = 47$ mV (the low value can be attributed to ethanol crossover⁴⁴) and a current of 1 mA at 0.81 V vs. DHE.

$$\eta_{cathode} = 1.23 \text{ V} - 0.81 \text{ V} + b \log(i/\text{mA}) \quad (4.11)$$

The average n_{av} at each potential in Figure 4.3 was used to calculate ε_F . Figure 4.6 shows the calculated DEFC efficiencies as a function of the current density.

It can be seen from the data in Figure 4.6 that the highest efficiency for a DEFC would have been obtained with the Pt/C anode over the whole current range. The PtSn/C anode would give the lowest efficiency at all currents, while PtRu/C would give slightly higher efficiencies and somewhat higher current densities. These results highlight the importance of developing catalysts with high selectivity for the oxidation of ethanol to CO₂, since this is the dominant factor influencing DEFC efficiency.

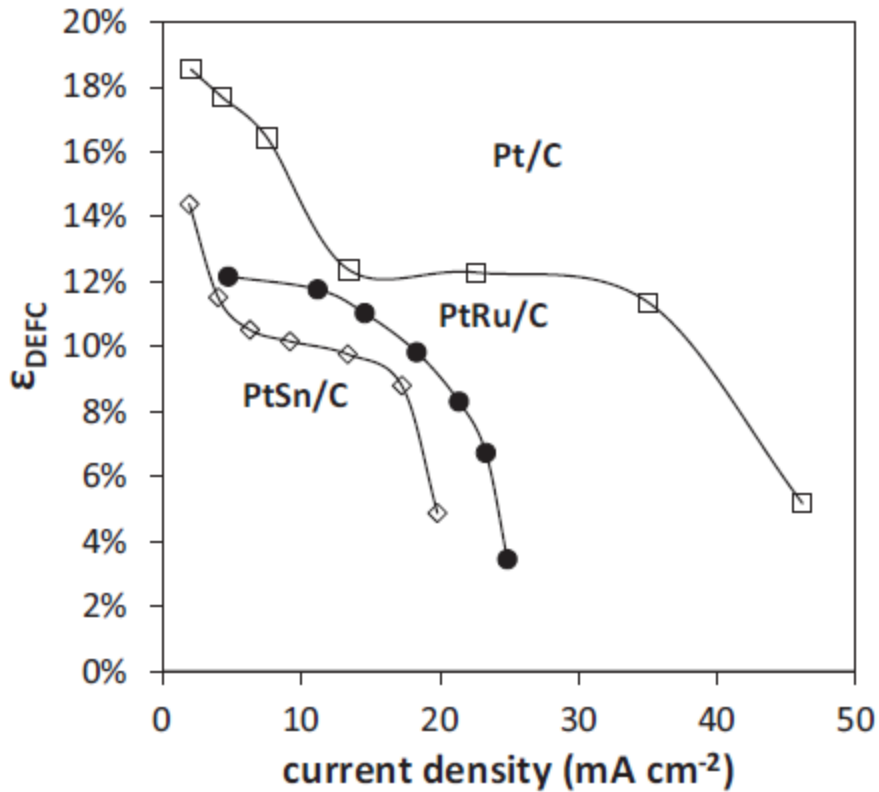


Figure 4.6. Predicted efficiency vs. current density for DEFCs operating at 80 °C with 0.1 M ethanol at 0.5 mL min⁻¹ with Pt/C (□), PtRu/C (●) and PtSn/C (◇) anodes.

It should be noted that the comparison of efficiencies calculated using eq. 4.10 depends on the cathode overpotentials employed. If the cathode overpotentials are higher, the PtRu/C anode can provide the highest overall efficiency in the intermediate current region, but the efficiencies with all anodes would be lower than shown in Figure 4.6. It should also be noted that the PtSn/C catalyst employed here had a significantly lower Pt loading than the Pt/C and PtRu/catalysts, which were also newer and more advanced. Consequently, the comparison of its efficiency with these state of the art catalysts does not accurately reflect the potential for advanced PtSn/C catalysts to contribute to DEFC and EEC technologies.

4.4 Conclusions

Proton NMR spectroscopy provides a simple, reliable, and accurate method for determining the stoichiometry, efficiency, and product distribution for ethanol electrolysis in fuel cell hardware. It is essential that the exhausts from both the anode and cathode are collected and analyzed because of the crossover of ethanol and all products through the membrane. However, the two exhausts can be combined for analysis unless knowledge of the extent of crossover is required. The combination of ethanol consumed and the quantities of acetic acid and acetaldehyde produced provide the necessary information without the need for analysis of the CO₂ produced, since the yield of CO₂ can be obtained from the mass balance.

The results for the commercial Pt/C, PtRu/C, and PtSn/C catalysts investigated here show that Pt/C would provide the highest efficiency for a fuel cell and for an electrolysis cell at high current densities, due to the higher stoichiometry of the ethanol oxidation reaction. However, PtRu/C provides better electrolysis efficiency than Pt/C at low current densities due to the lower overpotentials required. Also, PtRu/C will be the preferred catalyst if the acetic acid produced can be valorized.

References

1. S.P.S. Badwal, S. Giddey, A. Kulkarni, J. Goel, S. Basu, Direct ethanol fuel cells for transport and stationary applications – A comprehensive review, *Applied Energy*, 145 (2015) 80-103.
2. L. An, T.S. Zhao, Y. S. Li, Carbon-neutral sustainable energy technology: Direct ethanol fuel cells, *Renew. Sustain. Energy Rev.*, 50 (2015) 1462-1468.
3. S. Ramachandran, U. Stimming, Well to wheel analysis of low carbon alternatives for road traffic, *Energy Environ. Sci.*, 8 (2015) 3313-3324.

4. V. Bambagioni, M. Bevilacqua, C. Bianchini, J. Filippi, A. Lavacchi, A. Marchionni, F. Vizza, P. K. Shen, Self-Sustainable Production of Hydrogen, Chemicals, and Energy from Renewable Alcohols by Electrocatalysis, *ChemSusChem*, 3 (2010) 851-855.
5. C. Lamy, T. Jaubert, S. Baranton, C. Coutanceau, Clean hydrogen generation through the electrocatalytic oxidation of ethanol in a Proton Exchange Membrane Electrolysis Cell (PEMEC): Effect of the nature and structure of the catalytic anode, *J. Power Sources*, 245 (2014) 927-936.
6. A.R. de la Osa, A.B. Calcerrada, J.L. Valverde, E.A. Baranova, A. de Lucas-Consuegra, Electrochemical reforming of alcohols on nanostructured platinum-tin catalyst-electrodes, *Appl. Catal., B Env.*, 179 (2015) 276-284.
7. S. Rousseau, C. Coutanceau, C. Lamy, J.M. Leger, Direct ethanol fuel cell (DEFC): Electrical performances and reaction products distribution under operating conditions with different platinum-based anodes, *J. Power Sources*, 158 (2006) 18-24.
8. H. Wang, Z. Jusys, R.J. Behm, Ethanol Electrooxidation on a Carbon-Supported Pt Catalyst: Reaction Kinetics and Product Yields, *J. Phys. Chem. B*, 108 (2004) 19413-19424.
9. J. Friedl, U. Stimming, Model catalyst studies on hydrogen and ethanol oxidation for fuel cells, *Electrochim. Acta*, 101 (2013) 41-58.
10. E. Antolini, Catalysts for direct ethanol fuel cells, *J. Power Sources*, 170 (2007) 1-12.
11. Y. Wang, S.Z. Zou, W.B. Cai, Recent Advances on Electro-Oxidation of Ethanol on Pt- and Pd-Based Catalysts: From Reaction Mechanisms to Catalytic Materials, *Catalysts*, 5 (2015) 1507-1534.

12. M.A.F. Akhairi, S.K. Kamarudin, Catalysts in direct ethanol fuel cell (DEFC): An overview, *Int. J. Hydrogen Energy*, 41 (2016) 4214-4228.
13. N. Nakagawa, Y. Kaneda, M. Wagatsuma, T. Tsujiguchi, Product distribution and the reaction kinetics at the anode of direct ethanol fuel cell with Pt/C, PtRu/C and PtRuRh/C, *J. Power Sources*, 199 (2012) 103-109.
14. J. M. Jin, T. Sheng, X. Lin, R. Kavanagh, P. Hamer, P. J. Hu, C. Hardacre, A. Martinez-Bonastre, The origin of high activity but low CO₂ selectivity on binary PtSn in the direct ethanol fuel cell, J. Sharman, D. Thompsett, and W. F. Lin, *Phys. Chem. Chem. Phys.*, 16 (2014) 9432-9440.
15. J.P.I. deSouza, S.L. Queiroz, K. Bergamaski, E.R. Gonzalez, F.C. Nart, Electro-Oxidation of Ethanol on Pt, Rh, and PtRh Electrodes. A Study Using DEMS and in-Situ FTIR Techniques, *J. Phys. Chem. B*, 106 (2002) 9825-9830.
16. D.A. Cantane, W.F. Ambrosio, M. Chatenet, F.H.B. Lima, Electro-oxidation of ethanol on Pt/C, Rh/C, and Pt/Rh/C-based electrocatalysts investigated by on-line DEMS, *J. Electroanal. Chem*, 681 (2012) 56-65.
17. A. Kowal, M. Li, M. Shao, K. Sasaki, M.B. Vukmirovic, J. Zhang, N.S. Marinkovic, P. Liu, A.I. Frenkel, R.R. Adzic, Ternary Pt/Rh/SnO₂ electrocatalysts for oxidizing ethanol to CO₂, *Nature Materials*, 8 (2009) 325-330.
18. L.A. Soares, C. Morais, T.W. Napporn, K.B. Kokoh, P. Olivi, Beneficial effects of rhodium and tin oxide on carbon supported platinum catalysts for ethanol electrooxidation, *J. Power Sources*, 315 (2016) 47-55.
19. H. Mistry, A.S. Varela, S. Kuhl, P. Strasser, B.R. Cuenya, Nanostructured electrocatalysts with tunable activity and selectivity, *Nature Reviews Materials*, 1 (2016) 16009-16012.

20. H.F. Wang, Z. P. Liu, Comprehensive Mechanism and Structure-Sensitivity of Ethanol Oxidation on Platinum: New Transition-State Searching Method for Resolving the Complex Reaction Network, *J. Am. Chem. Soc.*, 130 (2008) 10996-11004.
21. R. Kavanagh, X.M. Cao, W.F. Lin, C. Hardacre, P. Hu, Origin of Low CO₂ Selectivity on Platinum in the Direct Ethanol Fuel Cell, *Angew. Chem. Int. Ed. Engl.*, 51 (2012) 1572-1575.
22. S. Sun, M.C. Halseid, M. Heinen, Z. Jusys, R.J. Behm, Ethanol electrooxidation on a carbon-supported Pt catalyst at elevated temperature and pressure: A high-temperature/high-pressure DEMS study, *J. Power Sources*, 190 (2009) 2-13.
23. Q. Wang, G.Q. Sun, L. Cao, L.H. Jiang, G.X. Wang, S.L. Wang, S.H. Yang, Q. Xin, High performance direct ethanol fuel cell with double-layered anode catalyst layer, *J. Power Sources*, 177 (2008) 142-147.
24. G. Andreadis, V. Stergiopoulos, S. Song, P. Tsiakaras, Direct ethanol fuel cells: The effect of the cell discharge current on the products distribution, *Appl. Catal., B Env.*, 100 (2010) 157-164.
25. Y. Katayanagi, Y. Yamazaki, Effect of Fuel Flow Rate, Fuel Concentration, and O₂ Concentration of the Cathode Gas on the CO₂ Evolution of a Direct Ethanol Fuel Cell, *Electrochemistry*, 78 (2010) 976-981.
26. A. Jablonski, P.J. Kulesza, A. Lewera, Oxygen permeation through Nafion 117 membrane and its impact on efficiency of polymer membrane ethanol fuel cell, *J. Power Sources*, 196 (2011) 4714-4718.
27. M.Y. Zhu, G.Q. Sun, Q. Xin, Effect of alloying degree in PtSn catalyst on the catalytic behavior for ethanol electro-oxidation, *Electrochim. Acta*, 54 (2009) 1511-1518.

28. I. Kim, O.H. Han, S.A. Chae, Y. Paik, S.H. Kwon, K.S. Lee, Y.E. Sung, and H. Kim, Catalytic Reactions in Direct Ethanol Fuel Cells, *Angew. Chem. Int. Ed. Engl.*, 50 (2011) 2270-22774.
29. J. Seweryn, A. Lewera, High selectivity of ethanol electrooxidation to carbon dioxide on platinum nanoparticles in low temperature polymer electrolyte membrane direct ethanol fuel cell, *Appl. Catal. B Environ*, 144 (2014) 129-134.
30. A.S. Arico, P. Creti, P.L. Antonucci, V. Antonucci, Comparison of Ethanol and Methanol Oxidation in a Liquid-Feed Solid Polymer Electrolyte Fuel Cell at High Temperature, *Electrochem. Solid. State. Lett*, 1 (1998) 66-68.
31. D.D. James, P.G. Pickup, Effects of crossover on product yields measured for direct ethanol fuel cells, *Electrochim. Acta*, 55 (2010) 3824-3829.
32. R.M. Altarawneh, P. Majidi, P.G. Pickup, Determination of the efficiency of ethanol oxidation in a proton exchange membrane electrolysis cell, *J. Power Sources*, 351 (2017) 106-114.
33. K. Alayavalli, D.L. Bourell, Fabrication of modified graphite bipolar plates by indirect selective laser sintering (SLS) for direct methanol fuel cells, *Rapid Prototyping Journal*, 16 (2010) 268-274.
34. C. Song, P.G. Pickup, Effect of Hot Pressing on the Performance of Direct Methanol Fuel Cells, *J. Appl. Electrochem*, 34 (2004) 1065-1070.
35. A. Ghumman, G.Li, D.V. Bennett, P.G. Pickup, Online analysis of carbon dioxide from a direct ethanol fuel cell, *J. Power Sources*, 194 (2009) 286-290.

36. A. Scheithauer, E. von Harbou, H. Hasse, T. Gruetzner, C. Rijksen, D. Zollinger, and W. R. Thiel, ^1H - and ^{13}C -NMR spectroscopic study of chemical equilibria in the system acetaldehyde + water, *AIChE J.*, 61 (2015) 177-187.
37. P. Majidi, R.M. Altarawneh, N.D.W. Ryan, P.G. Pickup, Determination of the efficiency of methanol oxidation in a direct methanol fuel cell, *Electrochim. Acta*, 199 (2016) 210-217.
38. F. Colmati, E. Antolini, E.R. Gonzalez, Ethanol Oxidation on Carbon Supported Pt-Sn Electrocatalysts Prepared by Reduction with Formic Acid, *J. Electrochem. Soc.*, 154 (2007) B39-B47.
39. F. Colmati, E. Antolini, E.R. Gonzalez, Effect of temperature on the mechanism of ethanol oxidation on carbon supported Pt, PtRu and Pt₃Sn electrocatalysts, *J. Power Sources*, 157 (2006) 98-103.
40. H. Wang, Z. Jusys, R.J. Behm, Ethanol electro-oxidation on carbon-supported Pt, PtRu and Pt₃Sn catalysts: A quantitative DEMS study, *J. Power Sources*, 154 (2006) 351-359.
41. A. Ghumman, P.G. Pickup, Efficient electrochemical oxidation of ethanol to carbon dioxide in a fuel cell at ambient temperature, *J. Power Sources*, 179 (2008) 280-285.
42. P. Majidi, P.G. Pickup, Improving carbon dioxide yields and cell efficiencies for ethanol oxidation by potential scanning, *J. Power Sources*, 269 (2014) 173-179.
43. G. Li, P.G. Pickup, Analysis of performance losses of direct ethanol fuel cells with the aid of a reference electrode, *J. Power Sources*, 161 (2006) 256-263.
44. V. Paganin, E. Sitta, T. Iwasita, W. Vielstich, Methanol crossover effect on the cathode potential of a direct PEM fuel cell, *J. Appl. Electrochem.*, 35 (2005) 1239-1243.

Chapter 5

Pt and PtRu Catalyst Bilayers Increase Efficiencies for Ethanol Oxidation in Proton Exchange Membrane Electrolysis and Fuel Cells

The principal author (Rakan M. Altarawneh) contributed to all aspects of the project as the main researcher including: literature review, performing all of the experiments, collecting and analyzing the data, designing some of the experiments, presenting and discussing the data and writing the first draft of the manuscript.

The corresponding author (Prof. Peter G. Pickup) was the principal investigator and developed the initial ideas for this research. He oversaw all aspects of the project, including supervision of the principal author (Rakan M. Altarawneh), the design of experiments, data analysis; he finalized and submitted the manuscript.

This chapter has been published as: -

(R.M. Altarawneh, P.G. Pickup, Pt and PtRu catalyst bilayers increase efficiencies for ethanol oxidation in proton exchange membrane electrolysis and fuel cells, *J. Power Sources*, 366 (2017) 27-32).

The raw data is provided in Appendix D.

5. Pt and PtRu Catalyst Bilayers Increase Efficiencies for Ethanol Oxidation in Proton Exchange Membrane Electrolysis and Fuel Cells

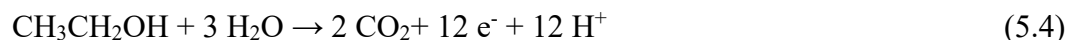
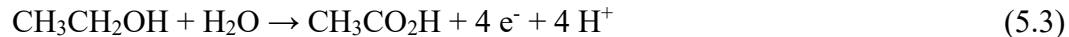
5.1 Introduction

Bio-ethanol is an attractive renewable fuel for use in fuel cells for many reasons, including its high energy density, relative safety, and the well-developed infrastructure for its production and distribution.¹⁻² Direct ethanol fuel cells (DEFC) are potentially one of the best low emission power sources for transportation,³ and have many other potential applications.^{2,4} Alternatively, ethanol can be oxidized in an ethanol electrolysis cell (EEC) to produce hydrogen for use in fuel cells.⁵ Hydrogen fuel cells are already well developed, and can provide much higher power densities than DEFCs.⁶⁻⁷

One of the fundamental advantages of fuel technology over the use of heat engines is the prospect of higher efficiencies. This will become increasingly important as renewable fuels are substituted for fossil fuels. The efficiency of a DEFC is determined by the thermodynamic efficiency ($\varepsilon_{rev} = 97\%$ at 25 °C),⁸ the potential efficiency ($\varepsilon_E = E_{cell}/E_{rev}$, where E_{cell} is the cell potential and E_{rev} is the reversible cell potential of ca. 1.15 V),⁸ the faradaic efficiency (ε_F), and fuel losses due to crossover of ethanol and oxygen through the membrane (ε_C), according to equation 5.1.¹

$$\varepsilon_{DEFC} = \varepsilon_{rev} \varepsilon_E \varepsilon_F \varepsilon_C \quad (5.1)$$

The faradaic term arises from the lower number of electrons transferred (n) for the partial oxidation of ethanol to acetaldehyde ($n = 2$; eq. 5.2) and acetic acid ($n = 4$; eq. 5.3), relative to complete oxidation to CO₂ ($n = 12$; eq. 5.4). It is the ratio of the average number of electrons transferred (n_{av}) to the maximum of 12 ($\varepsilon_F = n_{av}/12$).



The stoichiometry of the ethanol oxidation reaction (n_{av}) is also a central parameter in the electrolysis of ethanol, since it determines the ratio of hydrogen production to the consumption of ethanol. It can be determined more accurately in an EEC, where ethanol is only consumed electrochemically, than a DEFC where ethanol also reacts chemically with oxygen.⁹ In this work, n_{av} has been determined in an EEC by measurement of the amount of ethanol consumed (eq. 5.5),⁹

$$n_{av} = i/uF(C_{in} - C_{out}) \quad (5.5)$$

where i is the average current, u is the flow rate of the ethanol solution, C_{in} is the initial ethanol concentration, and C_{out} is the concentration of ethanol in the combined anode and cathode exhausts.

The multiplication of the potential and faradaic efficiency terms in eq. 5.1 means that both must be high to provide a competitive overall efficiency. However, this has not yet been achieved.¹ For proton exchange membrane cells, Pt anode catalysts can provide relatively high faradaic efficiencies,^{9, 11} but potential efficiencies are low. Alloying of Pt with Ru and/or Sn (for example) can significantly increase the potential efficiency,¹² but results in lower faradaic efficiencies.¹³⁻¹⁵ The purpose of the work reported in this chapter was therefore to explore the effects of combining discrete Pt and PtRu catalysts as a mixture or in separate layers in the anode of an EEC. It was postulated that the acetaldehyde intermediate formed at the PtRu catalyst could be oxidized at the Pt catalyst to increase the faradaic efficiency, while maintaining the higher potential efficiency of the PtRu catalyst.

5.2 Experimental

A commercial fuel cell (5 cm² active area; Fuel Cell Technology Inc.) with small modifications¹⁰ was used with a 4 mg cm⁻² Pt black cathode, Nafion™ 115 membrane (acidic polymer electrolyte) and various anodes. The gaskets were 0.25 mm fibre-glass reinforced Teflon on each side of the membrane. The compression was ca. 15 kg cm⁻².¹⁶ Ethanol (Commercial Alcohols Inc.) solution (0.100 M in water) was supplied to the anode at 0.2 or 0.5 mL min⁻¹ with a syringe pump and N₂ was passed over the cathode at 35 mL min⁻¹ to avoid interference from oxygen. The cathode acts a Dynamic Hydrogen Electrode (DHE). Electrochemical measurements were made at 80 °C under steady state conditions and constant cell potentials using a Hokuto Denko HA-301 potentiostat.

Anodes were prepared using commercial carbon supported Pt (HiSPEC® 13100, 70% Pt on a high surface area advanced carbon support (Alfa Aesar; Lot# M22A026)) and PtRu alloy (HiSPEC® 12100, 50% Pt and 25% Ru on a high surface area advanced carbon support (Alfa Aesar; Lot# P17B047)) catalysts. Suspensions of the catalyst in a ca. 1:1 mixture of 1-propanol and Nafion® solution (Dupont; 5% Nafion) were spread onto Toray™ carbon fiber paper (CFP; TGP-H-090) with a spatula to give a metal loading of 3.2 mg cm⁻². For preparation of the bilayer anodes, a 1.6 mg cm⁻² Pt layer was applied to the CFP, allowed to dry, and then coated with a 1.6 mg cm⁻² PtRu layer (designated as Pt on PtRu relative to the membrane; see Figure 5.2A), or vice versa (PtRu on Pt). Electrodes were allowed to dry overnight at ambient temperature to remove residual propanol. Smooth, uniform catalyst layers with a thickness of ca. 40 μm were obtained.

Each membrane and electrode assembly was broken in over a period of days. The cell was flooded with water for one day at room temperature to hydrate the membrane and then flushed with water at 80 °C for 1 h. It was then operated at 0.7 V for at least 2 h before recording

polarization curves from 0.7 V to 0.1 V and from 0.1 V to 0.7 V (0.05 V steps for 300 s). There was only minor hysteresis between the two curves. Preliminary CO₂ measurements were made and then the cell was shut-down and flushed with water. The reported measurements were made after one of more days of stable operation, from 0.7 to 0.1 V following operation at 0.7 V for at least 1 h.

For analysis of the reaction products and residual ethanol, the anode and cathode exhausts were combined in a trap cooled with a mixture of ice and dry ice. CO₂ remaining in the N₂ stream was measured in real time with a commercial non-dispersive infrared CO₂ monitor (Telaire 7001).¹⁵ The current and CO₂ readings were allowed to stabilize, and then averaged over a period of at least 100 s. The liquid collected in the trap was analyzed by ¹H-NMR as previously described.¹⁰ The measured concentrations of ethanol, acetic acid, acetaldehyde and CO₂ were used to determine the faradaic yield of each product. The average charge balance was $98.4 \pm 2.2\%$ and the average mass balance was $99.4 \pm 1.4\%$, indicating that the product collection efficiency was high and that no other products (such as CH₄ which would have been lost into the gas stream) were formed in significant quantities. Other possible minor products⁹ would have been seen in the NMR spectra if produced in significant quantities.

5.3 Results and Discussion

5.3.1 Polarization Curves

Figure 5.1 shows polarization curves for the oxidation of 0.100 M ethanol at anodes prepared with the Pt and PtRu catalysts individually, with a homogeneous mixture of the two catalysts, and with discrete layers of the catalysts. The data for the individual catalysts has been previously presented and discussed.⁹ The PtRu catalyst oxidizes ethanol at a lower potential than

Pt because Ru-OH is formed at lower potentials than Pt-OH. However, the main product is acetic acid rather than CO₂. Pt, which oxidizes as much as 50% of the ethanol to CO₂,⁹ provides higher currents than PtRu at potentials above ca. 0.45 V because of the higher number of electrons transferred per molecule of ethanol. Based on this analysis of the differences between Pt and PtRu, the mixed Pt + PtRu layer would be expected to provide higher currents than Pt alone at low potentials, but lower currents at high potentials, and that is what is observed in Figure 5.1. However, there was a narrow region at ca. 0.45 V where the mixed layer gave higher currents than either catalyst alone, indicating that there was a synergy between the two catalysts.

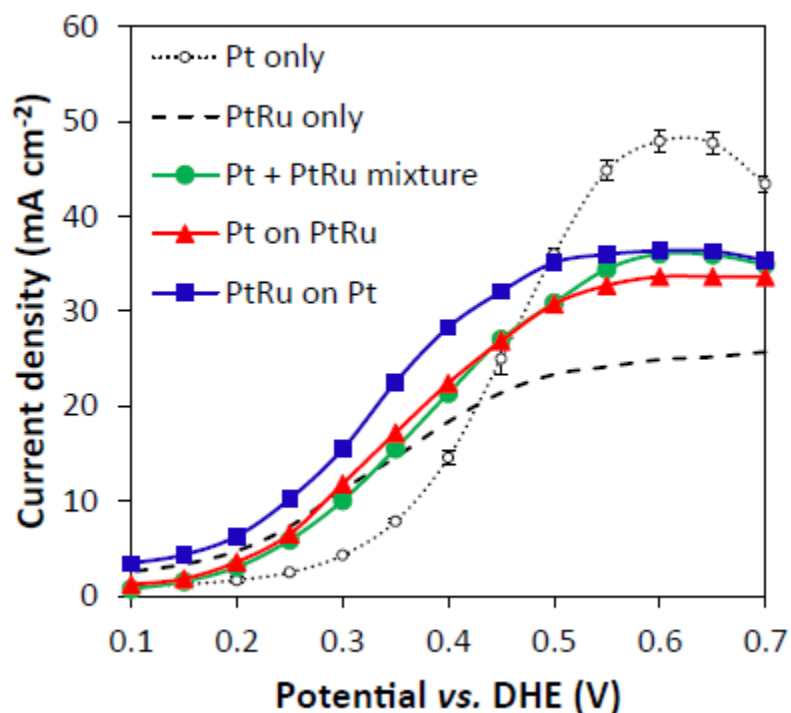
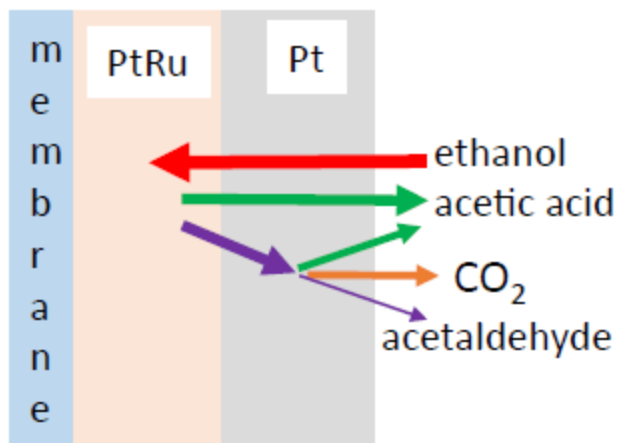


Figure 5.1. Polarization curves for the oxidation of 0.100 M ethanol (0.5 mL min⁻¹) at Pt (····), PtRu (- - -), Pt+ PtRu (●), Pt on PtRu (▲) and PtRu on Pt (■) anodes at 80 °C.

Since PtRu provides the fastest oxidation of ethanol at low potentials, and produces significant amounts of acetaldehyde at low potentials,⁹ it was envisaged that a Pt layer on top of a PtRu layer could be used to oxidize the acetaldehyde before it left the catalyst layer, and thereby

increase the overall efficiency of ethanol oxidation. This is shown schematically in Figure 5.2A. Because of the low activity of the Pt catalyst at low potentials, most of the ethanol will diffuse through the Pt layer to the PtRu layer, although some will be oxidized in the Pt layer (not shown in Figure 5.2A). However, the polarization curve for the Pt on PtRu bilayer in Figure 5.1 is not consistent with this scenario because the currents observed at potentials below 0.3 V were lower than at the PtRu anode, and the polarization curve was not significantly different from that for the mixture of Pt with PtRu. Curiously, reversing the order of the two catalyst layers produced higher currents than all of the other anodes for potentials below 0.5 V, although Pt produced higher currents at higher potentials.

A: Pt on PtRu



B: PtRu on Pt

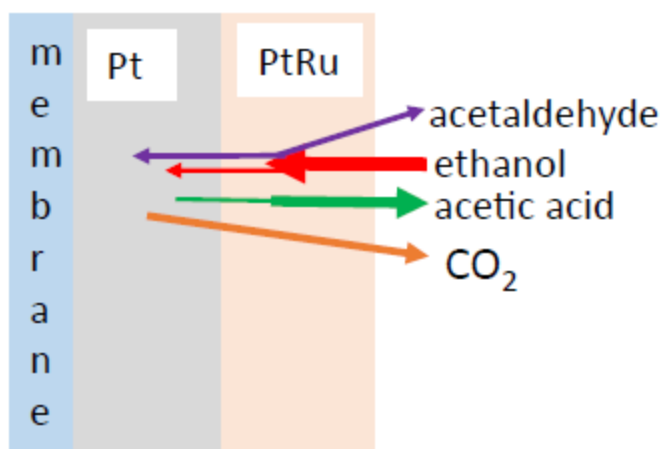


Figure 5.2. Schematic diagrams of some of the reactions and transport processes within bilayer anodes.

Overall, the mixed anode and both bilayers showed significant synergy between the Pt and PtRu catalysts. In order to understand this, and the differences seen in the polarization curves for the various anodes containing both Pt and PtRu, product distributions were measured as a function of potential. These, combined with the currents, allow the net rate of formation of each product to be obtained, which provides insight into the synergies between the two catalysts.

5.3.2 Product Distributions

Figure 5.3A shows faradaic yields of CO₂, acetic acid, and acetaldehyde obtained from analysis of the products in the cell exhaust. Two different Pt anodes were tested in order to check an anomalous dip in the CO₂ yield seen at ca. 0.4 V. Full product analysis for the second Pt anode focused on the 0.3 – 0.45 V region and so the data for the two Pt anodes is plotted separately. It has been speculated that the two peaks seen in the CO₂ yield at Pt may be due to a change in mechanism.⁹

The yields of CO₂ obtained for the bilayers and mixed Pt + PtRu layer were intermediate between those for Pt and PtRu alone, with the exception of the PtRu on Pt bilayer at 0.4 V which gave a slightly higher yield than Pt alone. At 0.2 and 0.3 V, the CO₂ yields for the bilayer and mixed anodes were closer to those for PtRu, but increased sharply at higher potentials to become closer to the values for Pt. This is highly significant because the CO₂ yield is the dominant factor determining the faradaic efficiency, and the high CO₂ yields for the bilayer anodes are obtained at much higher current densities than for Pt. Most notably, at 0.4 V the PtRu on Pt bilayer produced a CO₂ yield of 59% at 28 mA cm⁻², while the Pt anode provided 56% CO₂ at 13 mA cm⁻².

Acetic acid yields for the mixed and bilayer anodes were also intermediate between those for Pt and PtRu alone (Figure 5.3B), and closer to those for PtRu at low potentials and Pt at high potentials. However, acetaldehyde yields were generally lower at the mixed and bilayer anodes than either the Pt or PtRu anodes. For the PtRu on Pt anode, the yield of acetaldehyde was only 56% of the yield for the PtRu anode, on average. This validates the strategy of using Pt to oxidize the acetaldehyde produced by the more active PtRu catalyst before it can leave the anode, illustrated in Figure 5.2. Both the mixed and bilayers anodes gave very low yields of acetaldehyde at 0.35 V and higher.

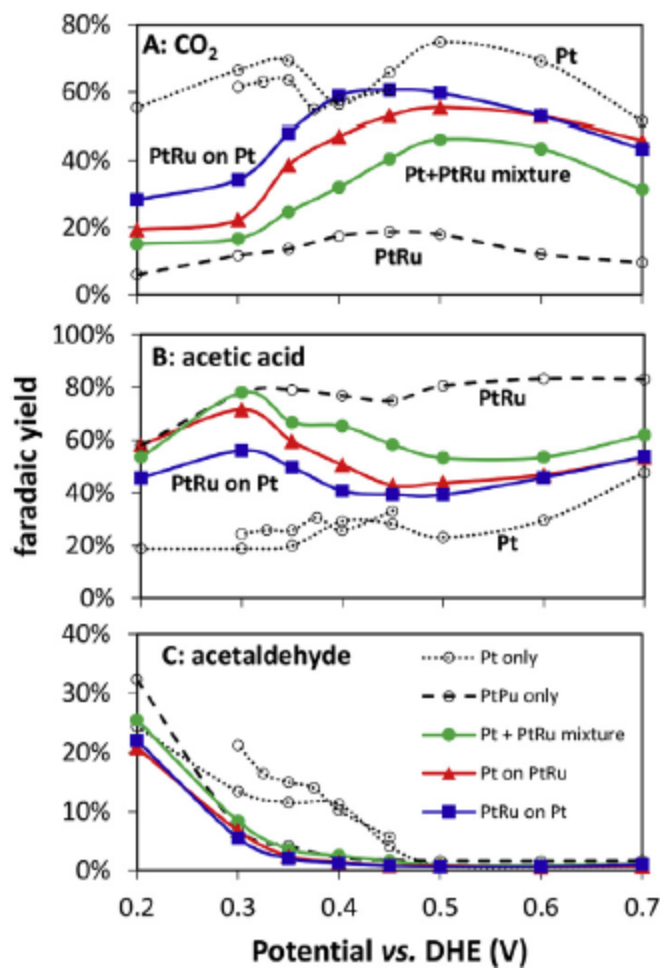


Figure 5.3. Faradaic yields of CO₂ (A), acetic acid (B), and acetaldehyde (C) vs. potential for oxidation of 0.100 M ethanol (0.2 mL min⁻¹) at Pt (·····), PtRu (- - -), Pt + PtRu (●), Pt on PtRu (▲) and PtRu on Pt (■) anodes at 80 °C.

The average acetaldehyde yield was only 1.1% for the PtRu on Pt anode over the potential range of 0.35 - 0.7 V. Neither the order of the two layers nor whether the catalysts were mixed affected the acetaldehyde yield significantly. This, together with the relatively small yields of acetaldehyde at all of the anodes at > 0.4 V (Figure 5.3C), indicates that there was some other, more important factor responsible for the high activity and CO₂ to acetic acid ratios for the PtRu on Pt bilayer anode.

5.3.3 Stoichiometry and Efficiency

Figure 5.4 shows n_{av} as a function of potential for the oxidation of ethanol at the Pt, PtRu, mixed and bilayer anodes, obtained from the concentration of ethanol consumed (eq. 5.5). At most potentials, n_{av} values for the mixed and bilayer anodes were intermediate between those for the Pt and PtRu catalysts alone, as would be expected. However, from 0.35 to 0.45 V n_{av} for the bilayer anodes was close to, and even exceeded, the values for Pt. n_{av} was generally lower for the mixed anode, and at low potentials was close to the values for PtRu alone.

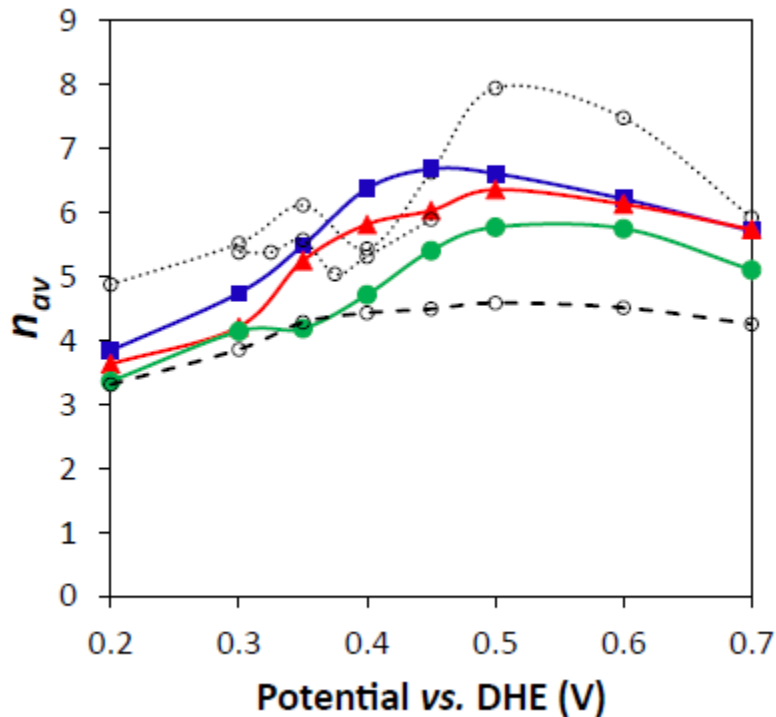


Figure 5.4. n_{av} from eq. 5.5 vs. potential for the oxidation of 0.100 M ethanol (0.2 mL min^{-1}) at Pt (·····; data for 2 different anodes), PtRu (- - -), Pt + PtRu (●), Pt on PtRu (▲) and PtRu on Pt (■) anodes at 80 °C.

The high n_{av} at 0.40 V for the bilayers, relative to Pt or PtRu alone, leads to significant increases in fuel efficiency for ethanol electrolysis, and the higher current densities would decrease

system costs. Use of the bilayers would also increase the thermal efficiency ($\epsilon_{rev} \epsilon_E$) and overall efficiency of a DEFC, because the cell potential would be higher and less ethanol would be consumed. However, this is difficult to demonstrate and quantify with a DEFC because of the effects of crossover of ethanol to the cathode, where it reacts chemically with oxygen.^{9,10,17} Consequently, representative DEFC efficiencies were calculated by using eq. 5.1, with E_{cell} estimated from the anode potentials vs. DHE in Figure 5.1 and a cathode polarization curve for the same cell.^{9,18} The results are shown in Figure 5.5 as functions of the power density (A) and current density (B) of the DEFC. Since the loss of fuel due to crossover will depend on many factors, including the membrane, cell design and operating conditions, it was not included in these efficiency estimates (i.e. $\epsilon_C = 1$ in eq. 5.1).

Surprisingly, the Pt catalyst would provide the best efficiency at the lowest power and current densities. Although the PtRu and PtRu on Pt anodes gave much higher currents at low potentials, which provide the highest potential efficiencies, this is more than offset by the lower stoichiometry (e.g. $n_{av} = 6.1$ for Pt at 7.5 mA cm^{-2} vs. $n_{av} = 3.8$ for PtRu on Pt at 6.3 mA cm^{-2}). At higher power densities (ca. $4 - 9 \text{ mW cm}^{-2}$), the PtRu on Pt anode would provide significantly higher efficiencies than Pt due to the lower anode potential, since the stoichiometries were similar. The Pt on PtRu anode would also be more efficient than Pt at ca. $5 - 7 \text{ mW cm}^{-2}$. Neither the PtRu anode nor the mixed Pt + PtRu anode would provide better efficiency or maximum power density than the Pt anode. These differences between the efficiencies of the anodes are paralleled in the plots of efficiency vs. current density.

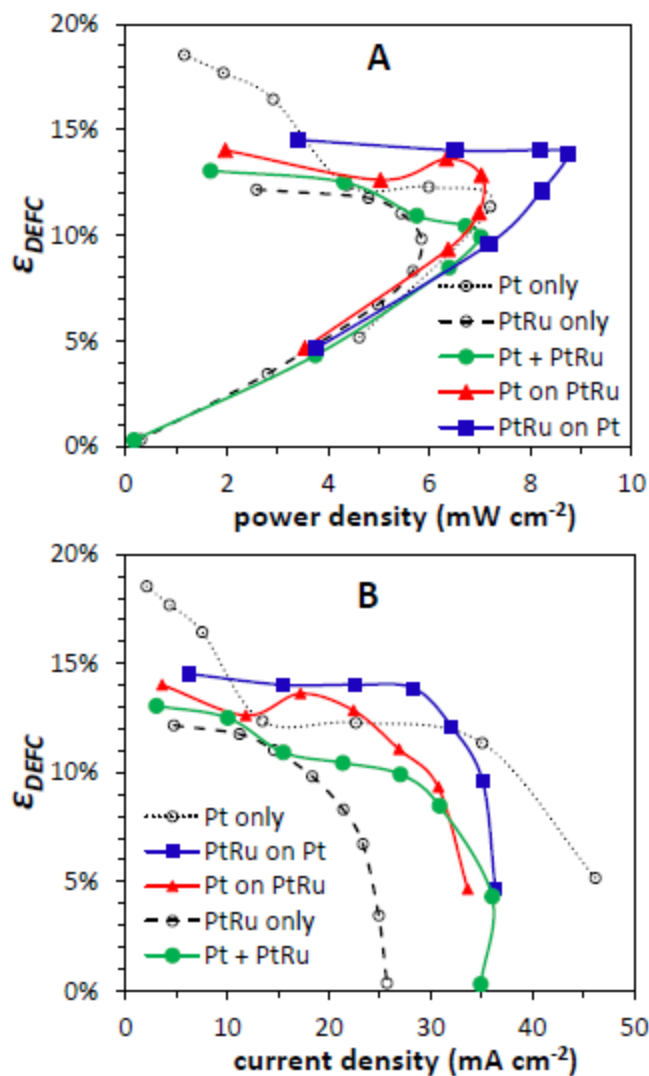


Figure 5.5. Predicted efficiency vs. power density (A) and current density (B) for DEFCs operating with 0.100 M ethanol at 80 °C at Pt (\cdots), PtRu ($-\ -$), Pt + PtRu (\bullet), Pt on PtRu (\blacktriangle) and PtRu on Pt (\blacksquare) anodes.

5.3.4 Reaction Rates

The polarization curves shown in Figure 5.1 are somewhat misleading because the currents are determined by the rates of three simultaneous reactions (eqs. 5.2 – 5.4). Since the relative rates of these reactions vary with potential, the current does not provide an accurate reflection of the

rate at which ethanol is oxidized (consumed). However, this can be extracted from the data by using eq. 5.6

$$\text{rate of ethanol oxidation (mol s}^{-1}\text{)} = i/n_{av}F \quad (5.6)$$

Figure 5.6 shows the calculated ethanol oxidation rates as a function potential, based on n_{av} values obtained from eq. 5.5, and the average currents measured during collection of the samples for NMR analysis. The rate of ethanol consumption at the Pt anode was initially very low because of the low currents and high CO_2 yields, but increased sharply at potentials above 0.35 V as the current increased. Ethanol consumption at low potentials was much faster at the other anodes, and began to level off at high potentials as the currents plateaued.

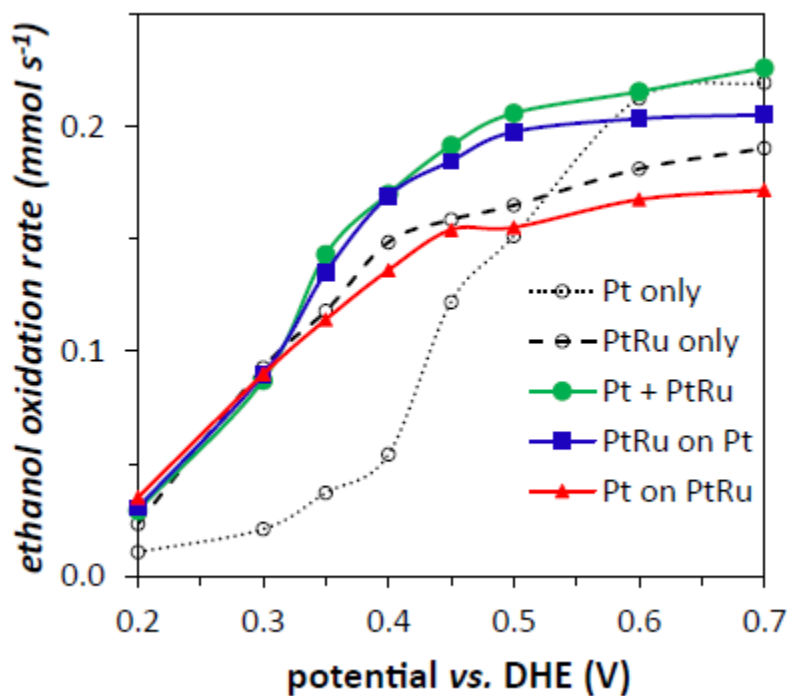


Figure 5.6. Ethanol consumption rate vs. potential for the oxidation of 0.100 M ethanol (0.2 mL min^{-1} and 80°C) at Pt (\cdots), PtRu ($- - -$), Pt+ PtRu (\bullet), Pt on PtRu (\blacktriangle) and PtRu on Pt (\blacksquare) anodes.

Curiously, the ethanol consumption rates were similar for the mixed, bilayer, and PtRu anodes, and increased approximately linearly with potential up to ca. 0.4 V. Thus, although the current increased exponentially with potential (Tafel behavior), indicating control by an electron transfer rate, the rate of ethanol consumption does not appear to have been limited by an electron transfer step.

Further insight into this behavior can be obtained from the potential dependence of the rate of formation of each product, shown in Figure 5.7. The rates of CO₂ formation increased approximately exponentially with potential between 0.2 and 0.4 V, as expected for a process limited by the rate of an electron transfer. It leveled off at higher potentials, presumably due to the effects of concentration polarization (mass transport limitation). The mixed and bilayer anodes produced CO₂ at similar rates to the Pt anode, while the rate was significantly lower at PtRu. It can therefore be concluded that CO₂ was produced primarily by the Pt catalyst in the mixed and bilayer anodes. The higher rate of CO₂ production at the PtRu on Pt anode relative to the Pt on PtRu anode or mixed anode appears to be inconsistent with this, since less ethanol would reach the Pt layer because of consumption in the PtRu layer, as illustrated in Figure 5.2B. However, this apparent anomaly can be explained by the increase in CO₂ yield that occurs at Pt anodes as the ethanol concentration is decreased.^{11,19,20} This is supported by, and explains, the higher CO₂ yields obtained with the PtRu on Pt anode (Figure 5.3).

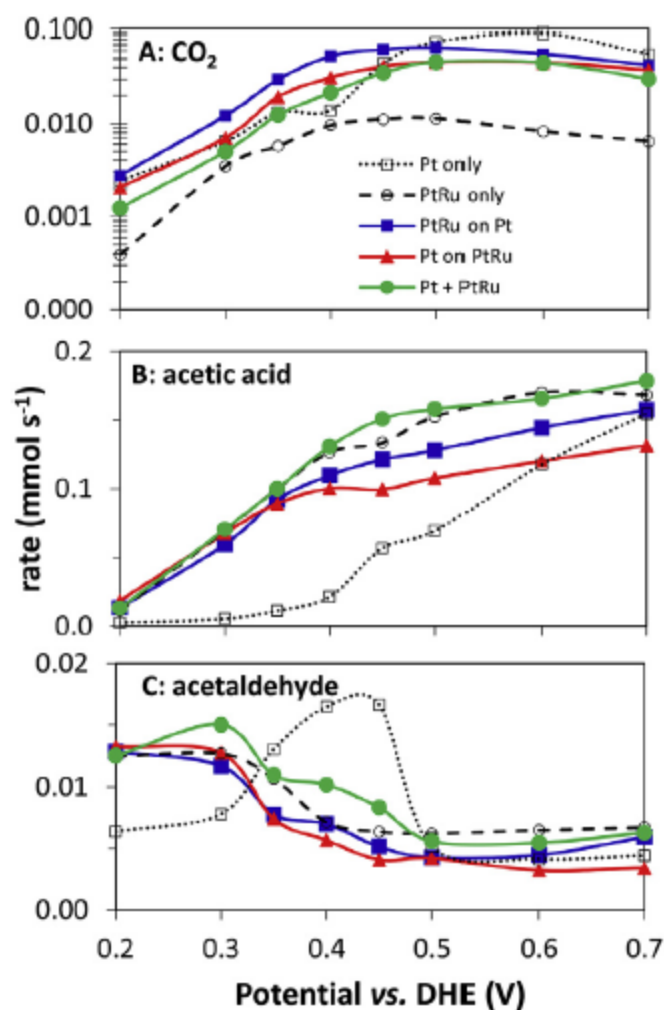


Figure 5.7. Product production rates vs. potential for the oxidation of 0.100 M ethanol (0.2 mL min^{-1} and $80 \text{ }^\circ\text{C}$) at Pt (\cdots), PtRu ($- - -$), Pt + PtRu (\bullet), Pt on PtRu (\blacktriangle) and PtRu on Pt (\blacksquare) anodes.

In contrast to the normal exponential dependence of the rate of CO_2 formation on potential, the rate of acetic acid formation increased linearly with potential for the PtRu, mixed and bilayer anodes at low potentials. This suggests that the rate of acetic acid formation at these anodes was controlled by a chemical step. The rate of acetaldehyde formation generally decreased with increasing potential, except for the Pt anode which gave a pronounced peak at ca. 0.4 V. The

complex variations in acetaldehyde production with potential arise because it is simultaneously produced and consumed by both catalysts.

At potentials from 0.2 V to 0.35 V, the rate of acetic acid production was very low at the Pt anode, due to the low currents and yields. Over this potential range, the PtRu, mixed and bilayer anodes produced acetic acid at similar rates that were much higher than for Pt. It can therefore be concluded that acetic acid was formed primarily by the PtRu in the mixed and bilayer anodes. The order of the layers did not have a significant effect because only a small amount of ethanol was consumed by the Pt catalyst at low potentials. At higher potentials, the increased consumption of ethanol by the Pt layers caused the rate of acetic acid formation to drop below the rate for the PtRu anode.

5.3.5 Mechanisms

Although the simple model illustrated in Figure 5.2 provides significant insight into the performances and product distributions obtained from the bilayer anodes, it does not explain why both bilayers provided better performances than a mixture of the Pt and PtRu catalysts, and much better performances than PtRu alone. Further insight can be obtained by considering mechanistic information and models that have been reported in the literature. It is generally accepted that the initial stages of ethanol oxidation at Pt based anodes proceed through two successive electrochemical dehydrogenation steps (eqs. 5.7 – 5.9) that lead to the formation of adsorbed acetaldehyde (eq. 5.8) and an adsorbed CH_3COH species (eq. 5.9).²¹⁻²²



Pt-C(CH₃)OH (i.e. CH₃COH_{ad}) is thought to be the precursor to the formation of acetic acid and CO₂,²³ while acetaldehyde is produced by desorption following reaction 5.8, or through the reaction of adsorbed ethanol with a surface hydroxyl group.²⁴

In contrast to the dehydrogenation of ethanol to adsorbed C₂ species, the C-C of acetaldehyde is broken during adsorption.²² Consequently, acetaldehyde generates adsorbed C₁ species at lower potentials than ethanol.^{22, 25} Cleavage of the C-C bond to form CO_{ad} and CH_{x,ad} is thought to be a chemical step.²⁶

These mechanistic differences between acetaldehyde and ethanol oxidation presumably play a significant role in the synergy observed here between layers of Pt and PtRu catalysts. In the low potential region between 0.2 and 0.4 V where the synergy is strongest, most of the ethanol is oxidized by the PtRu catalyst to produce acetaldehyde and acetic acid. For the Pt on PtRu anode, some of the acetaldehyde crosses the membrane to the cathode,¹⁰ but most diffuses into the Pt layer, where it can adsorb and dissociate to CO_{ad} and CH_{x,ad}. At the 80 °C operating temperature of the cell, these C₁ species are oxidized almost exclusively to CO₂ at Pt. This is indicated the excellent mass balances obtained for ethanol oxidation at all anodes, since significant formation of other, undetected C₁ products, such as CH₄, would lead to low mass balances. The high yields of CO₂ observed at 0.2 – 0.35 V for the Pt anode in Figure 5.3 demonstrate that Pt can efficiently oxidize the acetaldehyde intermediate to CO₂ under the conditions employed here, since ethanol is dehydrogenated to acetaldehyde prior to breaking of the C-C bond at low potentials.²² This is also supported by the >75% yield of CO₂ that has been reported for the oxidation of acetaldehyde at a carbon supported Pt anode at 80 °C.²⁷

It was envisaged that the Pt on PtRu bilayer configuration (Figure 5.2A) would be superior to the PtRu on Pt configuration (Figure 5.2B) because more of the acetaldehyde produced in the

PtRu layer would pass into the Pt layer. However, this effect appears to have been outweighed by the effect the PtRu layer on the concentration of ethanol in the Pt layer. Rationalization of the performance of the mixed anode relative to the bilayer anodes is more difficult. Having Pt nanoparticles close to all of the PtRu nanoparticles should be beneficial for oxidation of acetaldehyde, but this is not supported by the yields of acetaldehyde which were similar to (94% of, on average) those for PtRu alone. The effect of ethanol concentration for the mixed anode should have been intermediate between the effects for the two bilayer configuration, but the low CO₂ yields show that this was not the case. The main synergistic effect in the mixed electrode, seen at 0.4 V in the polarization curve (Figure 5.1), correlates with the anomaly in the product distribution at 0.4 V for Pt alone (Figure 5.3). The addition of PtRu eliminates the peak in acetaldehyde production seen for Pt alone in this region (Figure 5.3C), possibly by decreasing the local ethanol concentration.

5.4 Conclusions

The goals of combining Pt and PtRu catalysts to increase the low potential performance of anodes for ethanol oxidation, and decreasing acetaldehyde production, have been achieved. There is a synergy between the Pt and PtRu catalysts in both the mixed anode and bilayer structures that appears to be due to the oxidation at the Pt catalyst of acetaldehyde produced at the PtRu catalyst. The PtRu on Pt bilayer structure provides the added benefit that the PtRu layer decreases the ethanol concentration before it reaches the Pt layer, which leads to higher CO₂ yields. Since all of the anodes employed in this work had the same total metal loading (3.2 mg cm⁻²), the bilayer anodes contained less Pt than the Pt anode and so would lower the cost in addition to increasing performance and efficiency.

The importance of determining the stoichiometry of ethanol oxidation, and the product distribution, is demonstrated by the efficiencies presented in Figure 5.5 and the product production rates presented in Figure 5.7. Even with the strong synergy between the Pt and PtRu catalysts observed for the PtRu on Pt anode, the Pt catalyst alone produced the highest overall efficiency (18.5%). This highlights the need for further improvement of CO₂ yields at low potentials. The data in Figure 5.7 show that Tafel analysis of the total current will produce ambiguous results, since a large component of the current is not limited by electron transfer kinetics. Accurate analysis of the kinetics of ethanol oxidation will require fitting of the rates of each reaction to a detailed mechanistic model.

References

1. L. An, T.S. Zhao, Y.S. Li, Carbon-neutral sustainable energy technology: Direct ethanol fuel cells, *Renew. Sustain. Energy Rev.* 50 (2015) 1462-1468.
2. S.P.S. Badwal, S. Giddey, A. Kulkarni, J. Goel, S. Basu, Direct ethanol fuel cells for transport and stationary applications – A comprehensive review, *Applied Energy* 145 (2015) 80-103.
3. S. Ramachandran, U. Stimming, Well to wheel analysis of low carbon alternatives for road traffic, *Energy Environ. Sci.*, 8 (2015) 3313-3324.
4. H.R. Corti, E.R. Gonzalez, *Direct Alcohol Fuel Cells*, Springer: Dordrecht 2014.
5. V. Bambagioni, M. Bevilacqua, C. Bianchini, J. Filippi, A. Lavacchi, A. Marchionni, F. Vizza, P. K. Shen, Self - Sustainable Production of Hydrogen, Chemicals, and Energy from Renewable Alcohols by Electrocatalysis, *ChemSusChem*, 3 (2010) 851-855.

6. D. Banham, S.Y. Ye, Current Status and Future Development of Catalyst Materials and Catalyst Layers for Proton Exchange Membrane Fuel Cells: An Industrial Perspective, *ACS Energy Letters* 2 (2017) 629-638.
7. O.Z. Sharaf, M.F. Orhan, An overview of fuel cell technology: Fundamentals and applications, *Renew. Sustain. Energy Rev.* 32 (2014) 810-853.
8. U.B. Demirci, Direct liquid-feed fuel cells: Thermodynamic and environmental concerns, *J. Power Sources* 169 (2007) 239-246.
9. R.M. Altarawneh, P.G. Pickup, Product Distributions and Efficiencies for Ethanol Oxidation in a Proton Exchange Membrane Electrolysis Cell, *J. Electrochem. Soc.* 164 (2017) F861-F865.
10. R.M. Altarawneh, P. Majidi, P.G. Pickup, Determination of the efficiency of ethanol oxidation in a proton exchange membrane electrolysis cell, *J. Power Sources* 351 (2017) 106-114.
11. S. Sun, M.C. Halseid, M. Heinen, Z. Jusys, R.J. Behm, Ethanol electrooxidation on a carbon-supported Pt catalyst at elevated temperature and pressure: A high-temperature/high-pressure DEMS study, *J. Power Sources* 190 (2009) 2-13.
12. E. Antolini, Catalysts for direct ethanol fuel cells, *J. Power Sources* 170 (2007) 1-12.
13. S. Rousseau, C. Coutanceau, C. Lamy, J.M. Leger, Direct ethanol fuel cell (DEFC): Electrical performances and reaction products distribution under operating conditions with different platinum-based anodes, *J. Power Sources* 158 (2006) 18-24.
14. N. Nakagawa, Y. Kaneda, M. Wagatsuma, T. Tsujiguchi, Product distribution and the reaction kinetics at the anode of direct ethanol fuel cell with Pt/C, PtRu/C and PtRuRh/C, *J. Power Sources* 199 (2012) 103-109.

15. A. Ghumman, G. Li, D.V. Bennett, P. Pickup, Online analysis of carbon dioxide from a direct ethanol fuel cell, *J. Power Sources* 194 (2009) 286-290.
16. C. Song, P.G. Pickup, Effect of Hot Pressing on the Performance of Direct Methanol Fuel Cells, *J. Appl. Electrochem* 34 (2004) 1065-1070.
17. D.D. James, P.G. Pickup, Effects of crossover on product yields measured for direct ethanol fuel cells, *Electrochim. Acta* 55 (2010) 3824-3829.
18. G. Li, P.G. Pickup, Analysis of performance losses of direct ethanol fuel cells with the aid of a reference electrode, *J. Power Sources* 161 (2006) 256-263.
19. D.D. James, P.G. Pickup, Measurement of carbon dioxide yields for ethanol oxidation by operation of a direct ethanol fuel cell in crossover mode, *Electrochim. Acta* 78 (2012) 274-278.
20. P. Majidi, P.G. Pickup, Determination of the average number of electrons released during the oxidation of ethanol in a direct ethanol fuel cell, *Electrochim. Acta* 182 (2015) 856-860.
21. J. Florez-Montano, G. Garcia, O. Guillen-Villafuerte, J.L. Rodriguez, G.A. Planes, E. Pastor, Mechanism of ethanol electrooxidation on mesoporous Pt electrode in acidic medium studied by a novel electrochemical mass spectrometry set-up, *Electrochim. Acta* 209 (2016) 121-131.
22. J. Torrero, F.J. Perez-Alonso, M.A. Pena, C. Dominguez, A.O. Al-Youbi, S.A. Al-Thabaiti, S.N. Basahel, A.A. Alshehri, S. Rojas, In Situ Infrared Study of the Electrooxidation of Ethanol and Acetaldehyde in Acid Electrolyte, *Chemelectrochem* 3 (2016) 1072-1083.

23. R. Kavanagh, X.M. Cao, W.F. Lin, C. Hardacre, P. Hu, Origin of Low CO₂ Selectivity on Platinum in the Direct Ethanol Fuel Cell, *Angew. Chem. Int. Ed. Engl.* 51 (2012) 1572-1575.
24. R. Kavanagh, X.M. Cao, W.F. Lin, C. Hardacre, P. Hu, Acetaldehyde Production in the Direct Ethanol Fuel Cell: Mechanistic Elucidation by Density Functional Theory, *J. Phys. Chem. C* 116 (2012) 7185-7188.
25. M. Heinen, Z. Jusys, R.J. Behm, Ethanol, Acetaldehyde and Acetic Acid Adsorption/Electrooxidation on a Pt Thin Film Electrode under Continuous Electrolyte Flow: An in Situ ATR-FTIRS Flow Cell Study, *J. Phys. Chem. C* 114 (2010) 9850-9864.
26. A.B. Delpeuch, C. Cremers, M. Chatenet, Impact of water adsorbates on the acetaldehyde oxidation reaction on Pt- and Rh-based multimetallic electrocatalysts, *Electrochim. Acta* 188 (2016) 551-559.
27. S. Sun, M. Heinen, Z. Jusys, R.J. Behm, Electrooxidation of acetaldehyde on a carbon supported Pt catalyst at elevated temperature/pressure: An on-line differential electrochemical mass spectrometry study, *J. Power Sources* 204 (2012) 1-13.

Chapter 6

Determination of the Stoichiometry of Ethanol Oxidation from the Flow Rate Dependence of the Current in a Proton Exchange Membrane Electrolysis Cell

The principal author (Rakan M. Altarawneh) contributed to all aspects of the project as the main researcher including: literature review, performing all of the experiments, collecting and analyzing the data, designing some of the experiments, presenting and discussing the data and writing and revising the first draft of the manuscript.

The corresponding author (Prof. Peter G. Pickup) was the principal investigator and developed the initial ideas for this research. He oversaw all aspects of the project, including supervision of the principal author (Rakan M. Altarawneh), the design of experiments, data analysis and simulations; he finalized and submitted the manuscript.

This chapter has been published as: -

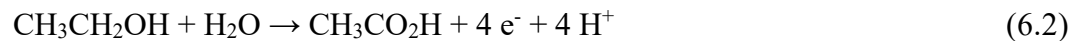
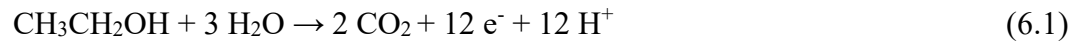
(R.M. Altarawneh, P.G. Pickup, Determination of the stoichiometry of ethanol oxidation from the flow rate dependence of the current in a proton exchange membrane electrolysis cell, J. Electrochem. Soc.,165 (2018) F479-F483).

The raw data is provided in Appendix E.

6. Determination of the Stoichiometry of Ethanol Oxidation from the Flow Rate Dependence of the Current in a Proton Exchange Membrane Electrolysis Cell

6.1 Introduction

Ethanol is an attractive fuel for direct liquid fuel cells.^{1, 2} However, the high theoretical efficiency of 97% for a direct ethanol fuel cell (DEFC) is based on complete oxidation of ethanol to CO₂ (eq. 6.1), which generates 12 electrons ($n = 12$), while the main products from a DEFC are acetic acid (eq. 6.2; $n = 4$) and acetaldehyde (eq. 6.3; $n = 2$).³⁻⁵



Since the overall efficiency of a DEFC is proportional to the number of electrons transferred,³ measurement of the stoichiometry of ethanol oxidation (average number of electrons transferred per molecule, n_{av}) plays a crucial role in the development of more efficient anode catalysts for DEFCs.^{3,6} Simple and fast methods are required for routine evaluation of the efficiency of catalysts over a wide range of conditions.

The faradaic efficiency (ϵ_F) of a DEFC is determined by the ratio of n_{av} to the maximum of $n = 12$ for the complete oxidation of ethanol to carbon dioxide ($\epsilon_F = n_{av}/12$), while n_{av} is determined by the product distribution according to eq. 6.4,⁷

$$n_{av} = \sum n_i f_i \quad (6.4)$$

where n_i is the number of electrons transferred to form product i and f_i is the fraction of ethanol converted to product i (CO₂, acetic acid and acetaldehyde account for > 99% of the ethanol consumed⁸). Various experimental methods are available for measuring n_{av} , including analysis of

the amount of ethanol consumed,^{9,10} the product distribution,^{7,10} and several electrochemical methods^{11,12}.

Determination of n_{av} from the dependence of the current on the flow rate of the ethanol solution, in proton exchange membrane fuel cell (PEMFC) hardware, is particularly convenient.^{11,13} In this method, the concentration of the ethanol solution decreases as it passes through the flow field, causing the local current to decrease. As the flow rate is decreased, the average concentration of ethanol in the flow field decreases, and so the current decreases. Modelling of this effect provides the following relationship (eq. 6.5) between the steady-state current (I) and the flow rate (u) of the ethanol solution:¹¹

$$I = n_{av} F C_{in} u \left(1 - \exp \left(- \frac{I_{lim}}{n_{av} F C_{in} u} \right) \right) \quad (6)$$

where C_{in} is the concentration of ethanol entering the cell and I_{max} is the current limit at high flow rates. In the derivation of this equation,¹¹ it was assumed that the current is proportional to the ethanol concentration, that there are negligible concentration gradients perpendicular to the flow direction, and that the effect of lateral diffusion along the flow field is negligible.

Eq. 6.5 has been shown to be valid for methanol oxidation in a number of cell configurations,¹³ including the anode polarization method employed in this work, and has provided reasonable accuracy for determining n_{av} values for both methanol¹³ and ethanol¹⁰ oxidation in the few cases where it has been tested. It can be routinely applied during polarization measurements (steady state current vs. potential) and avoids the need for analysis of the cell exhaust, which is complicated by crossover effects and loss of ethanol and products during their collection.¹⁰ However, further evaluation of the validity and accuracy of eq. 6.5 is necessary before it can be employed with confidence as a routine, stand-alone method. There is evidence that it can underestimate n_{av} when there is crossover of ethanol through the membrane, and overestimate n_{av}

when it varies significantly with concentration.¹⁰ The flux of ethanol crossing the membrane to the cathode is dependent on the concentration of ethanol at the interface between the anode and the membrane, which depends on the current and the properties of the catalyst layer (specific activity, thickness, porosity, etc.).

The purpose of the work described in this chapter was to comprehensively evaluate the accuracy of the eq. 6.5 (electrochemical method) by comparison with results from chemical analysis of the cell exhaust. Results are presented for six different anodes prepared from three different commercial catalysts and their combinations in a mixture and two bilayer structures. The cell was operated as an ethanol electrolysis cell (also described as anode polarization)^{13, 14} in which ethanol is oxidized at the anode, while protons are reduced to hydrogen at the cathode. This avoids inaccuracies that arise due to the chemical reaction of ethanol with oxygen when measurements are made in a DEFC.¹⁵ Chemical analysis of the cell exhaust by nuclear magnetic resonance (NMR) and infrared (IR) spectrometry has been reported previously for the same anodes,^{6, 8} with the accuracy of n_{av} verified by the mass and charge balances, and agreement of values obtained from the amount of ethanol consumed and the product distribution.

6.2 Experimental

A commercial PEMFC (5 cm² active area; Fuel Cell Technology Inc.), modified as previously described,¹⁰ was operated as an electrolysis cell by supplying 0.1 M ethanol (Commercial Alcohols Inc.) solution to the anode at flow rates of 0.02, 0.05, 0.09, 0.2 and 0.5 mL min⁻¹ with a syringe pump and dry N₂ to the cathode at 35 mL min⁻¹. The cell was operated at 80 °C in all experiments. Use of N₂ at the cathode produces a stable potential because protons are reduced to hydrogen, creating a dynamic hydrogen electrode (DHE).^{16, 17} Ren et al.¹⁶ have shown that overpotentials for hydrogen evolution in a similar cell were negligible, while Li and Pickup¹⁷

demonstrated that anode potentials in a direct methanol fuel cell did not differ significantly when measured against a hydrogen evolving cathode or an independent DHE. Since, hydrogen is produced within the cathode catalyst layer, it is unnecessary to supply hydrogen to the cathode.

Anodes were prepared with commercial carbon supported Pt (Pt/C; HiSPEC™ 13100, 70% Pt; Alfa Aesar), PtRu alloy (PtRu/C; HiSPEC™ 12100, 50% Pt and 25% Ru; Alfa Aesar), and PtSn alloy (PtSn/C; 40% Pt₃Sn; BASF Fuel Cell Inc.) catalysts, as previously described.^{6,8} Catalyst suspensions, prepared by dispersing the catalyst in a 1:1 mixture of 1-propanol and Nafion solution (Dupont; 5% Nafion) by sonication for 3 h, were spread onto Toray carbon fiber paper (CFP; TGP-H-090). Metal loadings of 3.2 mg cm⁻² and Nafion loadings of ca. 20 mass% were used for all anodes. Cathodes consisted of 4 mg cm⁻² Pt black. Membrane and electrode assemblies were prepared by pressing (room temperature; ca. 1.5 MPa) an anode and cathode onto a Nafion™ 115 membrane in the cell. Electrochemical measurements were made under steady state conditions at constant cell potentials using a Hokuto Denko HA-301 potentiostat.

For each anode, many preliminary experiments were conducted over a period of two days to condition the membrane and electrode assembly before collection of the electrochemical data reported here and the chemical analyses reported previously.^{6,8} This included flushing the cell with water, operating with ethanol at 0.7 V for at least 2 h and then recording polarization curves several times between 0.1 V and 0.7 V (0.05 V steps for 300 s). When applying the electrochemical method (eq. 5) for determination of n_{av} , the current at each potential was allowed to stabilize at each flow rate and then averaged over a period of at least 20 s. In order to ensure that steady-state currents were obtained, long stabilization times were employed, ranging from 300 s at 0.5 mL min⁻¹ to 2500 s at 0.02 mL min⁻¹.

The procedures for determining n_{av} by chemical analysis have been previously described.^{6,8} The cell was operated at constant potential with an ethanol flow rate of 0.2 mL min⁻¹. CO₂ was measured in real time with a commercial non-dispersive infrared CO₂ monitor (Telaire 7001), while residual ethanol, acetic acid, and acetaldehyde in a sample of the liquid exiting the cell were measured by proton NMR spectrometry. Three different methods were employed to determine n_{av} from each set of analysis results. These were based on the amount of ethanol consumed, the chemical yields of products, and the faradaic yields of products. This provides an assessment of precision, and the average of the three results minimizes inaccuracies due to loss of ethanol or products (mainly acetaldehyde) during collection of the cell exhaust.¹⁰

6.3 Results and Discussion

6.3.1 Polarization Curves

Figure 6.1 shows polarization curves for the oxidation of 0.1 M ethanol at various flow rates at a PtRu/C anode. The shape of the curves did not change greatly with flow rate, and all reached a limiting current at high potentials, where the current is limited by diffusion of ethanol through the carbon fiber paper backing layer of the anode.^{13, 18} The limiting current decreased as the ethanol flow rate was decreased (eq. 6.5) because a greater fraction of the ethanol entering the cell was consumed, and so the average ethanol concentration in the flow field was lower.

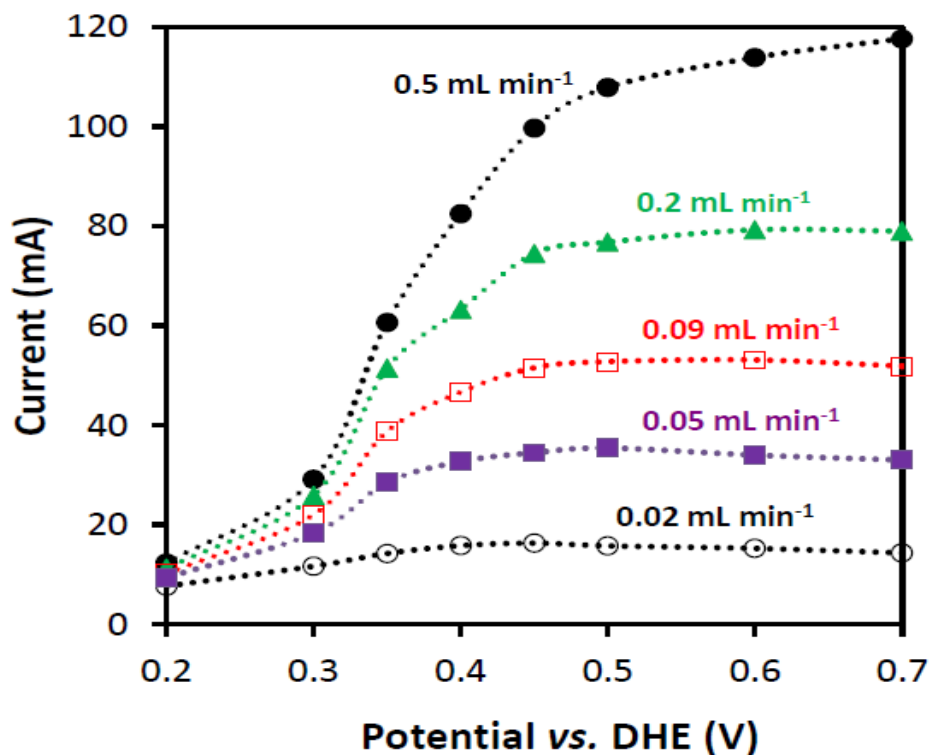


Figure 6.1. Polarization curves for the oxidation of 0.100 M ethanol at 0.02 (\circ), 0.05 (\blacksquare), 0.09 (\square), 0.2 (\blacktriangle) and 0.5 (\bullet) mL min⁻¹ at a PtRu/C anode and 80 °C.

6.3.2 Stoichiometry (n_{av}) from the Flow Rate Dependence of the Current.

Figure 6.2 shows plots of current vs. flow rate for selected data from Figure 6.1, together with the best fits (non-linear least squares)¹⁹ to eq. 6.5. Values of n_{av} from these fits are plotted in Figure 6.3 together with values obtained by analysis of the products and residue ethanol in the exhaust from the cell.⁸ The three different n_{av} obtained from the exhaust analysis reflect the uncertainties in the analyses,¹⁰ while the uncertainties from the fitting of eq. 6.5 are plotted as error bars showing the standard deviation calculated from Monte Carlo simulation.¹⁹

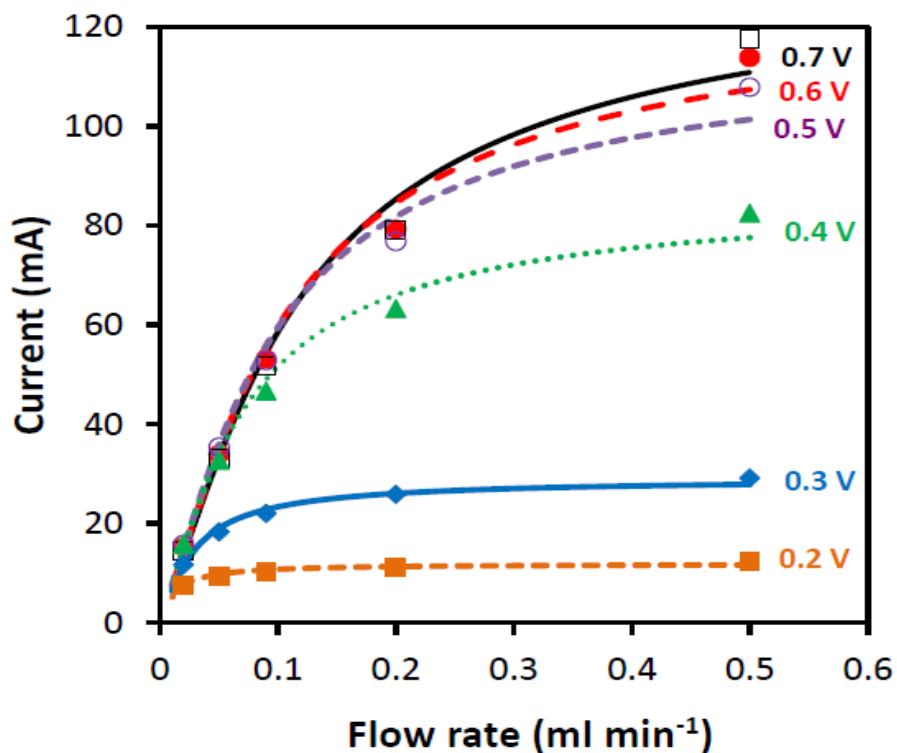


Figure 6.2. Plots of current vs. flow rate for selected data from Figure 6.1 (points) together with the best fits to eq. 6.5 (lines).

The agreement between the results in Figure 6.3 from the electrochemical method (eq. 6.5) and the chemical analysis methods is very good. Comparison of the average result and standard deviation from analysis of the exhaust at each potential with the value and standard deviation of the result from eq. 6.5, using a *t* test (95% confidence), indicates that there are no significant differences. This is a very important finding because eq. 6.5 was derived based on the assumption that the current was mass transport controlled. It should therefore be valid for the data in Figures 6.1 and 6.2 from 0.5 and 0.7 V, but could be inaccurate at lower potentials for a number of reasons. Firstly, there is crossover of ethanol through the membrane when the current is below the mass transport limit, and this leads to an additional decrease in the concentration of ethanol in the anode flow field.^{10, 13} Secondly, eq. 6.5 would become inaccurate if the electrochemical kinetics were not first order in ethanol, since a linear relationship between the current and concentration was

assumed in the derivation of eq. 6.5. However, the agreement between the electrochemical and chemical results in Figure 6.3 demonstrates that neither of these factors caused significant inaccuracies.

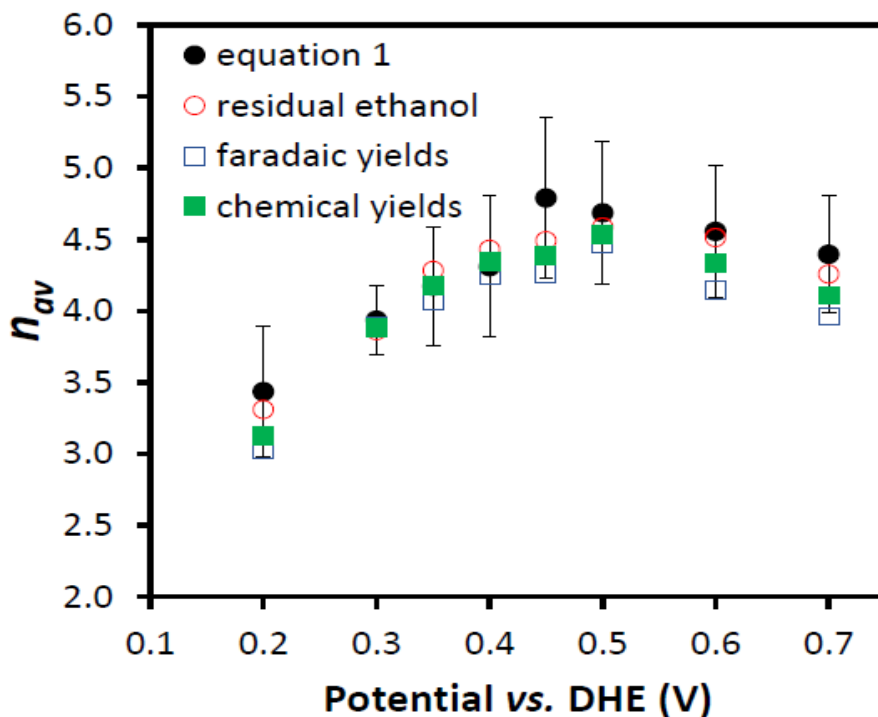


Figure 6.3. n_{av} vs. potential for the oxidation of 0.100 M ethanol at a PtRu/C anode at 80 °C. Black (●) points were obtained by using eq. 6.5, red (○) points are from the amount of ethanol consumed, blue (□) and green (■) points are from the faradaic and chemical yields of products, respectively. For clarity, error bars are only shown for the data from eq. 6.5.

The effect of crossover on the use of eq. 6.5 has previously been investigated for both methanol¹³ and ethanol¹⁰ oxidation. By simulation,¹³ it was shown that crossover produced a small underestimation of n_{av} for ethanol oxidation, typically by 2-5%.¹⁰ The results in Figure 6.3 reaffirm the conclusion that inaccuracies of eq. 6.5 due to crossover are not significant.

Figure 6.4 summarizes results for a number of other anodes, which all support the conclusion that eq. 6.5 provides good accuracy over the whole potential range from predominantly

kinetic control of the current at 0.2 V to mass transport control at potentials above ca. 0.5 V. For the mixed Pt/C + PtRu/C anode and the Pt/C on PtRu/C bilayer anode, there were no significant differences (95% confidence *t* test), between the n_{av} values from eq. 6.5 and chemical analysis.

For the PtSn/C anode the differences were statistically different at 0.2, 0.3, and 0.5 V. However, the standard deviation at 0.5 V from eq. 6.5 was unusually low and the difference in n_{av} values was only 7% (6.15 ± 0.16 from eq. 6.5 vs. 5.73 ± 0.11 from chemical analysis). The low n_{av} values from eq. 6.5 for the PtSn/C anode at 0.2 and 0.3 V can be attributed to the effects of crossover, since upward corrections of 2% and 7%, respectively, would bring them into agreement with the values from chemical analysis.

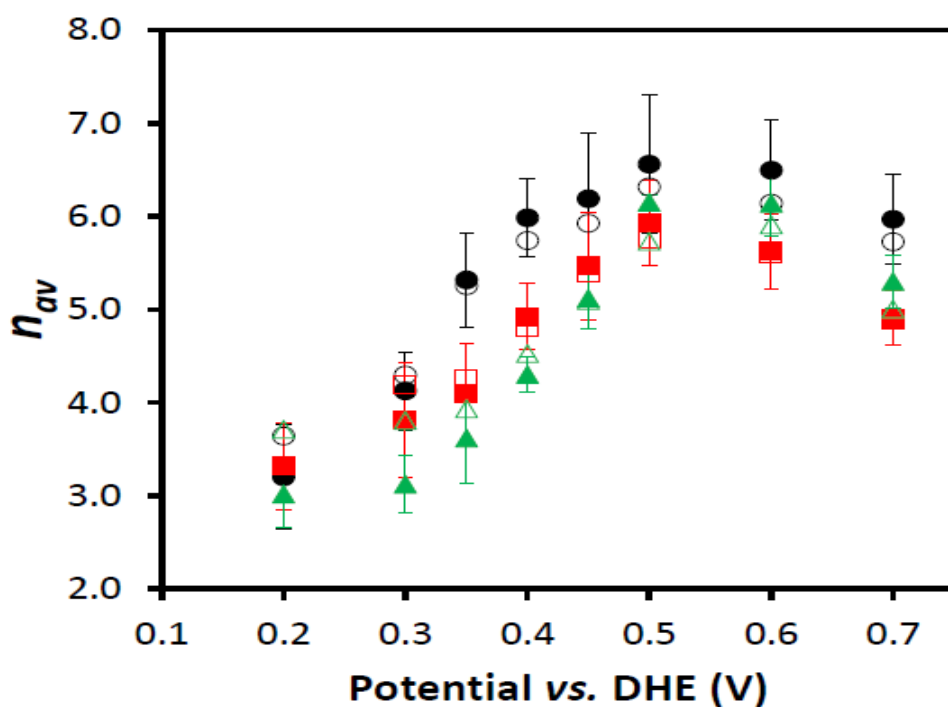


Figure 6.4. n_{av} vs. potential for the oxidation of 0.100 M ethanol at PtSn/C (green triangles), Pt/C + PtRu/C (red squares) and Pt/C on PtRu/C bilayer (black circles) anodes at 80 °C. Solid points are from eq. 6.5, while open points are from chemical analysis (averages from the amount of ethanol consumed and yields of products). For clarity, error bars are only shown for the values from eq. 6.5.

6.3.3 Discrepancies Between n_{av} Values from Eq. 6.5 and Chemical Analysis.

Previously, it has been found that eq. 6.5 can yield significantly higher n_{av} values than those obtained from chemical analysis, and this was attributed to a dependence of n_{av} on the concentration of ethanol.¹⁰ The data in Figures 6.3 and 6.4 show that this is not a significant effect in most cases, but it can become significant when yields of CO₂ are high. It is well established that at 80 °C the yield of CO₂ at Pt anodes increases sharply as the concentration of ethanol is decreased,^{20, 21} and it has been shown that this can significantly influence the accuracy of eq. 6.5 when data over a wide range of flow rates is employed.¹¹ In fact, eq. 6.5 has been used to demonstrate the flow rate dependence of n_{av} at a Pt black anode.¹¹

Figure 6.5 shows data for a Pt/C anode, which produced the highest yields of CO₂ (51-75% faradaic yields) of the electrodes that we have employed.⁶ In this case, n_{av} from eq. 6.5 only agreed with n_{av} from chemical analysis at 0.6 and 0.7 V. As the potential was decreased below 0.6 V, n_{av} from eq. 6.5 rose sharply to impossibly high values (greater than the value of 12 for complete oxidation of ethanol to CO₂) at potentials below 0.4 V.

In order to explore whether the failure of eq. 6.5 at potentials below 0.5 V for the Pt/C anode was due to a concentration dependence of n_{av} , the current vs. flow rate data points were analyzed in pairs using eq. 6.5. For example, use of the 0.09 mL min⁻¹ and 0.5 mL min⁻¹ data points at 0.4 V in eq. 6.5 yields an exact solution of $n_{av} = 6.9$. This is much closer to the value of 5.33 ± 0.11 from chemical analysis that was obtained at a flow rate of 0.2 mL min⁻¹ that is between these two flow rates (fitting of all of the data to eq. 6.5 gave $n_{av} = 11.4 \pm 0.6$ in this case). Use of the 0.05 mL min⁻¹ and 0.2 mL min⁻¹ data points in eq. 6.5 yields $n_{av} = 8.8$ at 0.4 V, showing that n_{av} increased with decreasing flow rate, as expected from the effect of ethanol concentration on the yield of CO₂. Use of the 0.02 mL min⁻¹ and 0.09 mL min⁻¹ data points at 0.4 V in eq. 6.5 yields n_{av}

= 13.5, which is greater than 12 and therefore unreasonable. These comparisons make it clear that the failure of eq. 6.5 when applied to all of the data point from 0.02 to 0.5 mL min⁻¹ was due to the concentration dependence of n_{av} .

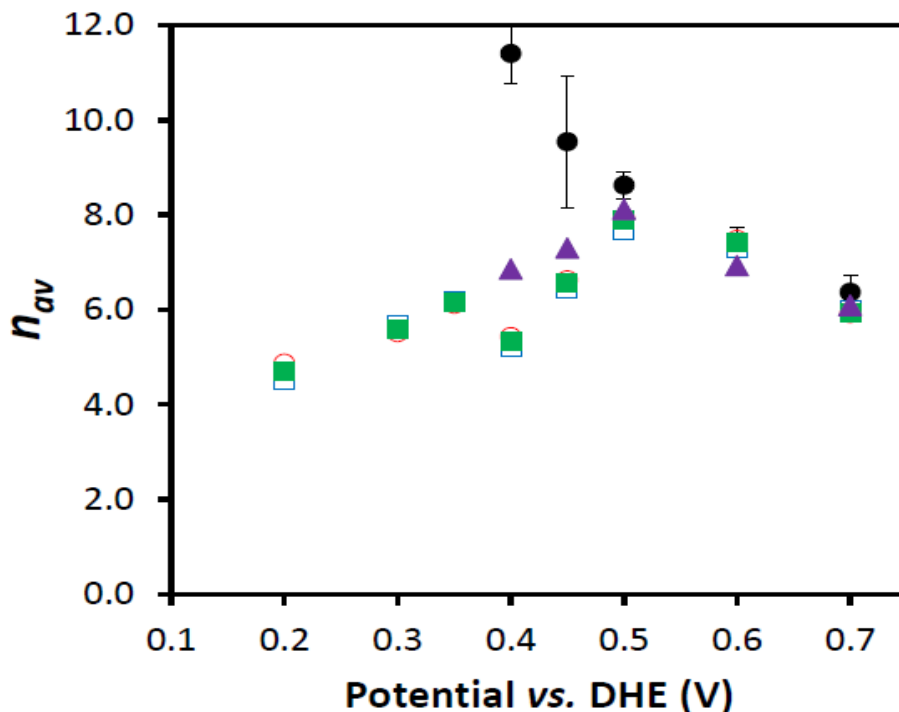


Figure 6.5. n_{av} vs. potential for the oxidation of 0.100 M ethanol at a Pt/C anode at 80 °C, from eq. 6.5 using the currents at all flow rates (●), the amount of ethanol consumed (○), and the faradaic (□) and chemical (■) yields of products. Triangular (purple) data points were obtained by fitting eq. 6.5 to the currents at 0.09, 0.2, and 0.5 mL min⁻¹.

In order to demonstrate this further, the effects of a linear dependence of n_{av} on ethanol concentration were simulated using a finite difference method that has previously been described.¹³ The best fit to the data for the Pt/C anode at 0.4 V is shown in Figure 6.6, together with the flow rate dependence of the current calculated from eq. 6.5 by using the n_{av} obtained by chemical analysis, and the flow rate dependence of n_{av} obtained from the best fit simulation. The best fit parameters used in the simulation (n_{av} for 0.1 M ethanol ($n_{av}(0.1 M)$) = 5.2; $dn_{av}/dC = -58 M^{-1}$; $I_{max} = 31.1$ mA) were obtained by minimizing the squares of the differences between the measured

and simulated currents and the concentration of ethanol exiting the cell. It was also assumed that there was crossover of 10% of the ethanol through the membrane, although this did not have a significant influence on the fitting parameters. Since inclusion of the concentration of ethanol exiting the cell forces n_{av} at 0.2 mL min^{-1} to be close to the value from chemical analysis, the simulation does not prove that the high n_{av} from eq. 6.5 is due to the concentration dependence of n_{av} . However, it does confirm that this is a reasonable explanation. It was not possible to obtain reasonable values of $n_{av}(0.1 \text{ M})$ and dn_{av}/dC without using the concentration of ethanol exiting the cell to constrain them, since a constant (and unreasonable) n_{av} of ca. 11 always gave a better fit to the current vs. flow rate data.

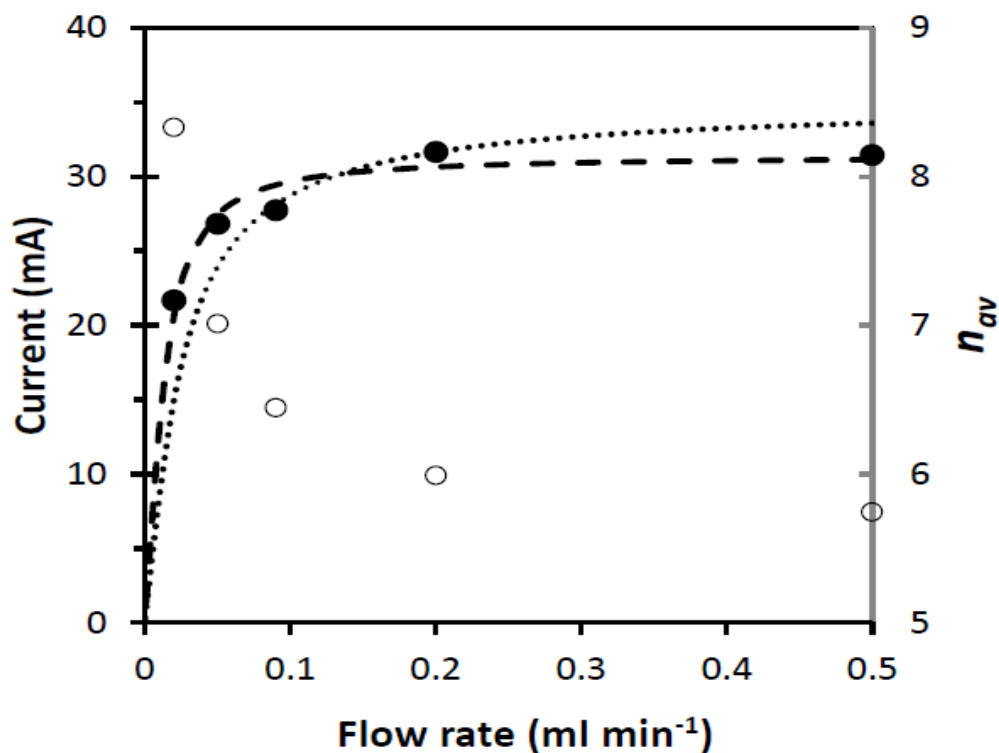


Figure 6.6. Plots of current (●) and n_{av} (○) vs. flow rate for the oxidation of 0.100 M ethanol at a Pt/C anode, at 0.4 V and 80 °C. The dashed line is the best fit obtained from a simulation based on a linear dependence of n_{av} on ethanol concentration (see text), while the dotted line was obtained by using in eq. 6.5 with $n_{av} = 5.33$ from chemical analysis.

Simulation of the 0.35 V data for the Pt/C anode gave a best fit with $n_{av}(0.1 M) = 6.2$ and $dn_{av}/dC = -58 M^{-1}$, while eq. 6.5 gave an unreasonable n_{av} of 33. Simulations of the data at 0.3 and 0.2 V also gave reasonable fits and values relative to those from chemical analysis, as shown in Figure 6.7. At these potentials there was very little dependence of the current on flow rate because the effect of ethanol consumption was cancelled by the change in n_{av} . The fact that the experimental current vs. flow rate profiles at different potentials can be reproduced by the simulation, using similar n_{av} profiles, provides strong evidence that the unreasonable n_{av} values from eq. 6.5 are due to the concentration dependence of n_{av} .

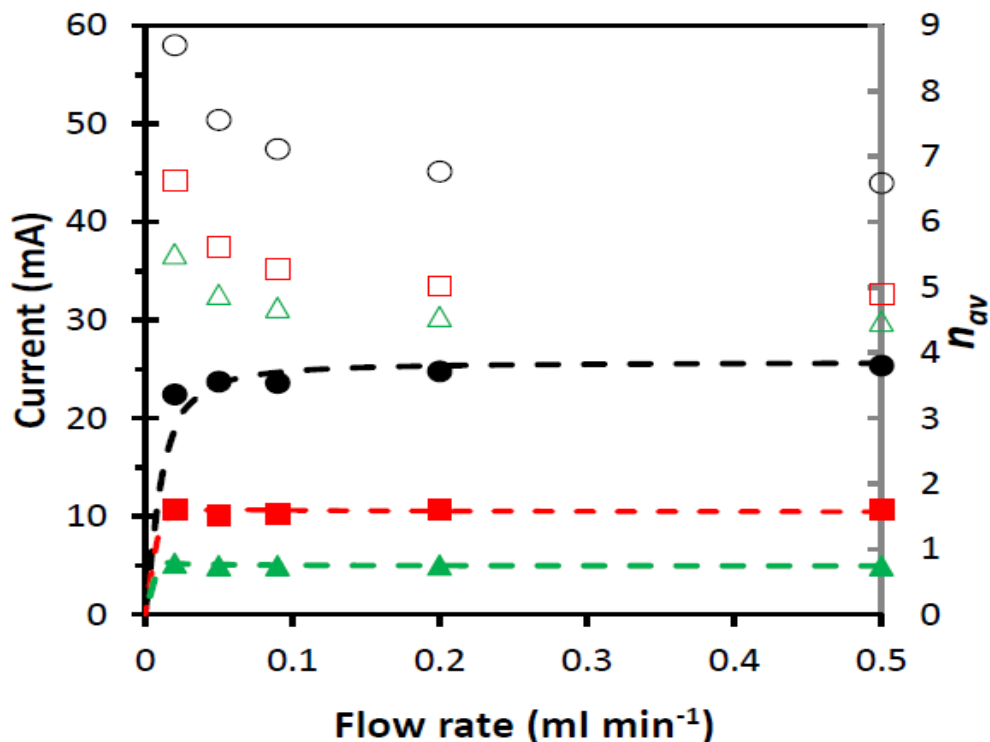


Figure 6.7. Plots of current (solid points) and n_{av} (open point) vs. flow rate for the oxidation of 0.100 M ethanol at a Pt/C anode at 80 °C, at 0.2 V (▲), 0.3 V (■), and 0.35 V (●) V. Lines show simulations of the current based on $n_{av}(0.1 M) = 4.1$ and $dn_{av}/dC = -79 M^{-1}$ at 0.2 V, $n_{av}(0.1 M) = 4.5$ and $dn_{av}/dC = -75 M^{-1}$ at 0.3 V, and $n_{av}(0.1 M) = 6.2$ and $dn_{av}/dC = -58 M^{-1}$ at 0.35 V.

Errors due to the concentration dependence of n_{av} can generally be mitigated by employing a smaller range of flow rates. This is illustrated in Figure 6.5 by the triangular (purple) data points which were obtained by fitting eq. 6.5 to the currents at just 0.09, 0.2, and 0.5 mL min⁻¹. This method also provided more accurate n_{av} values for a PtRu/C on Pt/C bilayer anode, as shown in Figure 6.8. In this case, n_{av} from the full fit (0.02 to 0.5 mL min⁻¹) was too high at most potentials, while the 0.09 to 0.5 mL min⁻¹ fit gave values that were generally in better agreement with those from chemical analysis.

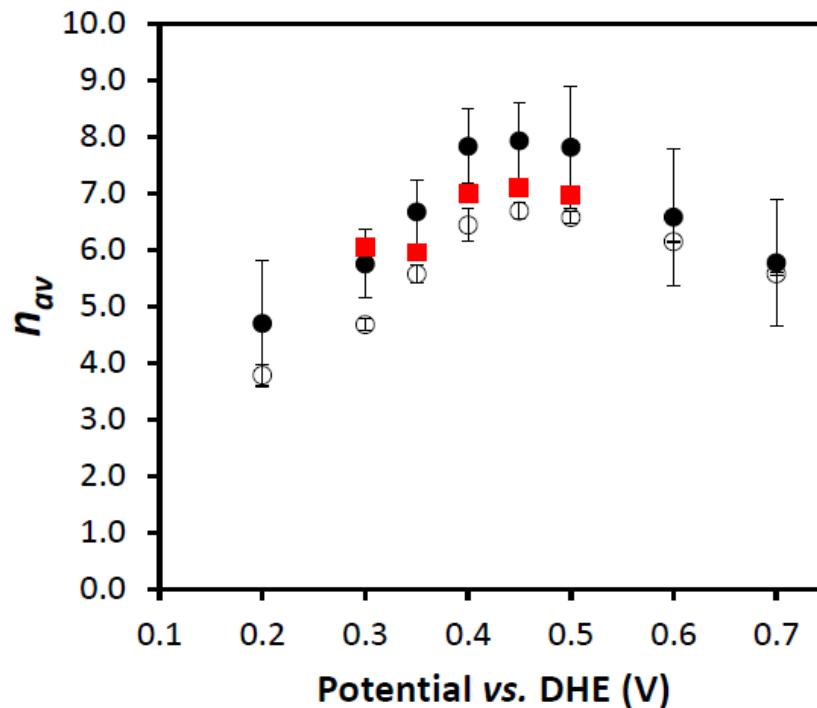


Figure 6.8. n_{av} vs. potential for the oxidation of 0.100 M ethanol at a PtRu/C on Pt/C bilayer anode at 80 °C. Solid points are from eq. 6.5 (● for 0.02 to 0.5 mL min⁻¹; ■ for 0.09 to 0.5 mL min⁻¹), while open points are from chemical analysis (average and standard deviation from the amount of ethanol consumed and yields of products).

6.4 Conclusions

The dependence of the current of a PEM electrolysis cell on the ethanol flow rate (eq. 6.5) has been shown to consistently provide accurate stoichiometries for ethanol oxidation at various anodes over a full range of potentials. Errors due to crossover are small, and variations in stoichiometry with concentration can be identified by comparing results over different flow rate ranges. When there are significant changes in n_{av} with concentration, a restricted range of flow rates should be employed.

Determination of n_{av} by using eq. 6.5 is a valuable method for rapid assessment of a catalyst's electrochemical performance (potential efficiency) and fuel efficiency (faradaic

efficiency); the two key factors that determine the overall efficiency of a DEFC.⁸ The faradaic efficiency ($n_{av}/12$) can be obtained concurrently with measurement of a polarization curve without any additional equipment. The methodology can be routinely applied, and is well suited for rapid assessment of the effects of operating conditions (potential, temperature, concentration, pressure) and changes over time.

References

1. B.C. Ong, S. K. Kamarudin, S. Basri, Direct liquid fuel cells: A review, *Int. J. Hydrogen Energy*, 42 (2017) 10142-10157.
2. S.P.S. Badwal, S. Giddey, A. Kulkarni, J. Goel, S. Basu, Direct ethanol fuel cells for transport and stationary applications – A comprehensive review, *Applied Energy*, 145 (2015) 80-103.
3. L. An, T.S. Zhao, Y.S. Li, Carbon-neutral sustainable energy technology: Direct ethanol fuel cells, *Renew. Sustain. Energy Rev.* 50 (2015) 1462-1468.
4. J. Friedl, U. Stimming, Model catalyst studies on hydrogen and ethanol oxidation for fuel cells, *Electrochim. Acta*, 101 (2013) 41-58.
5. M.A.F. Akhairi, S. K. Kamarudin, Catalysts in direct ethanol fuel cell (DEFC): An overview, *Int. J. Hydrogen Energy*, 41 (2016) 4214-4228.
6. R.M. Altarawneh, P.G. Pickup, Pt and PtRu catalyst bilayers increase efficiencies for ethanol oxidation in proton exchange membrane electrolysis and fuel cells, *J. Power Sources*, 366 (2017) 27-32.
7. H. Wang, Z. Jusys, R.J. Behm, Ethanol Electrooxidation on a Carbon-Supported Pt Catalyst: Reaction Kinetics and Product Yields, *J. Phys. Chem. B*, 108 (2004) 19413-19424.

8. R.M. Altarawneh, P.G. Pickup, Product Distributions and Efficiencies for Ethanol Oxidation in a Proton Exchange Membrane Electrolysis Cell, *J. Electrochem. Soc.*, 164 (2017) F861-F865.
9. H. Hitmi, E. M. Belgsir, J. M. Leger, C. Lamy, R. O. Lezna, A kinetic analysis of the electro-oxidation of ethanol at a platinum electrode in acid medium, *Electrochim. Acta*, 39 (1994) 407-415.
10. R.M. Altarawneh, P. Majidi, P.G. Pickup, Determination of the efficiency of ethanol oxidation in a proton exchange membrane electrolysis cell, *J. Power Sources*, 351 (2017) 106-114.
11. P. Majidi, P. G. Pickup, Determination of the average number of electrons released during the oxidation of ethanol in a direct ethanol fuel cell, *Electrochim. Acta*, 182 (2015) 856-860.
12. I. Mahesh, R. Jaithaliya, A. Sarkar, Efficient electrooxidation of ethanol on Bi@Pt/C nanoparticles: (i) Effect of monolayer Bi deposition on specific sites of Pt nanoparticle (ii) Calculation of average number of e^- s without help of chemical analysis, *Electrochim. Acta*, 258 (2017) 933-941.
13. P. Majidi, R. M. Altarawneh, N. D. W. Ryan, P. G. Pickup, Determination of the efficiency of methanol oxidation in a direct methanol fuel cell, *Electrochim. Acta*, 199 (2016) 210-217.
14. C. Lamy, T. Jaubert, S. Baranton, C. Coutanceau, Clean hydrogen generation through the electrocatalytic oxidation of ethanol in a Proton Exchange Membrane Electrolysis Cell (PEMEC): Effect of the nature and structure of the catalytic anode, *J. Power Sources*, 245 (2014) 927-936.

15. D.D. James and P.G. Pickup, Effects of crossover on product yields measured for direct ethanol fuel cells, *Electrochim. Acta*, 55 (2010) 3824-3829.
16. X. Ren, T.E. Springer and S. Gottesfeld, Water and Methanol Uptakes in Nafion Membranes and Membrane Effects on Direct Methanol Cell Performance, *J. Electrochem. Soc.*, 147 (2000) 92-98.
17. G. Li, P.G. Pickup, Measurement of single electrode potentials and impedances in hydrogen and direct methanol PEM fuel cells, *Electrochim. Acta*, 49 (2004) 4119-4126.
18. T.M. Brueckner, P.G. Pickup, Kinetics and Stoichiometry of Methanol and Ethanol Oxidation in Multi-Anode Proton Exchange Membrane Cells, *J. Electrochem. Soc.*, 64 (2017) F1172-F1178.
19. W. Hu, J. Xie, H.W. Chau, B.C. Si, Evaluation of parameter uncertainties in nonlinear regression using Microsoft Excel Spreadsheet, *Environmental Systems Research*, 4 (2015) 4-17.
20. S. Sun, M.C. Halseid, M. Heinen, Z. Jusys, R.J. Behm, Ethanol electrooxidation on a carbon-supported Pt catalyst at elevated temperature and pressure: A high-temperature/high-pressure DEMS study, *J. Power Sources*, 190 (2009) 2-13.
21. D.D. James, P.G. Pickup, Measurement of carbon dioxide yields for ethanol oxidation by operation of a direct ethanol fuel cell in crossover mode, *Electrochim. Acta*, 78 (2012) 274-278.

Chapter 7

Product Distributions and Efficiencies for Ethanol Electrolysis at PtNi Octahedra

All of the experimental work in this chapter was performed by Rakan M. Altarawneh.

The raw data is provided in Appendix F.

Data analysis was performed by Rakan M. Altarawneh and Prof. Peter Pickup.

This chapter was written by Rakan M. Altarawneh.

7. Product Distributions and Efficiencies for Ethanol Electrolysis at PtNi Octahedra

7.1 Introduction

Growing environmental concerns are driving the development of alternative kinds of renewable and clean energy sources with low CO₂ emissions. In this context, ethanol is one of the most important renewable energy sources because it is relatively safe, easily transported, and has a high energy density. It is widely used in gasoline, and can potentially be used more efficiently in fuel cells, either directly in direct ethanol fuel cells (DEFC) or following reforming, or electrolysis, to produce hydrogen.¹⁻³

Nevertheless, the large-scale commercialization of DEFCs or electrolysis cells (EECs) has been obstructed by obstacles that need to be overcome such as the low current densities for the ethanol oxidation reaction (EOR), crossover through the membrane and low faradaic efficiencies.⁴⁻⁶ The complete oxidation of ethanol to carbon dioxide is still the major problem in electrocatalysis. For efficient use of ethanol in DEFCs or EECs, it should be oxidized completely to carbon dioxide at the anode to generate 12 electrons, while oxygen is reduced to water at the cathode in a DEFC or water is reduced to hydrogen in an EEC. However, the main products from DEFCs and EECs are acetaldehyde and acetic acid, which provide low faradaic efficiency by only generating 2 and 4 electrons, respectively.^{7,8}

The catalysts most commonly used in DEFCs and EECs are based on platinum nanoparticles, which provide a high number of low coordination atoms and have relatively high selectivity for cleavage of the C–C bond of ethanol.⁹⁻¹³ Following adsorption on the active sites of Pt, the ethanol molecules can dissociate and oxidize to various species through two or more pathways. One path produces strongly adsorbed CO and CH_x intermediates and a second path mainly leads to the

formation of acetic acid and/or acetaldehyde. Further oxidation of intermediates requires OH_{ad} species to form CO_2 . However, Pt is easily poisoned by adsorbed oxygenated species such as CO_{ad} at low overpotentials and OH_{ad} at high overpotentials. CO_{ad} and OH_{ad} are adsorbed very strongly on the surface of the Pt at low and high overpotentials, respectively. Even small amounts of these species can block the catalyst's active sites, leading to a decrease in the catalytic activity and the selectivity by inhibiting the adsorption, dissociation, and further oxidation of ethanol.¹⁴⁻¹⁶ Since dissociative adsorption of water to form OH_{ad} is necessary for the complete oxidation of CO_{ad} and CH_x to CO_2 , the formation of OH_{ad} species is the rate limiting step for the complete oxidation at low overpotentials, while the cleavage of the C-C bond is the rate limiting step at high overpotentials. Therefore, modification of existing catalysts and synthesis of new catalysts are required to activate the formation of OH_{ad} species at low overpotentials and to enhance the cleavage of the C-C bond at high overpotentials. Using oxophilic metals such as Ru, Sn, Ni, Co, Fe, Cu and Pd, as well as controlling the morphology (crystalline facets) of the catalyst surface can improve the efficiency and performance of DEFCs and EECs by facilitating the complete oxidation of ethanol.^{11,17-20}

In recent years, modification of Pt nanoparticles with oxophilic metals to form bi and trimetallic alloy nanostructures has attracted great interest.¹⁹⁻²¹ This strategy is one of the most important methods used to reduce the catalyst cost and mitigate the effect of CO poisoning. The formation of OH_{ad} on the surface of the oxophilic metal at low overpotentials promotes CO_{ad} oxidation, while changes in the electronic structure of the surface Pt atoms can result in weaker binding of CO_{ad} .¹⁴ However, measurements of product distributions have shown that the modification of Pt with Ru and/or Sn decreases the selectivity of the catalysts for complete oxidation of ethanol to CO_2 .^{21,22}

Nickel has been shown to promote the catalytic activity of Pt for ethanol oxidation.^{14,23,24} An octahedral PtNi/C nanocatalyst was applied for the study of ethanol oxidation at ambient temperature.²³ The electrochemical performance of the PtNi/C octahedra was found to be much higher than commercial Pt/C.^{23,24} In situ FTIR measurements showed that the poisoning effect of CO_{ad} was significantly less at PtNi/C as compared with commercial Pt/C.²³

The aim of the work described in this chapter was to measure the performance and the selectivity of the reported octahedral PtNi/C alloy catalyst in a proton exchange membrane ethanol electrolysis cell (PEM-EEC). In particular, this work focusses on the stoichiometry, product distributions and efficiencies for ethanol oxidation at octahedral PtNi/C, and comparison with a commercial Pt/C catalyst. It is important to know whether Ni increases the selectivity for C-C bond cleavage, like Rh, or decreases it like Ru and Sn.

7.2 Experimental

7.2.1 Chemicals and Materials

Carbon supported Pt (Pt/C; HiSPECTM 13100, 70% Pt; Alfa Aesar), platinum acetylacetonate (Pt(acac)₂, 97%, Aldrich Chem. Co.), nickel acetylacetonate (Ni(acac)₂, 95%, Aldrich Chem. Co.), anhydrous ethanol (Commercial Alcohols Inc.), acetic acid (99.7%, Caledon Lab. Chemicals), oleylamine (70%, Aldrich Chem. Co.), oleic acid (90%, Aldrich Chem. Co.), benzyl ether (98%, Alfa Aesar), tungsten hexacarbonyl (W(CO)₆, 97%, Alfa Aesar), Nafion solution (5%, DuPont) and carbon black (Vulcan XC-72, Cabot) were used as received in this work. The as-received NafionTM 115 and 117 membranes were pre-treatment before using as follows: they cut into square pieces and heated in 3% H₂O₂ for 1 h at 80°C. Using distilled water, the membranes were rinsed until cooled down and immersed for 15 min at ambient temperature. Then the pieces of membranes

were heated at 80°C in 1 M sulfuric acid for 1 h followed by heating at 80°C for 3 h in distilled water, after rinsing.

7.2.2 Synthesis of the PtNi/C Catalyst

A sampled of the carbon supported PtNi (~30 wt% metal on carbon) catalyst was initially prepared following the procedure reported in ref.^{23,24}. A larger batch was then prepared by the same method as follows. 200 mg of Pt(acac)₂ and 100 mg of Ni(acac)₂ in 20 mL of oleylamine, 10 mL of oleic acid and 70 mL of benzyl ether were heated to 130 °C under N₂ protection with vigorous stirring. Then 600 mg of W(CO)₆ was rapidly added and the mixture was heated at 225°C for 40 min under N₂. Toluene (5 mL) and ethanol (15 mL) were added to the cooled solution followed by sonication for 5 min. The PtNi nanoparticles were isolated by centrifugation at 6000 rpm for 10 min, and then dispersed in toluene by sonication for 10 min. A carbon black suspension, prepared by sonication for 10 min of 200 mg of carbon in toluene (5 mL), was added and the mixture was then sonicated for 3 h, filtered and the PtNi/C catalyst was washed several times with toluene and ethanol.^{23,24} For further purification,²⁴ batches of the PtNi/C catalyst were mixed with 20 mL of acetic acid and then heated at 60 °C for 2 or 4 h. The suspensions were filtered, washed several times with ethanol and dried at 70 °C in an oven for 30 min.

7.2.3 Physical Characterization

The crystal structure of the PtNi/C octahedral catalyst was investigated by using X-ray powder diffraction (XRD; Rigaku Ultima IV X-ray diffractometer with a copper X-ray source (Cu K α radiation, $\lambda = 1.5406 \text{ \AA}$) and a scintillation counter detector). The composition of the PtNi/C octahedral catalyst was determined by thermal gravimetric analysis (TGA; TA Instruments Q500

TGA) and inductively coupled plasma optical emission spectrometry (ICP-OES). The sample for ICP-OES was prepared by mixing ca. 6 mg of catalyst with 6 mL of HCl and 2 mL of HNO₃ and heated at 65 °C for 22 h. The final solution was filtered and diluted to 15 mL of water and then analyzed using a Perkin-Elmer 5300 DV inductively coupled plasma – optical emission spectrometer. Transmission electron microscopy (TEM) was used to study the morphology of the PtNi/C octahedral catalyst including the particle size and distribution, with a JEOL 2011 scanning transmission electron microscope.

7.2.4 Electrochemical Characterization

Electrochemical characterization of the catalysts was performed with a potentiostat/galvanostat using EC-Lab electrochemical software (CV measurements) as well as a 5 cm² commercial proton exchange membrane fuel cell hardware operated as an EEC^{22,25} and nine anode PEM-EEC cell²⁶.

A conventional three-electrode glass cell was used for cyclic voltammetry (CV). The counter electrode was a platinum wire and the reference electrode was a saturated calomel electrode (SCE). A catalyst coated glassy carbon disk was used as the working electrode. All CV experiments were carried out in a N₂-purged 1.0 M sulfuric acid electrolyte at ambient temperature, and potentials are referred to SCE. The working electrode was prepared by suspension of ca. 2 mg of PtNi/C or Pt/C catalyst in 120 μL of water, 30 μL of 2-propanol and 50 μL of 5% Nafion solution. Following sonication for 2 h, 3 μL of the catalyst suspension was pipetted onto a polished glassy carbon disk and allowed to dry overnight at ambient temperature. Before measurement of the ethanol oxidation activity, the working electrodes were cycled from -0.2 to 0.8 V at 100 mV s⁻¹ in 1 M H₂SO₄ for 3 cycles. Then each working electrode was cycled between -0.2 V and 0.8 V in 0.1 M ethanol + 1.0

M H₂SO₄ solution at scan rate of 10 mV s⁻¹ for 3 cycles. For each sample, three cycles of CV were collected and the last two cycles were averaged.

The 5 cm² commercial fuel cell setup, software and apparatus have been previously described.^{25,28} The cell was operated in anode polarization mode to avoid the chemical reaction between oxygen and ethanol.²⁵ The anode was prepared by mixing ca. 52 mg of PtNi/C catalyst, after treatment with acetic acid for 4 h, with ca. 258 μL of 5% Nafion and 200 μL of 1-propanol, and sonication for 3 h at ambient temperature. The resulting suspension was spread onto Toray carbon fiber paper (CFP; TGP-H-090) to give a metal (Pt+Ni) loading of 3.2 mg cm⁻² and a Nafion loading of ca. 20 mass%. The cathode consisted of 4 mg cm⁻² Pt black on TGP-H-090. A similar cell with nine 0.236 cm² anodes,²⁶ operated as an EEC in crossover mode, was used to provide kinetic and stoichiometric information for the ethanol oxidation reaction.

7.3 Results and Discussion

7.3.1 Physical Characterization of the PtNi/C Catalyst

Herein, the large batch of PtNi/C was used for the physical characterization, before treatment with acetic acid. The XRD spectrum of the PtNi/C catalyst is presented in Figure 7.1. Alloy formation was confirmed by comparing the peak positions of the as-prepared PtNi/C catalyst and peak positions for pure Pt and Ni from the ICDD (International Centre for Diffraction Data, PDF # 03-065-9445) database. The XRD shows peaks for the face centered cubic (fcc) structure of crystalline Pt. All the diffraction peaks of the PtNi/C were slightly shifted to higher and lower angles as compared with those for Pt and Ni, respectively, which confirm alloy formation. The mean size of the PtNi particles was estimated to be 8.3 nm by applying the Scherrer equation to the most intense PtNi alloy (111) peak,²⁷ which is near to the average size of 9.0 nm reported by

Choi et al.²⁴. Heating in acetic acid at 60 °C for 4 h produced only minor changes in the XRD (Fig. 7.1), with small shifts to lower angles and a slight broadening, indicating a decrease in the average particle size to 8.0 nm. This is consistent with the loss of Ni.

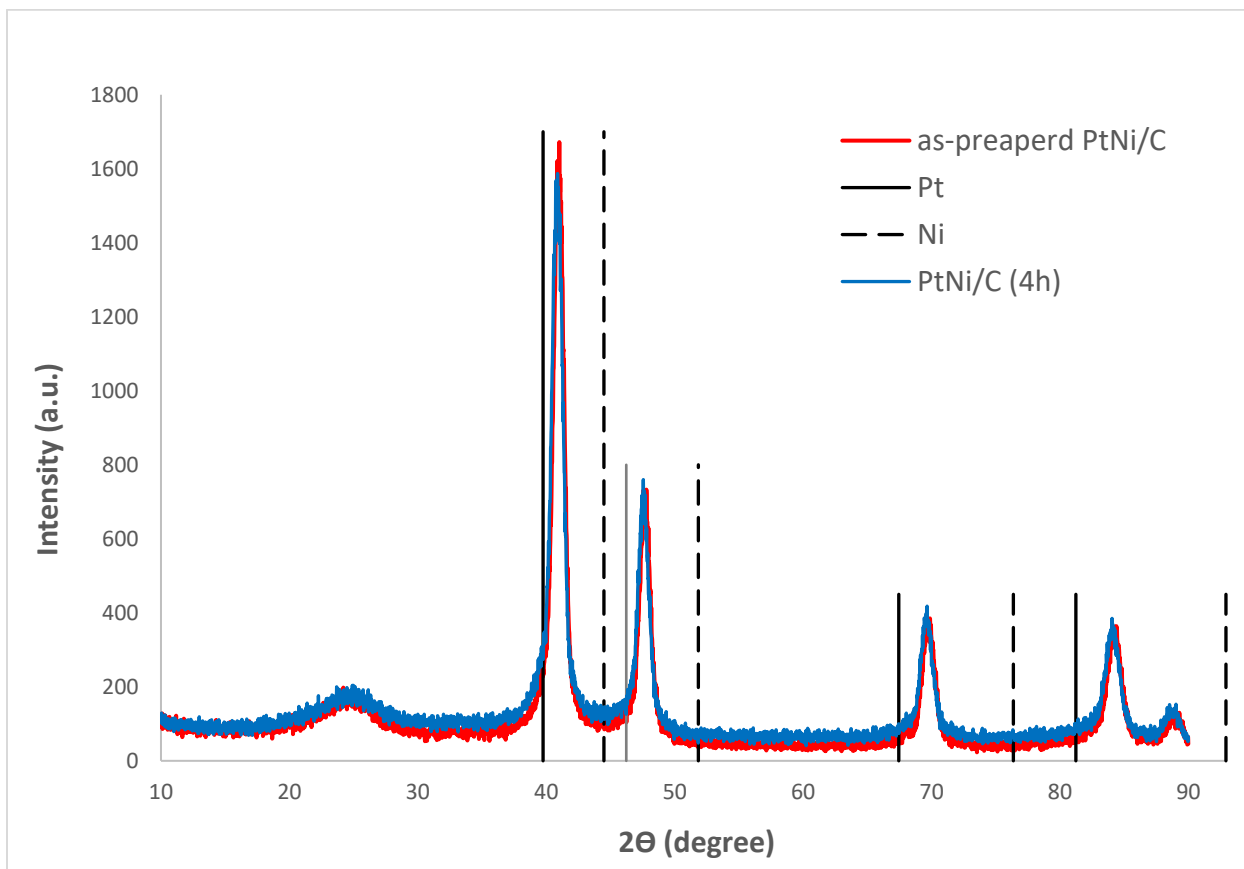


Figure 7.1. X-ray diffraction patterns of the as prepared bulk PtNi/C sample, and follow treatment with acetic acid for 4 h.

Several quantitative analysis techniques were used to determine the loadings of the metals in the catalyst. TGA showed that the loading of metals (Pt and Ni) in the PtNi/C catalyst was 30.96% before treatment with acetic acid and decreased slightly following treatment with acetic acid for 2 h and 4 h, to 30.62% and 30.30%, respectively. These results are in good agreement with ref²⁴ which indicate that some loss of Ni occurred when the catalyst was treated with acetic acid.

Furthermore, the loadings of Pt and Ni based on ICP-OES for the PtNi/C catalyst before treated with acetic acid were 23.6 mass% and 4.4 mass% respectively. These results show a

difference between the TGA and ICP-OES techniques. This difference can be attributed to the experimental errors such as loss some carbon or metals during the sample transfer or sample preparation, resulting in the TGA and ICP-OES results being overestimated and underestimated, respectively. The Pt:Ni atomic ratio determined by ICP-OES was close to 1.6 ($\text{Pt}_{63}\text{Ni}_{37}/\text{C}$) which is the same as one value reported previously,²⁴ but less than 2.3 that is another value that has been reported in the literature.²³ There was also a small amount of W (0.5%) from the $\text{W}(\text{CO})_6$ employed in the synthesis. Heating the as prepared catalyst in acetic acid at 60 °C for 4 h increased Pt content to 24.9 mass% and decreased the Ni and W contents to 3.4% and 0.4%, respectively. The increase in the Pt:Ni atomic ratio to 2.2 is consistent with the previously reported preferential loss of Ni from the catalyst surface.²⁴

The morphology of the PtNi/C catalyst was characterized by TEM and selected images are displayed in Figure 7.2. It is clear from Figure 7.2 that the PtNi nanoparticles (dark) have relatively homogenous structures with a typically octahedral shape, in good agreement with refs.^{23,24}. These images showed that the PtNi nanoparticles were distributed and dispersed well over the carbon support. The mean edge length of the PtNi nanoparticles is ca. 9.0 ± 1 nm, which is in good agreement with the mean particles size obtained from XRD and reported previously.^{23,24}

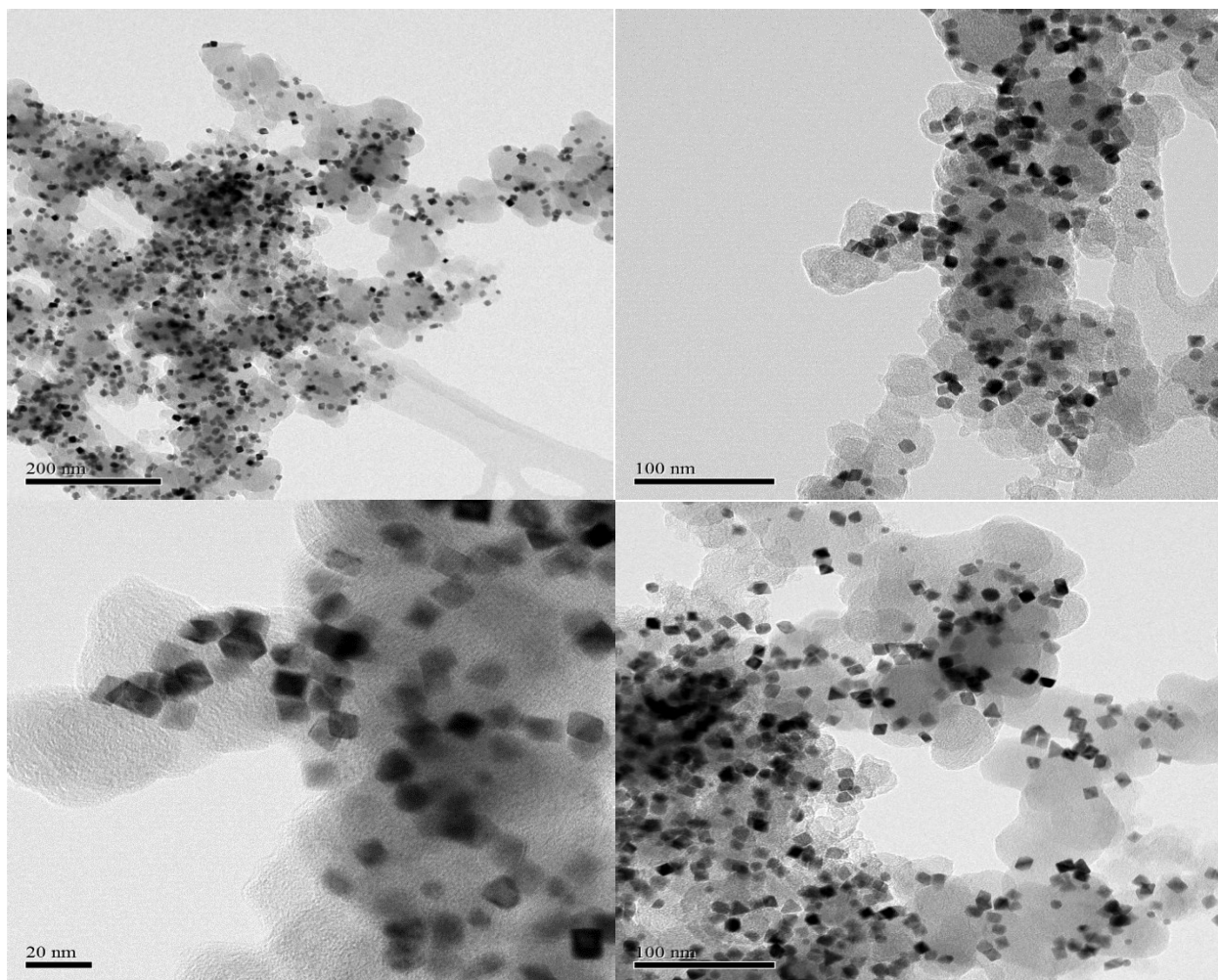


Figure 7.2. TEM images of the PtNi/C catalyst before treatment with acetic acid.

7.3.2 Electrochemical Measurements

7.3.2.1 Cyclic Voltammetry

CVs for the PtNi/C catalyst before and after treatment with acetic acid and for a commercial Pt/C catalyst are shown in Figures 7.3 and 7.4. These experiments were carried out at ambient temperature in 1.0 M sulfuric acid. The CVs are normalized in terms of the mass of Pt (A per mg of Pt) and all of the potentials reported in this section (CV measurements) are versus SCE. Figure 3 shows the CVs for PtNi/C and Pt/C catalysts carried out in sulfuric acid electrolyte in the absence

of ethanol. It is clear from this figure that the catalysts exhibit peaks with different areas in the hydrogen adsorption-desorption region from -0.20 V to 0.15 V. The area under the peaks in this region is proportional to the area of Pt that is electrochemically active. Although quantitative comparisons are difficult because of the differences in background currents (comparisons are shown in Table 7.1), it can be seen that the PtNi/C catalyst initially had a low active area relative to Pt/C. Following 2 h of treatment with acetic acid almost the same behavior was observed over all potentials, indicating no significant change in active area. In contrast, the PtNi/C after 4 h treatment with acetic acid showed higher activity in the hydrogen region, which indicates that this sample had a higher number of Pt active sites relative to the other samples. After 4 h treatment with acetic acid, the PtNi/C showed larger current than those on the Pt/C and other PtNi/C samples in the electronic double-layer region (between 0.15 and 0.6 V vs. SCE). The as-prepared and 2 h treatment samples did not show high activities (large current) over all potentials and this can be attributed to the non-alloyed Ni and residual organic solvents that strongly adsorbed on the active sites including the carbon supported and effect on the activity of the catalyst. Previous studies have shown that transition metals such as Ni and Sn can block Pt active sites and decrease the charge in the hydrogen region.^{28,29} In general, the larger current in the electronic double-layer region is characteristic of carbon supported catalysts.³⁰⁻³² Thus, the larger current for the PtNi/C after 4 h treatment can be attributed to removal of the residual oleic acid and oleyl amine from the carbon surface. In conclusion, treatment of the catalyst with acetic acid for 4 h is necessary to remove the non-alloyed Ni atoms and the residual organic solvents blocking the active sites and this provides a higher number of Pt active sites and increase the catalytic activity.

Table 7.1. Surface areas and utilizations of the PtNi/C and Pt/C catalysts determined from the hydrogen desorption charges in Fig. 7.3.

Catalyst	Geometric area (cm²)	Electrochemical area (cm²)	Utilization (%)
Pt/C	16	6.7	41
As-prepared PtNi/C	4.4	0.60	13
2 h treatment PtNi/C	4.0	0.66	16
4 h treatment PtNi/C	4.1	1.2	30

Generally, catalyst properties such as the shape and size of particles, as well as composition and alloying, have a significant influence on the activity of catalysts that have the same mass of Pt due to differences in active areas.^{23,24,33,34} Although the comparison in Figure 7.3 is on a Pt mass basis, the PtNi/C catalyst showed significantly lower activity in the hydrogen region than the Pt/C catalyst after subtracting the background current. This indicates that the PtNi/C sample had a lower number of Pt active sites than Pt/C for the same mass (content) of Pt.

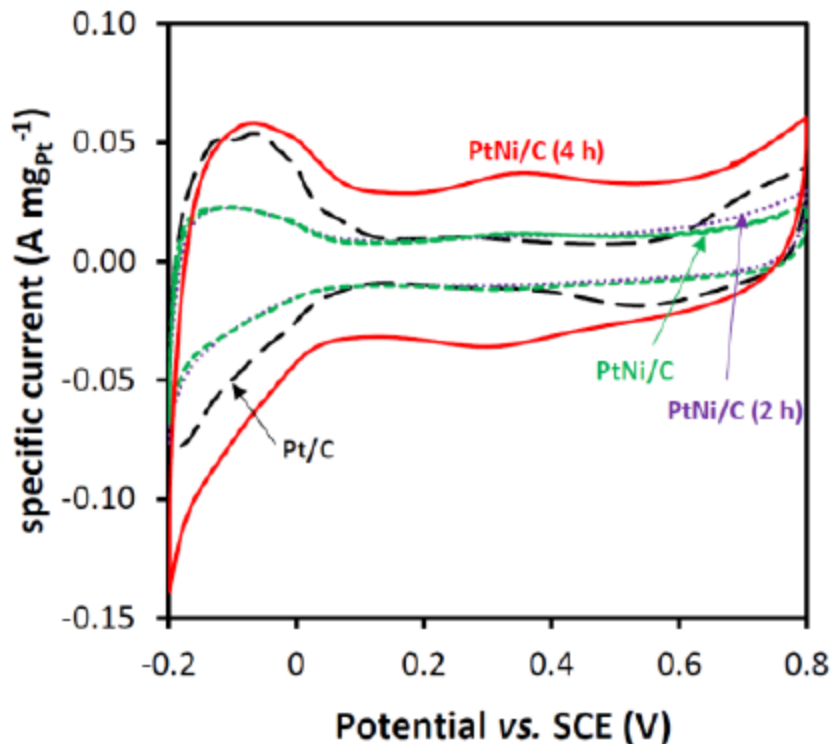


Figure 7.3. Cyclic voltammograms (100 mV s^{-1} ; $1 \text{ M H}_2\text{SO}_4(\text{aq})$) of Pt/C (—; $0.32 \text{ mg Pt cm}^{-2}$), the as prepared PtNi/C (\cdots ; $0.11 \text{ mg Pt cm}^{-2}$) and PtNi/C following treatment with acetic acid for 2 h (- -; $0.10 \text{ mg Pt cm}^{-2}$) and 4 h (—; $0.11 \text{ mg Pt cm}^{-2}$).

Figure 7.4 shows the ethanol oxidation reaction characteristics using CV for the PtNi/C and Pt/C catalysts in an aqueous solution of 0.1 M ethanol and 1.0 M sulfuric acid. At potentials lower than 0.65 V, the PtNi/C catalyst exhibited higher catalytic activity as compared with Pt/C in both scans, which can be attributed to easier dissociative adsorption of water to form OH_{ad} species at low potentials on the catalyst's surface in the presence of Ni,^{35,36} resulting in less poisoning effect and higher catalytic activity. The different samples of PtNi/C had similar catalytic activities on the reverse scan at low potentials. At higher potentials ($\geq 0.65 \text{ V}$), the PtNi/C catalyst after treatment with acetic acid for 4 h showed significantly higher catalytic activity relative to the Pt/C and the other samples of PtNi/C in both the forward and reverse scans. Furthermore, the PtNi/C after 2 h treatment with acetic acid had higher catalytic activity than the PtNi/C before treatment

at potentials lower than 0.65 V. While the PtNi/C before and after 2 h treatment had similar behavior at high potentials and their catalytic activities were higher than Pt/C at intermediate potentials and similar at higher potentials. In comparison with Pt/C, the forward current peak for the PtNi/C catalyst was shifted to lower potential which indicates that the PtNi/C surface had less poisoning effect over this range of potentials.

The differences in the voltammogram for ethanol oxidation at the PtNi/C and Pt/C catalysts can be explained as follow: generally, the ethanol oxidation reaction is enhanced (promoted) significantly with increasing the active areas and/or decreasing the poisoning effect. Based on the results in Table 7.1 and Figure 7.3, the PtNi/C had a lower number of Pt active sites than Pt/C for the same mass of Pt. In contrast, the presence of Ni increases the dissociative adsorption of water to form OH_{ad} and weaken the Pt-CO bond, which lead to a decrease in the poisoning effect at low potentials.^{35,36} Thus, this can provide higher catalytic activity at the PtNi/C as well as decrease the onset potential (close to 0.2 V) and shift the forward current peak to low potential. Whereas, the Pt/C had higher active area, the poisoning effect played a central role at low potentials where the surface is blocked with CO_{ad} and this inhibits the ethanol oxidation reaction, resulting in lower catalytic activity and a shift in the onset potential and the forward current peak to higher potential.

The PtNi/C catalyst following treatment with acetic acid showed different behaviors for ethanol oxidation and this can be explained by the effect of poisoning species particularly the residual organic solvents and the non-alloyed Ni atoms. The active sites of the as-prepared catalyst were blocked by these species. Following 4 h of treatment the active area was increased (as shown in Table 7.1 and Figure 7.3) by removing these species and this increased the catalytic activity over all potentials. While 2 h of treatment did not affect significantly the active area, it did have a

significant effect on the onset potential and catalytic activity at intermediate potentials as shown in Figure 7.4.

Moreover, the CV curves of the PtNi/C catalyst present broad and higher current peak on the reverse scan as compared to the forward scan. This indicates that the PtNi/C catalyst had higher activity and less poisoning effect (higher CO tolerance) at low potentials.^{23,37} While Pt/C had lower current peak on the reverse scan and this can be explained by the strongly adsorbed CO_{ad} that rapidly blocks the active sites as the potentials decreased, which decreases the catalytic activity. Generally, strong Pt-OH and Pt-O bonds were formed and accumulated at high potentials leading to blocking of the active sites, ethanol adsorption and surface reaction, resulting in decreased catalytic activity.^{16,38,39} This can be used to explain the sharp fall in current at potentials higher than ca. 0.6 V in the forward scan, as shown in Figure 7.4. The free electrochemical active sites increased on the reverse scan OH and O species are desorbed from the Pt surface (reduction of surface Pt(II)) with decreasing the potentials.^{38,39} Following the reverse scan at the PtNi/C, the ability of the reactive species like ethanol to adsorb on the free active sites and even displace the strongly adsorbed OH and O species can be increased significantly with decreasing the potential. This can increase the dissociative adsorption of ethanol to form CO_{ad} and thus increased complete oxidation of ethanol to CO₂ by reacting CO_{ad} and OH_{ad} species at the PtNi/C surface, resulting higher in an activity.

Treatment of the PtNi/C catalyst with acetic acid had a significant effect on the current for ethanol oxidation on the forward scan, but a much smaller effect on the reverse scan. Notably, the onset of ethanol oxidation was shifted to a much lower potential following 4 h in acetic acid, while the shift was much smaller for 2 h in acetic acid. Additionally, the forward current peak was shifted to lower potential following 4 h treatment as compared to 2 h treatment with acetic acid, which

indicates higher catalytic activity obtained for 4 h treatment with acetic acid. Residual organic solvents from the synthesis and non-alloyed Ni atoms may block the Pt active sites and have a negative effect on the ethanol oxidation reaction leading to a decrease in the catalytic activity. Therefore, removing the residual organic solvent and the non-alloyed Ni atoms, which is easier than for alloyed Ni atoms, is necessary, and can be accomplished by treatment with acetic acid. Choi et al.²⁴ reported that the Ni content decreased with increasing treatment time.

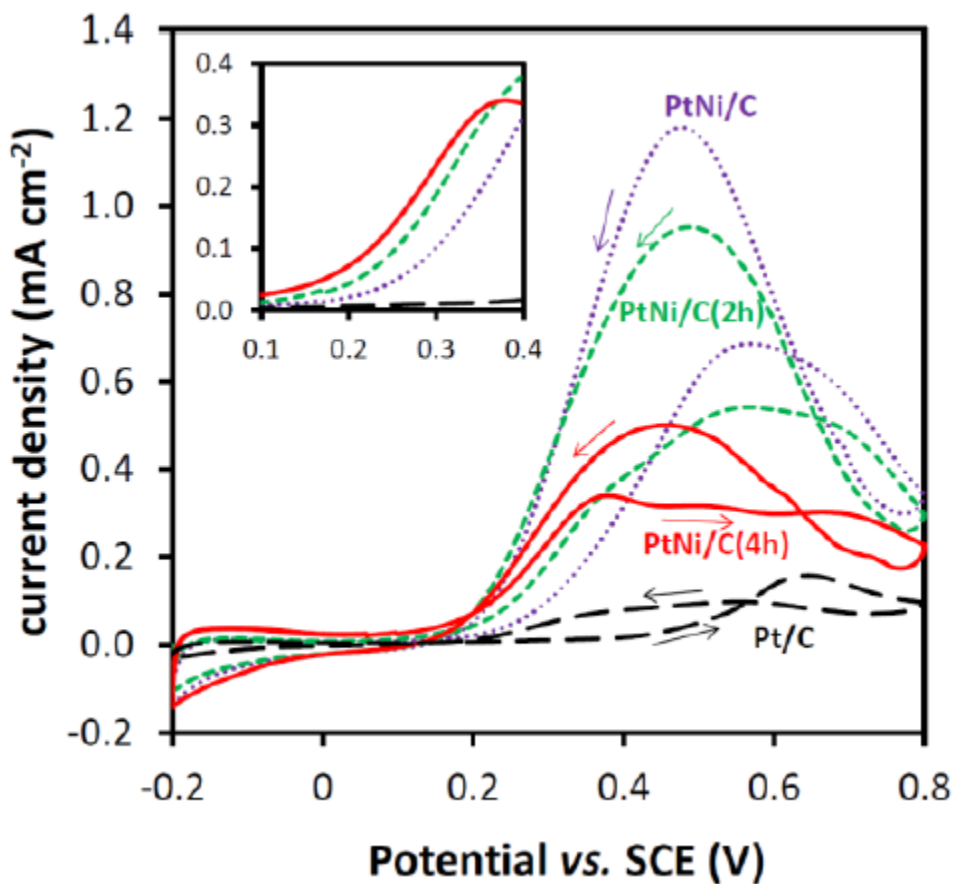


Figure 7.4. Active area normalized cyclic voltammograms (10 mVs^{-1}), in $1 \text{ M H}_2\text{SO}_4(\text{aq})$ containing 0.1 M ethanol, at Pt/C (— —), the as prepared PtNi/C (····) and PtNi/C following treatment with acetic acid for 2 h (- - -) and 4 h (—). The inset shows an expansion of the 0.1 to 0.4 V region on the forward scan.

7.3.2.2 Ethanol Electrolysis in a Multi-Anode PEM Cell at 80 °C.

A multi-anode cell was used for preliminary evaluation of the PtNi/C for ethanol oxidation at 80 °C in a PEM cell, and for assessing the effects of treatment with acetic acid. This cell allows several catalysts to be tested and compared under the same conditions at the same time. Three electrodes prepared with each catalyst were used in order to assess the significance of differences between catalysts and to determine the reproducibility of the electrodes. All potentials reported in this section are versus DHE. The cell was operated in crossover mode in order to avoid the loss of ethanol due to crossover. In this mode, ethanol was fed through the cathode while N₂ was passed through the anode at a flow rate of ca. 30 mL min⁻¹. Then the ethanol would cross through the membrane to the anode where it is electrochemically oxidized.^{6,26}

Figure 7.5 shows polarization curves for the oxidation of 0.1 M ethanol at different samples of PtNi/C catalyst and at Pt/C. Two batches of PtNi/C catalyst were prepared by using the same method on a small (black line) and large (red line) scale and tested in the nine-anode cell. The sample from the first batch was used without treatment with acetic acid, while the sample from the second batch was treated with acetic acid for 4 h. Note that the second batch (large scale preparation) was used for the physical characterization and the other electrochemical measurements (including measurements in a 5 cm² cell) in this chapter. Figure 7.5 shows that the two PtNi/C samples had almost the same activity at all potentials, which indicates that the catalyst treatment with acetic acid did not affect the catalytic activity at 80 °C in the PEM cell. This observation indicates that the species that blocked the Pt surface in the CV experiments were removed during start-up and conditioning of the PEM cell. In comparison with Pt/C, the PtNi/C had similar current at low potentials but lower current at high potentials.

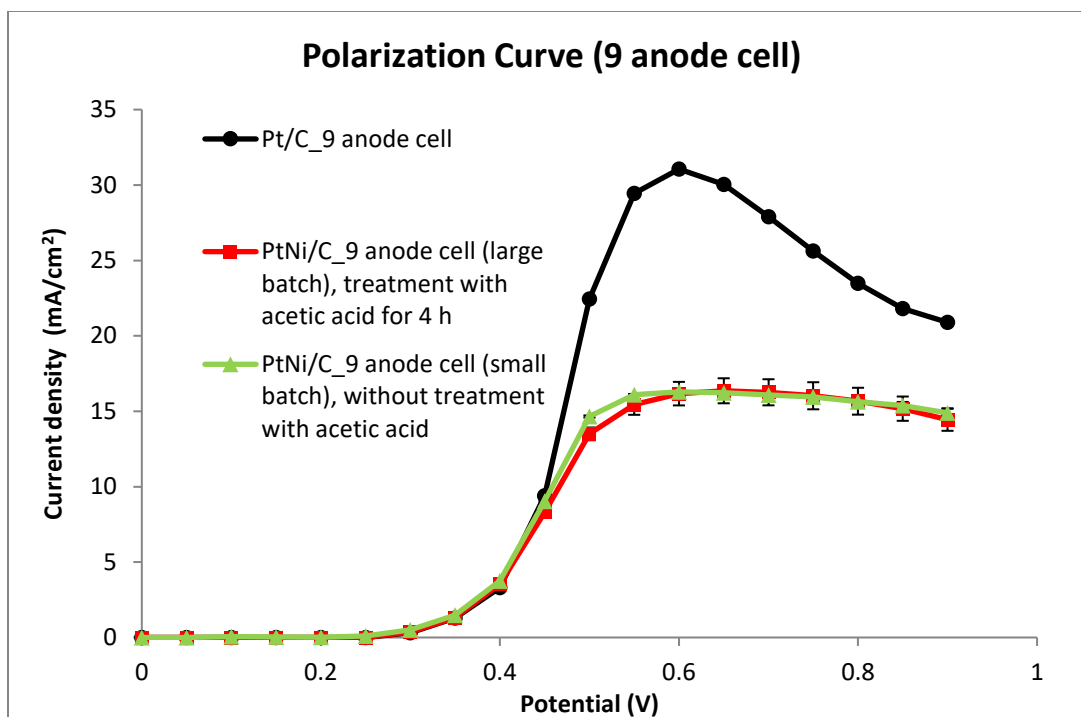


Figure 7.5. Polarization curves for the oxidation of 0.100 M ethanol in a nine-anode PEM cell in crossover mode at Pt/C and different samples of PtNi/C at 0.5 mL min⁻¹ and 80 °C.

The nine-anode cell was also used to measure the efficiency of the PtNi/C catalyst for the complete oxidation of ethanol, by passing the N₂ from the cell exhaust through a CO₂ detector. Figure 7.6 shows faradaic yields of CO₂ for the two samples of PtNi/C catalyst and for Pt/C at 0.5 V. The relatively stable CO₂ readings demonstrate, for the first time, that the nine-anode cell is suitable for CO₂ measurements. The average yield of CO₂ increased from 21% to 30% after the PtNi/C catalyst was treated with acetic acid for 4 h while the CO₂ yield was 80% for the Pt/C. At this potential, the PtNi/C showed less selectivity for complete oxidation relative to the Pt/C. The increase in selectivity for the complete oxidation at the PtNi/C can be attributed to the increase in number of Pt active sites after treatment of the catalyst with acetic acid for 4 h and changing the Pt:Ni ratio at the catalyst surface, as discussed earlier. Hence, the treatment with acetic acid did not affect the catalytic activity but significantly affected the selectivity of the catalyst.

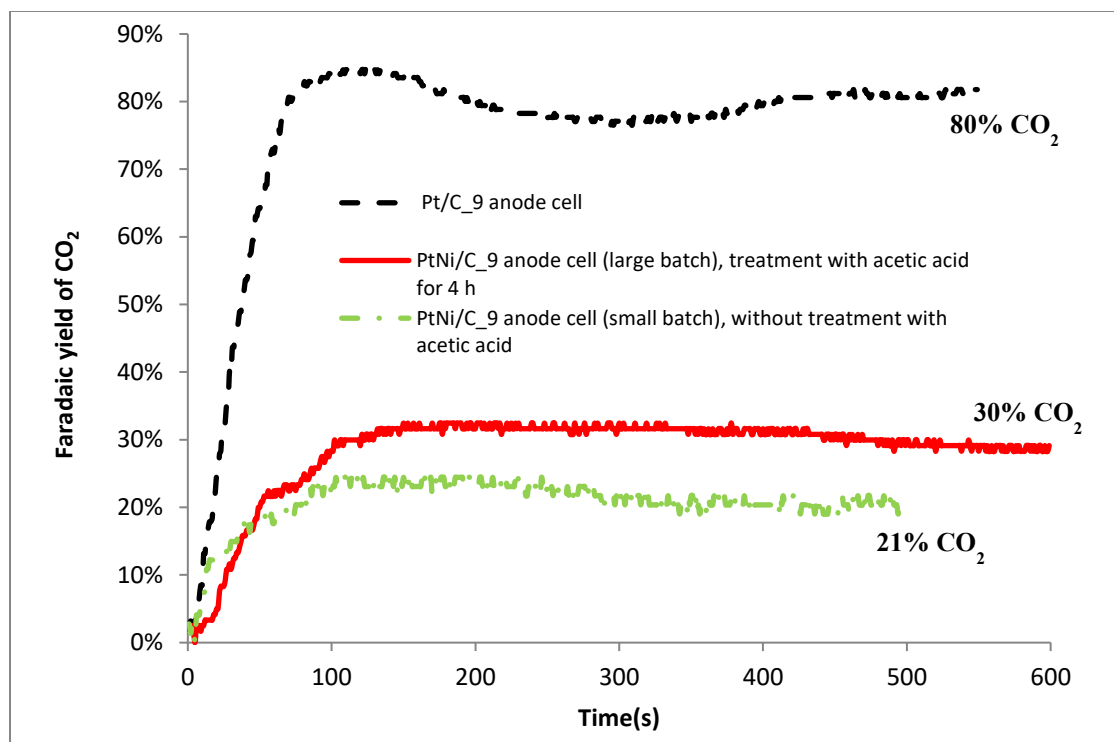


Figure 7.6. Faradaic yields of CO₂ for the oxidation of 0.100 M ethanol in a nine-anode PEM cell in crossover mode at Pt/C and different samples of PtNi/C at 0.2 mL min⁻¹, 0.5 V and 80 °C.

7.3.2.3 Ethanol Electrolysis in a 5 cm² PEM Cell at 80 °C

Polarization Curve. — The PtNi/C catalyst was treated with acetic acid for 4 h and tested in a 5 cm² PEM cell in anode polarization mode at 80 °C. The anode polarization mode provides higher current and faradaic efficiencies compared with the cross over mode and can be used to evaluate performances of anode catalysts for DEFCs.

Figure 7.7 shows polarization curves for the oxidation of 0.1 M ethanol at PtNi/C, Pt/C and PtRu/C anodes. The data for Pt/C and PtRu/C have been presented and discussed in Chapter 4.²² The PtNi/C and Pt/C catalysts had very similar performances at potentials lower than 0.35 V, while at potentials higher than 0.4 V the PtNi/C showed lower currents than Pt/C. In comparison with PtRu/C, the PtNi/C had lower performance at low and high potentials but similar performance at

intermediate potentials as shown in Figure 7.7. Generally, the effect of Ni and Ru can be explained as follow: the presence of Ni and Ru can enhance the bifunctional mechanism and ligand (electronic) effect of the catalyst which increases the formation of the adsorbed OH_{ad} species and weakens the CO_{ad} bonds, but the most dominate effect of Ru is the bifunctional mechanism.^{35,36,40–42} This effect should improve the ethanol oxidation reaction at low potentials where the OH_{ad} could form and react with CO_{ad} , resulting more free active sites and thus higher catalytic activity should be observed. While at the Pt/C catalyst, high potentials are required to increase the catalytic activity by enhancing the dissociative adsorption of water to form OH_{ad} to oxidize the CO_{ad} species and clear the Pt active sites for further ethanol oxidation.

Herein, the CVs did not give a good indication of what would happened in a fuel cell particularly at low potentials where the current measured in the PEM cell at the PtNi/C was similar and lower than those measured at the Pt/C and PtRu/C, respectively. The CVs (Figure 7.4) showed the effect of Ni by enhancing the catalytic activity of the PtNi/C at low potentials as compared with Pt/C. The poor performance of the PtNi/C in the 5 cm² cell at low potentials compared with Pt/C can be attributed to the lower Pt active areas for the same content of Pt, less amount of Pt and large Pt particle size (9 nm compared with 3.6 nm for the Pt/C), where the current in this region is proportional to the Pt active areas, and poisoning effect. At potentials higher than 0.45 V, the differences in the catalytic activity between the PtNi/C and Pt/C can be attributed to a difference in average number of electrons (n_{av}), which is discussed in Section 7.3.3.

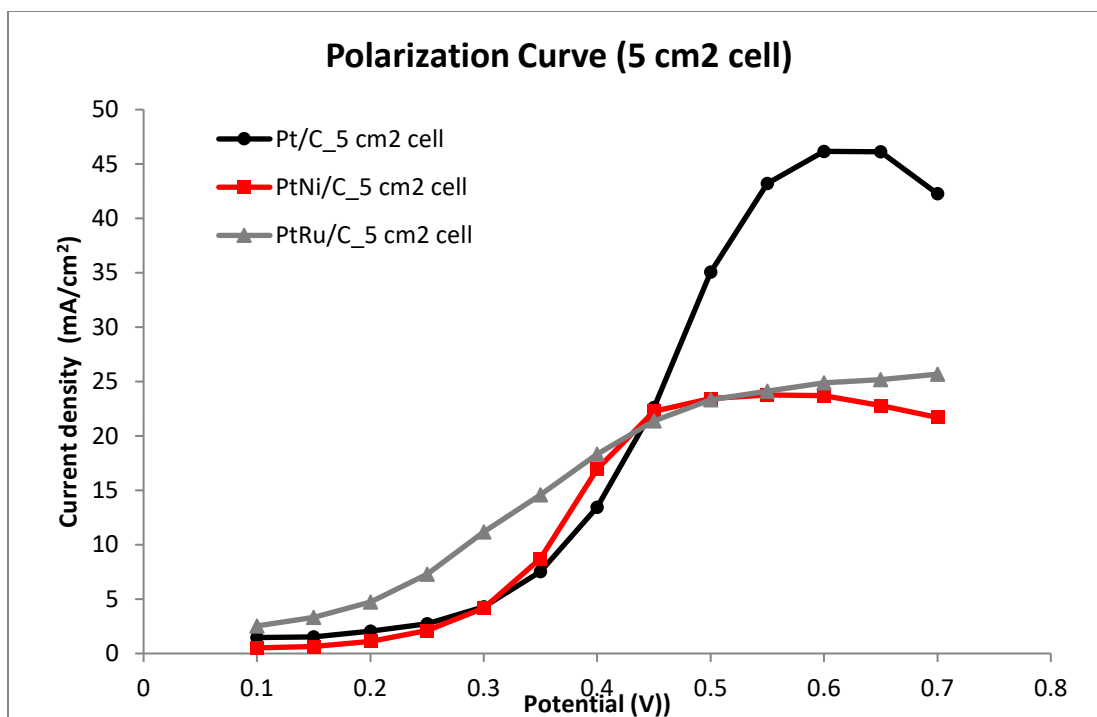


Figure 7.7. Polarization curves for the oxidation of 0.100 M ethanol in anode polarization mode at Pt/C, PtRu/C and PtNi/C at 0.5 mL min⁻¹ and 80 °C.

7.3.3 Stoichiometry and Product distribution

7.3.3.1 Average Number of Electrons (n_{av})

Table 7.2 shows n_{av} values for the oxidation of 0.10 M ethanol at a PtNi/C anode at 80°C, obtained by using three different methods: analysis of the amount of ethanol consumed (ΔC) and from the product distribution (faradaic and chemical).^{21,22,25} Figure 7.8 compares the average values of n_{av} obtained for the PtNi/C and Pt/C anodes under the same conditions, which can be used to determine the faradaic efficiency. At lower potentials (≤ 0.4 V), the PtNi/C had higher efficiency than Pt/C with a maximum n_{av} of 6.90 at 0.35 V. While at potentials ≥ 0.45 V, the PtNi/C had lower efficiency than Pt/C with n_{av} decreasing to 4.74 at 0.70 V for the PtNi/C.

Table 7.2. n_{av} vs. potential for the oxidation of 0.100 M ethanol (0.2 mL min^{-1}) at PtNi/C anode at $80 \text{ }^\circ\text{C}$.

Potential (V)	n_{av} (ΔC)	n_{av} (Faradaic)	n_{av} (Chemical)
0.70	4.80	4.65	4.74
0.60	4.99	5.01	5.00
0.50	5.17	5.29	5.22
0.45	5.60	5.67	5.63
0.40	6.90	6.64	6.82
0.35	6.90	6.88	6.90
0.30	6.79	6.81	6.80
0.20	6.51	6.57	6.53

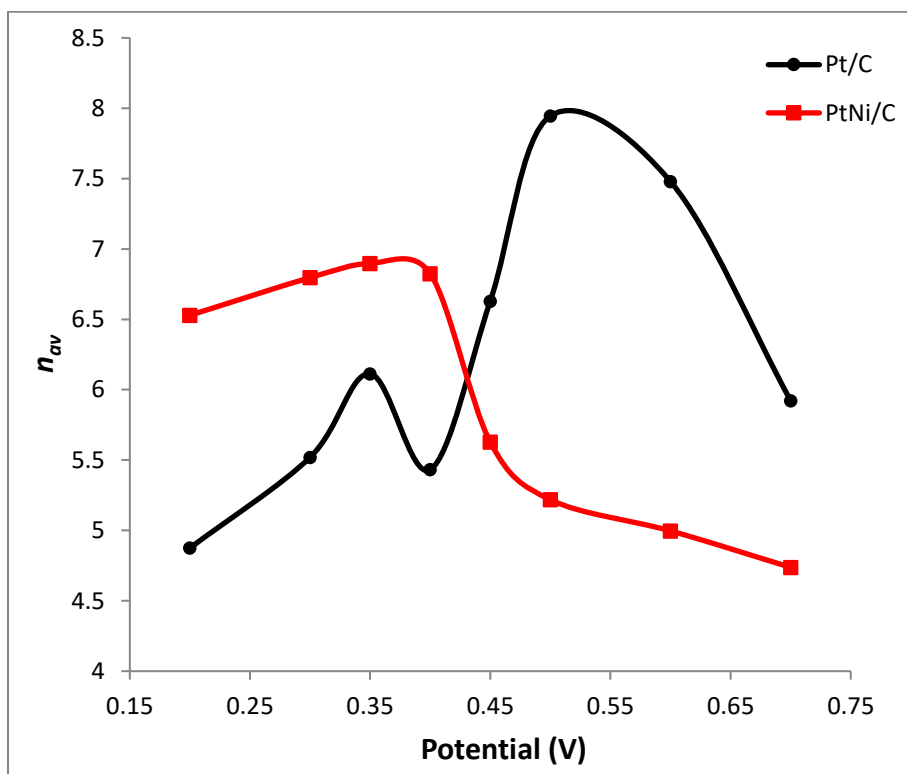


Figure 7.8. n_{av} vs. potential for the oxidation of 0.100 M ethanol (0.2 mL min^{-1}) at Pt/C and PtNi/C anodes at $80 \text{ }^\circ\text{C}$.

7.3.3.2 Product Distribution

The reaction mechanism of the ethanol oxidation reaction is complex and involves many adsorbed intermediates and products. Determining the product distribution in conjunction with electrochemical measurements is important for understanding the mechanism and how the rates of the desired pathways can be enhanced. This can lead to development of more efficient catalyst for commercialization of DEFCs and EECs. Figure 7.9 shows the faradaic and chemical yields of CO₂, acetic acid and acetaldehyde obtained from the analysis of the products in the cell exhaust. The current produced and the measured quantities of CO₂, acetic acid and acetaldehyde were used to calculate the faradaic yields, while the chemical yields were calculated based on the measured quantities of these products and the amount of ethanol consumed. A NDIR detector was used to determine CO₂ while amounts of ethanol consumed, and acetic acid and acetaldehyde produced were measured by using ¹H NMR spectroscopy.²⁵ The chemical yield of CO₂ obtained for PtNi/C was almost constant at low potentials and decreased at high potentials, from 40% at 0.2 V to 10% at 0.7 V. In contrast, higher acetic acid yields were obtained at high potentials, reaching 86% at 0.7 V. The high yield of acetic acid at high potentials indicates that acetic acid was easily formed when the catalyst surface was covered with OH_{ad} species.

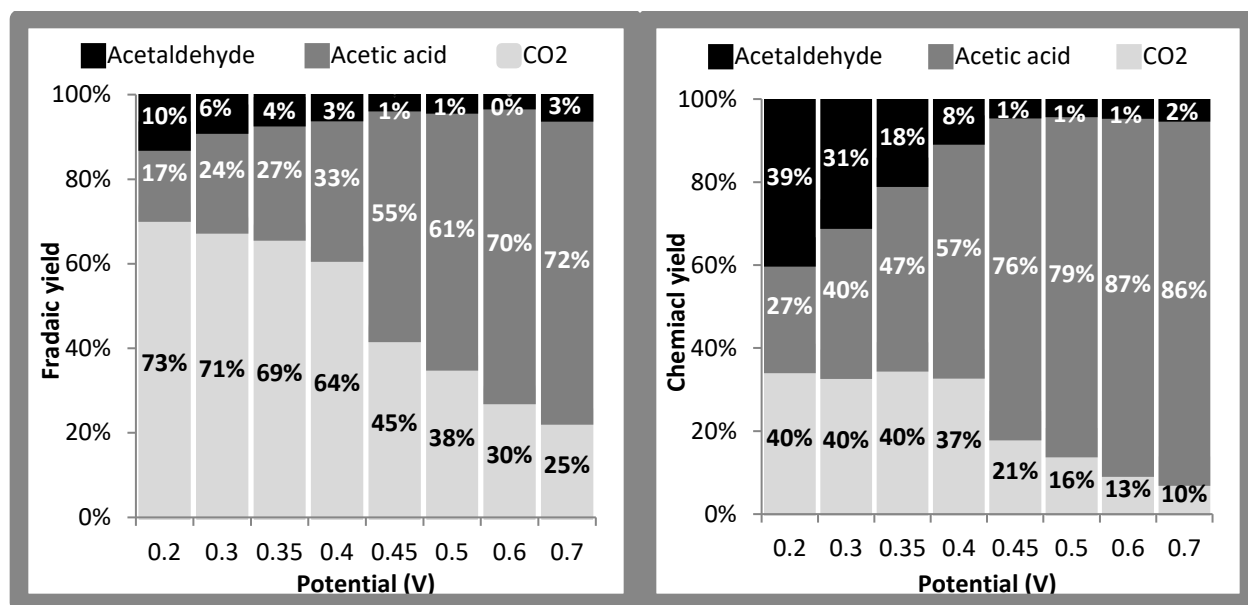


Figure 7.9. Faradaic and chemical yields of CO₂, acetic acid, and acetaldehyde as a function of potential for oxidation of 0.100 M ethanol at a PtNi/C anode at 80 °C.

Figure 7.10 shows a comparison between the yields of CO₂ for PtNi/C and Pt/C under the same conditions. It can be seen from Figure 7.10 that the potential dependence of the CO₂ yields for both the PtNi/C and Pt/C are similar to those for the n_{av} values, shown in Figure 7.8. This can be attributed to the high number of electrons transferred during CO₂ formation, relative to acetaldehyde and acetic acid formation. PtNi/C provided higher selectivity than Pt/C for the complete oxidation of ethanol to CO₂ at low potentials, while at high potentials, PtNi/C was less selective for the complete oxidation of ethanol to CO₂ than Pt/C.

In comparison with the product distributions of Pt/C and PtRu/C reported in ref.²², the measured product distributions for PtNi/C clearly demonstrates the effects of Ni and octahedral shape on the selectivity and efficiency (Figure 7.8) of the PtNi/C catalyst. The selectivity for the complete oxidation was higher for PtNi/C than for the Pt/C at low potentials and for the PtRu/C at all potentials. The enhancement of the selectivity and efficiency of PtNi/C toward oxidation of ethanol at low potentials compared with Pt/C can be attributed to the formation of OH_{ad} and

weakening of the CO_{ad} bond. The different behaviors of the poisoning species (CO_{ad} and OH_{ad}) at low and high potentials can be observed at the surface of PtNi/C and Pt/C.^{35,36,42,43} Increasing the potential, more OH_{ad} and O species would be adsorbed strongly on the PtNi/C surface occupying most of the active sites (oxidation of the Pt surface), where they adsorbed on Pt even more strongly than CO, lead to inhibition of C-C bond cleavage. At Pt/C, OH_{ad} can form at high potentials and react with the accumulated adsorbed CO, resulting higher selectivity. It can be seen from the data in Figure 7.10 that CO_2 yields were decreased significantly at potentials higher than 0.5 V at Pt/C. This can be attributed to the increasing coverage of OH_{ad} species that block the active sites. Previous studies have shown that a high coverage of surface oxidants (particularly OH and O species) inhibits the ability of the catalyst to cleave the C-C bond and thus decreases CO_{ad} formation.^{16,38,39}

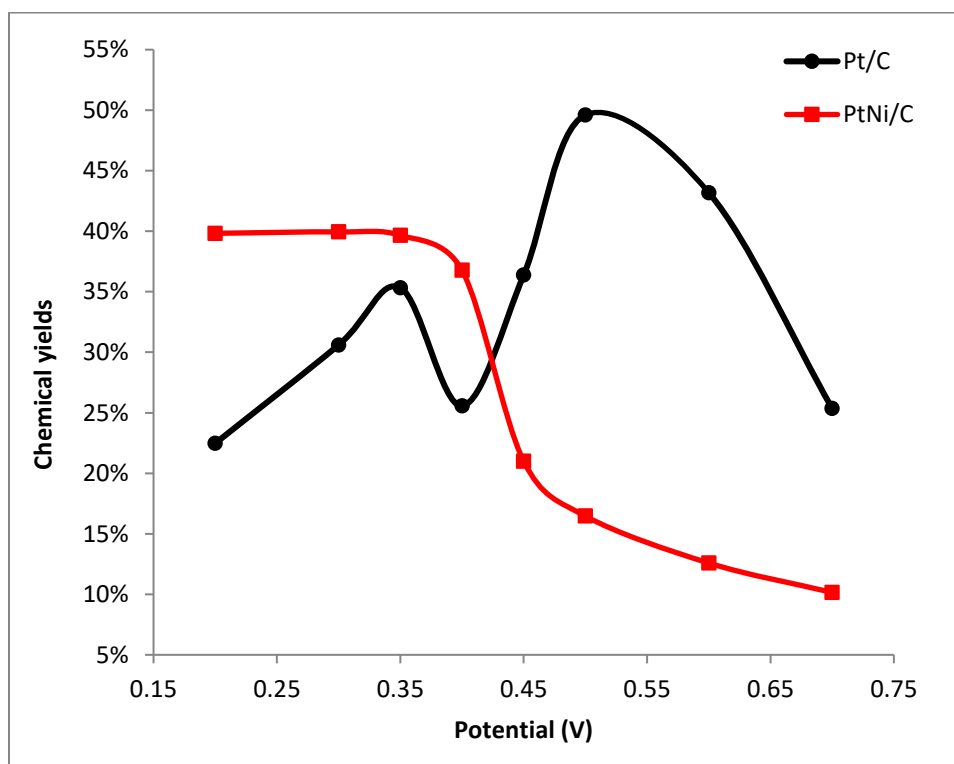


Figure 7.10. Chemical yields of CO_2 vs. potential for oxidation of 0.100 M ethanol at Pt/C and PtNi/C anodes at 80 °C.

The acetaldehyde yields were higher at low potentials compared to the yields at high potentials. Since the acetaldehyde is an intermediate that can be easily further oxidized in the cell, bilayer catalyst can be used to enhance the further oxidation of acetaldehyde to CO₂ and acetic acid and thus increase the faradaic efficiency of ethanol oxidation.²¹

A comparison of the present performance results with the literature is the best way to get insight on the promoting effect of the temperature and the electrolyte. In situ FTIR was used to monitor the intermediates and products of the ethanol oxidation reaction on the octahedral PtNi/C at ambient temperature in a liquid electrolyte.²³ Sulaiman reported that the PtNi/C catalyst exhibits higher current than Pt/C (46% Pt), but based on the IR results acetic acid was the main product at all potentials on PtNi/C. The CO₂ yields were almost constant at low potentials and increased at high potentials, which indicates that the PtNi/C had higher selectivity for the complete oxidation at higher potentials.²³ Increasing temperature leads to increased catalytic activity and efficiency due to the effect of temperature on the kinetics and mass transport. DEFCs operate at elevated temperatures (> 70 °C) with a polymer electrolyte. Consequently, the catalytic activity, selectivity and efficiency of new catalysts should be evaluated under these conditions, in addition to studies at ambient temperature in a liquid electrolyte. Our results show that the selectivity of Pt for complete oxidation of ethanol to CO₂ can be increased at low potentials by modification with Ni.

7.3.4 Efficiency

In this work, the cell was operated as an ethanol electrolysis cell (EEC) to obtain accurate n_{av} values by avoiding the chemical reaction between oxygen and ethanol that occurs in a DEFC. These accurate n_{av} values were used to estimate the efficiencies of DEFCs as described previously.²² Figure 7.8 shows the overall efficiency (ϵ_{DEFC}) of a DEFC vs. current density (A)

and power density (B). It can be seen from Figure 7.11 that the PtNi/C would provide higher efficiencies than Pt/C at the lowest current and power densities, while PtNi/C would give lower efficiencies at the highest current and power densities. Consequently, from the best of our knowledge, the PtNi/C is the best catalyst at low potentials whereas the best catalyst at higher potentials is still Pt/C. The latter could provide higher current densities at higher potentials as compared to the PtNi/C. Although the PtNi/C and Pt/C had similar performances at low potentials, the higher n_{av} values for PtNi/C provide higher faradaic efficiencies at low potentials. These results indicate that the selectivity of the catalyst has a vital effect on the efficiency. Developing catalysts with high selectivity for the complete oxidation of ethanol to CO₂ can improve the efficiency of a DEFC.

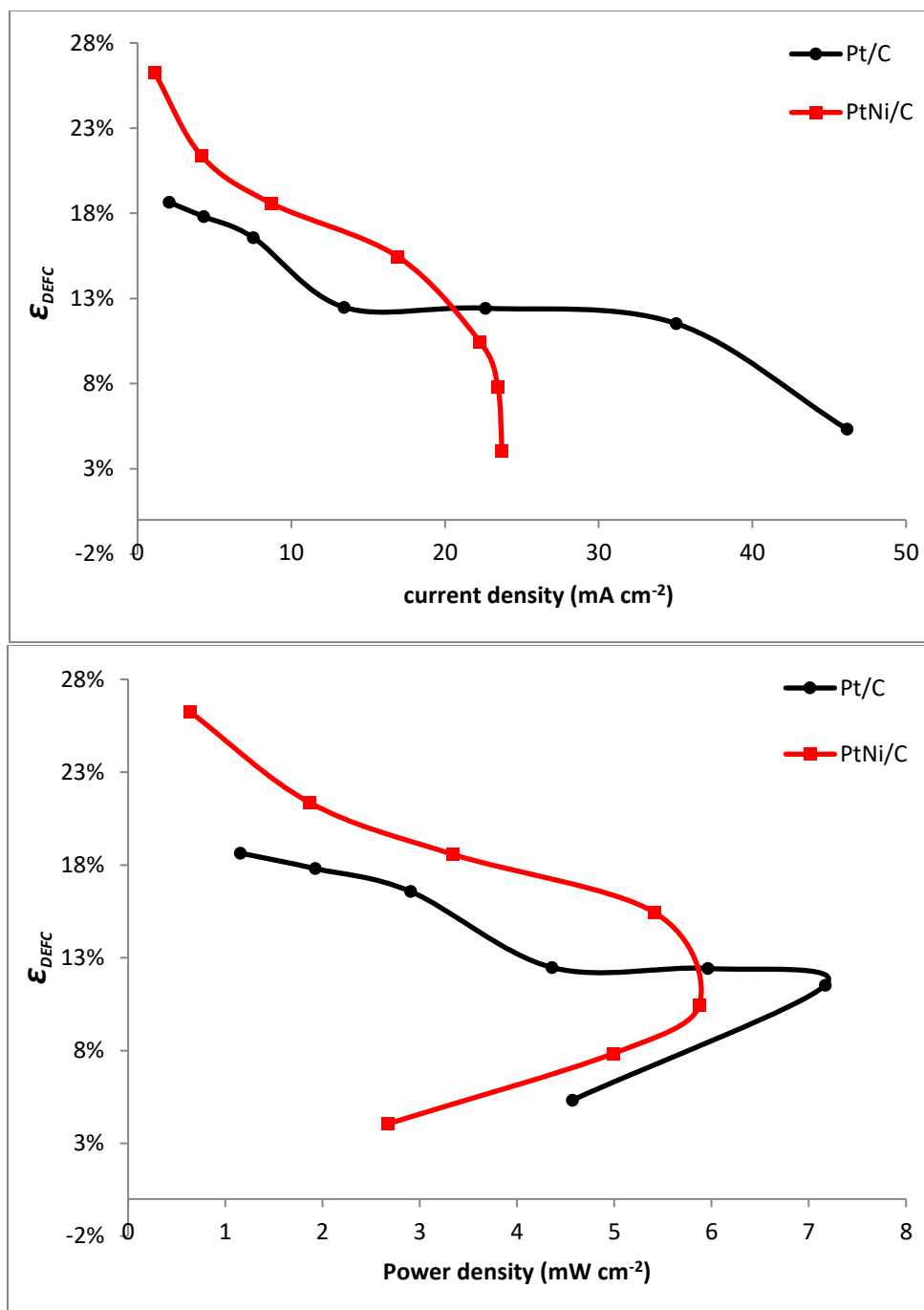


Figure 7.11. Efficiency vs. current density (A) and power density (B) for DEFCs operating with 0.100 M ethanol at 80°C at PtNi/C and Pt/C anodes.

7.4 Conclusions

In summary, the treatment of the PtNi/C octahedra with acetic acid for 4 h had a large effect on the activity and selectivity for ethanol oxidation. It was found that increasing the treatment time increased the active Pt area by removing residual organic solvents and non-alloyed Ni atoms. Following 4 h treatment the current in CVs was enhanced and the selectivity for complete oxidation significantly increased in the nine-anode cell compared with as-prepared PtNi/C. In comparison with the polarization curves, the CVs did not give a clear insight into the performance of the PtNi/C catalyst under fuel cell conditions. The selectivity was increased significantly at the PtNi/C compared with Pt/C at low potentials, but acetic acid was the main product at high potentials. The n_{av} values and product distributions showed that the presence of the alloyed Ni atoms with an octahedral shape increased the faradaic efficiency of the catalyst at low potentials and thus the PtNi/C has the highest faradaic efficiencies at low potentials.

References

1. Y. Wang, K.S. Chen, J. Mishler, S.C. Cho, X.C. Adroher, A review of polymer electrolyte membrane fuel cells: Technology, applications, and needs on fundamental research, *Appl. Energy*. 88 (2011) 981–1007.
2. A. Ghumman, P.G. Pickup, Efficient electrochemical oxidation of ethanol to carbon dioxide in a fuel cell at ambient temperature, *J. Power Sources*. 179 (2008) 280–285.
3. S. Song, P. Tsiakaras, Recent progress in direct ethanol proton exchange membrane fuel cells (DE-PEMFCs), *Appl. Catal. B Environ.* 63 (2006) 187–193.
4. G. Li, P.G. Pickup, Analysis of performance losses of direct ethanol fuel cells with the aid of a reference electrode, *J. Power Sources*. 161 (2006) 256–263.
5. G. Andreadis, P. Tsiakaras, Ethanol crossover and direct ethanol PEM fuel cell

- performance modeling and experimental validation, *Chem. Eng. Sci.* 61 (2006) 7497–7508.
6. D.D. James, P.G. Pickup, Effects of crossover on product yields measured for direct ethanol fuel cells, *Electrochim. Acta.* 55 (2010) 3824–3829.
 7. S. Rousseau, C. Coutanceau, C. Lamy, J.M. Léger, Direct ethanol fuel cell (DEFC): Electrical performances and reaction products distribution under operating conditions with different platinum-based anodes, *J. Power Sources.* 158 (2006) 18–24.
 8. D.D. James, D. V. Bennett, G. Li, A. Ghumman, R.J. Helleur, P.G. Pickup, Online analysis of products from a direct ethanol fuel cell, *Electrochem. Commun.* 11 (2009) 1877–1880.
 9. K.I. Ozoemena, Nanostructured platinum-free electrocatalysts in alkaline direct alcohol fuel cells: catalyst design, principles and applications, *RSC Adv.* 6 (2016) 89523–89550.
 10. W. Hong, J. Wang, E. Wang, Facile synthesis of PtCu nanowires with enhanced electrocatalytic activity, *Nano Res.* 8 (2015) 2308–2316.
 11. W.P. Zhou, M. Li, C. Koenigsmann, C. Ma, S.S. Wong, R.R. Adzic, Morphology-dependent activity of Pt nanocatalysts for ethanol oxidation in acidic media: Nanowires versus nanoparticles, *Electrochim. Acta.* 56 (2011) 9824–9830.
 12. D. Ruan, F. Gao, Z. Gu, Enhanced Electrochemical Properties of Surface Roughed Pt Nanowire Electrocatalyst for Methanol Oxidation, *Electrochim. Acta.* 147 (2014) 225–231.
 13. J. Seweryn, A. Lewera, High selectivity of ethanol electrooxidation to carbon dioxide on platinum nanoparticles in low temperature polymer electrolyte membrane direct ethanol fuel cell, *Appl. Catal. B Environ.* 144 (2014) 129–134.
 14. B. Li, H. Fan, M. Cheng, Y. Song, F. Li, X. Wang, R. Wang, Porous Pt–NiO_x nanostructures with ultrasmall building blocks and enhanced electrocatalytic activity for the ethanol oxidation reaction, *RSC Adv.* 8 (2018) 698–705.

15. H.F. Wang, Z.P. Liu, Comprehensive mechanism and structure-sensitivity of ethanol oxidation on platinum: New transition-state searching method for resolving the complex reaction network, *J. Am. Chem. Soc.* 130 (2008) 10996–11004.
16. R. Kavanagh, X.M. Cao, W.F. Lin, C. Hardacre, P. Hu, Origin of low CO₂ selectivity on platinum in the direct ethanol fuel cell, *Angew. Chemie - Int. Ed.* 51 (2012) 1572–1575.
17. Y.W. Lee, M. Kim, Z.H. Kim, S.W. Han, One-Step Synthesis of Au@Pd Core-Shell Nanooctahedron, *J. Am. Chem. Soc.* 131 (2009) 17036–17037.
18. M.T.M. Koper, Structure sensitivity and nanoscale effects in electrocatalysis, *Nanoscale.* 3 (2011) 2054.
19. E. Antolini, F. Colmati, E.R. Gonzalez, Ethanol oxidation on carbon supported (PtSn)alloy/SnO₂ and (PtSnPd)alloy/SnO₂ catalysts with a fixed Pt/SnO₂ atomic ratio: Effect of the alloy phase characteristics, *J. Power Sources.* 193 (2009) 555–561.
20. E. Antolini, F. Colmati, E.R. Gonzalez, Effect of Ru addition on the structural characteristics and the electrochemical activity for ethanol oxidation of carbon supported Pt-Sn alloy catalysts, *Electrochem. Commun.* 9 (2007) 398–404.
21. R.M. Altarawneh, P.G. Pickup, Pt and PtRu catalyst bilayers increase efficiencies for ethanol oxidation in proton exchange membrane electrolysis and fuel cells, *J. Power Sources.* 366 (2017) 27–32.
22. R.M. Altarawneh, P.G. Pickup, Product Distributions and Efficiencies for Ethanol Oxidation in a Proton Exchange Membrane Electrolysis Cell, *J. Electrochem. Soc.* 164 (2017) F861–F865.
23. J.E. Sulaiman, S. Zhu, Z. Xing, Q. Chang, M. Shao, Pt-Ni Octahedra as Electrocatalysts for the Ethanol Electro-Oxidation Reaction, *ACS Catal.* 7 (2017) 5134–5141.

24. S. Il Choi, S. Xie, M. Shao, J.H. Odell, N. Lu, H.C. Peng, L. Protsailo, S. Guerrero, J. Park, X. Xia, J. Wang, M.J. Kim, Y. Xia, Synthesis and characterization of 9 nm Pt-Ni octahedra with a record high activity of 3.3 A/mg Pt for the oxygen reduction reaction, *Nano Lett.* 13 (2013) 3420–3425.
25. R.M. Altarawneh, P. Majidi, P.G. Pickup, Determination of the efficiency of ethanol oxidation in a proton exchange membrane electrolysis cell, *J. Power Sources.* 351 (2017) 106–114.
26. T.M. Brueckner, P.G. Pickup, Kinetics and Stoichiometry of Methanol and Ethanol Oxidation in Multi-Anode Proton Exchange Membrane Cells, *J. Electrochem. Soc.* 164 (2017) F1172–F1178.
27. V.K. Puthiyapura, S. Pasupathi, S. Basu, X. Wu, H. Su, N. Varagunapandiyan, B. Pollet, K. Scott, $\text{Ru}_x\text{Nb}_{1-x}\text{O}_2$ catalyst for the oxygen evolution reaction in proton exchange membrane water electrolyzers, *Int. J. Hydrogen Energy.* 38 (2013) 8605–8616.
28. P.G. Corradini, N.A. Santos, J. Perez, Pt-Sn-Eu/C Catalysts: Application of Rare Earth Metals as Anodes in Direct Ethanol Fuel Cells, *Fuel Cells.* 18 (2018) 73–81.
29. L.S. Parreira, J.C.M. Da Silva, M. D’Villa -Silva, F.C. Simões, S. Garcia, I. Gaubeur, M.A.L. Cordeiro, E.R. Leite, M.C. Dos Santos, PtSnNi/C nanoparticle electrocatalysts for the ethanol oxidation reaction: Ni stability study, *Electrochim. Acta.* 96 (2013) 243–252.
30. K. Juodkazis, J. Juodkazyte, T. Juodiene, V. Šukiene, I. Savickaja, Alternative view of anodic surface oxidation of noble metals, *Electrochim. Acta.* 51 (2006) 6159–6164.
31. S. Tanaka, M. Umeda, H. Ojima, Y. Usui, O. Kimura, I. Uchida, Preparation and evaluation of a multi-component catalyst by using a co-sputtering system for anodic oxidation of ethanol, *J. Power Sources.* 152 (2005) 34–39.

32. J. Ribeiro, D.M. dos Anjos, K.B. Kokoh, C. Coutanceau, J.M. Léger, P. Olivi, A.R. de Andrade, G. Tremiliosi-Filho, Carbon-supported ternary PtSnIr catalysts for direct ethanol fuel cell, *Electrochim. Acta.* 52 (2007) 6997–7006.
33. K.W. Park, J.H. Choi, B.K. Kwon, S.A. Lee, Y.E. Sung, H.Y. Ha, S.A. Hong, H. Kim, A. Wieckowski, Chemical and electronic effects of Ni in Pt/Ni and Pt/Ru/Ni alloy nanoparticles in methanol electrooxidation, *J. Phys. Chem. B.* 106 (2002) 1869–1877.
34. C. Te Hsieh, J.Y. Lin, Fabrication of bimetallic Pt-M (M = Fe, Co, and Ni) nanoparticle/carbon nanotube electrocatalysts for direct methanol fuel cells, *J. Power Sources.* 188 (2009) 347–352.
35. Y. Zhao, X. Li, J.M. Schechter, Y. Yang, Revisiting the oxidation peak in the cathodic scan of the cyclic voltammogram of alcohol oxidation on noble metal electrodes, *RSC Adv.* 6 (2016) 5384–5390.
36. J. Rossmeisl, J.K. Nørskov, C.D. Taylor, M.J. Janik, M. Neurock, Calculated phase diagrams for the electrochemical oxidation and reduction of water over Pt(111), *J. Phys. Chem. B.* 110 (2006) 21833–21839.
37. Y.H. Fang, Z.P. Liu, Surface phase diagram and Oxygen coupling kinetics on flat and stepped Pt surfaces under electrochemical potentials., *J. Phys. Chem. C.* 113 (2009) 9765–9772.
38. O. Sahin, H. Kivrak, A comparative study of electrochemical methods on Pt-Ru DMFC anode catalysts: The effect of Ru addition, *Int. J. Hydrogen Energy.* 38 (2013) 901–909.
39. P. Liu, A. Logadottir, J.K. Nørskov, Modeling the electro-oxidation of CO and H₂/CO on Pt, Ru, PtRu and Pt₃Sn, *Electrochim. Acta.* 48 (2003) 3731–3742.
40. Z. Zhang, L. Xin, K. Sun, W. Li, Pd-Ni electrocatalysts for efficient ethanol oxidation

- reaction in alkaline electrolyte, *Int. J. Hydrogen Energy*. 36 (2011) 12686–12697.
41. V.R. Stamenkovic, B. Fowler, B.S. Mun, G. Wang, P.N. Ross, C.A. Lucas, N.M. Marković, Improved Oxygen Reduction Activity on Pt₃Ni(111) via Increased Surface Site Availability, *Science* (80-.). 315 (2007) 493 LP-497.
 42. N. Erini, V. Beermann, M. Gocyla, M. Gliech, M. Heggen, R.E. Dunin-Borkowski, P. Strasser, The Effect of Surface Site Ensembles on the Activity and Selectivity of Ethanol Electrooxidation by Octahedral PtNiRh Nanoparticles, *Angew. Chemie - Int. Ed.* 56 (2017) 6533–6538.
 43. M. Arenz, K.J.J. Mayrhofer, V. Stamenkovic, B.B. Blizanac, T. Tomoyuki, P.N. Ross, N.M. Markovic, The Effect of the Particle Size on the Kinetics of CO Electrooxidation on High Surface Area Pt Catalysts, *J. Am. Chem. Soc.* 127 (2005) 6819–6829.
 44. A. Ruban, B. Hammer, P. Stoltze, H.L. Skriver, J.K. Nørskov, Surface electronic structure and reactivity of transition and noble metals, *J. Mol. Catal. A Chem.* 115 (1997) 421–429.

Chapter 8

Summary and Future Work

8. Summary and Future Work

8.1 Summary

New methodologies for determining the product distribution in a proton exchange membrane ethanol electrolysis cell were developed that allowed accurate analysis of residual ethanol and products from both the anode and cathode exhausts. Nitrogen was used at the cathode to avoid chemical reaction between oxygen and ethanol. Moreover, the accuracy of the results was tested by comparing four different methods to measure the stoichiometry (n_{av}) of ethanol oxidation: a purely electrochemical method, analysis of the amount of ethanol consumed (ΔC) and from the product distribution (faradaic and chemical). The results from chemical analysis were found to be in a good agreement with those from the electrochemical method in most cases, and discrepancies were used to guide refinement of the methods.

The methodology developed in this work for measurement of products and residual ethanol from ethanol electrolysis can also be applied to DEFCs. However, the effects of crossover need to be avoided or corrections need to be made. The loss of ethanol and products through the membrane to the cathode was quantified by analysis of the anode and cathode exhausts separately. It was shown that inaccuracies due to crossover were avoided when the anode and cathode exhausts were combined prior to analysis.

Many research groups have evaluated catalysts and determined product yields in cells with liquid electrolytes at ambient temperature. In this work, the effects of temperature were examined in fuel cell hardware. It was found that the performance and efficiency of the EOR were increased at higher temperatures, in good agreement with other reported in the literature. Furthermore, the effect of potential on the product distribution and efficiency was investigated for various commercial catalysts in an electrolysis cell at elevated temperature. Pt was found to provide higher

selectivity for the complete oxidation of ethanol to CO₂ than either PtRu or PtSn at all potentials and the current was higher than both at high potentials, but lower than for PtRu at low potentials. Also, the effect of combining Pt and PtRu catalysts as a mixture and in bilayer electrodes was measured as a function of potential. A synergistic effect was discovered, that was particularly strong for a PtRu on Pt bilayer. It was found that the decrease in the ethanol concentration in the PtRu layer, before it reaches the Pt layer, leads to higher CO₂ yields. Furthermore, the Pt layer can oxidized acetaldehyde produced in the PtRu layer to CO₂, resulting in a high faradaic efficiency while maintain the high potential efficiency of PtRu. From our results, it was found that the selectivity had higher influence than performance on the efficiency of the cell.

Finally, the selectivity, performance and efficiency of the EOR in an electrolysis cell were investigated for an octahedral PtNi catalyst at elevated temperature. Also, the effect of treatment with acetic acid for different periods of time was examined. It was found that there was a significant increase in selectivity for CO₂ after 4 h treatment with acetic acid. The PtNi catalyst was found to be much more selective for the complete oxidation, and therefore more efficient than Pt/C at low potentials. While at higher potentials, the PtNi had lower selectivity and efficiency compared to Pt.

In this work, the efficiencies of the DEFCs were accurately estimated for the first time as a function of current and power density based on full product analysis from both anode and cathode exhausts. The accurate determination of n_{av} allows different anodes to be compared based on the overall efficiency.

8.2 Future Work

Based on the results obtained in this work, there are some areas that should be further explored. Since an electrochemical method has been used to determine the stoichiometry of the EOR, further work is required to solve the discrepancy in the n_{av} values obtained from this method and from the amount of ethanol consumed and product analysis. Also, further work is required to understand the effect of Ni and octahedral shape on the EOR. Using a normal cell at ambient temperature, in situ infrared spectroscopy (IR) and CO stripping voltammetry could be useful techniques to provide a general idea about the behavior of adsorbed CO species on the catalyst surface in order to understand the mechanism in more detail.

Since the octahedral PtNi catalyst had higher selectivity at low potentials than the Pt, further work is required to test normal and spherical PtNi nanoparticles to compare with octahedral shape in order to study the effect of the particle shape. In addition, modification with other metals and variation of the particle size and composition can be studied. Since PtRu had the highest performance at low potentials but lowest selectivity for the complete oxidation, modification of PtNi with Ru and other metals such as Sn, Rh, and Ir, to make binary and tertiary catalysts could enhance the performance and efficiency. The performance of a PtNi catalyst was found to increase significantly at low potentials after modification with Ru and Sn.¹⁻³ Also, the modification of the catalysts can be conducted by the same procedure as the preparation of octahedral PtNi to form octahedral particles or other active shapes with more edges and corners such as polyhedra. There are lots of promising anode candidates in the literature that should be tested and compared with each other.

It can be said that the preparation method and desired metals as well as controlling size, composition, shape, uniformity and morphology are very powerful and efficient tools that can be

applied to a broad range of catalysts to enhance the performance and efficiency. A variety of such techniques can be considered for the synthesis of nanoparticles catalysts, metal oxides and supported materials and to enhance the selectivity and catalytic activity by the synergetic effect between the catalyst and support such as PtRh/SnO₂.⁴ Another option would be to use mixed and bilayer electrodes to increase the efficiency and performance of catalysts. In order to do this, bilayer electrode of PtNi and PtRu may increase the efficiency and performance of fuel cells. This means that PtNi should provide high selectivity resulting higher faradaic efficiency, while the PtRu can maintain the higher output potential which leads to increase the potential efficiency.

Finally, the selectivity, activity and efficiency of catalysts could also be affected by using oxygen at the cathode, which was influence the overall performance of the fuel cell. Therefore, these catalysts should be tested in a DEFC with oxygen at the cathode in order to study the effect of oxygen on the efficiency and performance.

References

1. D. Li, H. Lv, Y. Kang, N.M. Markovic, V.R. Stamenkovic, Progress in the Development of Oxygen Reduction Reaction Catalysts for Low-Temperature Fuel Cells, *Annu. Rev. Chem. Biomol. Eng.* 7 (2016) 509–532.
2. E. Ribadeneira, B.A. Hoyos, Evaluation of Pt-Ru-Ni and Pt-Sn-Ni catalysts as anodes in direct ethanol fuel cells, *J. Power Sources.* 180 (2008) 238–242.
3. S. Beyhan, C. Coutanceau, J.M. Léger, T.W. Napporn, F. Kadirgan, Promising anode candidates for direct ethanol fuel cell: Carbon supported PtSn-based trimetallic catalysts prepared by Bönemann method, *Int. J. Hydrogen Energy.* 38 (2013) 6830–6841.

4. L.A. Soares, C. Morais, T.W. Napporn, K.B. Kokoh, P. Olivi, Beneficial effects of rhodium and tin oxide on carbon supported platinum catalysts for ethanol electrooxidation, *J. Power Sources*. 315 (2016) 47–55.

Appendix A

CO₂ and NMR Measurements

A. CO₂ and NMR Measurements

A1. CO₂ Measurements

A1.1 Faradaic Yield

The faradaic yield of the CO₂ is determined by the experimental and theoretical rates of CO₂ formation according to eq. A1,

$$\text{faradaic } CO_2 \text{ yield} = \frac{\text{experimental rate of } CO_2 \text{ formation}}{\text{theoretical rate of } CO_2 \text{ formation}} \quad (A1)$$

The experimental CO₂ rate in mol s⁻¹ is obtained from the CO₂ detector and is determined by eq. A2. While the theoretical CO₂ rate is calculated based on the measured current (eq. A3). The theoretical moles of CO₂ is determined by eq. A4.

$$\text{experimental rate of } CO_2 = \frac{CO_2 \text{ (ppm)} * \text{flow rate of nitrogen (L min}^{-1}\text{)}}{60 * 10^6 * V_m} \quad (A2)$$

$$\text{theoretical rate of } CO_2 = \frac{\text{average current (mA)}}{nF} \quad (A3)$$

$$\text{theoretical moles of } CO_2 = \frac{Q}{nF} = \frac{It}{nF} \quad (A4)$$

Where V_m is the volume of any gas in L mol⁻¹, Q is the charge produced from the EOR, n is the number of electrons transferred to form one molecule of CO₂ and $F = 96500 \text{ A s mol}^{-1}$ is the faraday constant. The CO₂ reading ($CO_2 \text{ (ppm)}$) was allowed to stabilize and then average over a period of at least 100 s.

In chapter 3 (and appendix B), the experimental rate of CO₂ from the anode can be calculated according to eq. A5.

$$\text{experimental rate of } CO_2 = \frac{CO_2(\text{ppm})_a * t_{CO_2} * \text{flow rate of nitrogen (L min}^{-1}\text{)}}{60 * 10^6 * V_m * t_{exp}} \quad (A5)$$

Where $CO_2 (ppm)_a$ is the average of all CO_2 readings from the anode, t_{CO_2} is the time in seconds required to flush the collected CO_2 from the anode through the CO_2 detector, while t_{exp} is the length of experiment in seconds.

A1.2 Chemical Yield

The chemical yield of CO_2 is calculated according to eq. A6,

$$\text{chemical } CO_2 \text{ yield} = \frac{\text{mol of } CO_2 / 2}{\text{mol of ethanol consumed}} \quad (A6)$$

Where the moles of CO_2 (determined by eq. A7) is divided by 2 since two moles of CO_2 are produced from one mole of ethanol. While the moles of ethanol consumed is determined by NMR.

$$\text{mol of } CO_2 = \text{experimental rate of } CO_2 * \text{time (s)} \quad (A7)$$

A2. NMR Measurements

The concentration of the analyte (residual ethanol, acetic acid and acetaldehyde) was determined by its NMR area according to eq. A8.

$$\text{analyte concentration} = \frac{\text{normalized area for analyte} * \text{standard concentration}}{\text{normalized area for standard}} \quad (A8)$$

Where the normalized area is the NMR peak area of the analyte or internal standard divided by the number of protons that contribute to the peak.

A3. Faradaic Yields of Acetic Acid and Acetaldehyde

The faradaic yields of acetic acid and acetaldehyde can be calculated by eq. A9,

$$\text{faradaic yield} = \frac{C_A u}{IFn} \quad (A9)$$

Where C_A is the concentration in mM obtained from NMR, u is the flow rate of ethanol in mL s^{-1} , I is the measured current in mA, F is the faraday constant, and n is the number of electrons transferred to form acetic acid ($n = 4$) and acetaldehyde ($n = 2$).

Appendix B

Current and CO₂ Traces for Pt black

B. Current and CO₂ Traces for Pt black

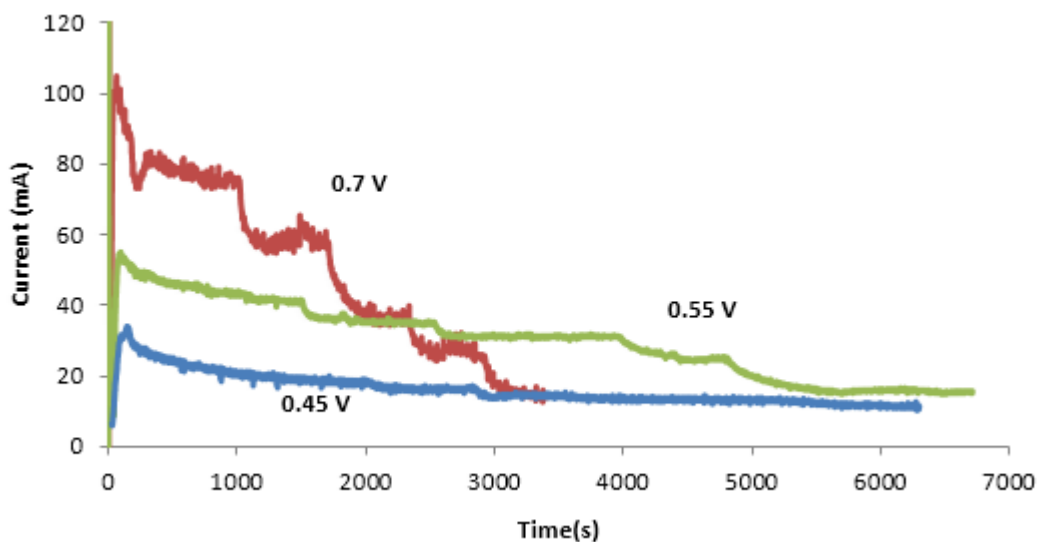


Figure B1. Current at different potentials vs. time for oxidation of 0.100 M ethanol at 50°C at Pt black anode. At each potential, the cell was running at different flow rates (0.5, 0.2, 0.09, 0.05 and 0.02 mL min⁻¹).

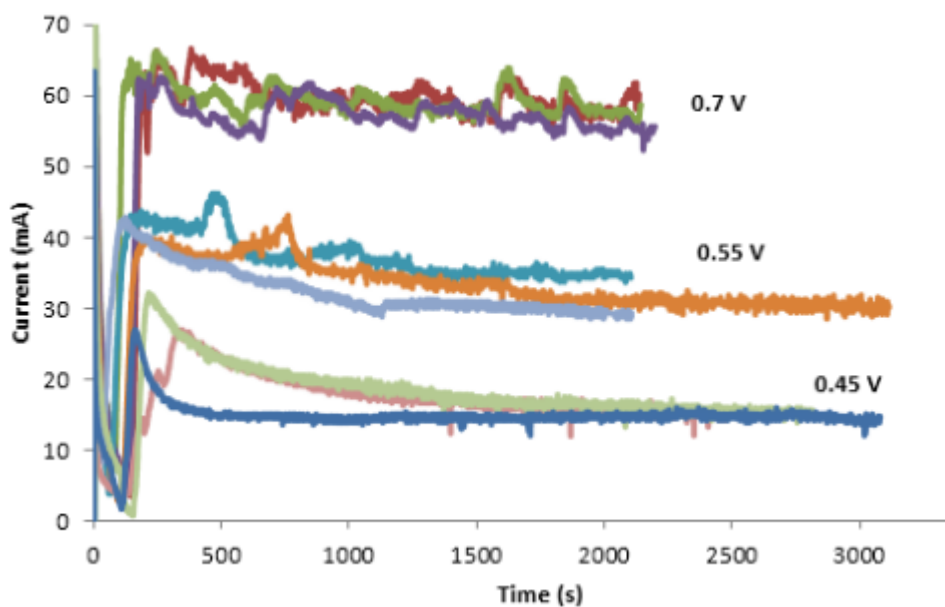


Figure B2. Current at different potentials vs. time for oxidation of 0.100 M ethanol at 50°C at Pt black anode. At each potential, the experiment was performed in triplicate at 0.2 mL min⁻¹.

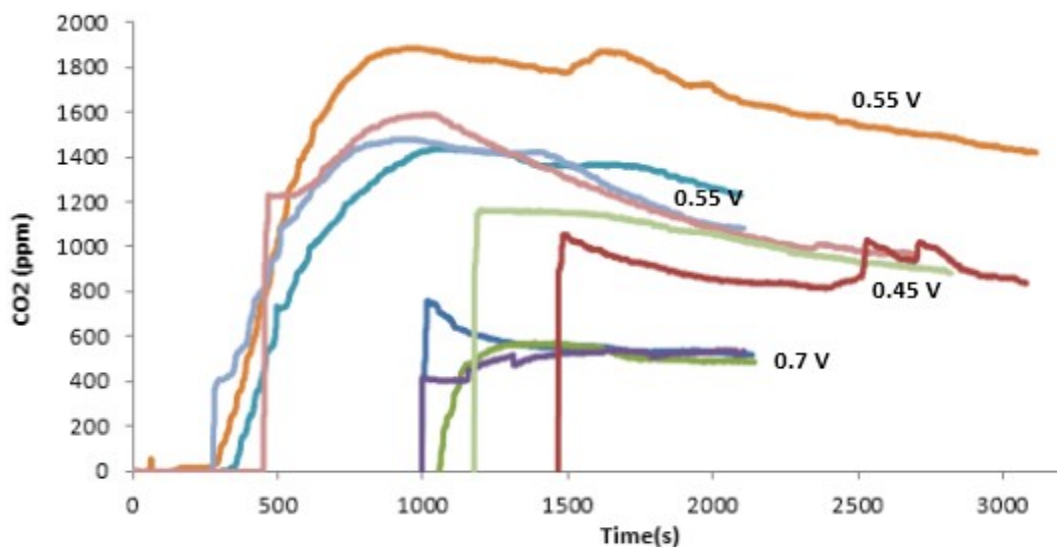


Figure B3. CO₂ (from cathode) at different potentials vs. time for oxidation of 0.100 M ethanol at 50°C at Pt black anode. At each potential, the experiment was performed in triplicate at 0.2 mL min⁻¹. The data collection started between 300 s to 1500 s after the current stabilized.

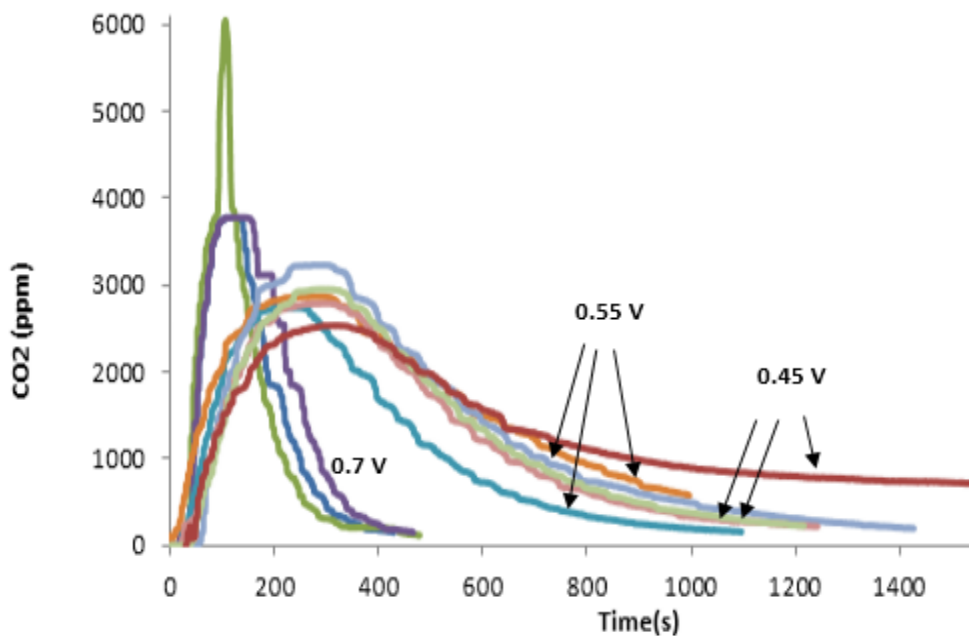


Figure B4. CO₂ (from anode) at different potentials vs. time for oxidation of 0.100 M ethanol at 50°C at Pt black anode. At each potential, the experiment was performed in triplicate at 0.2 mL min⁻¹.

Table B1. Concentrations of residual ethanol and products in mM for oxidation of 0.100 M ethanol at 50°C at Pt black anode (0.2 mL min⁻¹). Note that the CO₂ concentration is the value that would be obtained if it remains in the ethanol solution, and that only 0.5 mol of ethanol are consumed to produce 1 mol of CO₂.

Potential (V)	CO ₂	AA	AAL	AAL dimer	ethanol
0.7 (1)	7.41	28.85	2.24	1.94	53.88
0.7 (2)	7.31	26.87	2.53	1.78	50.63
0.7 (3)	7.57	29.73	2.45	1.86	55.77
0.55 (1)	5.38	17.05	2.37	1.50	74.90
0.55 (2)	4.75	13.59	0.82	0.76	79.35
0.55 (3)	5.12	11.56	1.79	1.75	82.42
0.45 (1)	4.08	4.35	2.67	1.47	87.35
0.45 (2)	4.03	4.95	1.84	2.03	85.76
0.45 (3)	3.67	4.01	3.25	1.67	88.16

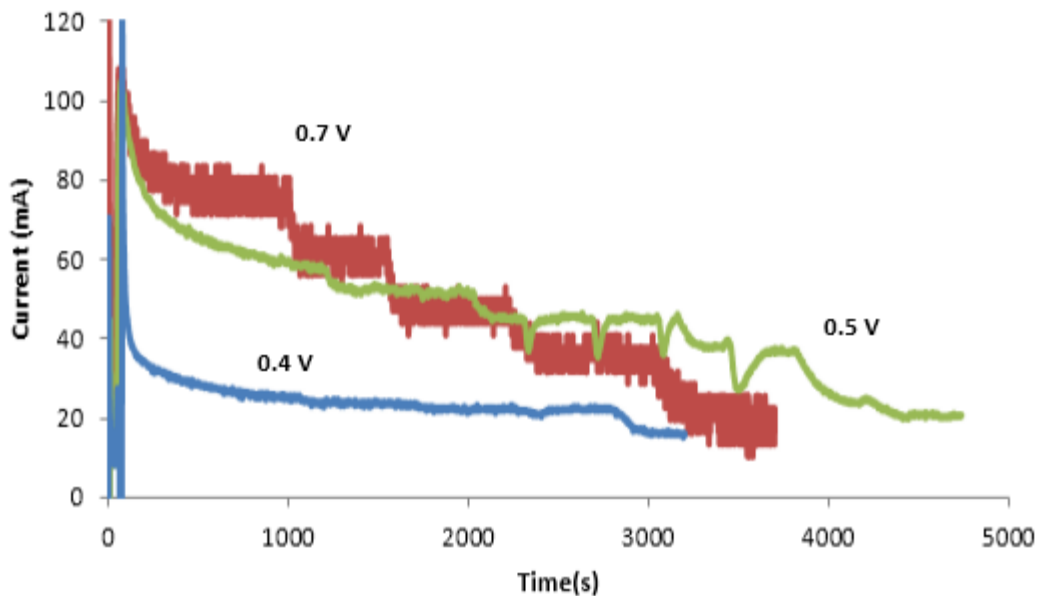


Figure B5. Current at different potentials vs. time for oxidation of 0.100 M ethanol at 80°C at Pt black anode. At each potential, the cell was running at different flow rates (0.5, 0.2, 0.09, 0.05 and 0.02 mL min⁻¹).

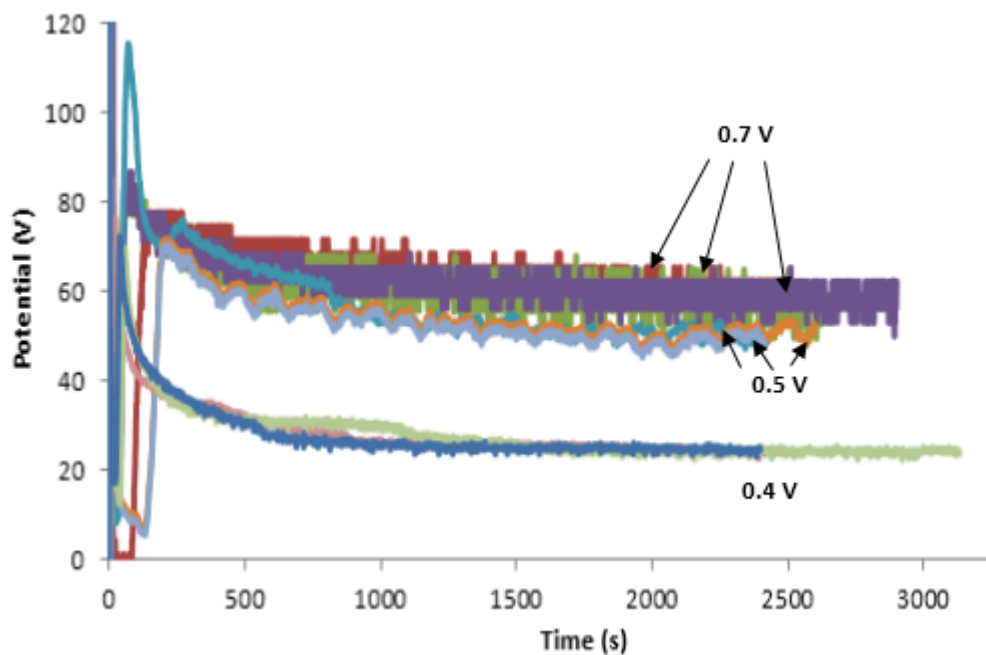


Figure B6. Current at different potentials vs. time for oxidation of 0.100 M ethanol at 80°C at Pt black anode. At each potential, the experiment was performed in triplicate at 0.2 mL min⁻¹.

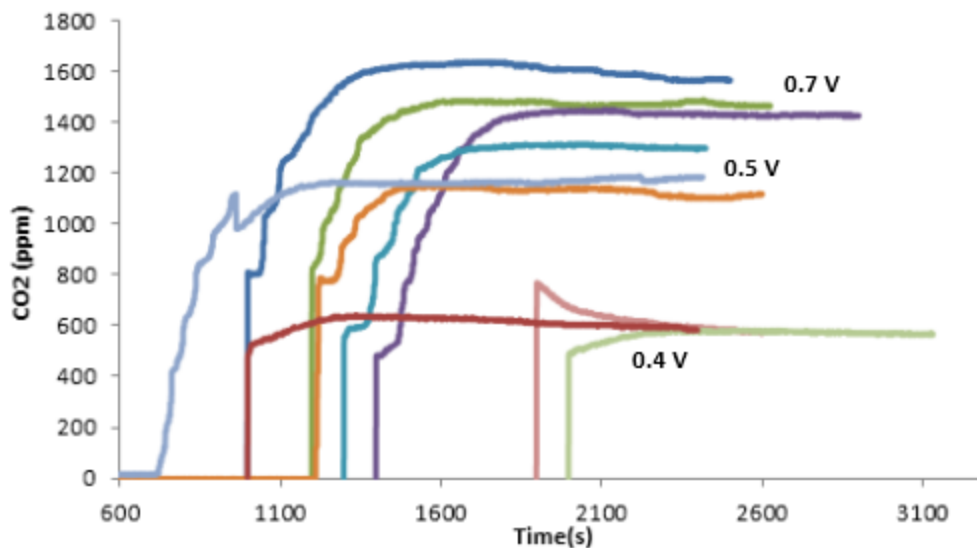


Figure B7. CO₂ (from cathode) at different potentials vs. time for oxidation of 0.100 M ethanol at 80°C at Pt black anode. At each potential, the experiment was performed in triplicate at 0.2 mL min⁻¹. The data collection started between 700 s to 2000 s after the current stabilized.

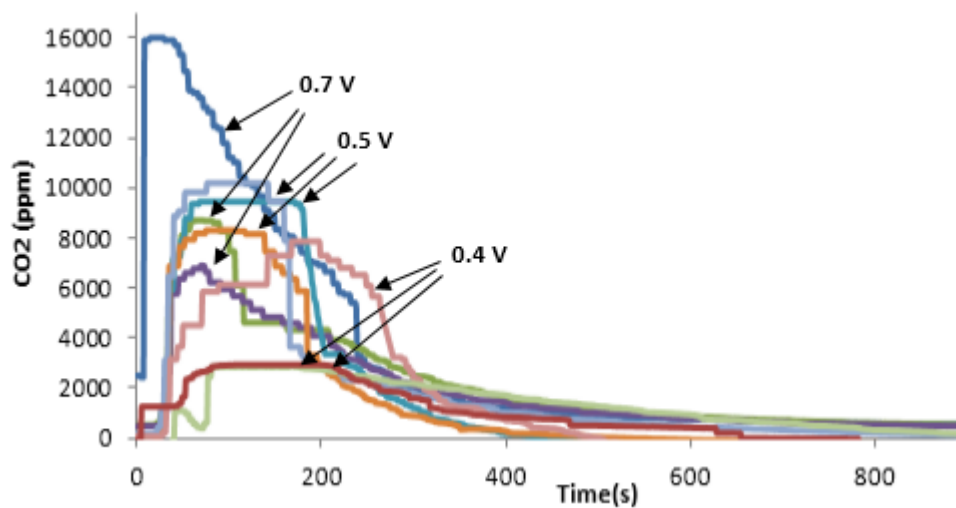


Figure B8. CO₂ (from anode) at different potentials vs. time for oxidation of 0.100 M ethanol at 80°C at Pt black anode. At each potential, the experiment was performed in triplicate at 0.2 mL min⁻¹.

Table B2. Concentrations of residual ethanol and products in mM for oxidation of 0.100 M ethanol at 80°C at Pt black anode (0.2 mL min⁻¹). Note that the CO₂ concentration is the value that would be obtained if it remains in the ethanol solution, and that only 0.5 mol of ethanol are consumed to produce 1 mol of CO₂.

Potential (V)	CO ₂	AA	AAL	AAL dimer	ethanol
0.7 (1)	19.52	16.28	1.19	1.18	64.77
0.7 (2)	19.76	15.44	1.98	1.16	64.92
0.7 (3)	19.06	15.40	1.47	1.37	62.84
0.5 (1)	15.41	14.21	1.86	1.21	73.55
0.5 (2)	15.93	14.07	2.35	1.31	72.94
0.5 (3)	15.85	14.30	1.77	1.28	73.63
0.4 (1)	8.81	6.11	3.09	2.03	86.49
0.4 (2)	7.23	6.90	2.54	2.30	87.19
0.4 (3)	7.74	7.15	2.66	2.13	87.08

Appendix C

Current and CO₂ Traces for Pt/C, PtRu/C and PtSn/C

C. Current and CO₂ Traces for Pt/C, PtRu/C and PtSn/C

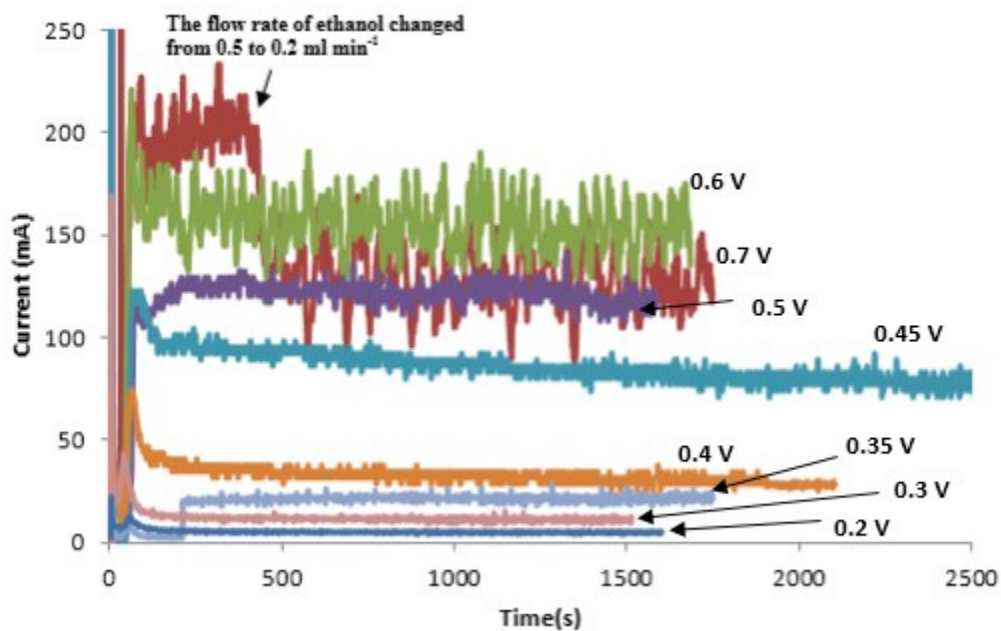


Figure C1. Current at different potentials vs. time for oxidation of 0.100 M ethanol at 80°C at Pt/C anode (0.2 mL min⁻¹).

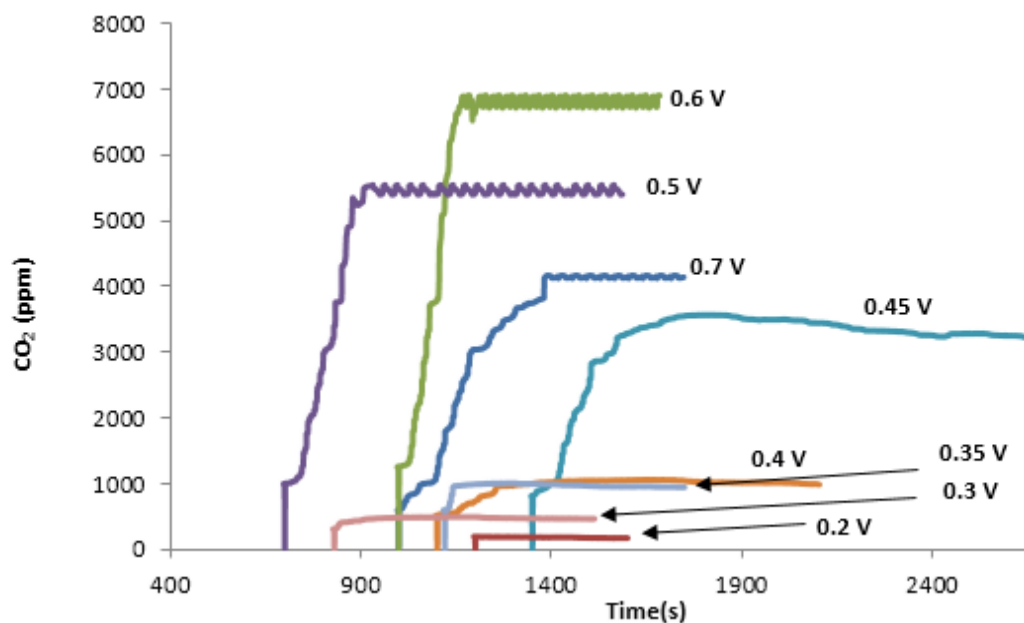


Figure C2. CO₂ at different potentials vs. time for oxidation of 0.100 M ethanol at 80°C at Pt/C anode (0.2 mL min⁻¹). The data collection started between 700 s to 1400 s after the current stabilized.

Table C1. Concentrations of residual ethanol and products in mM for oxidation of 0.100 M ethanol at 80°C at Pt/C anode (0.2 mL min⁻¹). Note that the CO₂ concentration is the value that would be obtained if it remains in the ethanol solution, and that only 0.5 mol of ethanol are consumed to produce 1 mol of CO₂.

Potential (V)	CO ₂	AA	AAL	AAL dimer	ethanol
0.7	33.38	46.35	0.79	0.54	34.18
0.6	55.05	35.24	0.65	0.59	36.26
0.5	45.01	20.82	0.99	0.55	54.62
0.45	26.61	17.06	3.11	1.89	63.41
0.4	8.32	6.46	2.92	2.03	83.72
0.35	7.87	3.39	2.14	1.78	88.85
0.3	3.87	1.64	1.27	1.08	93.68
0.2	1.45	0.74	1.09	0.82	96.76

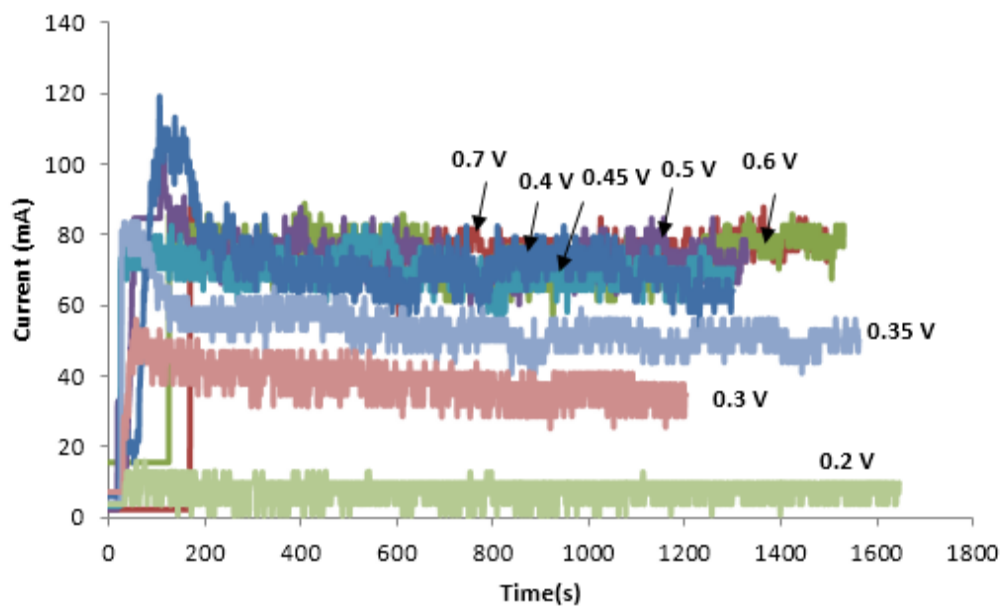


Figure C3. Current at different potentials vs. time for oxidation of 0.100 M ethanol at 80°C at PtRu/C anode (0.2 mL min⁻¹).

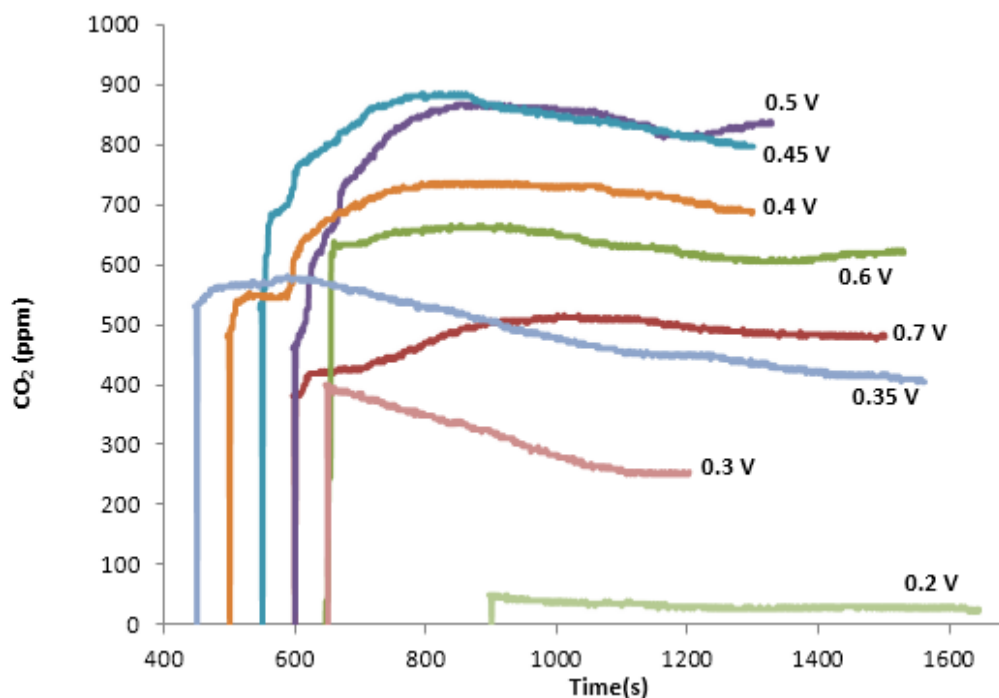


Figure C4. CO₂ at different potentials vs. time for oxidation of 0.100 M ethanol at 80°C at PtRu/C anode (0.2 mL min⁻¹). The data collection started between 500 s to 1400 s after the current stabilized.

Table C2. Concentrations of residual ethanol and products in mM for oxidation of 0.100 M ethanol at 80°C at PtRu/C anode (0.2 mL min⁻¹). Note that the CO₂ concentration is the value that would be obtained if it remains in the ethanol solution, and that only 0.5 mol of ethanol are consumed to produce 1 mol of CO₂.

Potential (V)	CO ₂	AA	AAL	AAL dimer	ethanol
0.7	3.87	50.44	0.95	1.07	42.92
0.6	4.97	51.03	1.14	0.80	45.66
0.5	6.97	45.71	0.89	0.97	50.51
0.45	6.66	40.02	1.12	0.79	52.44
0.4	5.75	37.91	1.07	1.07	55.44
0.35	3.44	29.95	1.73	1.47	64.62
0.3	2.08	20.90	1.86	1.95	72.17
0.2	0.23	3.36	1.95	1.79	92.99

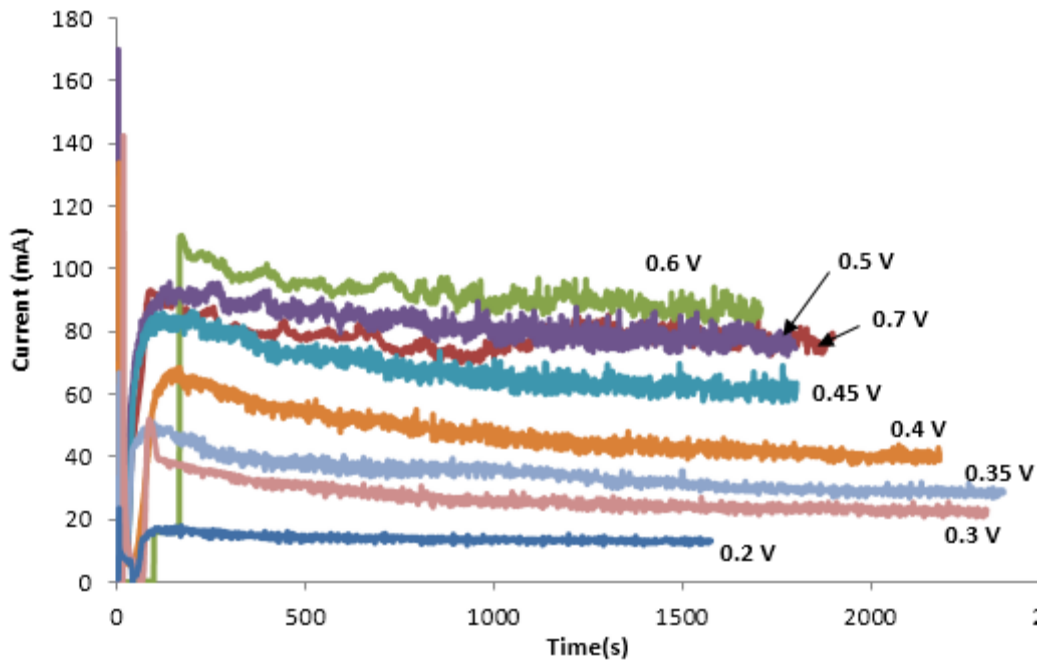


Figure C5. Current at different potentials vs. time for oxidation of 0.100 M ethanol at 80°C at PtSn/C anode (0.2 mL min⁻¹).

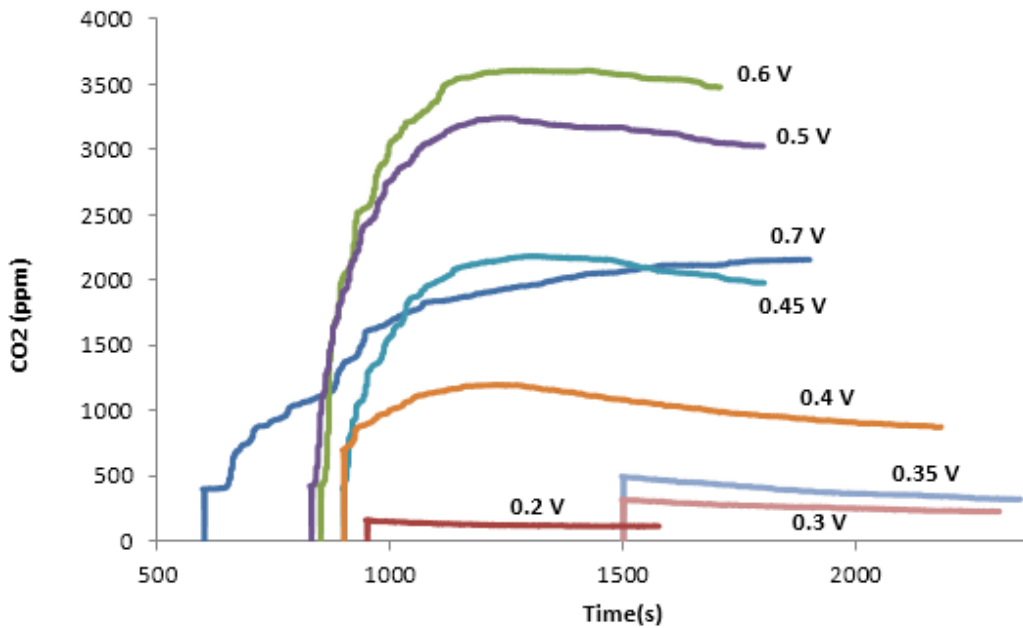


Figure C6. CO₂ at different potentials vs. time for oxidation of 0.100 M ethanol at 80°C at PtSn/C anode (0.2 mL min⁻¹). The data collection started between 600 s to 1500 s after the current stabilized.

Table C3. Concentrations of residual ethanol and products in mM for oxidation of 0.100 M ethanol at 80°C at PtSn/C anode (0.2 mL min⁻¹). Note that the CO₂ concentration is the value that would be obtained if it remains in the ethanol solution, and that only 0.5 mol of ethanol are consumed to produce 1 mol of CO₂.

Potential (V)	CO ₂	AA	AAL	AAL dimer	ethanol
0.7	14.62	34.79	3.02	2.41	52.58
0.6	24.11	28.98	1.98	1.30	54.41
0.5	20.91	26.68	2.07	1.56	57.40
0.45	13.81	24.72	2.54	2.36	61.43
0.4	6.02	21.27	2.17	2.70	70.51
0.35	2.39	17.11	2.92	2.37	76.11
0.3	1.59	14.52	2.09	1.92	79.44
0.2	0.78	8.05	1.51	0.89	88.32

Appendix D

Current and CO₂ Traces for Pt/C and PtRu/C catalyst bilayers

D. Current and CO₂ Traces for Pt/C and PtRu/C catalyst bilayers

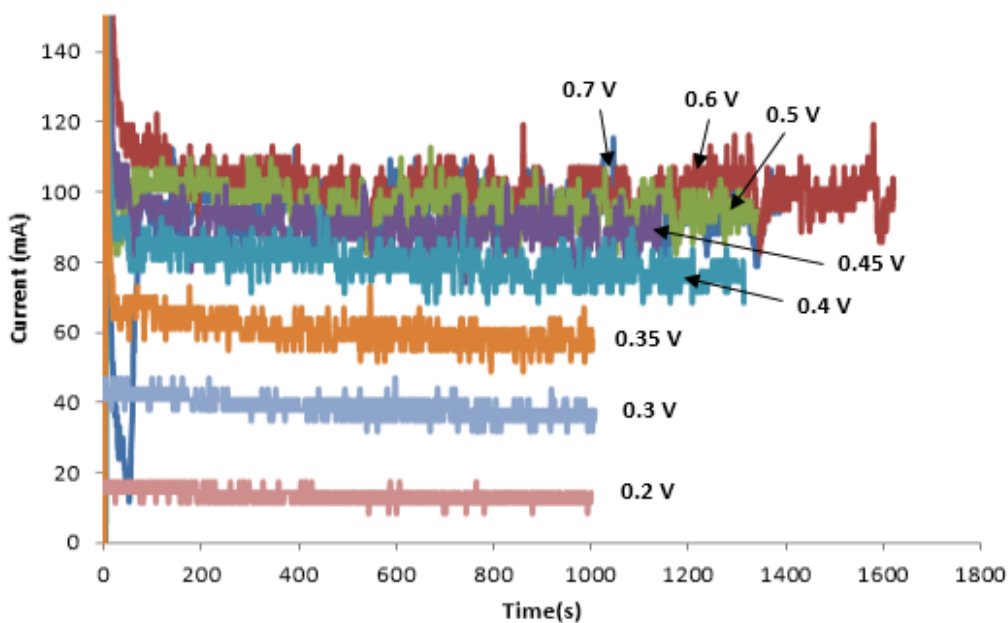


Figure D1. Current at different potentials vs. time for oxidation of 0.100 M ethanol at 80°C at Pt on PtRu anode (0.2 mL min⁻¹).

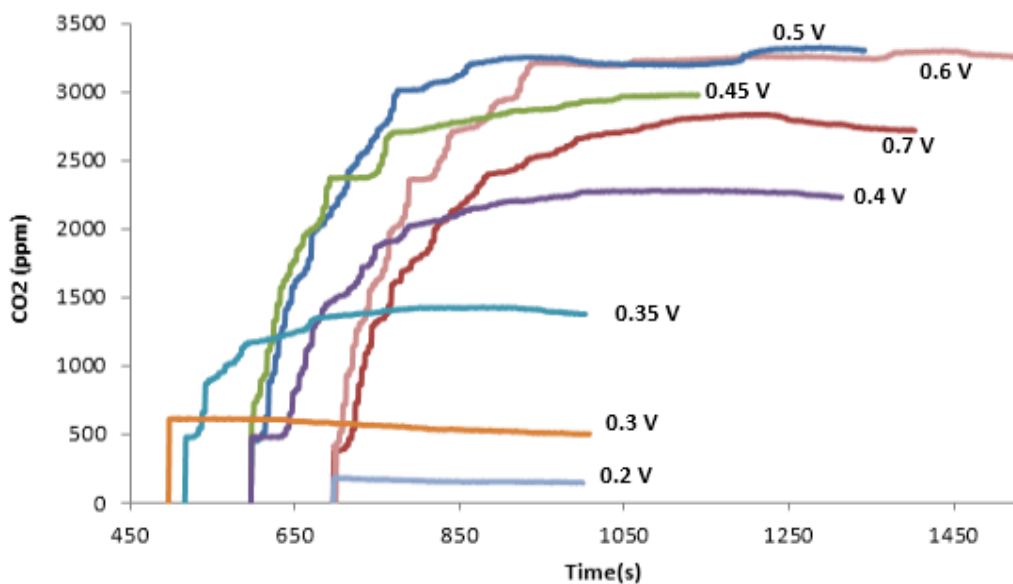


Figure D2. CO₂ at different potentials vs. time for oxidation of 0.100 M ethanol at 80°C at Pt on PtRu anode (0.2 mL min⁻¹). The data collection started between 500 s to 700 s after the current stabilized.

Table D1. Concentrations of residual ethanol and products in mM for oxidation of 0.100 M ethanol at 80°C at Pt on PtRu anode (0.2 mL min⁻¹). Note that the CO₂ concentration is the value that would be obtained if it remains in the ethanol solution, and that only 0.5 mol of ethanol are consumed to produce 1 mol of CO₂.

Potential (V)	CO ₂	AA	AAL	AAL dimer	ethanol
0.7	22.63	39.44	0.56	0.47	48.50
0.6	27.16	36.02	0.55	0.42	49.76
0.5	27.34	32.31	0.59	0.67	53.47
0.45	24.59	29.83	0.63	0.60	53.78
0.4	18.68	29.99	0.82	0.88	59.17
0.35	11.60	26.73	1.05	1.17	65.76
0.3	4.23	20.30	1.97	1.86	73.05
0.2	1.24	5.57	1.89	2.09	89.45

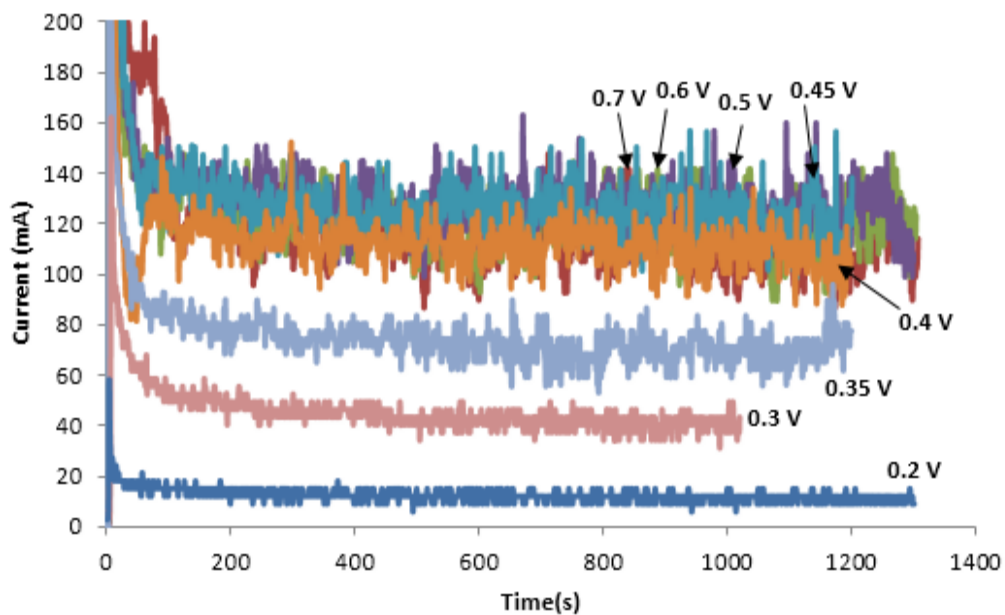


Figure D3. Current at different potentials vs. time for oxidation of 0.100 M ethanol at 80°C at PtRu on Pt anode (0.2 mL min⁻¹).

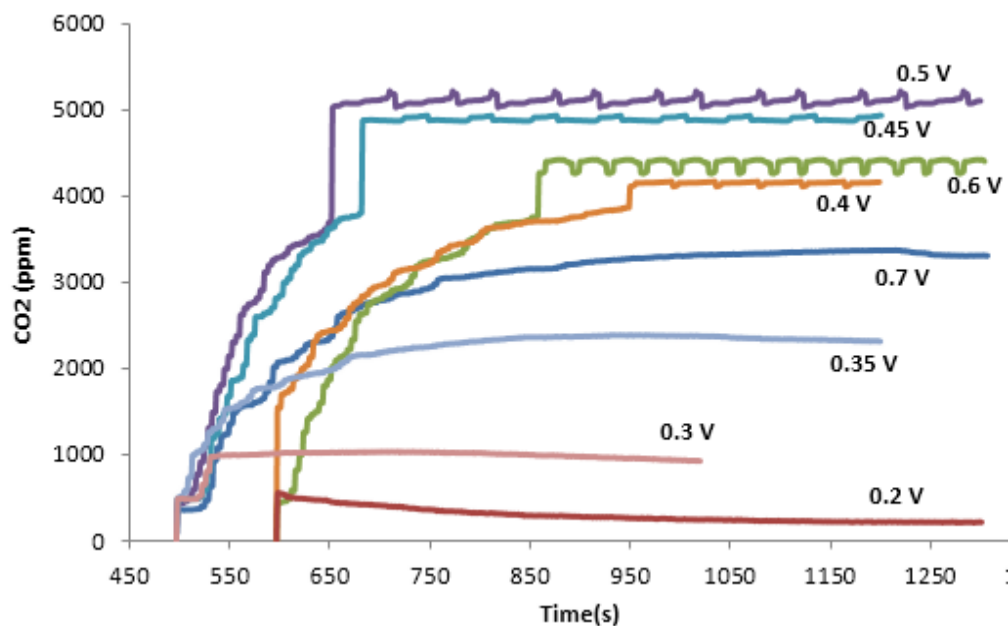


Figure D4. CO₂ at different potentials vs. time for oxidation of 0.100 M ethanol at 80°C at PtRu on Pt anode (0.2 mL min⁻¹). The data collection started between 500 s to 700 s after the current stabilized.

Table D2. Concentrations of residual ethanol and products in mM for oxidation of 0.100 M ethanol at 80°C at PtRu on Pt anode (0.2 mL min⁻¹). Note that the CO₂ concentration is the value that would be obtained if it remains in the ethanol solution, and that only 0.5 mol of ethanol are consumed to produce 1 mol of CO₂.

Potential (V)	CO ₂	AA	AAL	AAL dimer	ethanol
0.7	25.48	47.20	1.04	0.74	38.45
0.6	33.48	43.31	0.85	0.49	38.98
0.5	39.02	38.39	0.79	0.49	40.73
0.45	37.04	36.35	0.74	0.81	44.60
0.4	31.72	32.90	1.28	0.82	49.25
0.35	17.79	27.57	1.19	1.14	59.47
0.3	7.31	17.85	1.85	1.65	73.08
0.2	1.66	4.02	2.11	1.75	90.84

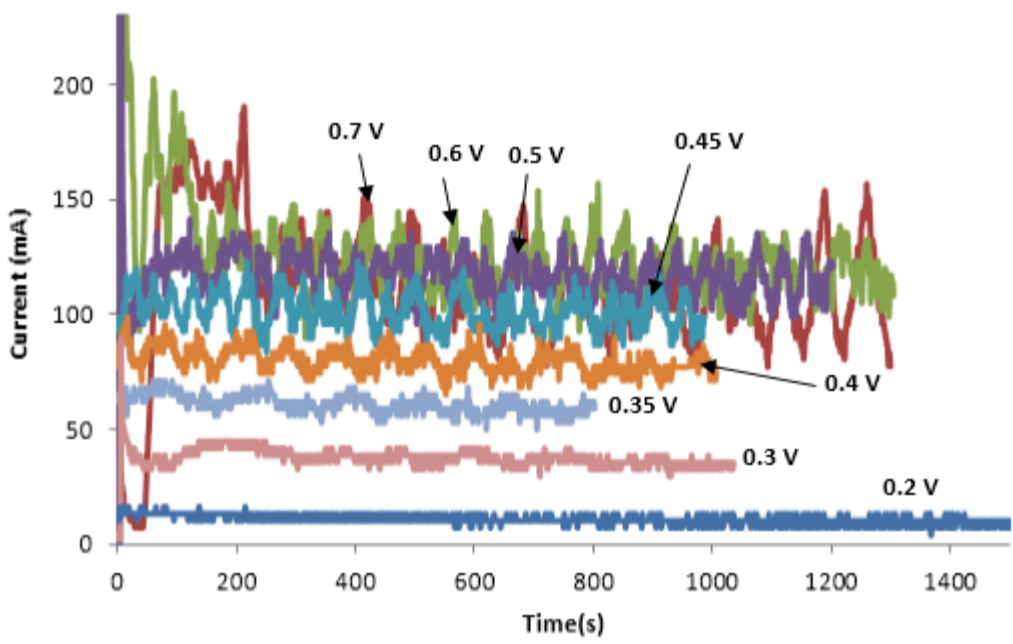


Figure D5. Current at different potentials vs. time for oxidation of 0.100 M ethanol at 80°C at Pt + PtRu anode (0.2 mL min⁻¹).

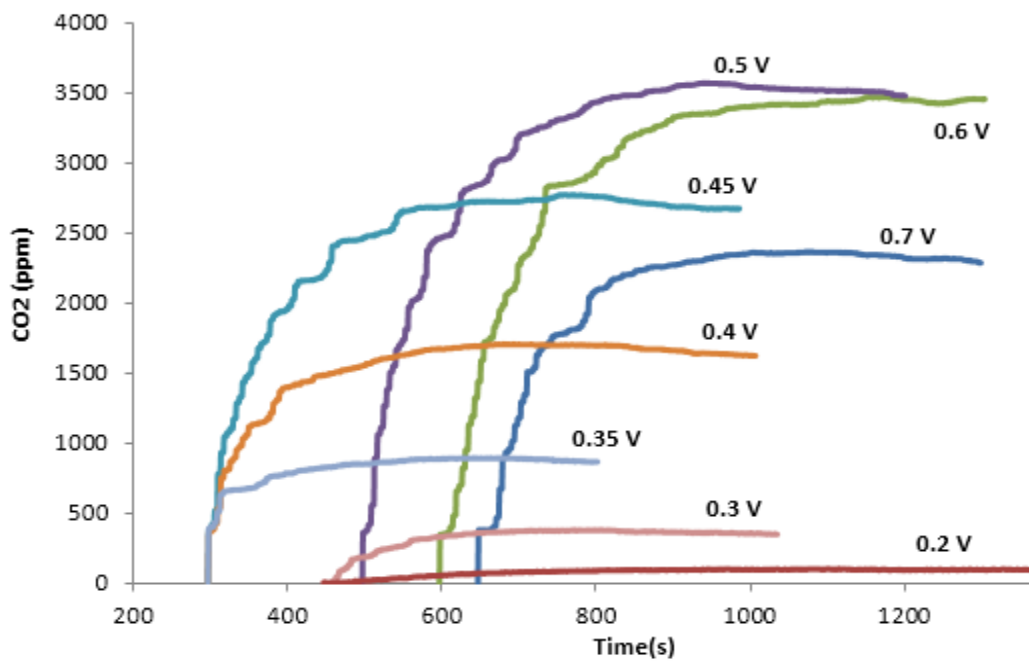


Figure D6. CO₂ at different potentials vs. time for oxidation of 0.100 M ethanol at 80°C at Pt + PtRu anode (0.2 mL min⁻¹). The data collection started between 500 s to 700 s after the current stabilized.

Table D2. Concentrations of residual ethanol and products in mM for oxidation of 0.100 M ethanol at 80°C at Pt + PtRu anode (0.2 mL min⁻¹). Note that the CO₂ concentration is the value that would be obtained if it remains in the ethanol solution, and that only 0.5 mol of ethanol are consumed to produce 1 mol of CO₂.

Potential (V)	CO ₂	AA	AAL	AAL dimer	ethanol
0.7	18.13	53.53	0.89	0.99	32.21
0.6	27.00	49.67	0.89	0.75	35.37
0.5	27.51	47.39	0.90	0.77	38.25
0.45	21.00	45.22	1.27	1.22	42.54
0.4	12.84	39.23	1.68	1.37	49.00
0.35	7.40	29.98	1.69	1.59	57.07
0.3	3.01	21.12	2.38	2.13	73.86
0.2	0.75	3.96	2.08	1.68	91.20

Appendix E

Determination of the stoichiometry of ethanol oxidation from the flow rate dependence of the current in a proton exchange membrane electrolysis cell

E. Determination of the stoichiometry of ethanol oxidation from the flow rate dependence of the current in a proton exchange membrane electrolysis cell

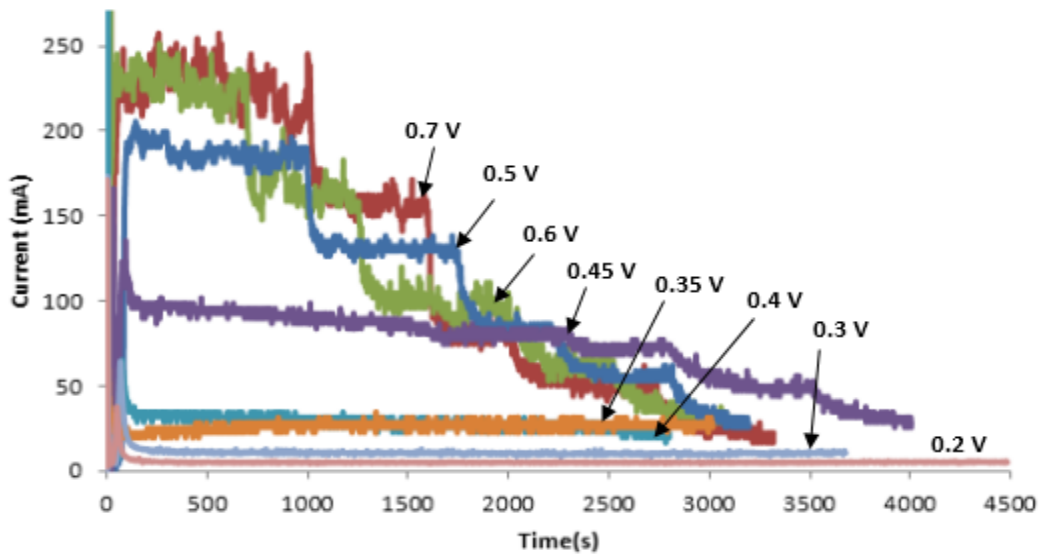


Figure E1. Current at different potentials vs. time for oxidation of 0.100 M ethanol at 80°C at Pt/C anode. At each potential, the cell was running at different flow rates (0.5, 0.2, 0.09, 0.05 and 0.02 mL min⁻¹).

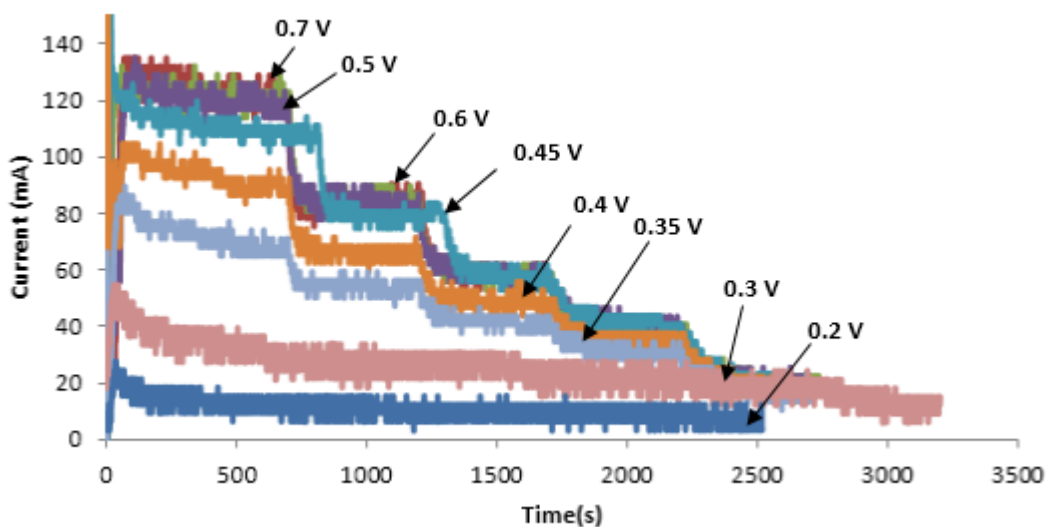


Figure E2. Current at different potentials vs. time for oxidation of 0.100 M ethanol at 80°C at PtRu/C anode. At each potential, the cell was running at different flow rates (0.5, 0.2, 0.09, 0.05 and 0.02 mL min⁻¹).

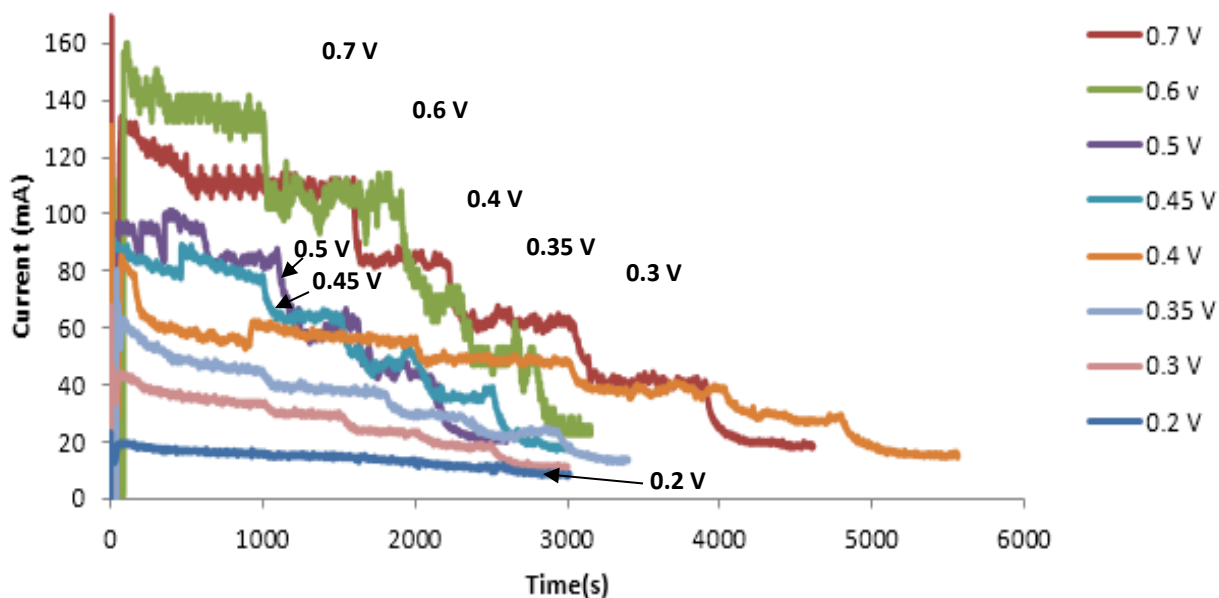


Figure E3. Current at different potentials vs. time for oxidation of 0.100 M ethanol at 80°C at PtSn/C anode. At each potential, the cell was running at different flow rates (0.5, 0.2, 0.09, 0.05 and 0.02 mL min⁻¹).

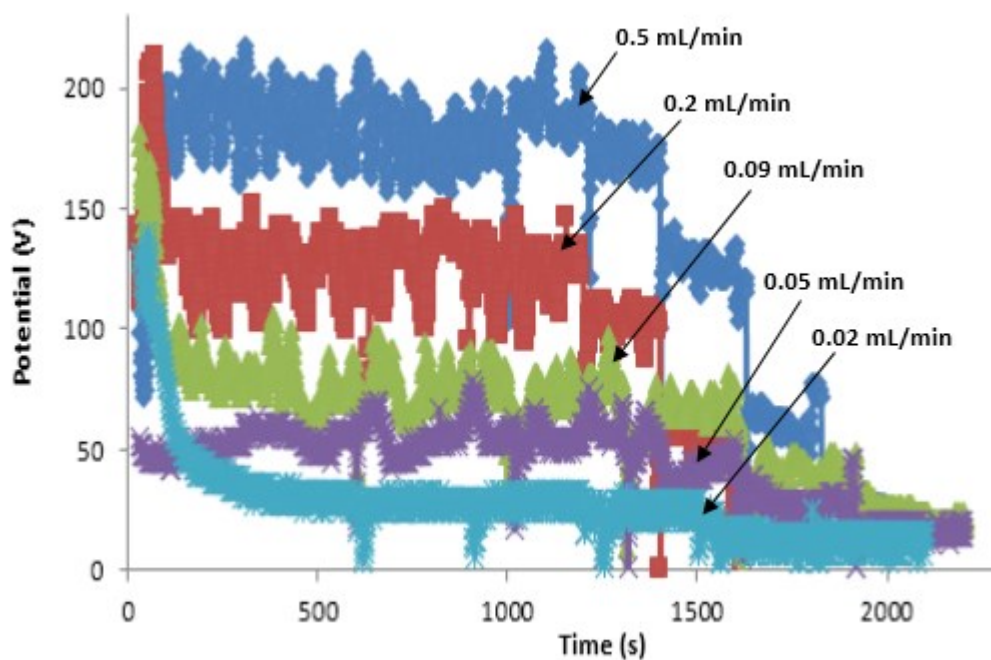


Figure E4. Current at different flow rates vs. time for oxidation of 0.100 M ethanol at 80°C at Pt on PtRu anode. At each flow rate, the cell was running at different potentials (0.7, 0.6, 0.5, 0.4, 0.3 and 0.2 V).

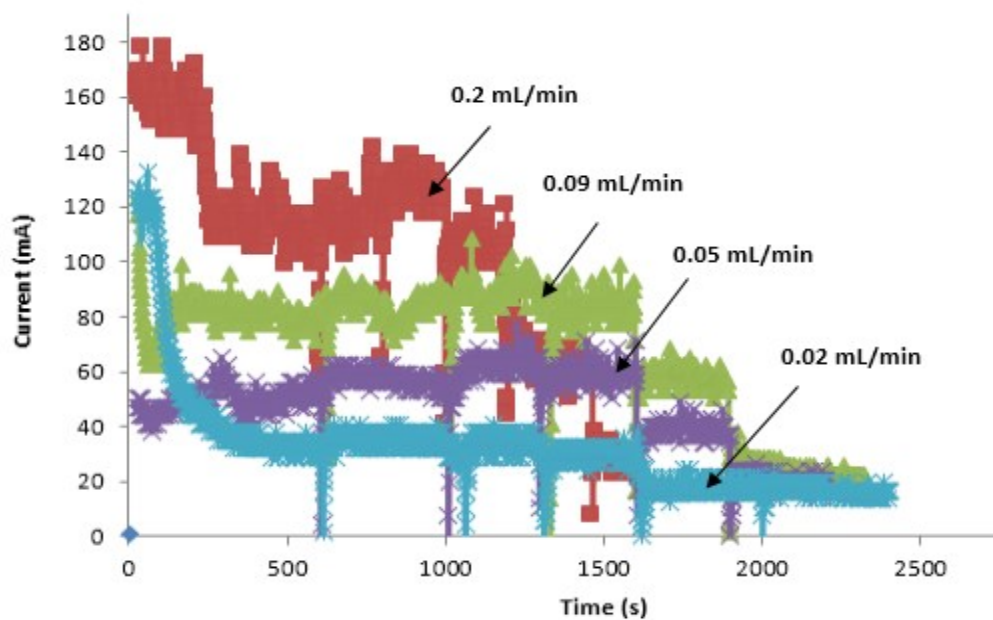


Figure E5. Current at different flow rates *vs.* time for oxidation of 0.100 M ethanol at 80°C at PtRu on Pt anode. At each flow rate, the cell was running at different potentials (0.7, 0.6, 0.5, 0.4, 0.3 and 0.2 V).

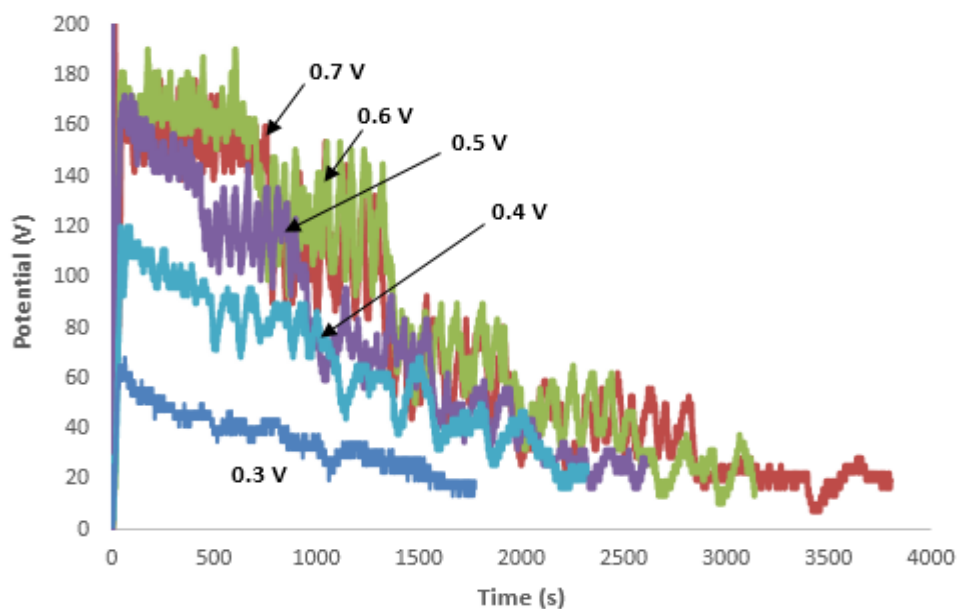


Figure E6. Current at different potentials *vs.* time for oxidation of 0.100 M ethanol at 80°C at Pt + PtRu anode. At each potential, the cell was running at different flow rates (0.5, 0.2, 0.09, 0.05 and 0.02 mL min⁻¹).

Appendix F

Product distributions and efficiencies for ethanol oxidation at PtNi octahedra

F. Product distributions and efficiencies for ethanol oxidation at PtNi octahedra

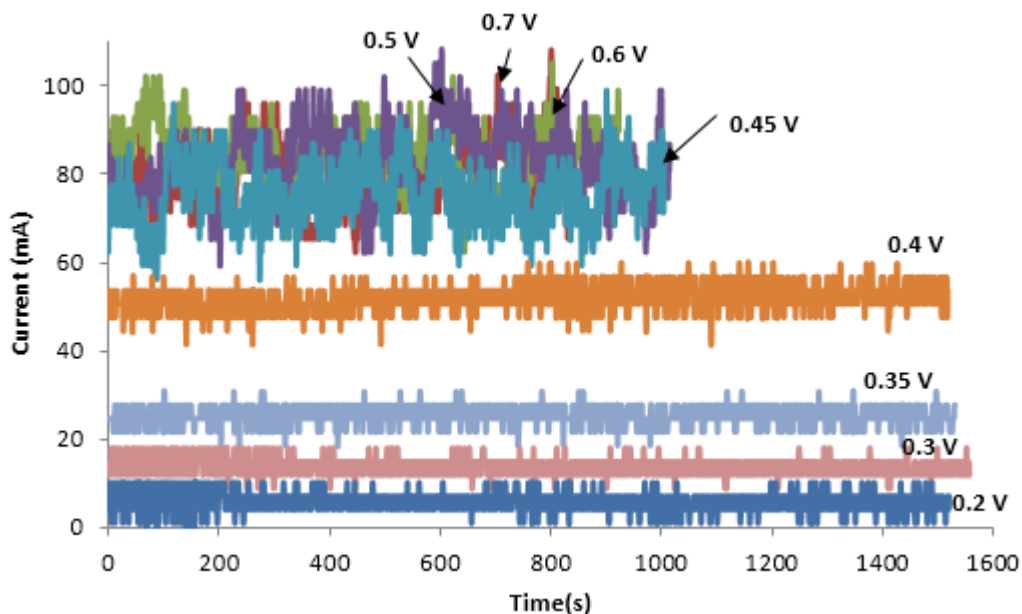


Figure F1. Current at different potentials vs. time for oxidation of 0.100 M ethanol at 80°C at PtNi anode (0.2 mL min^{-1}).

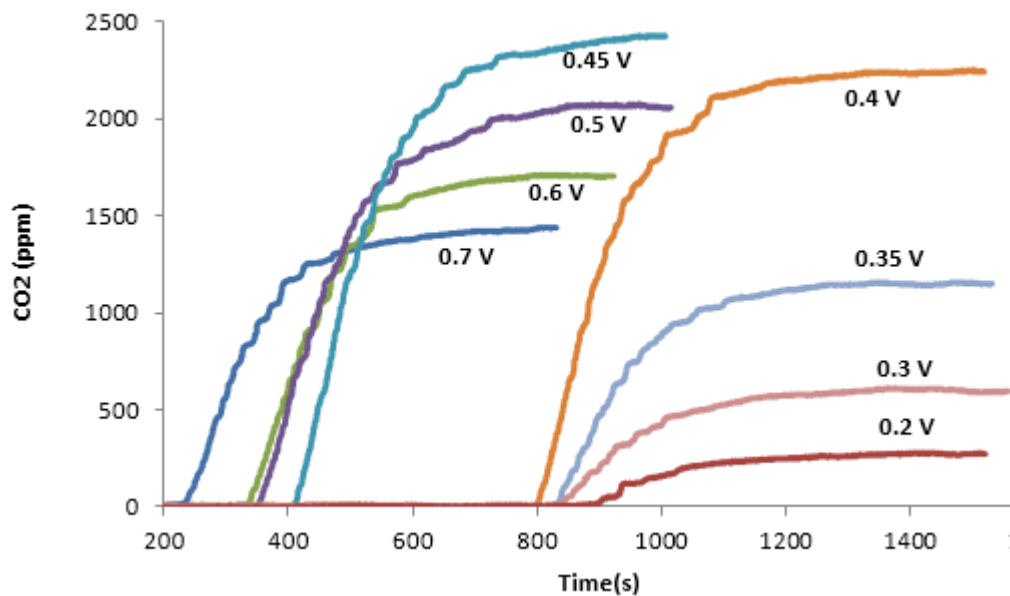


Figure F2. CO_2 at different potentials vs. time for oxidation of 0.100 M ethanol at 80°C at PtNi anode (0.2 mL min^{-1}). The data collection started between 200 s to 900 s after the current stabilized.

Table F1. Concentrations of residual ethanol and products in mM for oxidation of 0.100 M ethanol at 80°C at PtNi anode (0.2 mL min⁻¹). Note that the CO₂ concentration is the value that would be obtained if it remains in the ethanol solution, and that only 0.5 mol of ethanol are consumed to produce 1 mol of CO₂.

Potential (V)	CO ₂	AA	AAL	AAL dimer	ethanol
0.7	11.17	47.38	0.59	0.45	45.49
0.6	13.40	46.26	0.31	0.34	47.28
0.5	16.23	38.73	0.17	0.22	51.22
0.45	18.96	34.50	0.22	0.31	55.35
0.4	17.58	13.71	0.86	0.94	76.60
0.35	9.01	5.29	1.00	1.10	89.14
0.3	4.74	2.38	0.89	0.93	94.57
0.2	2.14	0.73	0.68	0.37	97.81

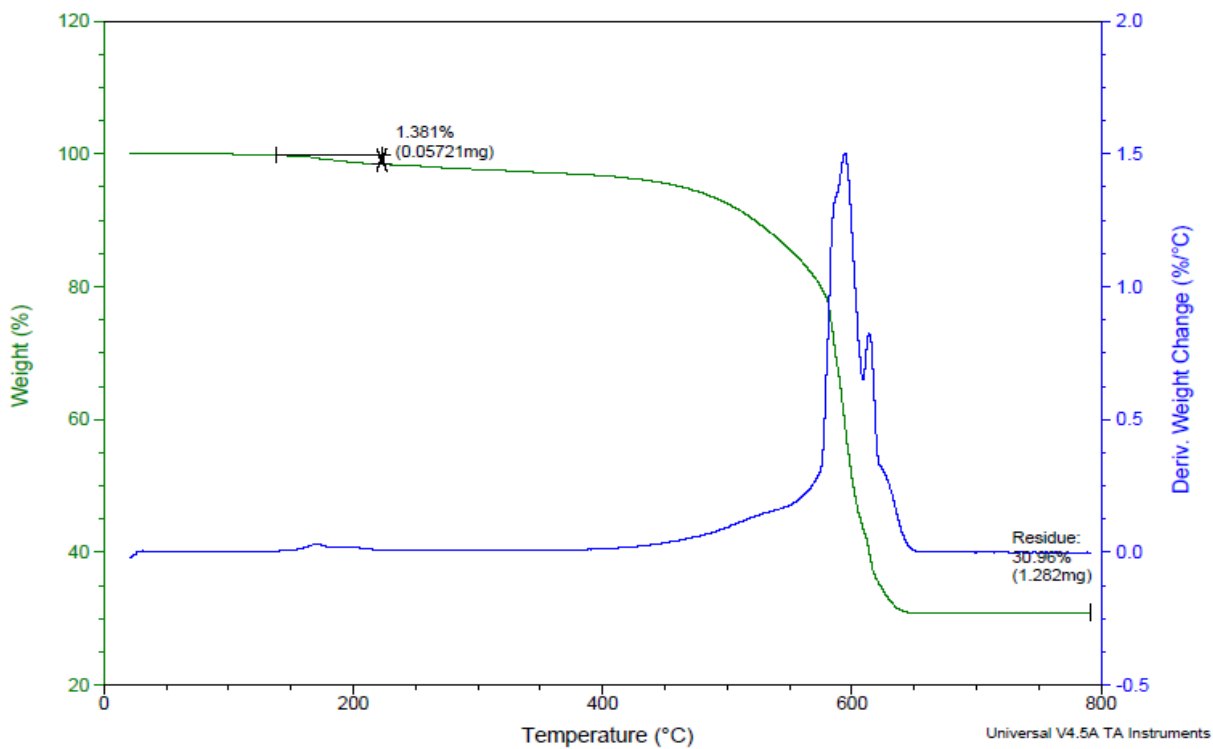


Figure F3. Thermogravimetry of the as-prepared bulk sample of PtNi/C.

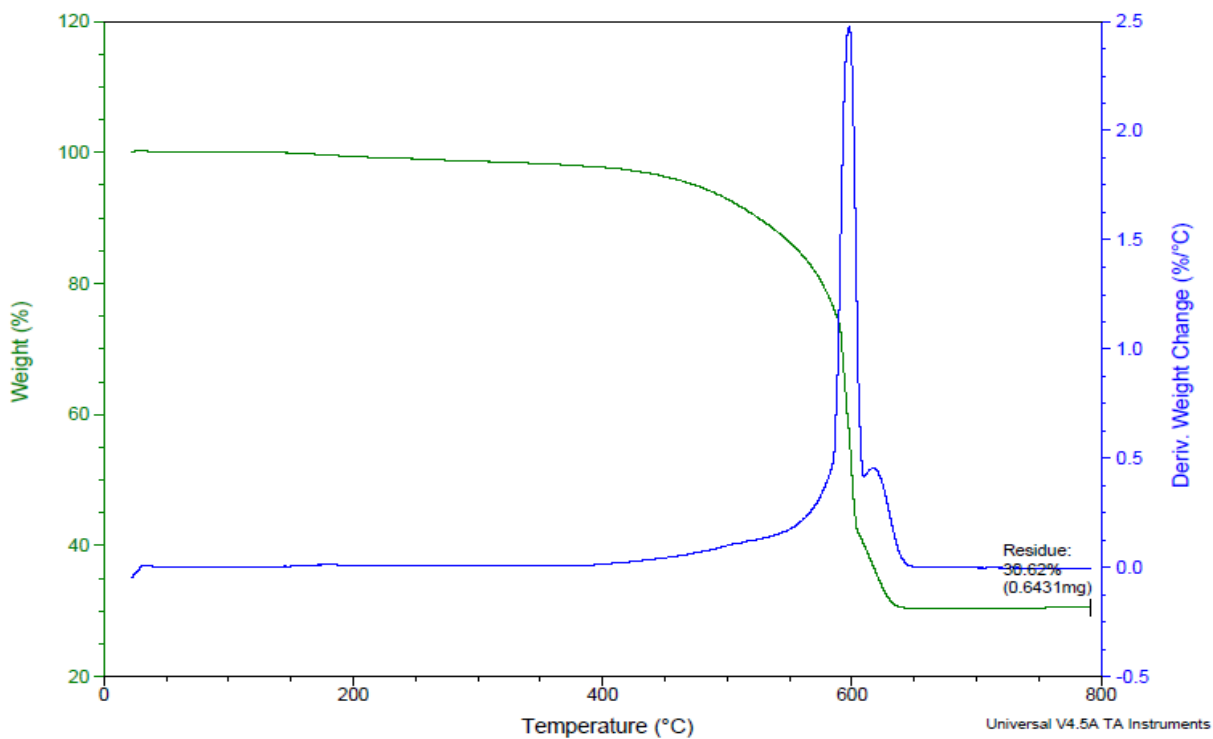


Figure F4. Thermogravimetry of the bulk sample of PtNi/C following heating in acetic acid at 60 °C for 2 h.

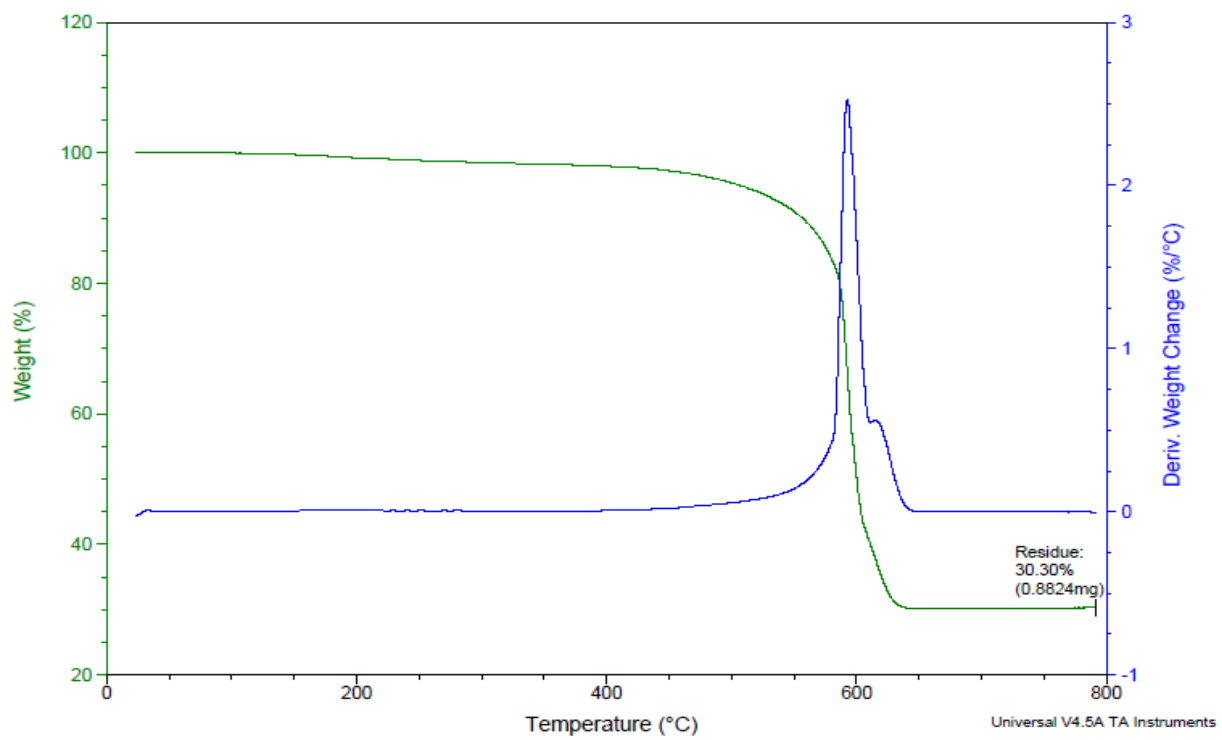


Figure F5. Thermogravimetry of the bulk sample of PtNi/C following heating in acetic acid at 60 °C for 4 h.